Investigating the mechanisms regulating retrograde transport and signalling of neurotrophin receptors in neuronal cells

Marta Izabela Budzinska

Institute of Neurology

Academic supervisors:

Prof. Giampietro Schiavo and Prof. Linda Greensmith (UCL)

Industrial supervisors:

Wheaton T. Little and Jill Richardson (GSK)

A thesis submitted for the degree of Doctor of Philosophy

University College London

May 2019

Declaration

I, Marta Budzinska, confirm that the work presented in this thesis is my own. Where information has been derived from other sources, I confirm that this has been indicated in the thesis.

Abstract

Signalling by target-derived growth factors called neurotrophins (NT) is essential for the development of the nervous system and its maintenance throughout life. Neurons have very complex morphology, reaching up to a metre in length in humans, and strongly rely on fast axonal transport for the efficient delivery of biological molecules to ensure their homeostasis. It is therefore not surprising that perturbations connected to long-range trafficking and signalling are associated with neurological conditions. Although the transport of NT and their receptors (NTRs) is a well-characterized process, the molecular mechanism controlling the somatic sorting of activated NTRs towards a specific destination, such as recycling or degradation, is not completely understood.

Recently, our laboratory demonstrated that the dynein motor adaptor, Bicaudal D1 (BICD1), is a main regulator of NTR sorting towards lysosomal degradation. Following the identification of protein tyrosine phosphatase, non-receptor type 23 (PTPN23) in the BICD1 interactome, I characterized their interaction using biochemical approaches and confocal microscopy. PTPN23 is a non-canonical member of the endosomal sorting complexes required for transport (ESCRT) family, which in non-neuronal cells mediates the turnover of transmembrane receptors, such as epidermal growth factor receptor (EGFR). By silencing PTPN23 expression and using an anti-NTR-antibody accumulation assay, I highlighted its novel role in NTR sorting in neuronal cells.

The long-range trafficking machinery is also essential for effective responses to environmental insults, such as oxidative stress, which in healthy cells, including neurons, results in the formation of stress granules (SGs). In the second part of this project, I characterized BICD1 as a novel component of neuronal SGs, following a previous report identifying this molecule as a factor necessary for SG assembly. Furthermore, I demonstrated that oxidative stress decreases the sensitivity of neurons to NTs, revealed by the specific downregulation of NTR trafficking and signalling in response to BDNF stimulation.

Impact statement

Neurotrophin receptors (NTRs) are transmembrane signalling receptors, regulating neuronal growth, proliferation and survival in response to target-derived growth factors. Due to their complexity, these processes have to be tightly regulated on several levels, such as endocytosis, transport and signalling. As expected, their misregulation is associated with the severe human disorders, such as neurodegeneration and cancer. While neurotrophins (NT) and their receptors have been the focus of intense research for several decades, there are still outstanding questions with regards to their turnover. In addition, the regulation of the NT pathway in pathological conditions, such as upon activation of the integrated stress response (ISR), characterized by the presence of stress granules (SG), is not completely understood. There is a strong connection between perturbed trafficking, signalling and SG dynamics and neurodegenerative diseases, such as amyotrophic lateral sclerosis (ALS), as well as cancer. It is therefore essential to further our understanding on how these processes are regulated in order to improve the chances of finding new effective therapies.

The work described in this thesis characterizes a novel molecular interaction between BICD1 and PTPN23, as well as the role of PTPN23 in the endocytic flow of NTRs. In addition, the association of BICD1 with neuronal SGs was demonstrated. Lastly, this thesis provides evidence of perturbed NT signalling and transport in motor neurons undergoing oxidative stress.

Insights from this study are of particular interest to cell biologists investigating the mechanisms of receptor homeostasis in healthy and pathological conditions, as well as studies deciphering the regulation of SG dynamics. Taken together, findings presented in this thesis will contribute to academic and industrial research, across disciplines ranging from neurodevelopment to neurodegeneration and cancer.

Acknowledgements

I would like to thank my primary supervisor Prof. Giampietro Schiavo, for giving me the opportunity to join his lab and learn from his expertise; for his invaluable guidance and support throughout my PhD. Thank you for all the freedom in my project and all your kindness, I could not hope for a better supervisor.

Further thanks go to my secondary supervisor, Prof. Linda Greensmith, who is truly inspirational. I could not thank you enough for taking me under your wings earlier in my studies.

Many thanks go to Wheaton T. Little, for his constructive comments and enthusiasm about this project, as well as Jill Richardson for showing me the world of pharma, and invaluable career advice.

I cannot express enough gratitude to David Villarroel-Campos. Thank you for joining me on the PTPN23 project and for your help, support and knowledge that you offered throughout my PhD. Most warm thanks go to Dr. Sergey Novoselov, who always came to my rescue when I first started and had no clue what I was doing.

Further thanks go to Dr. Marco Terenzio and Dr. Matthew Golding, who kindly offered guidance with my early experiments, as well as Dr. Solene Debaisieux, who taught me everything I know about embryonic stem cells. I would especially like to thank Dr. Bilal Malik for all the discussions in the corridor, and all present and past members of the Schiavo and Greensmith labs for their help and support, as well as BBSRC and GSK for my funding.

Most of all I would like to thank Luke, I could never have done this without you. Lastly, I would like to thank my dear mamus Iza for her continuous support.

Table of Contents

List of figures

List of tables

Abbreviations

AD	Alzheimer’s disease
ALG2	Alpha-1,3-mannosyltransferase
ALIX	ALG-2-interacting protein X
ALS	Amyotrophic lateral sclerosis
AKT	RAC-alpha serine/threonine-protein kinase
AMP-PNP	Adenosine 5-(β,ɣ-imido)triphosphate
ATP	Adenosine triphosphate
BafA1	Bafilomycin A1
BDNF	Brain-derived neurotrophic factor
BICD1/2	Bicaudal D1/2
βME	β-mercaptoethanol
bp	Base pair
BrefA	Brefeldin A
BSA	Bovine serum albumin
CC	Coiled coil
cGMP	Cyclic guanosine monophosphate
CGN	*Cis*-Golgi network
CHMP4b	Charged multivesicular body protein 4b
CHX	Cycloheximide
CNTF	Ciliary neurotrophic factor
Co-IP	Co-immunoprecipitation
COPD	Chronic obstructive pulmonary disease
CRD	Cysteine-rich domain
CTB	Cholera toxin subunit B
DAPI	4',6-diamidino-2-phenylindole
Dcp1a	mRNA-decapping enzyme 1A
DI/L/HC	Dynein intermediate/light/heavy chain
DMEM	Dulbecco's modified Eagle's medium
DMSO	Dimethyl sulfoxide

ECL	Enhanced chemiluminescence
EDTA	Ethylenediaminetetraacetic acid
EGF	Epidermal growth factor
EGFR	Epidermal growth factor receptor
Egl	Egalitarian
EGTA	Ethylene glycol-bis(β-aminoethyl ether)-N,N,N',N'-tetraacetic acid
EHNA	Erythro-9-(2-hydroxy-3-nonyl)adenine
eIF2	Eukaryotic Initiation Factor 2
ER	Endoplasmic reticulum
ERK1/2	Extracellular signal–regulated kinase 1/2
ESC	Embryonic stem cell
ESCRT	Endosomal sorting complexes required for transport
ES-MN	Embryonic stem cell-derived motor neuron
FBS	Foetal bovine serum
FMRP	Fragile X mental retardation protein
FRAP	Fluorescence recovery after photobleaching
FTLD	Frontotemporal lobal degeneration
FUS	Fused in sarcoma
G3BP	Ras GTPase-activating protein-binding protein 1
GAPDH	Glyceraldehyde 3-phosphate dehydrogenase
GCN2	General control nonderepressible 2
GDNF	Glial-derived neurotrophic factor
GFP	Green fluorescent protein
GSK3β	Glycogen synthase kinase 3-β
GST	Glutathione S-transferase
H_20_2	Hydrogen peroxide
HA	Human influenza hemagglutinin
HcT	Tetanus toxin binding fragment
HD	Huntington’s disease
HDAC6	Histone deacetylase 6

HI-HS	Heat-inactivated horse serum
HRI	Heme-regulated initiation factor 2α kinase
HRP	Horseradish peroxidase
HRS	Hepatocyte growth factor-regulated tyrosine kinase substrate
Htt	Huntingtin
ICC	Immunocytochemistry
IDR	Intrinsically-disordered region
IF	Immunofluorescence
IgG	Immunoglobulin G
ILV	Intraluminal vesicle
IPTG	Isopropyl β-D-1-thiogalactopyranoside
ISR	Integrated stress response
JNK	C-Jun N-terminal kinase
kDa	Kilodalton
Kidins220/Arms	Kinase D interacting substrate of 220 kDa/ankyrin repeat-rich membrane spanning
KO	Knockout
LatB	Latrunculin B
LB	Luria Broth
LCD	Low complexity domain
LLPS	Liquid-liquid phase separation
LSB	Laemmli sample buffer
MHC	Major histocompatibility complex
MION	Monocrystalline iron oxide nanoparticles
MN	Motor neuron
MSC	Mesenchymal stromal cell
Mt	Microtubules
MVB	Multivesicular body
MW	Molecular weight
$NaAsO_2$	Sodium arsenite

NB	Neurobasal
NGF	Nerve growth factor
Noc	Nocodazole
NT	Neurotrophin
NT3/4	Neurotrophin-3/4
NTR	Neurotrophin receptor
$p75^{NTR}$	Low-affinity nerve growth factor receptor
PABP-1	Polyadenylate-binding protein-1
P-body	Processing body
PBS	Phosphate buffered saline
PBST	Phosphate buffered saline-Tween 20
PBSTx	Phosphate buffered saline-Triton X-100
PCR	Polymerase chain reaction
PD	Parkinson’s disease
PDGFR	Platelet-derived growth factor receptor
PERK	PKR-like endoplasmic reticulum (ER) kinase
PenStrep	Penicillin-streptomycin
PFA	Paraformaldehyde
PI3K	Phosphoinositide 3-kinase
PKR	Protein kinase RNA-activated
PLC	Phospholipase C
pMN	Primary motor neuron
PMSF	Phenylmethylsulfonyl fluoride
PQC	Protein quality control
PTPN23	Protein tyrosine phosphatase, non-receptor type 23
p-Ub	Polyubiquitinated
PVDF	Polyvinylidene fluoride
RA	Retinoic acid
RanBP2	RAN-binding protein 2
RBP	RNA-binding protein
RIPA	Radioimmunoprecipitation assay

RNA	Ribonucleic acid
RNP	Ribonucleoprotein particle
ROS	Reactive oxygen species
RPM	Revolutions per minute
RT	Room temperature
RTK	Receptor tyrosine kinase
SAG	Smoothened agonist
SDS-PAGE	Sodium dodecyl sulphate polyacrylamide gel electrophoresis
SG	Stress granule
shRNA	Short hairpin RNA
siRNA	Small interfering RNA
SMA	Spinal muscular atrophy
SMN1	Survival motor neuron 1
SNX	Sorting nexin
STAM2	Signal transducing adapter molecule 2
TBE	Tris/Borate/EDTA
TDP-43	TAR DNA-binding protein 43
TeNT	Tetanus neurotoxin
TGN	*Trans*-Golgi network
TIA-1	T-cell-restricted intracellular antigen-1
TM	Transmembrane
TNF	Tumor necrosis factor
Ub	Ubiquitin
UBAP1	Ubiquitin-associated protein 1
UPS	Ubiquitin-proteasome system
VCP	Valosin-containing protein
Vinc	Vincristine
Vps	Vacuolar protein sorting
WB	Western blotting

1 Introduction

1.1 Long range signalling by axonal transport

Various transmembrane receptors enable cells to communicate with the extracellular milieu. Their activation initiates downstream signalling cascades, which regulate vital cellular functions, such as growth, differentiation, proliferation and survival (Uings and Farrow, 2000). This route is shared by many cell types, is highly conserved throughout evolution, and is often mediated by the endocytosis and trafficking of ligand-activated signalling receptors to an appropriate cellular destination, which determines their fate – degradation or recycling (Le Roy and Wrana, 2005). Active intracellular cargo transport is an essential cellular function, and cells rely on it to shuttle proteins, lipids, RNAs and organelles to and from a particular sub-cellular location (Maday et al., 2014). A striking example of this dependence is provided by neurons, which, due to their highly complex function and morphology, face a number of logistical challenges to maintain their homeostasis and accurate communication with their targets (Terenzio et al., 2017). Similarly to other cell types, neurons rely on the molecular motor complexes, kinesins and cytoplasmic dynein, for the fast delivery of essential biological molecules from the soma to growth cones and synapses, and vice versa (Figure 1.1) (Gibbs et al., 2015). In axons, kinesin motors canonically travel to the distal ends, located near the “plus” end of the microtubule (MT^{+}) network, whereas dynein walks back towards the cell body, or the MT “minus” end (MT^{-}). Perturbations in long-range axonal transport contribute to the development of a broad spectrum of neurodegenerative diseases, including amyotrophic lateral sclerosis (ALS), Alzheimer’s disease (AD) and Huntington’s disease (HD) (Schreij et al., 2016).

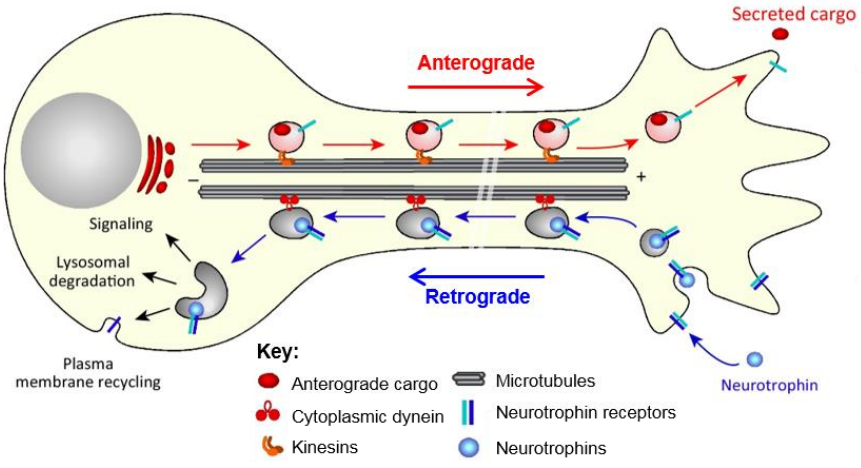

Figure 1.1 Schematic of axonal transport.

Molecular motor machineries mediate directional trafficking in axons. Kinesins travel in anterograde fashion, away from the soma. Dynein enables retrograde transport of cargoes, such as signalling endosomes, from distal ends to the soma. During their transport, these specialized organelles provide a signalling platform for neurotrophin receptors (NTRs), en route to their sorting towards degradation or recycling (adapted from Gibbs et al., 2015).

1.2 Neurotrophin signalling

Retrograde transport of target-derived neurotrophins (NTs) is crucial for the precise development of the nervous system (Ernfors, 2001). These growth factors play an important role in neuronal differentiation, dendritic branching and axonal growth and guidance (Oppenheim, 1989; Ascano et al., 2012; Emdal et al., 2015; Garcia et al., 2009). During development, they are available in restricted amounts, accessible only to a subpopulation of peripheral neurons, thereby selectively supporting their survival (Ernfors, 2001). NTs not only promote neuronal survival and guidance - they also have important non-trophic roles, as they can elicit the activation of the apoptotic pathway, leading to neuronal loss as a part of normal developmental process (Lanser and Fallon, 1984; Oppenheim et al., 1990; Frade et al. 1996; Anastasia et al. 2015). The importance of target-derived NTs for neuronal survival and correct innervation of their targets was uncovered in studies using the *limbless* chick embryo. The removal of the limb bud resulted in increased apoptosis of the spinal neurons – motor neurons in particular – without affecting initial neuronal proliferation and growth (Lanser and Fallon, 1984; Lanser et al., 1986; Lanser and Fallon, 1987; Oppenheim, 1996; Calderó et al., 1998). In addition, NTs contribute to neuronal plasticity, and are therefore crucial for the establishment of higher functions, such as learning, memory and behaviour (Cunha et al., 2010). In adulthood, these growth factors provide trophic support for neurons, thus maintaining they health and survival, while NT withdrawal has been associated with perturbed cognitive function and neurodegeneration (reviewed below) (Mitre et al., 2016).

1.2.1 Components of the neurotrophin cascade

The NT family comprises nerve growth factor (NGF), brain derived neurotrophic factor (BDNF), neurotrophin-3 (NT-3), and NT-4/5. They exist in two forms: as larger precursors (pro-NTs), or as mature NTs lacking the “pro” domain (Roux and Barker, 2002). Proteolytic cleavage of the “pro” domain can be achieved extracellularly or intracellularly by the target tissue, which secretes NTs, such as

the muscle, or by the neurons themselves (Gray and Ellis, 2008). As dimers, NTs bind and activate two distinct classes of receptors, tropomyosin receptor kinase (Trk), which belongs to the receptor tyrosine kinase (RTK) family, and the low-affinity nerve growth factor receptor ($p75^{NTR}$; Figure 1.2) (Chao, 2003). NGF binds preferentially to TrkA, BDNF and NT-4/5 to TrkB, and NT-3 to TrkC, however NT-3 may also bind the other two Trk receptors (Huang and Reichardt, 2001). While all NTs can bind $p75^{NTR}$, mature growth factors have a preference for their cognate Trk receptor, and pro-NTs for $p75^{NTR}$, signalling of which is further enhanced by the Sortilin receptor (Frade et al., 1996; Nykjaer et al., 2004). NT binding promotes Trk receptor dimerization, and autophosphorylation of the tyrosine kinase domain, which leads to receptor autoactivation and phosphorylation of several sites spanning the cytoplasmic domain of these receptors, subsequently activating the downstream signalling cascades (Senger and Campenot, 1997). However, not all Trk receptors support signalling. For instance, different splice variants of TrkB can produce either full length (TrkB-FL) or a truncated form of the receptor (TrkB-T1), lacking the crucial autoactivation kinase domain. Dimerization of TrkB-T1 and TrkB-FL has a dominant-negative effect, thereby blocking the TrkB-FL activity in response to growth factor binding (Stoilov et al., 2002; Haapasalo et al., 2002; Gupta et al., 2013). Interestingly, $p75^{NTR}$ can also heterodimerize with Trk receptors. By influencing a conformational change in Trks, $p75^{NTR}$ increases the specificity, affinity and the level of activation of Trk receptors by mature NTs (Esposito et al., 2001; Nykjaer et al., 2005).

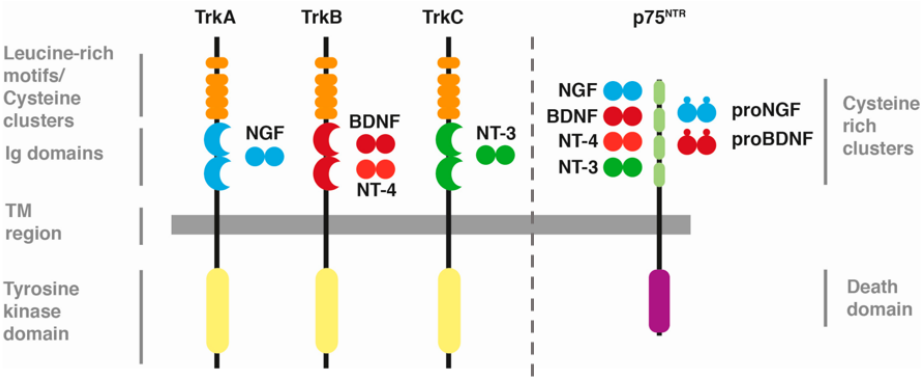

Figure 1.2 NTs bind Trk and $p75^{NTR}$ receptors with high specificity.

The schematic representation of Trk and $p75^{NTR}$ receptors, depicting common structural motifs. Intracellular kinase domain of Trk receptors promotes receptor dimerization and autoactivation in response to NT binding, and several cytoplasmic phosphorylation sites activate different signalling cascades. The death domain of $p75^{NTR}$ activates apoptosis when activated by pro-NTs (adapted from Sánchez-Sánchez and Arévalo, 2017). Ig = immunoglobulin; TM = transmembrane.

1.2.2 Signalling by neurotrophin receptors

Given the complexity of the NT signalling network and the unique, highly compartmentalized morphology of neurons, proper spatial and temporal integration of signalling inputs is of great importance for neuronal homeostasis. Numerous steps, including receptor activation and its endocytosis, retrograde transport, and somatic sorting of activated NT-receptor complexes, contribute to a correct signalling outcome (Barford et al., 2017). Activated NTRs signal from the surface of specialized signalling endosomes, on their journey along the highly polarized microtubule network from the synapses to the soma (Yamashita & Kuruvilla 2016). The main executors of Trk signalling are PI3K/AKT, Ras/ERK and PLCγ pathways, which elicit transcriptional responses promoting neuronal survival, differentiation and growth (Figure 1.3) (Zhang et al. 2000; Kaplan & Miller 2000). These kinases are activated when distinct sites on the cytoplasmic face of Trk receptor are phosphorylated, and these sites are highly conserved between different Trk receptors. For instance, phosphorylation of a juxtamembrane tyrosine (Tyr490-TrkA; Tyr515-TrkB; Tyr516-TrkC) leads to the binding and phosphorylation of Shc, acting upstream of Ras and PI3K cascades, and a phospho-tyrosine located in the tail of Trk receptor (Tyr790-TrkA; Tyr816-TrkB; Tyr820-TrkC) promotes binding and activation of PLCγ (Mitre et al., 2016; Gromnitza et al., 2018). In contrast, pro-NT binding to $p75^{NTR}$ activates the c-Jun N-terminal kinase (JNK) signalling pathway, and therefore promotes apoptosis (Frade et al., 1996; Harrington et al., 2002). Interestingly, the activity of Trks can supress constitutively-active pro-apoptotic $p75^{NTR}$ signalling (Barrett and Bartlett, 2006), as well as $p75^{NTR}$ signalling in response to binding mature growth factors (Bamji et al., 1998), further cementing the importance of Trk receptors in neuronal survival. Trk and $p75^{NTR}$ also interact with the transmembrane scaffolding protein, Kinase D interacting substrate of 220 kDa/ankyrin repeat-rich membrane spanning (Kidins220/ARMS), which is a modulator of neuronal survival, differentiation and plasticity (Higuero et al., 2010; Schmieg et al., 2014). Kidins220 is involved in regulation of neurite outgrowth, by modulating the activities of Rac1 (Neubrand et al., 2010). Importantly, Kidins220 regulates TrkB/BDNF synaptic and retrograde signalling, and may promote the association of Trk receptors with ion channels, as well as synaptic transmission (Scholz-Starke and Cesca, 2016). Moreover, Kidins220 directly contributes to sustained

ERK1/2 activation, specifically in response to NT stimulation (Arévalo et al., 2006a).

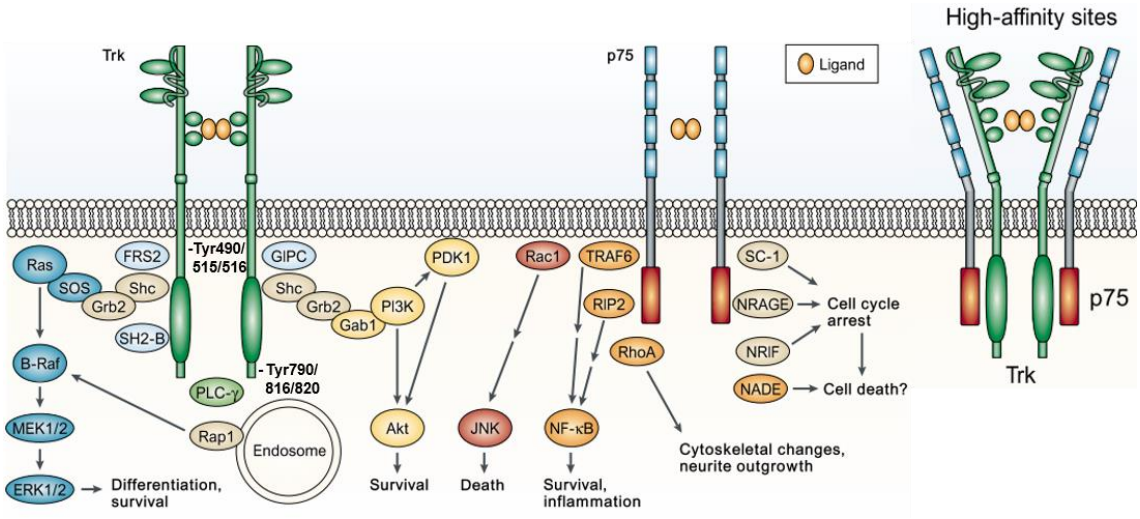

Figure 1.3 The downstream signalling pathways activated by Trks and p75^{NTR}.

Schematic representation of the signalling cascades downstream of NT-activated receptors. While Trk receptors activate PI3K/AKT, Ras/ERK and PLCγ signalling, promoting neuronal survival and differentiation, p75^{NTR} facilitates apoptosis via the JNK pathway. Cross-regulation of p75^{NTR} and Trk activities results in high-specificity interaction of Trks with NTs, and inhibition of p75^{NTR} apoptotic signalling (adapted from Chao, 2003).

1.2.3 Regulation of transport and sorting of NTs and their receptors

Endocytosis and axonal retrograde transport of activated NTRs are key to relay target-derived signals in neurons, necessary for proper neuronal development and survival (Heerssen et al., 2004). This has been demonstrated in compartmentalized cultures, where somato-dendritic application of NTs leads to retraction of axons (Campenot, 1977), strongly suggesting that distal NT retrograde trafficking is essential for signalling supporting neuronal function and morphology, and vice versa (Barford et al., 2017).

Caveolin/clathrin-dependent and -independent endocytosis, as well as micropinocytosis, all contribute to NTR internalization and activation of associated downstream signalling (Howe et al., 2001; Shao et al., 2002; Miaczynska et al., 2004; Zheng et al., 2008). Trk-related signalling effectors act to propagate signalling in response to NTs, and also directly contribute to the early steps of endocytosis and retrograde transport. For instance, PLCγ activity in NGF-stimulated sympathetic neurons is crucial for TrkA endocytosis (Bodmer et al., 2011), while PI3K directly facilitates TrkA retrograde transport (Kuruvilla et

al., 2000). Pharmacological inhibition of these signalling kinases results in reduced endocytosis and somatic accumulation of TrkA upon NGF stimulation. In addition, TrkA itself ensures its own retrograde propagation. In synaptic terminals, TrkA recruits cofilin and Rac1 to facilitate the depolymerization of the surrounding actin mesh, thus promoting axonal entry and retrograde transport of TrkA-containing endosomes (Harrington et al., 2011).

NTR-containing signalling endosomes are retrogradely transported by cytoplasmic dynein complex; and Trk receptors can directly interact with the dynein light chain (DLC) (Yano et al., 2001a). In addition, transport of NTR is regulated by several accessory proteins. For instance, an interaction between unphosphorylated huntingtin (Htt) and the dynein intermediate chain (DIC) stimulates retrograde transport of NTR-signalling endosomes and other cargos (Colin et al., 2008). In addition, Htt promotes association of signalling endosomes with glyceraldehyde 3-phosphate dehydrogenase (GAPDH), which is expected to supply the ATP required for the fast processivity of dynein motor (Zala et al., 2013). These process are perturbed in Huntington's diseases (HD), due to polyglutamine (poly-Q) expansion in Htt, which causes a toxic gain-of-function and formation of misfolded protein aggregates (Caviston and Holzbaur, 2009).

Early endocytic compartments decide the fate of endocytosed NTRs, and the Rab family of GTPases play an important role in this process. For instance, Rab5 is involved in the biogenesis and trafficking of early endosomes (Sönnichsen et al., 2000; Zerial et al., 2012), while conversion to Rab7 promotes maturation of early endosomes to late endosomes, en route to degradation in the lysosomes (Bucci et al., 2000; Rink et al., 2005). However, not all receptors destined for degradation will travel to the soma, as receptor proteolysis may occur locally (Ure and Campenot, 1997; Yamashita and Kuruvilla, 2016). In active, GTP-bound state, these proteins frequently associate with motor adaptor proteins, which ultimately act as Rab effectors, thus promoting the directional transport of a cargo (Akhmanova and Hammer, 2010). NTRs, including TrkA, TrkB and $p75^{NTR}$, prominently co-localize with endosomes marked by Rab5 and Rab7 (Delcroix et al., 2003; Deinhardt et al., 2006). In motor neurons, Rab7-positive endosomes constitute the highly processive transported fraction, while organelles marked by Rab5, although distributed throughout axon, show reduced motility (Deinhardt et al., 2006; Goto-Silva et al., 2019). Therefore, Rab7 can be used to identify

actively transported signalling endosomes. Rab11, on the other hand, associates with endosomes promoting receptor recycling, and marks endosomes travelling in anterograde direction (Ullrich et al., 1996; Green et al., 1997). The association of TrkA and TrkB with Rab11-recycling endosomes is particularly evident when these receptors are endocytosed at the cell soma and the dendrites, rather than the axon. This is especially true during early neurogenesis, when processes such as dendritic branching and axonal growth and guidance are highly reliant on rapid NTR turnover, thereby increasing the sensitivity of neurons to growth factor stimulation (Ascano et al., 2009; Lazo et al., 2013). Although transport of Rab7-positive late endosomes is usually associated with the degradative pathway, these receptors can re-enter the anterograde Rab11 recycling route. While it is not known whether receptors can be retrieved directly from late endosomes labelled with Rab7, it has been suggested that Rab7 late endosomes can transcytose receptors onto the somatic plasma membrane, which allows receptor reinternalization and anterograde synaptic recycling (Barford et al., 2017). Indeed, a recent report characterized this positive-feedback loop for TrkA in sympathetic neurons. Upon NGF binding at the distal ends, TrkA is retrogradely transported to the soma where it undergoes transcytosis onto the somatic plasma membrane. Following the second round of TrkA endocytosis, this receptor is then dephosphorylated by PTP1B to prevent its degradation, transported anterogradely in Rab11-positive endosomes to the distal ends and transcytosed onto synaptic membranes (Yamashita et al., 2017).

Vectorial transport towards the *trans*-Golgi network (TGN) is enabled by the retromer complex, comprising sorting nexins (SNX) and vacuolar protein sorting (Vps) families of proteins (Seaman, 2012), while the endosomal sorting complexes required for transport (ESCRT) direct cargo retrieval for degradation in lysosomes. Sequential polymerization of the ESCRT complexes 0-III on the endosome surface mediates recognition of ubiquitinated cargo, its deubiquitination and packing into intraluminal vesicles (ILVs), a process which downregulates the signalling capacity of transmembrane receptors (Hurley, 2010). The inward membrane sculpting is the basis for the biogenesis of multivesicular bodies (MVBs), contents of which are later degraded in the lysosomes (Shields and Piper, 2011) or secreted as exosomes (Kowal et al., 2014). Internalized NGF and Trk receptors accumulate in MVBs (Claude et al., 1982; Valdez et al., 2005). However, discovery of TrkA within MVBs, as well as

on their surface, suggested that MVBs may also act as specialized retrograde signalling platforms regulating NT-mediated signalling, in addition to their role in cargo turnover, although they are not highly represented in the axon (Sandow et al., 2000; Bronfman et al., 2007). Another interesting hypothesis is that MVBs act as signal-limiting carriers, which specifically relay distally-acquired signals in the soma, or provide means for receptor transcytosis (Villarroel-Campos et al., 2018).

Different isoforms of Trk receptors play a role in receptor fate-decisions. For instance, BDNF-activated TrkB-FL is degraded with much higher kinetics than TrkB-T1, which is preferentially rerouted back to the plasma membrane to recycle BDNF (Li et al., 2009). However, BDNF-activated TrkB-FL can also enter the recycling pathway, and both processes, degradation and recycling of ubiquitinated TrkB-FL, are dependent on the kinase activity of hepatocyte growth factor-regulated tyrosine kinase substrate (HRS), an ESCRT-0 component (Li et al., 2009).

Although the exact mechanism behind receptor fate decisions is not fully understood, NTR ubiquitination appears to play a deciding role in receptor degradation, and may contribute to the amplitude and duration of NTR-mediated signalling. An interesting example was demonstrated in a study investigating the differences in TrkB signalling upon its activation by either BDNF or NT-4 (Proenca et al., 2016). Stimulation with NT-4, rather than BDNF, resulted in more sustained TrkB, AKT and ERK1/2 signalling, which was related directly to the ubiquitination status of TrkB and the endocytic pH. BDNF, rather than NT-4 binding, resulted in much higher ubiquitination and degradation of TrkB, although TrkB phosphorylation levels in response to BDNF and NT-4 binding were comparable, suggesting that ligands directly influence the trafficking and signalling of NTRs (Proenca et al., 2016). The E3 ubiquitin ligase Nedd4-2 promotes TrkA, but not TrkB or TrkC, ubiquitination, retrograde trafficking to late endosomes and degradation in response to NGF stimulation (Arévalo et al., 2006b), while its deficits increase TrkA recycling (Yu et al., 2011). Ubiquitination of TrkA therefore regulates the internalization and signalling of this receptor. This process is also partially mediated by the association of TrkA with $p75^{NTR}$, which promotes the recruitment of E3 ubiquitin ligase TRAF6, and p62, both of which influence the targeting of TrkA for degradation. TRAF6/p62 are potential candidates determining the ubiquitination status of all Trk receptors, as well as of $p75^{NTR}$

(Sanchez-Sanchez and Arevalo, 2017). Furthermore, c-Cbl and Cbl-b ubiquitin ligases, acting on TrkA, promote the downregulation of NGF-elicited signalling. NTRs can be deubiquitinated to facilitate their recycling or degradation, although, as yet, no convincing candidates for this process have been identified (Sanchez-Sanchez and Arevalo, 2017). Overall, posttranslational modifications and the balance between receptor degradation over recycling determine the amplitude and duration of NT-elicited signalling, and therefore have to be tightly regulated.

1.3 BICD1 and NTR sorting

Although many components of the NT pathway have been studied and described extensively over the years, an in-depth understanding of the mechanism contributing to cargo recognition and sorting towards a particular destination is still missing. Recently, the Schiavo's laboratory identified Bicaudal D1 (BICD1) as an important player in this process, using a high-throughput siRNA screen performed in embryonic stem cell-derived motor neurons (ES-MNs) (Terenzio et al., 2014b). More precisely, BICD1 controls the downregulation of BDNF-activated TrkB/$p75^{NTR}$ receptors, while silencing BICD1 expression leads to increased somatic accumulation of internalized NTRs receptors in large amorphous membrane compartments. Because of deficits in lysosomal delivery of NTRs upon BICD1 knockdown, ubiquitinated TrkB receptors enter an alternative, proteasomal degradation route (Terenzio et al., 2014a). Furthermore, lack of BICD1 causes increased plasma membrane recycling of TrkB-T1 receptor, which ultimately affects BDNF-elicited signalling, leading to decreased amplitude of AKT and ERK1/2 activation in response to BDNF stimulation, while at the same time leading to more sustained signalling by these kinases. The correct balance between TrkB-FL/TrkB-T1 is essential for neuronal health, as its misregulation may promote neuronal death due to excitotoxicity (Vidaurre et al., 2012).

In spite of its known function as a dynein adaptor and postulated involvement in retrograde transport in neuronal cell lines (Wanschers et al., 2007), BICD1 does not appear to be essential for the transport of NTR-containing signalling endosomes in motor neurons *per se*, as signalling endosome velocity and frequency were not grossly perturbed in ES-MNs with downregulated BICD1

expression (Terenzio et al., 2014a). In addition, BICD1 was not identified in the mass spectrometry screen characterizing the composition of signalling endosomes purified from ES-MNs (Debaisieux et al., 2016). The same screen and work by others suggest that the Hook family of dynein adaptors are more likely to mediate the retrograde trafficking of NTR-containing signalling endosomes (Debaisieux et al., 2016; Reck-Peterson et al., 2018). Similarly, BICD1 depletion does not affect the morphology and the branching complexity of the neurite network of motor neurons (Terenzio et al., 2014a). Transmission electron microscopy performed on ES-MNs depleted of BICD1 revealed the presence of enlarged endosomes, which accumulated TrkB, $p75^{NTR}$ and the non-pathogenic binding fragment (HcT) of tetanus neurotoxin (TeNT) (Terenzio et al., 2014a). HcT is a useful tool used to monitor the axonal retrograde transport pathway, which shares the retrograde trafficking route of NTRs (Lalli & Schiavo 2002; Deinhardt et al., 2006; Bercsenyi et al., 2014). The morphology of these organelles (Huotari and Helenius, 2011), together with the spatial segregation of HcT, TrkB and $p75^{NTR}$, are highly suggestive of an impairment of NTR degradation due to BICD1 depletion (Terenzio et al., 2014a).

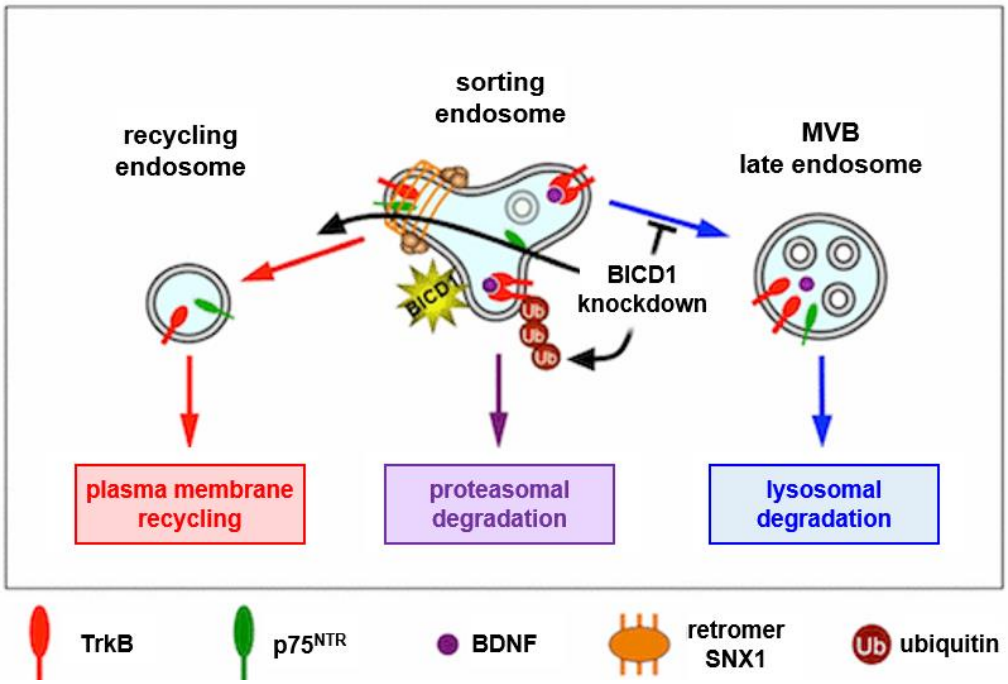

Figure 1.4 Proposed role of BICD1 in somatic NTR sorting.

BICD1 facilitates the delivery of activated NTR to multivesicular bodies for their later degradation in the lysosome. BICD1 knockdown results in the plasma membrane recycling of these receptors and rerouting towards proteasomal degradation, which ultimately affects NT signalling and leads to changes in receptor composition at the plasma membrane (adapted from Terenzio et al., 2014a).

The role of BICD1 in NTR turnover and signalling might be particularly important in the early developmental stages of the nervous system. In fact, BICD1 expression in the mouse embryo is highest in the spinal cord and the brain up to embryonic day 12.5 (E12.5), after which it rapidly decreases and is only retained in dorsal root ganglia (DRG) and upregulated in non-neuronal tissues, such as skeletal muscles and heart ventricles (Terenzio et al., 2014a).

1.3.1 BICD adaptors participate in various trafficking events

The BICD family of dynein adaptors is conserved amongst species. Mammals have two orthologues of the *Drosophila* BicD: BICD1 and BICD2 (Baens and Marynen, 1997), and two related but less conserved proteins, BICDR1 and BICDR2 (Figure 1.5B,C) (Schlager et al., 2010). Although they do not contain structural domains, their main feature are the α-helical coiled coils (CCs) dispersed throughout protein, referred to as N-terminal CC1, middle CC2, and C-terminal CC3 (Hoogenraad and Akhmanova, 2016). BICD proteins form axially-asymmetric parallel homodimers (Terawaki et al., 2015). Flexible linker regions between their CCs allow their collapse into an autoinhibited state in the absence of ligands. This could act as an autoregulatory mechanism, preventing its otherwise high-affinity interaction with dynein in the absence of cargo. Canonically, cargo binding to CC3 releases this autoinhibition, thus promoting dynein recruitment by CC1 and a proximal portion of CC2 (Figure 1.5A). Binding of BICDs to dynein not only promotes the processivity of this motor (Hoogenraad et al., 2003), but it also increases its force against the activated kinesin, which can be present on the same cargo (Belyy et al., 2016).

First characterized in *Drosophila melanogaster*, BicD was identified as one of the determinants of embryo polarity along the anterior-posterior axis; its deficit led to development of a double abdomen phenotype (Mohler & Wieschaus 1986, Steward & Nüsslein-Volhard 1986). BicD participates in different stages of oogenesis (Suter et al., 1989); it also mediates transport of mRNAs and positioning of the oocyte and the photoreceptor nuclei (Swan et al., 1999; Bullock and Ish-Horowicz, 2001).

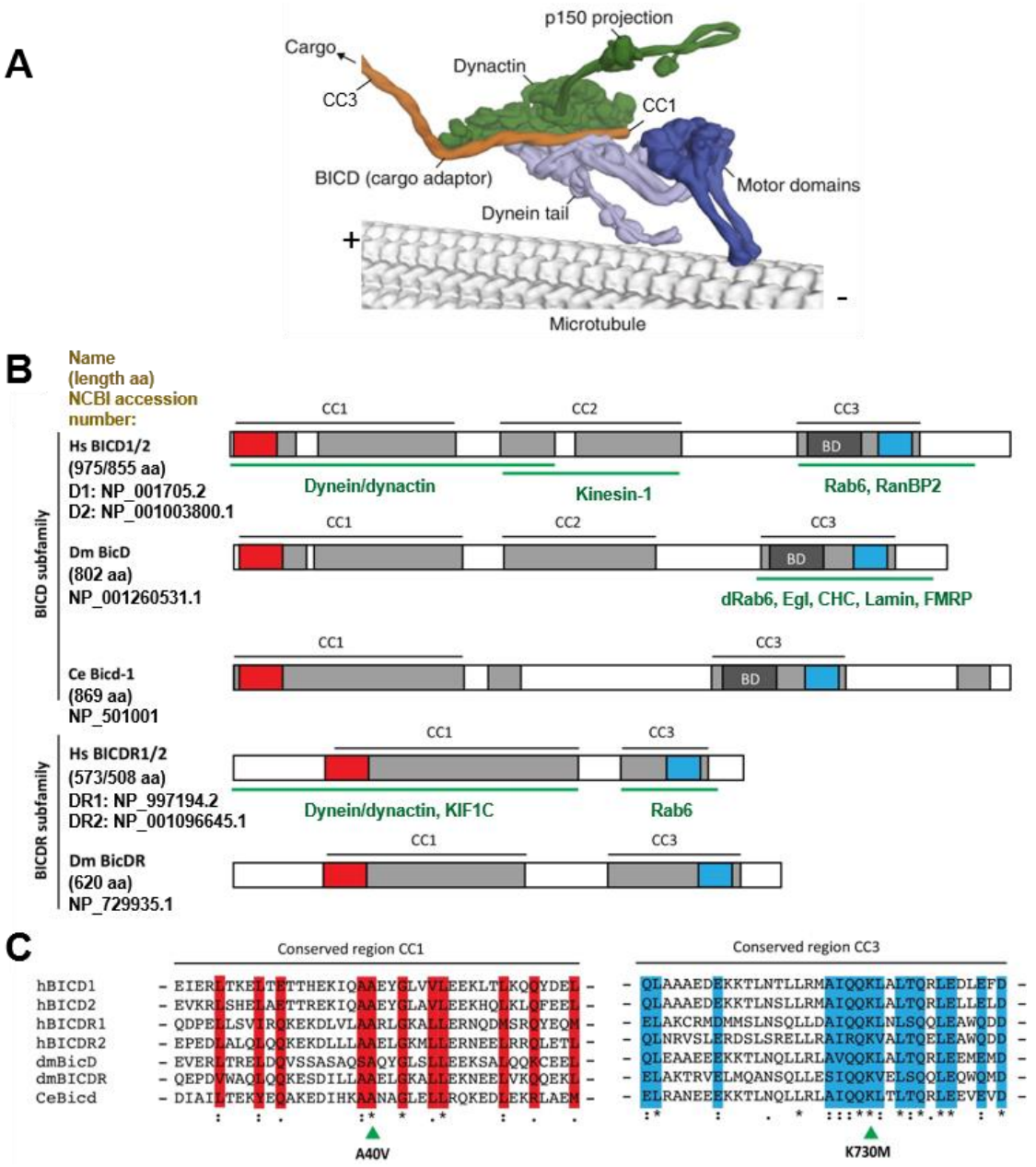

Figure 1.5 Structure of BICD family members.

A) Model of dynein/dynactin motor in complex with BICD. Binding of cargo to BICD is mediated by its C-terminus, which facilitates recruitment and binding of the motor complex by the N-terminal end of BICD. BICD N-terminus runs parallel to dynactin and sits in the groove of dynein tail. Binding of all three components results in a conformational change of the dynein motor domain and the activation of processive movement along microtubules (adapted from Carter et al. 2016). B) Schematic representation of the domain architecture of BICD proteins. BICDs contain characteristic coiled coil (CC) domains (grey boxes). Regions conserved between different species, contained within CC1 and CC3, are marked by red and blue boxes, respectively. Known binding partners and regions they interact with are below in green. C) Alignment of CC1 (red) and CC3 (blue) conserved sequences. Depicted A40V mutation (BICD2, BICDR1) reduces association with dynein; K730M mutation interferes with cargo binding (adapted from Hoogenraad & Akhmanova 2016). AA = amino acid; Ce = *Caenorhabditis elegans*; CHC = clathrin heavy chain; Dm = *Drosophila melanogaster*; Egl = egalitarian; FMRP = Fragile X mental retardation protein; h = human; KIF1C = Kinesin-like protein; RanBP2 = Ran binding protein 2.

In mammalian neurons and mitotic cells, BICD1/2 can be found enriched at MT^- end, localized in the perinuclear region (Hoogenraad et al., 2001, Fumoto et al., 2006). These adaptors are involved in regulation of cytoskeletal function and intracellular transport (Figure 1.6A). Indeed, BICD1/2 interact with guanosine-5'-triphosphate (GTP)-bound Rab6 GTPase present on the TGN-derived vesicles, thus facilitating their retrograde transport to the ER, in the coat complex coatomer protein I (COP-I)-independent pathway (Matanis et al., 2002). BICD1 also mediates the retrograde transport of Rab6B-positive vesicles in neurites of human neuroblastoma cells SK-N-SH (Wanschers et al., 2007). By regulating the secretion of Rab6-exocytic vesicles, BICD proteins participate in neurogenesis fine-tuning, during which time they can also associate with kinesins (Schlager et al., 2010). BICDR1 overexpression supresses neurite outgrowth, by simultaneously accumulating dynein and a weak kinesin motor, Kif1C, on Rab6-positive vesicles in the pericentrosomal region, thus inhibiting their anterograde transport (Schlager et al., 2010). When BICDR1 expression ceases, BICD2 promotes the anterograde transport of secretory Rab6 vesicles, thus restoring neurite outgrowth (Grigoriev et al., 2007). Interestingly, activation of dynein by BICDR1 increases its force and velocity to a much higher extent than BICD2 binding, although both of these adaptors interact with dynein via the same conserved N-terminal region (Schlager et al., 2014).

BICD2 plays an important role during mitosis (Splinter et al., 2010). In the G2 stage of the cell cycle, this dynein adaptor associates with the large scaffold nucleoporin protein, RAN-binding protein 2 (RanBP2), which facilitates the recruitment of dynein as well as kinesin-1 (KIF5A). The tug-of-war between these motors along microtubule tracks then promotes accurate positioning of the nucleus prior to mitosis (Figure 1.6B). Because binding of Rab6 and RanBP2 to BICD2 is mutually exclusive, it suggests that dynein adaptors mediate specialized events important for cell reorganization at different stages of development and cell cycle. In fact, glycogen synthase kinase-3β (GSK-3β) interaction with BICD1 is necessary for microtubule anchorage at the centrosomes, suggesting that BICD1 directly participates in organization of the cytoskeletal network (Fumoto et al., 2006). In addition, these adaptors participate in a variety of cellular processes, including the integrated stress response (ISR; reviewed below; Loschi et al., 2009).

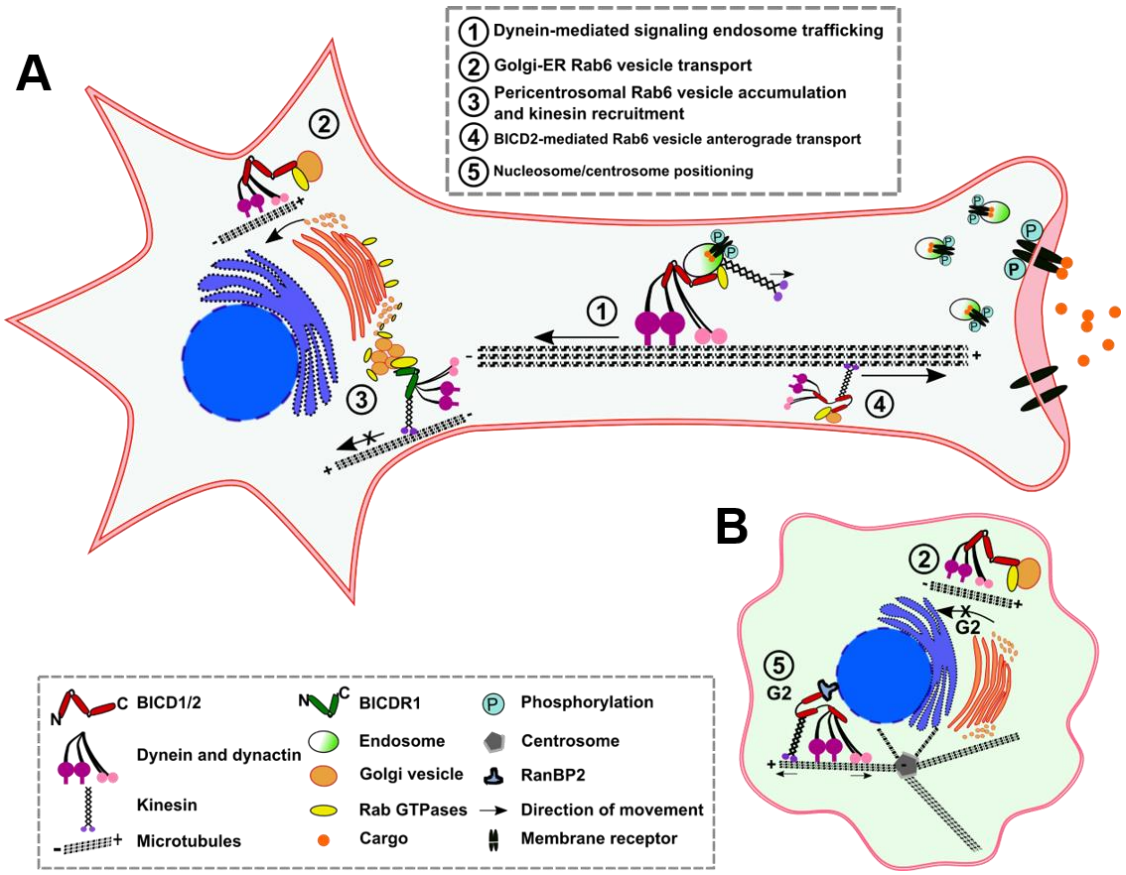

Figure 1.6 Diverse functions of BICD proteins in mammalian cells.

BICDs participate in diverse trafficking events in neurons (A) and mitotic cells (B). In neurons (A), they mediate retrograde transport (1), and shuttling of cargos between the Golgi apparatus and the ER in a COP-I-independent pathway (2). Additionally, BICDR1 inhibits neurite outgrowth by blocking the action of kinesin (3), which is restored when BICDR1 expression decreases and BICD2 replaces it on Rab6 exocytic vesicles, thus facilitating their anterograde trafficking (4). In mitotic cells (B), by binding to the nuclear pore complex protein RanBP2, as well as dynein and kinesin, BICD2 helps to position the nucleus and centrosome in the G2 stage of the cell cycle before mitosis (5). During that time, binding to Rab6 vesicles by BICD2 is abolished (2) (adapted from Budzinska et al., 2017).

1.3.2 Search for novel BICD1-interacting candidates

To further our understanding of the molecular mechanism by which BICD1 directs the turnover of NTRs (Terenzio et al., 2014a), a mass spectrometry proteomic screen was performed to identify novel BICD1-binding proteins in N2A cells stably expressing FLAG-tagged TrkB (N2A-FLAG-TrkB) and in ES-MNs (Appendix 1; Golding and Schiavo, unpublished). Protein tyrosine phosphatase, non-receptor type 23 (PTPN23; or his domain-containing protein tyrosine phosphatase, HD-PTP) was one of the most enriched and interesting hits, chosen for this study.

At the time of writing this thesis, the function of PTPN23 in the mammalian nervous system had not been explored in great detail (Gingras et al., 2009a). However, the association of PTPN23 and BICD1 with the neurotrophin pathway is supported by findings from other studies. PTPN23 was identified in the proteomic screen characterizing the composition of signalling endosomes, purified from ES-MNs after 10, 30 and 60 min of incubation with HcT conjugated to monocrystalline iron oxide nanoparticles (MIONs) (Debaisieux et al., 2016). Interestingly, the association of PTPN23 with signalling endosomes increases with the time (Debaisieux et al., 2016), suggesting that PTPN23 may play a role in NTR trafficking and/or cargo sorting, when signalling endosomes approach the soma compartment. In addition, both BICD1 and PTPN23 were identified as potential binding partners of TrkA (Emdal et al., 2015). Furthermore, a large proteomic screen identifying a novel protein interactome found a possible association between Kidins220 and PTPN23 (Hein et al., 2015).

1.3.3 PTPN23 regulates the sorting of transmembrane receptors in non-neuronal cells

PTPN23 has a well-established function in sorting of transmembrane receptors into MVBs in non-neuronal cells. This non-canonical member of the ESCRT family is essential for the downregulation of ligand-activated epidermal growth factor receptor (EGFR) (Doyotte et al., 2008). More importantly, the effect of PTPN23 knockdown on the endocytic sorting of EGFR in HeLa cells recapitulates the increased NTR accumulation in aberrant early endosomes, and increased plasma membrane receptor recycling observed after BICD1 downregulation in ES-MNs (Doyotte et al., 2008; Terenzio et al., 2014a). Similarly to the increased TrkB ubiquitination after BICD1 knockdown, silencing of PTPN23 results in accumulation of ubiquitinated proteins on swollen early endosomes. Importantly, PTPN23 is essential for the biogenesis of MVBs, and its silencing significantly increases the sizes of late endosomes and lysosomes (Doyotte et al., 2008), suggesting that loss of PTPN23 significantly perturbs endocytic flow in cells.

Other studies reported similar observations after PTPN23 knockdown. PTPN23 mediates the downregulation of diverse classes of receptors, including platelet-derived growth factor receptor (PDGFR) (Ma et al., 2015), α5β1 integrin (Kharitidi et al., 2015), major histocompatibility complex (MHC) class I (Parkinson et al.,

2015) and transforming growth factor β/bone morphogenetic protein (TGFβ/BMP) receptors (TGFβ/BMP) (Gahloth et al., 2017b).

1.3.4 PTPN23 is an ESCRT module

PTPN23 belongs to the “Bro domain”-containing family of proteins, which includes ALG-2-interacting protein X (ALIX) and yeast Bro1 (Figure 1.7). These “Bro” proteins are accessory factors for the ESCRT machinery, and participate in membrane sculpting and scission events, such as cytokinesis, viral budding and biogenesis of intraluminal vesicles (ILV) within MVBs (Bissig and Gruenberg, 2014; Doyotte et al., 2008). However, the function of PTPN23, unlike other Bro proteins, appears to be restricted to supporting ESCRT function in cargo sorting within the endocytic pathway (Doyotte et al., 2008; Parkinson et al., 2015; Gahloth et al., 2016).

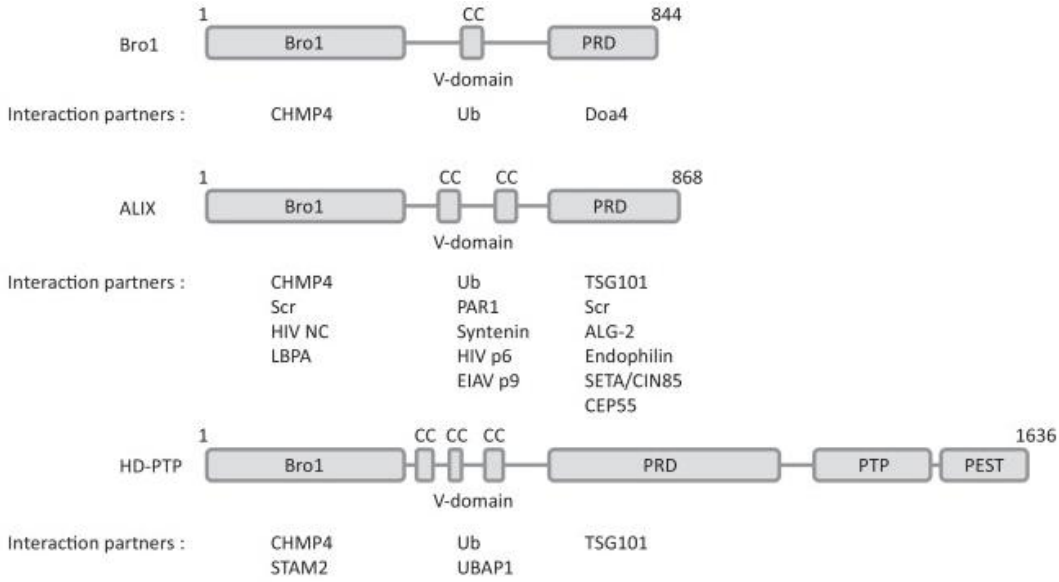

Figure 1.7 The Bro family of the ESCRT-interacting proteins.

A schematic depicting the structural architecture and common domains shared between the Bro proteins, as well as their interaction partners (adapter from Bissig and Gruenberg, 2014).

PTPN23 is a predominantly cytoplasmic protein of approximately 185 kDa, composed of five distinct domains: Bro1, V/CC, PRD/HD, PTP and PEST (Figure 1.7). The N-terminal Bro1, the coiled coil V-shaped domain (V/CC) and proline-rich domain (PRD) are homologous to yeast Bro1, and mammalian ALIX (Kim et al., 2005; Sette et al. 2011; Fisher et al. 2007). Together, the Bro1 and V/CC domains are the minimal functional unit of PTPN23 supporting its function in

receptor sorting and binding to the core ESCRT-complex proteins, such as STAM2 and CHMP4b (Doyotte et al. 2008; Lee et al. 2016). The central portion of PTPN23 is occupied by PRD, with multiple SRC Homology 3 (SH3) domain-binding motifs (Toyooka et al., 2000; Bissig and Gruenberg, 2014). This region promotes the recruitment of the ESCRT-I protein – Tumor susceptibility gene 101 (TSG101), the brain-specific endophilin A1, involved in synaptic vesicle endocytosis and receptor trafficking (Ichioka et al., 2007), as well as the EGFR adaptor protein Grb2 (Tanase, 2010). The presence of a proteolytic degradation-targeting motif PEST (proline-, glutamic acid-, serine- and threonine-rich) at the C-terminus, suggests that PTPN23 is a short-lived protein (Rogers et al., 1986).

The polymerization of ESCRT-0/I complexes on early endosomes determines the early steps of cargo recognition and recruitment for their degradation in lysosomes (Frankel and Audhya, 2018). In this pathway, ubiquitin is a key posttranslational modification that labels a cargo it for targeting to MVBs. Several ESCRT modules possess ubiquitin binding domains, which facilitate the formation of a specialized domain on early endosome membranes (Tabernero and Woodman, 2018). In the process of cargo sorting, PTPN23 acts as a molecular ESCRT “switch”, enabling the sequential recruitment of different ESCRT complexes. First, PTPN23 interacts with ESCRT-0 component, STAM2, via a highly conserved binding pocket within the Bro1 domain and a binding motif on the PRD domain (Ali et al., 2013), as well as ESCRT-I member TSG101 (Stefani et al., 2011). STAM2 and PTPN23 also engage USP8 to promote ubiquitin recycling, which is necessary for receptor downregulation (Ali et al., 2013). The key component of the ESCRT-III machinery mediating formation of MVBs is CHMP4b, which, via its polymerization on the endosome membrane, promotes membrane sculpting and biogenesis of ILVs (Hurley, 2010). CHMP4b competes with STAM2 for interaction with the conserved binding region within the PTPN23 Bro1 domain, leading to the ESCRT-0/I release and capture of deubiquitinated cargoes within MVBs (Figure 1.8) (Gahloth et al., 2017a). For all these reasons, PTPN23 is a promising candidate as a BICD1 interacting protein that has a role in NTR sorting.

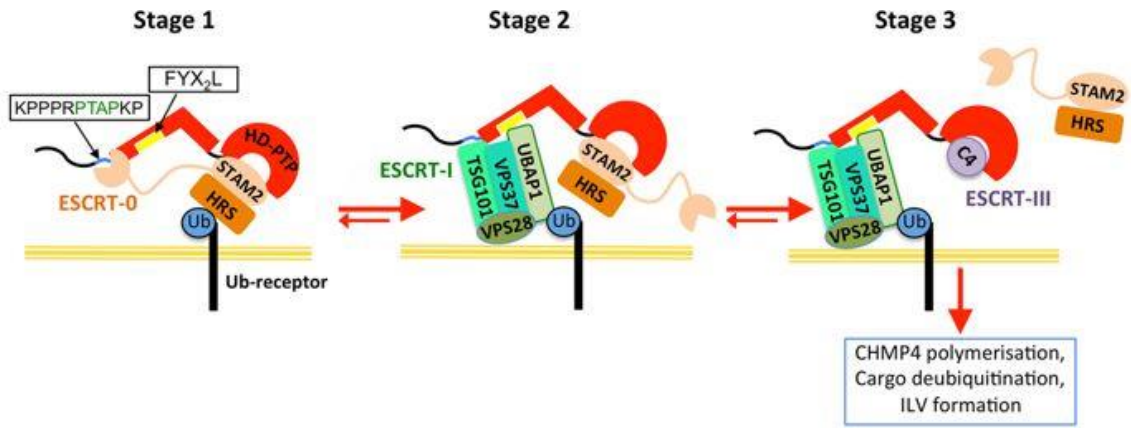

Figure 1.8 The mechanism of ESCRT recruitment by PTPN23.

The schematic depicting the steps of cargo recognition and engagement of different ESCRT modules by PTPN23 (adapted from Gahloth et al., 2017a).

1.3.4.1 PTPN23 is a non-canonical phosphatase

What makes PTPN23 unique and unlike other canonical phosphatases, is its catalytic domain PTP. Different groups have produced contradictory results regarding its phosphatase activity, with some describing it as functional (Lin et al. 2011; Castiglioni et al. 2007), and others as non-functional (Gingras et al., 2009b). The main reason for this discrepancy is the presence of a cysteine residue in the highly-conserved active site. However, pivotal studies by Toyooka et al. (2000) and Gingras et al. (2009b) argue that its catalytic activity is impaired due to a conversion of alanine to serine at the position 1394, downstream of the catalytic cysteine (VH**C**SAG to VH**C**SSG). Interestingly, a serine to alanine mutation restores the phosphatase function of PTPN23. In spite of the lack of catalytic activity of endogenous PTPN23, it plays an important regulatory role by binding to tyrosine-phosphorylated proteins, such as survival motor neuron (SMN) complex, thus maintaining their high phosphorylation state that is necessary to support their function (Lin et al., 2011; Husedzinovic et al., 2014).

1.3.5 PTPN23 is deleted in cancers

The gene encoding *PTPN23* is localized in the tumor-suppressor gene cluster on chromosome 3p21.3, which, in humans, is often deleted in cancer (Toyooka et al., 2000; Ji et al. 2005). Loss of PTPN23 is therefore associated with tumorigenesis and poor prognosis in cancer, in humans and in animal models, which is likely to be correlated to perturbed sorting of mitogenic receptors (Manteghi et al., 2016; Gingras et al., 2017; Zhang et al., 2017). Loss of PTPN23

may also directly contribute to metastasis and angiogenesis, as PTPN23 controls cell migration by regulating the phosphorylation state of focal adhesion kinase (FAK) and the plasma membrane levels of E-cadherin (Castiglioni et al., 2007; Lin et al., 2011). Additionally, *PTPN23* was identified as an “essential” gene in a synthetic lethality screen (Blomen et al., 2015). Indeed, PTPN23 is necessary for embryo development, as its homozygous deletion in a mouse is lethal at E9.5 (Gingras et al., 2009a).

1.3.6 PTPN23 is necessary for the development of the nervous system

While PTPN23 has been indicated as one of the key players regulating the lysosomal sorting of various transmembrane receptors (Doyotte et al., 2008; Ali et al., 2013; Ma et al., 2015), its function in the mammalian nervous system, especially in the context of NT signalling, has not been investigated. However, findings from studies exploring the function of the *Drosophila* orthologue of PTPN23, myopic, suggest that its function in the nervous system may extend beyond receptor sorting. Myopic plays a role in development of the *Drosophila* nervous system by participating in processes such as synaptic pruning (Loncle et al., 2015) and FMRF neuropeptide gene transcription, related to cell-fate specification (Bivik et al., 2015). In the adult fly, myopic regulates activity-dependent synaptic neuropeptide (insulin-like peptide 2; Dilp-2) release from dense core vesicles at the neuromuscular junction (Bulgari et al., 2018), implying that it contributes to synaptic transmission. Functional PTPN23 is also essential for the development of the mammalian nervous system, as recently identified mutations in *PTPN23* were linked with developmental epileptic encephalopathy with hypomyelination, brain atrophy and global developmental delay in humans (Alazami et al., 2015; Sowada et al., 2017; Smigiel et al., 2018). In animal models, PTPN23 is highly expressed during development, in particular in the nervous tissue. In adulthood it can be found in the epithelial lining of many organs, as well as in the brain and cerebellum (Gingras et al., 2009a). These findings suggest that PTPN23 plays an important role in the development and maintenance of the adult nervous system; therefore, its role in trafficking, especially of NTRs, should be investigated.

1.4 Integrated stress response and RNA granules

Exposure to environmental stressors poses a threat to cellular health and survival. Eukaryotes have a sophisticated, and highly conserved, protective mechanism, termed the integrated stress response (ISR), activation of which results in changes to housekeeping functions. The major feature of ISR is the silencing of translational machinery (Kimball et al., 2003), and formation of large (0.2-2 μm) cytoplasmic RNA-protein depots, called stress granules (SGs) (Kedersha et al., 1999; Souquere et al., 2009; Fay and Anderson, 2018). In literature, SGs are often described as dynamic “membrane-less organelles”, ribonucleoparticle (RNP) foci or RNA granules. As these names suggest, they lack a surrounding membrane, and they comprise a unique species of translationally-repressed mRNAs (Anderson and Kedersha, 2008; Mollet et al., 2008; Khong et al., 2017). In addition, SGs contain several species of RNA-binding proteins (RBPs) involved in mRNA metabolism (Kedersha et al., 1999; Hua and Zhou, 2004; McDonald et al., 2011; Aulas et al., 2012), and elements of stalled translation initiation complexes (Kedersha et al., 2002; Kimball et al., 2003; Mokos et al., 2009), which distinguishes them from other types of RNA granules. Approximately 50% of identified SG-related proteins have functions not directly related to mRNA dynamics, including metabolic enzymes (Protter and Parker, 2016), activators of senescence (Omer et al., 2018), and pro-apoptotic molecules (Kim et al., 2005b; Arimoto et al., 2008; Tsai and Wei, 2010). It has been demonstrated in numerous studies, using fluorescence recovery after photobleaching (FRAP), that SG constituents, such as mRNAs and proteins, are highly dynamic and shuttle in-and-out of SGs in an ATP-dependent process (Kedersha et al., 2005; Mollet et al., 2008; Gareau et al., 2013; Jain et al., 2016; Van Treeck and Parker, 2019).

Tight regulation of SG dynamics is essential, as their hypo- and hyper-regulation has been linked to neurodegeneration and cancer (Mahboubi and Stochaj, 2017), reviewed in more details below. At present, the exact mechanism of SG assembly and clearance is still not fully understood. Further work is necessary to decipher the principles of SG dynamics, which may facilitate the development of new therapeutics.

1.4.1 Mechanism of ISR and SG assembly

1.4.1.1 Induction of a stress response

In mammalian cells, four kinases mediate stress sensing and activation of ISR (Figure 1.9): 1) heme-regulated initiation factor 2α kinase (HRI), activated by heme deprivation and redox imbalance, and a commonly-used oxidative stress inducer, sodium arsenite ($NaAsO_2$) (McEwen et al., 2005); 2) PKR-like endoplasmic reticulum (ER) kinase (PERK), activated by ER stress (Harding et al., 1999; Harding et al., 2000); 3) protein kinase RNA-activated (PKR), activated by UV radiation, viral infections and heat shock (Srivastava et al., 1998); 4) general control nonderepressible 2 (GCN2), activated by amino acid starvation and UV radiation (McEwen et al., 2005; Aulas et al., 2017). Activation of these kinases leads to phosphorylation of a common downstream target, eukaryotic initiation factor 2α (eIF2α) on Ser51 (Kedersha et al., 1999), which in turn reduces the availability of the eIF2-GTP-$tRNA_i^{Met}$ ternary complex, necessary for translation initiation (Figure 1.9). As a result, recruitment of translation-initiating 60S ribosomal unit to 48S preinitiation complex is blocked, ultimately leading to polysome disassembly and translational stall (Kedersha et al., 2002; Aulas et al., 2017). Translational inhibition, however, is not immediate, as it does not affect ribosomes already engaged in elongation (Shenton et al., 2006). The phosphorylation of eIF2α leads to nucleation and formation of canonical, *bona fide*, SGs, a process which is reversible in cells exposed to sublethal doses of stress (Kedersha et al., 1999). In addition, non-canonical SGs can be induced independently of eIF2α phosphorylation, by molecules such as hydrogen peroxide, which interfere with activities of eIF4A/eIF4E/eIF4G translation initiation factors (Emara et al., 2012; Panas et al., 2016).

SGs are easily identifiable by immunocytochemistry and microscopy. Widely-used markers include Ras GTPase-activating protein-binding protein (G3BP), T-cell-restricted intracellular antigen-1 (TIA-1) and polyadenylate-binding protein 1 (PABP-1) (Van Treeck and Parker, 2019). However, in certain conditions SGs may contain distinct signatures, directly related to the type of stress, cell or subcellular localization (Kedersha et al., 1999; Aulas et al., 2017; Markmiller et al., 2018). It is therefore recommended to verify their background using at least two different markers. For instance, UV-induced SGs, although positive for G3BP, lack canonical translation initiation factors and are largely deficient in

polyadenylated (poly-A) mRNA (Aulas et al., 2017). As components of SGs are in dynamic equilibrium with translating polysomes, agents modifying polysome stability can be used to validate *bona fide* SGs. Disrupting polysome stability by puromycin facilitates SG assembly in the presence of stress, while polysome stabilizing, or “freezing”, drugs, such as emetine or cycloheximide, lead to SG disassembly (Kedersha et al., 2000; Kedersha and Anderson, 2007).

Overall, stress leads to reduced translation of approximately 25% of total mRNA, with only 10% of mRNA localizing to SGs – many of which encode housekeeping proteins, such as glyceraldehyde 3-phosphate dehydrogenase (GAPDH) or β-actin. Individual transcripts are not equally recruited to SGs either, and preference is given to longer transcripts that translate less-efficiently (Anderson and Kedersha, 2008; Khong et al., 2017).

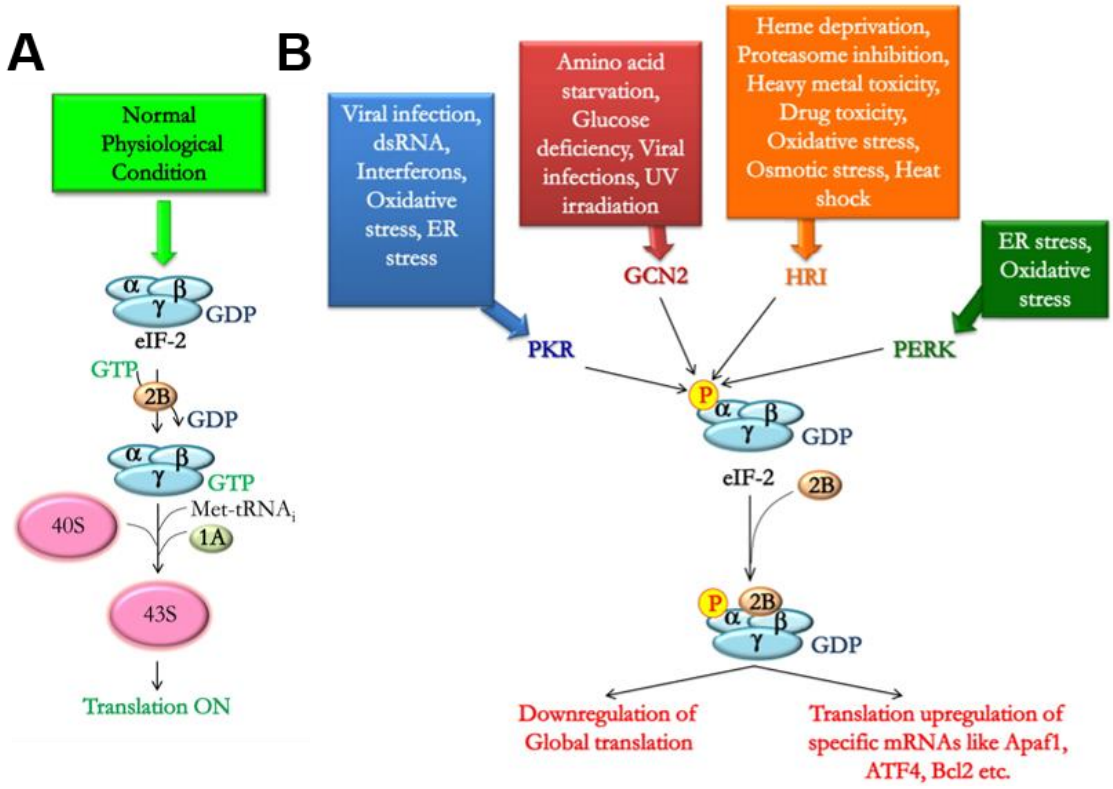

Figure 1.9 Regulation of translation by eIF2α and its kinases.

Schematic of translation regulation by the eIF2 complex under physiological (A) and stressed (B) conditions. Activation of a stress-sensing kinase, PKR, GCN2, HRI or PERK, leads to phosphorylation of eIF2α. This in turn blocks the formation of the ternary translation preinitiation complex, leading to global inhibition of protein synthesis. During stress recovery, translation is slowly restored (adapted from Joshi et al., 2013).

1.4.1.2 SG nucleation

In recent years, due to evidence of perturbed SG dynamics and accumulation of SG-like aggregates in neurodegeneration (reviewed below), a lot of attention has been dedicated to elucidating the mechanism of SG formation and disassembly. Here, the principles of canonical, p-eIF2α-dependent SGs formation, and two general models of SG assembly favoured in the literature, are reviewed.

1.4.1.2.1 The LLPS theory

Phosphorylation of eIF2α and polysome disassembly lead to increased local concentration of stalled pre-initiation complexes (Kedersha et al., 2002) and RBPs, such as G3BP (Tourrière et al., 2003) and TIA-1 (Gilks et al., 2004), which promote the nucleation of SGs. Several SG-associated RBPs, such as TIA-1, fused in sarcoma (FUS), TAR DNA-binding protein 43 (TDP-43) or survival motor neuron-1 (SMN1), are native to the nucleus, where they mediate RNA processing. These proteins translocate to the cytoplasm upon induction of stress, suggesting that stress downregulates their nuclear functions (Buchan et al., 2013). SG nucleation is driven by weak electrostatic and hydrophobic interactions of protein-protein (Jain et al., 2016), protein-mRNA (Gilks et al., 2004), and mRNA-mRNA (Van Treeck et al., 2018) components. RBPs, including those related to SGs, contain intrinsically disordered regions (IDRs) abundant in low complexity domains (LCDs) (Kedersha et al., 2013), characterized by low amino acid diversity and high net charges, which favour homotypic interactions and association with RNAs (Uversky, 2017). Defining these properties of RBPs, and studying their behaviour *in vitro*, led to a hypothesis that SGs may form by liquid-liquid phase separation (LLPS), favourable under stress conditions (Brangwynne et al., 2009; Perez-Pepe et al., 2018). *In vitro* studies had helped to define many characteristics of normal and aberrant SGs. One such example was the work characterizing LLPS of FUS, which demonstrated that frontotemporal dementia (FTD)-related mutant FUS favoured gel, rather than liquid, transition, contributing to impaired function of SGs (Qamar et al., 2018). In addition, Kato et al. (2012) determined that LCDs within RBPs directly promote phase separation. Authors demonstrated that LCD-containing RBPs can be specifically precipitated from lysates in the absence of stress using biotinylated isoxazole (b-isox), and proteins identified using this method overlapped with the SG proteome (Kato et al., 2012).

1.4.1.2.2 Biphasic structure of SGs

Although *in vitro* work provided a lot of insights into the biophysical properties and behaviour of SG-related proteins, an outstanding question regarding the role of LLPS in SG formation in mammalian cells remained. Recently, it came to light that mature SGs are not uniform and they possess discreet, biphasic substructures, defined as the core and the shell. SG cores (approximately 0.2 μm in diameter) are denser and less dynamic than the shell, and they are resistant to lysis conditions, suggesting that complex protein-protein interactions are the basis for the SG core stability. In contrast, components of the SG shell, which behave like a “liquid”, are held by weak interactions, which allow them to dynamically exchange their material with polysomes (Figure 1.10C). This property, however, suggests that components of the SG shell dissociate upon cell lysis. Although the LLPS-like behaviour is the major obstacle to identify the SG proteome, recent advances in purification of SG cores enabled the identification of several new SG-related candidate proteins, many of which await validation (Jain et al., 2016; Wheeler et al., 2017). There has also been progress in defining SG transcriptome (Khong et al., 2017; Khong et al., 2018a).

1.4.1.2.3 Two models of SG assembly – the shell or core first?

To resolve the SG “core vs. shell” assembly conundrum, Wheeler et al. (2016) presented an elegant study, converging on the works conducted *in vitro* and *in vivo*. Their leading hypotheses were based on two different models of SG formation (Figure 1.10A).

The first model, based on findings from *in vitro* studies, proposes the initial LLPS-mediated assembly of loosely-associated shell-like structure, which increases in size over time. Continuous recruitment of LCD-containing substrates leads to their deposition, and subsequent formation of stable cores. These assemblies should grow and mature over time into large SGs, in a process mediated by active, microtubule-based transport (Figure 1.10A).

The second model favours formation of stable cores first, which, once developed, do not increase in size. These cores then act as nucleation sites for dynamic, LLPS-mediated, shell development, subsequently leading to the assembly of larger deposits, promoted by LLPS and active transport (Figure 1.10A). Following the second model, mature SGs should contain multiple cores surrounded by a

vast shell, and these assemblies would be of irregular shape – a point of argument for a sole LLPS involvement in this process, which favours structures of more uniform shape. Through their work, Wheeler et al. were in favour of the second model. The authors demonstrated basic principles of mammalian SG assembly using a combination of approaches, but primarily by correlating their microscopy and SG core purification findings, thereby contradicting many claims of solely *in vitro*-based studies (Figure 1.10B) (Wheeler et al., 2016). Moreover, the same group demonstrated that ATP drives SG dynamics: their formation and clearance, fusion and fission, transport, and exchange of material between its layers (Figure 1.10C), further strengthening their point against solely LLPS-driven SG dynamics, and/or as means of force counterbalancing LLPS (Jain et al., 2016).

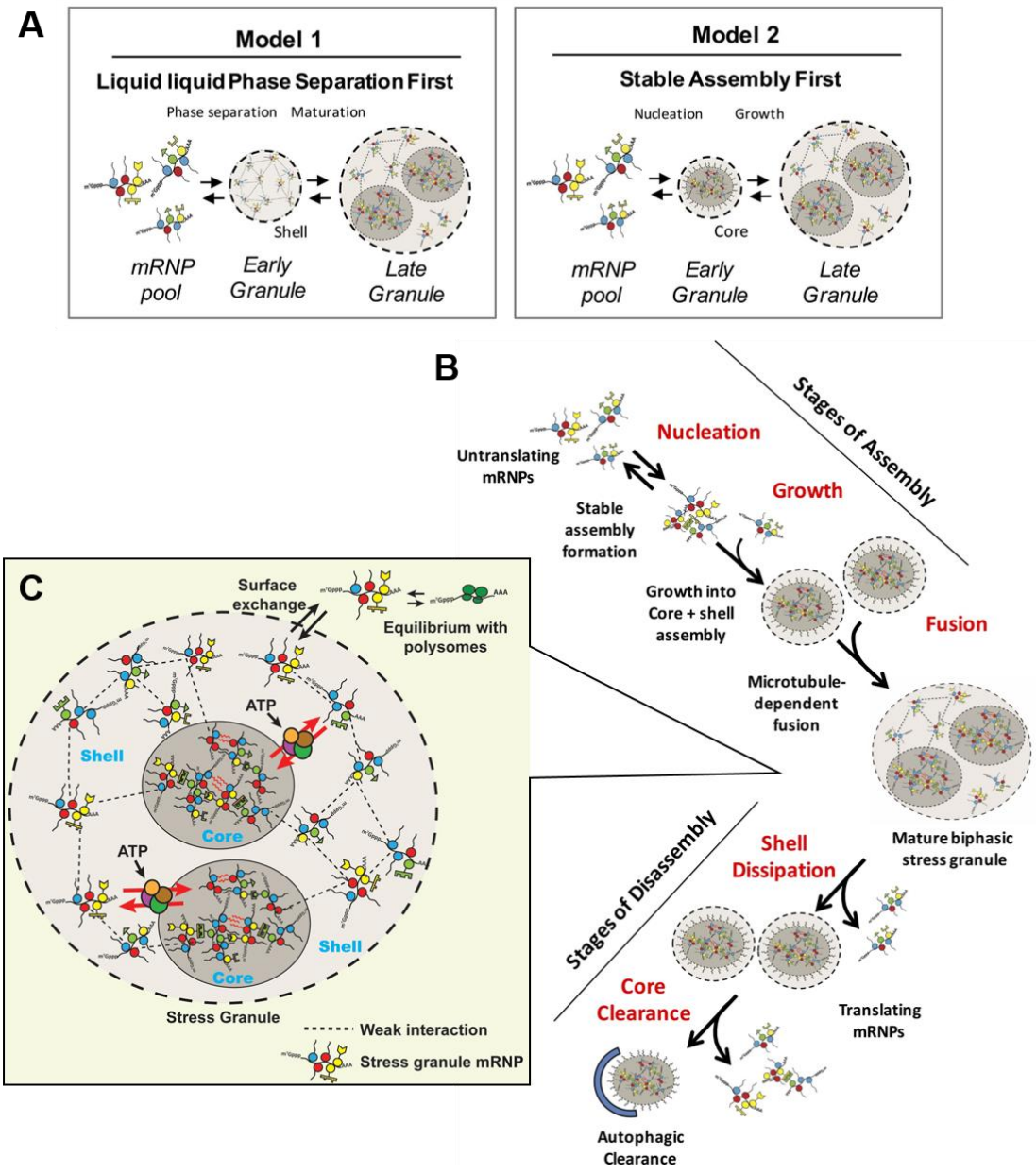

Figure 1.10 Model of SG formation and disassembly.

A) Two proposed models of SG formation. Model 1 favours initial nucleation of the shell via LLPS, while Model 2 – initial formation of stable cores. B) Step-wise formation and clearance of SGs, based on Model 2 in A. Formation of stable cores surrounded by a dynamic shell is an early event in SG formation, maturation of which is facilitated by molecular motors (adapted from Wheeler et al., 2016). C) Mature SGs, formed as a consequence of fusion of smaller foci, may contain multiple cores. Exchange of SG core and shell material is mediated by ATP, and shell material, rather than core, is in dynamic equilibrium with polysomes (adapted from Jain et al., 2016).

1.4.1.3 Regulation of SG dynamics

1.4.1.3.1 Microtubules as tracks for mature SG formation

Studying SG assembly by live microscopy using fluorescently-labelled SG-nucleating proteins, such as GFP-G3BP or -TIA-1, has shed light on the principles of SG formation, clearance and dynamics. For their formation, the general observation is that within 5-15 minutes of stress application numerous foci emerge, which grow in size and then rapidly move and fuse together, resulting in fewer but larger SGs (Ohshima et al., 2015; Wheeler et al., 2016). This later step is dependent on the microtubule network, but not on actin filaments. This was demonstrated by several groups using agents modifying cytoskeleton integrity, such as nocodazole and taxol (microtubule depolymerization and stabilization, respectively) or latrunculin B (actin depolymerization) (Ivanov et al., 2003; Chernov et al., 2009; Fujimura et al., 2009; Kolobova et al., 2009; Nadezhdina et al., 2010; Ohshima et al., 2015).

Microtubules primarily provide a network which allows transport of structural components and rapid SG maturation in response to stress. Once mature, SGs show relatively low motility, and integrity of microtubule tracks is not necessary for mature SGs persistence (Kedersha et al., 2005; Nadezhdina et al., 2010). Interestingly, FRAP analyses revealed that disruption of microtubules does not affect the recovery rate of individual components, such as PABP-1; they are, however, crucial for SG clearance, demonstrated by SG persistence after addition of cycloheximide in cells with depolymerized microtubules (Nadezhdina et al., 2010). In addition, α/β-tubulin co-purifies with SG components (Jain et al., 2016). Studying the recruitment or composition of SG cores at the early stage of their assembly, or in cells with depolymerized microtubules, might thus reveal the principal constituents involved in the early nucleation events, as well as determinants promoting their active transport and maturation.

1.4.1.3.2 Molecular motors regulate SG dynamics

The transport of RNP foci along microtubule tracks, and assembly into mature SG, is promoted by dynein and BICD1 (Kwon et al., 2007; Loschi et al., 2009; Tsai et al., 2009). Loschi et al. (2009) demonstrated that downregulating dynein heavy chain 1 (DHC1) and BICD1, but not DHC2 or BICD2, inhibits SG formation. In addition, DHC and dynein intermediate chain (DIC) are enriched in SGs (Loschi et al., 2009), and were identified in the SG proteome (Jain et al., 2016; Markmiller et al., 2018). In contrast, the recruitment or the proteomic identification of BICD1 and other known dynein adaptors in SGs have not been reported to date. Interestingly, the transcripts of DHC but not DIC or DLC, and BICD2 but not BICD1 are enriched within SGs (Khong et al., 2017), suggesting that expression of various retrograde machinery components might be differently regulated during stress.

Loschi et al. (2009) also demonstrated that silencing the expression of kinesin heavy chain 1 (KHC1, or KIF5) and kinesin light chain 1 (KLC1), but not KLC2, perturbs disassembly of SGs. Similarly to dynein, KHC and KLC are enriched in SGs (Loschi et al., 2009). The same study shows that cells depleted of both motors simultaneously displayed unperturbed SG dynamics, and the authors of the study concluded that lack of one motor compensates for the deficit of the other. This explanation does not appear plausible, since the lack of cytoplasmic dynein inhibits SG formation in the first place.

Studies conducted in *Drosophila* also imply that the role of BICD1 in SG formation, and its localization to these organelles in mammalian cells, should be investigated further. The fly BicD, complexed with dynein, interacts with the RBPs Egalitarian (Egl) and fragile X mental retardation (FMRP), both of which mediate mRNA transport (Bullock and Ish-Horowicz, 2001; Dienstbier et al., 2009; Bianco et al., 2010; McClintock et al., 2018). In addition, Egl and FMRP are components of fly (Gareau et al., 2013; Perez-Pepe et al., 2018) and mammalian (FMRP only) SGs (Mazroui et al., 2002).

The findings of Loschi et al. (2009) regarding the role of molecular motors in SG dynamics only partially correlate with the work of Tsai et al. (2009). Using pharmacological inhibitors of dynein and kinesin motors activity (erythro-9-(2-hydroxy-3-nonyl)adenine [EHNA], and adenosine 5-(β,γ-imido)triphosphate

[AMP-PNP], respectively), and monitoring SG formation and clearance, they found that dynein, but not kinesin, is essential for both dynamic processes. As EHNA is known to have targets other than dynein motor, such as cyclic guanosine monophosphate (cGMP) (Podzuweit et al., 1995), further validation, in particular dynein-mediated SG disassembly, is necessary using alternative dynein inhibitors.

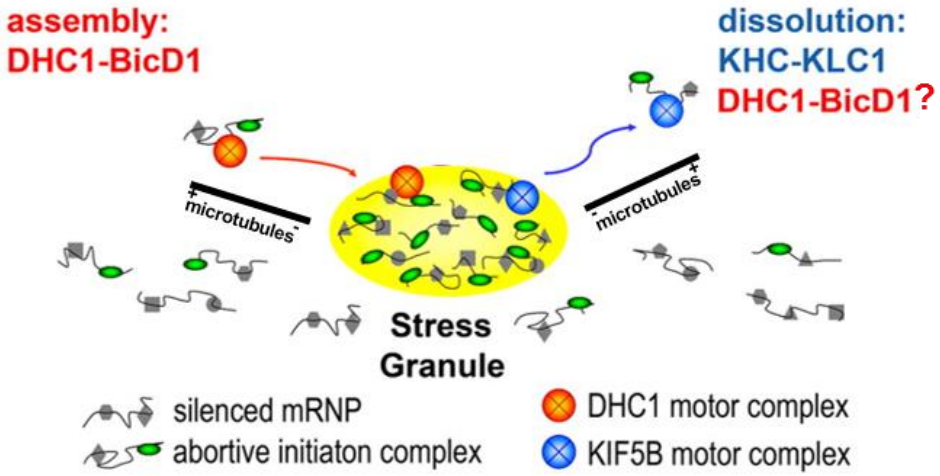

Figure 1.11 Dynein and kinesin motors contribute to SG dynamics.

Model of SG dynamics regulation by molecular motors. While dynein-BICD1 promotes SG formation, kinesin mediates SG disassembly. The role of dynein, and potentially BICD1, in the latter is yet to be confirmed (adapted from Loschi et al., 2009).

1.4.1.3.3 HDAC6 is a dynein co-factor regulating SG assembly

An important factor contributing to SG dynamics is histone deacetylase 6 (HDAC6). Amongst its many cytoplasmic functions, HDAC6 regulates the kinetics of dynein- and kinesin-mediated vesicular trafficking by deacetylating microtubules and organelle adaptors (Reed et al., 2006; Dompierre et al., 2007; Gao et al., 2010; Kalinski et al., 2019), while deacetylation of cortactin promotes assembly of the actin cortex necessary for autophagosome maturation (Lee et al., 2010). More importantly, HDAC6 binds ubiquitinated (Ub) proteins and promotes the recruitment of deubiquitinating enzymes (Hook et al., 2002), while its downregulation result in accumulation of Ub proteins, due to their inefficient delivery to aggresomes in cells with compromised proteasome (Hideshima et al., 2005). SGs accumulate Ub proteins, and HDAC6 may act as a multivalent adaptor linking G3BP, SG-related Ub-proteins and, potentially, dynein (Figure 1.12) (Kwon et al., 2007). HDAC6 localizes to canonical SGs, with kinetics

comparable to G3BP; and its deacetylase and Ub binding activities are both crucial for SG formation (Kwon et al., 2007). However, further experimental evidence is needed to confirm its direct association with Ub-proteins in SGs. In addition, the chaperone activity of HSP90 is maintained by HDAC6-mediated deacetylation (Bali et al., 2005), which contributes to SG dynamics (Matsumoto et al., 2011). Because of the requirement for HDAC6 in SG formation (Kwon et al., 2007), and its high affinity for free tubulin (Hubbert et al., 2002), it would be tempting to speculate that the latter may underlie the lack of SGs in cells treated with microtubule depolymerizing agents. Although it was demonstrated that HDAC6 co-immunoprecipitates dynein from mammalian cell lysates (Kawaguchi et al., 2003; Hideshima et al., 2005), it is still not known whether HDAC6 can bind dynein directly or via an intermediate adaptor, such as BICD1. This molecular interaction should be explored further, as it may uncover the mechanism of dynein recruitment necessary for SG maturation and transport. Interestingly, TDP-43 positively regulates transcription of HDAC6 (Fiesel et al., 2010), and poly-Ub cytoplasmic TDP-43 inclusions are a hallmark or ALT/FTD (Neumann et al., 2006).

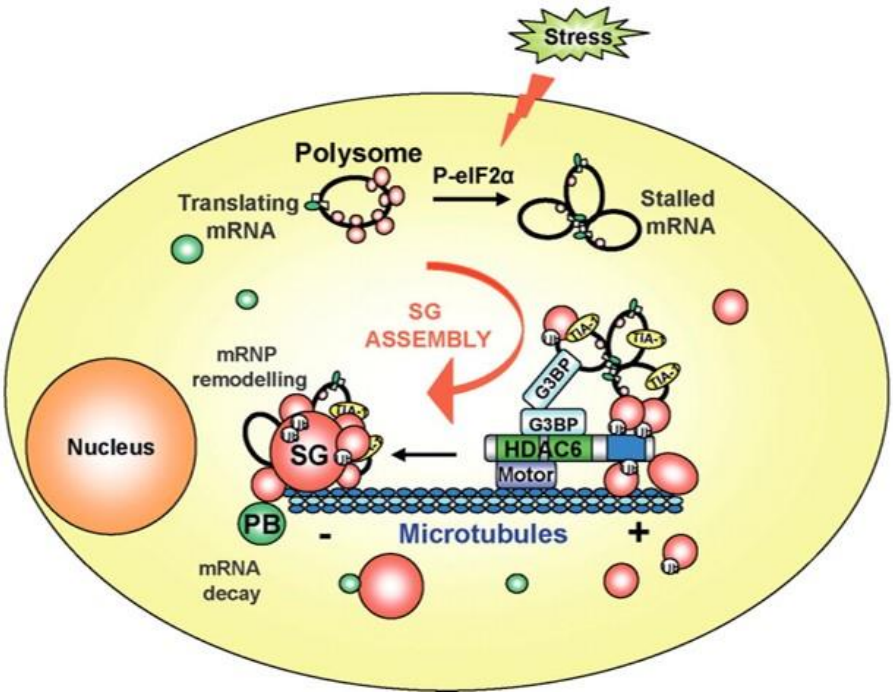

Figure 1.12 HDAC6 mediates SG formation.

Hypothesized role of HDAC6 in SG formation and transport. HDAC6 acts as a multivalent adaptor, linking G3BP and Ub-proteins with dynein, allowing SG maturation (adapted from Kwon et al., 2007).

1.4.1.3.4 Ubiquitin modifying enzymes in SG dynamics

The role of ubiquitin-related proteins in SG dynamics gained more attention in recent years. Ubiquitin can be detected in SGs induced by stress or by pharmacological inhibition of the ubiquitin-proteasome system (UPS) (Mazroui et al., 2007; Mateju et al., 2017; Xie et al., 2018), which, as discussed above, may potentiate the association of HDAC6 with G3BP and dynein (Kwon et al., 2007). Although HDAC6 was previously shown to recruit deubiquitinating enzymes (Hook et al., 2002), at present it is not known whether it mediates this process in SGs. Interestingly, in addition to ubiquitin, several ubiquitin-modifying enzymes were recently identified in the SG proteome (Jain et al., 2016; Markmiller et al., 2018). To date, the role of only a few of these proteins in SG dynamics has been explored experimentally.

Ubiquitin-associated protein 2-like (UBAP2L) is necessary for SG assembly, and localizes to SGs. Expression of mutant UBAP2L, lacking the Ub-associated domain, induces formation of aggregates which contain canonical SG markers, G3BP and FMRP, in the absence of additional stress (Markmiller et al., 2018). Moreover, ubiquilin-2 (UBQLN2) also resides within SGs (Alexander et al., 2018; Dao et al., 2018). UBQLN2 assists the protein quality control (PQC), by promoting the binding and transport of Ub-cargo for degradation by the proteasome and autophagy (N'Diaye et al., 2009; Hjerpe et al., 2016). Mutations in UBQLN2 are linked to ALS, and UBQLN2 is present in pathological inclusions in neurodegenerative diseases (Dao et al., 2018; Picher-Martel et al., 2018). Its interaction with HSP70, which mediates SG and protein clearance (Teyssou et al., 2017), promotes UBQLN2 recruitment to SGs, suggesting that SGs may provide an environment that facilitates the interaction of Ub substrates and their modifying enzymes. The binding of Ub to UBQLN2 reduces the LLPS propensity of UBQLN2, which was suggested to potentiate the extraction of SG-related Ub-proteins for degradation (Dao et al., 2018). In addition, UBQLN2 was demonstrated to negatively modulate the LLPS propensity of FUS, thereby delaying SG formation. However, it drives SG assembly during stress, suggesting that UBQLN2, and potentially other PQC proteins, act as regulators of SG dynamics at different stages of SG formation, by modulating the biochemical properties of SG-related proteins (Alexander et al., 2018).

Deubiquitinating enzymes also play a role in SG dynamics (Kedersha et al., 2016; Xie et al., 2018). In the absence of stress, G3BP specifically binds ubiquitin specific protease 10 (USP10), thereby inhibiting its deubiquitinase (Soncini et al., 2001) and antioxidant activities (Takahashi et al., 2013). As USP10 localizes to SGs during stress, its antioxidant function is restored (Takahashi et al., 2013). This might be partially modulated by the competitive binding of a SG nucleating factor, Caprin1, to G3BP, which releases its association with USP10. The USP10-G3BP complex inhibits SG formation, while Caprin1-G3BP promotes it (Kedersha et al., 2016). This suggests that USP10 and Caprin1 may act as molecular switches facilitating the dynamic behaviour of G3BP in SGs (Figure 1.13) (Kedersha et al., 2005), and USP10-G3BP regulate each other's activities in the absence and presence of stress. In addition, the deubiquitinase activity of USP10 on certain SG proteins may promote assembly of SGs (Nostramo et al., 2016), whilst USP5 and USP13 regulate assembly and clearance, respectively, of heat shock-induced SGs (Xie et al., 2018).

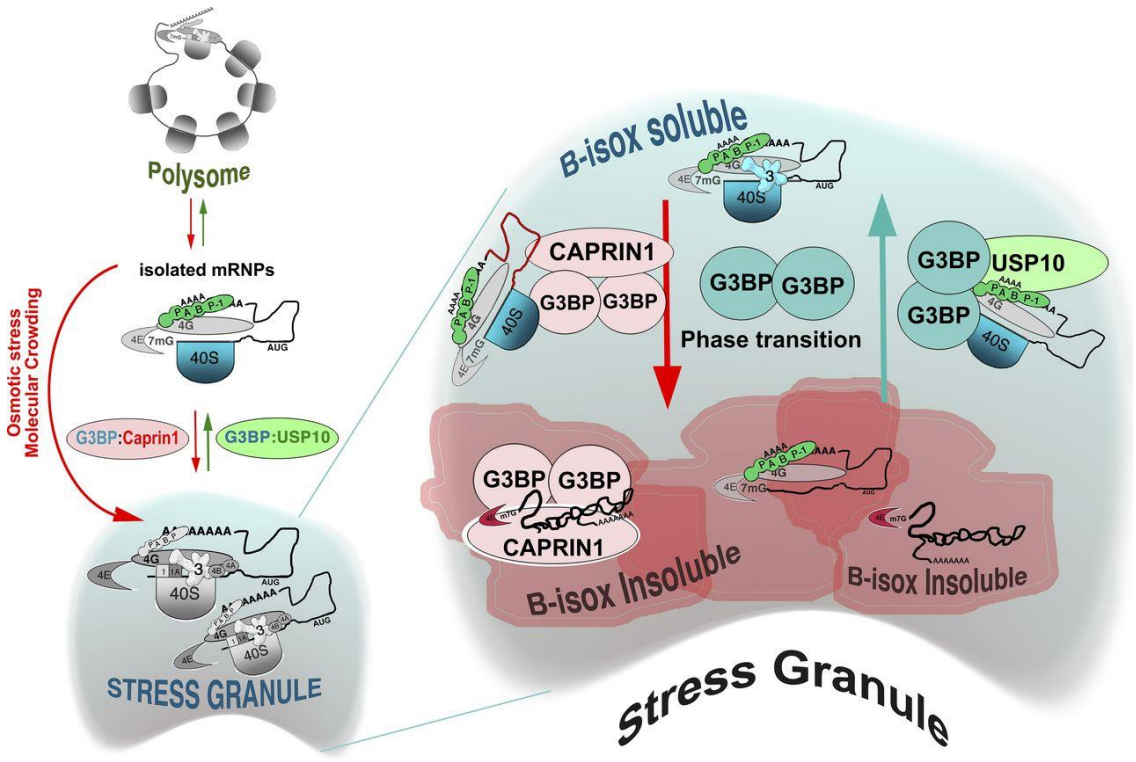

Figure 1.13 USP10/Caprin1 modulate the dynamic behaviour of G3BP during stress.

G3BP dynamics are promoted by switching between different phases, which is modulated by its association with USP10 or Caprin1. Caprin1 facilitates recruitment of G3BP and nucleation of SGs, while USP10 promotes shuttling out of G3BP (adapted from Kedersha et al., 2016).

1.4.1.4 SG clearance

While mature SGs are microscopic and easily detectable, studying the mechanisms of SG clearance is limited using traditional microscopy methods, due to the nanoscopic size of the disassembling foci. In addition, SGs are complex, multiprotein assemblies, therefore findings from studies using overexpressed SG proteins might be biased, as these proteins may favour certain interactions or dynamics (Kedersha and Anderson, 2007; Anderson and Kedersha, 2008). The exact mechanism of SG disassembly has been only partially characterized. Like SG formation, disassembly is a step-wise process, that includes dissipation of the SG shell and their fission into smaller structures, followed by the clearance of SG cores (Figure 1.10B) (Wheeler et al., 2016). As discussed above, molecular motors, their adaptors and tubulin posttranslational modifications are likely to play a role in this process (Loschi et al., 2009; Tsai et al., 2009; Ohshima et al., 2015). However, further experimental evidence is needed to decipher the precise mechanism. Posttranslational modifications, such as phosphorylation, ubiquitination, glycosylation, polyADP-ribosylation or acetylation, influence SG dynamics. G3BP methylation status also directly affects its ability to nucleate or promote disassembly of SGs (Alam and Kennedy, 2019).

Components released from disassembling SGs may be reverted back to translation, or targeted for autophagy (Figure 1.10B) (Protter and Parker, 2016). Valosin-containing protein (VCP), a HDAC6 binding partner (Boyault et al., 2006), segregates Ub proteins for degradation. VCP knockdown phenocopies inhibition of autophagy, which results in perturbed SG disassembly upon stress recovery (Buchan et al., 2013), suggesting a potential pathomechanism related to defective protein clearance in a variety of human Mendelian proteinopathies, including ALS/FTD (Johnson et al., 2010). ATPases and molecular chaperones, such as HSP70, also assist SG clearance, and decide the fate of its components, while their deficits result in persistent SGs (Walters et al., 2015). Furthermore, yeast HSP40 proteins, Ydj1 and Sis1, promote translational recovery and autophagic clearance of SGs, respectively (Walters et al., 2015). Stress recovery also leads to activation of focal adhesion kinase (FAK), which in turn phosphorylates growth factor receptor-bound protein 7 (Grb7), both of which localize to SGs, thereby weakening its interaction with SG components, such as

Hu antigen R (HuR), TIA-1 or mRNA, leading to SG disassembly (Tsai et al., 2008).

1.4.2 Function of SGs

The exact function of SGs, in mRNA metabolism in particular, is somewhat enigmatic. Because of the abundance of RBPs and mRNAs in SGs, they were initially considered solely as a storage organelle during stress (Wilczynska et al., 2005) – a hypothesis which was partially dismissed after the discovery of robust mRNA dynamics by FRAP (Mollet et al., 2008). During stress, SGs mediate mRNA triage, deciding between repression, reinitialization of translation or degradation of selected transcripts, which could be further regulated by direct interaction between SGs and processing bodies (P-bodies) (Anderson and Kedersha, 2008). The actual role of SG enlargement during stress remains unclear. Perhaps it facilitates the development of a specialized regulatory microenvironment, by locally increasing the concentration of various factors. In addition, fewer and larger SGs might be easier to target for later autophagic clearance (Buchan et al., 2013). The environment of SGs may additionally protect mRNAs and proteins from environmental insults, in turn promoting the translation of proteins necessary for the stress response, such as HSPs, as well as basal translation of selected transcripts with housekeeping functions (Perez-Pepe et al., 2018). As HSPs play an important role in preventing protein aggregation, their expression, together with 25% of other mRNAs, increases during stress. Interestingly, HSP transcripts are excluded from SGs (Kedersha and Anderson, 2002; Kolobova et al., 2009). With recent advances in identification of SG components (Jain et al., 2016; Khong et al., 2017), it is anticipated that the function of these RNP foci is much more complex. Their composition suggests that they exert tight posttranscriptional and posttranslational regulation of many mRNA and protein species, thereby regulating the efficacy of ISR, carefully adapted to the needs of cells undergoing stress (Kedersha et al., 2013). In addition, targeting of enzymes and signalling proteins to SGs was shown to directly modulate their function and the efficiency of the stress response, suggesting that SGs may act as complex signalling hubs (Kedersha et al., 2013).

The presence of SGs *per se* is not necessary for translational repression (Kwon et al., 2007). However, the occurrence of SGs in acute, sublethal stresses, increases resistance and cell survival, while inhibition of SG formation sensitizes

cells to environmental insults and may induce premature apoptosis (Tsai and Wei, 2010; Zou et al., 2011; Orrù et al., 2016). Interestingly, localization of activated Ras homolog gene family member A (RhoA), and its target, Rho-associated, coiled-coil containing protein kinase 1 (ROCK1) to SGs, prevents the interaction of ROCK1 with JNK-interacting protein 3 (JIP-3), and subsequent activation of cell death by c-Jun N-terminal kinase (JNK) in acute stress. In contrast, inhibition of SG formation by cycloheximide or EHNA leads to activation of JNK by JIP-3 via RhoA/RACK1 under stressed conditions, suggesting direct involvement of SG in survival (Figure 1.14) (Arimoto et al., 2008; Buchan and Parker, 2009; Tsai and Wei, 2010). JNK, however, can be activated by chronic stress, and enhances the localization of TDP-43 to SGs, which may facilitate their progression into ubiquitinated aggregates (Meyerowitz et al., 2011; Neumann et al., 2006).

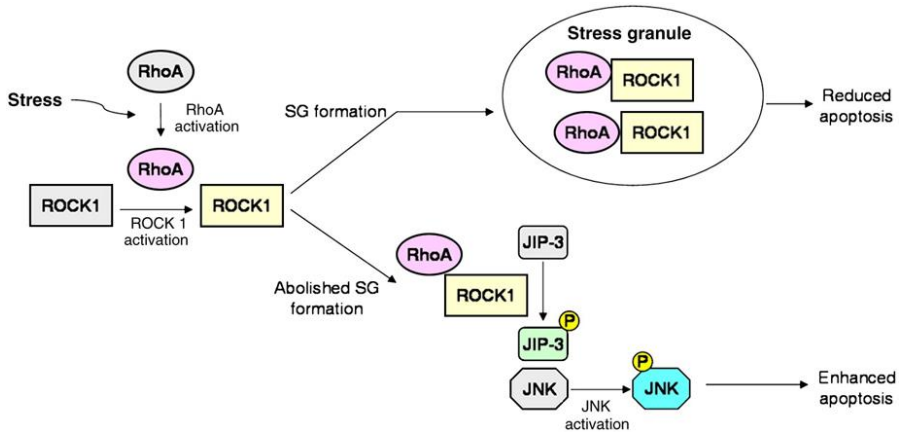

Figure 1.14 SGs inhibit JNK-induced apoptosis by sequestering RhoA and ROCK1.

Stress activated RhoA-ROCK1 complex localizes to SGs, preventing phosphorylation of JIP-3 and activation of apoptosis by JNK. Inhibition of SG assembly releases the complex and activates the JNK cell death signalling pathway (adapted from Tsai and Wei, 2010).

SGs also directly affect nucleocytoplasmic transport, as localization of nucleocytoplasmic transport elements to these organelles downregulates communication with the nuclear milieu (Zhang et al., 2018). This raises the question, whether prominent localization of dynein and kinesin motor components (Loschi et al., 2009), as well as HDAC6 (Dompierre et al., 2007; Kwon et al., 2007) to SGs may alter certain cytoplasmic trafficking events in cells undergoing stress. As mature SGs show relatively little motility (Nadezhdina et al., 2010), yet are abundant in motor proteins (Loschi et al., 2009), perhaps the analysis of motor proteins dynamics by FRAP would reveal whether they are

passively contained within SGs, or mediate active transport. As axonal transport defects and SG-related protein aggregates are a common pathological feature of neurodegeneration (De Vos and Hafezparast, 2017), the regulation of SG dynamics and transport in cells undergoing stress needs to be further investigated (Morfini et al., 2009).

1.5 Cancer cells hijack ISR to promote their survival

Due to high metabolic demands for growth and proliferation, stress is often induced in cancer cells (Figure 1.15). SGs are detected in many tumors, and they promote their survival and metastasis (Somasekharan et al., 2015; Mahboubi and Stochaj, 2017). Cancer cells may additionally utilize ISR to reduce the efficacy of radiation and some chemotherapeutic drugs. Canonical, pro-survival SGs, are detected in tumors targeted with bortezomib, MG132, 6-thioguanine, 5-azacytidine and 5-fluorouracil (Anderson et al., 2015). Inhibition of ISR was shown to be successful in restoring the effectiveness of these tumor suppressors, demonstrating that modulation of ISR is a potential therapeutic target promoting the effectiveness of chemotherapeutic agents (Anderson et al., 2015).

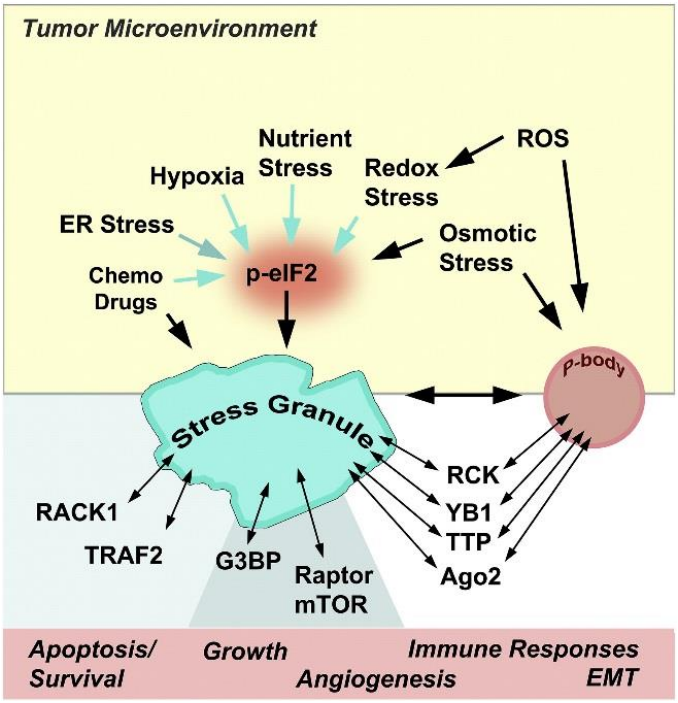

Figure 1.15 Cancer cells use ISR to promote their survival and as a defence mechanism against chemotherapeutics.

Due to high metabolic demands, ISR is often activated in unfavourable tumor environments. ISR increases survival of cancer cells and metastasis. In addition, cancer cells may utilize this pathway to decrease their sensitivity to chemotherapy (adapted from Anderson et al., 2015).

Although cancer cells are well-adapted to intracellular ROS imbalance, they are more vulnerable to exogenously applied stress. Inhibition of eIF2α and its upstream kinases promotes senescence in cancer cells, and increases the effectiveness of anti-cancer drug and oxidative stress inducer, doxorubicin (Rajesh et al., 2013). In addition, several SG-related proteins, including eIF4E, RACK1 or HuR, are oncogenic, and their elevated expression is often detected in cancer. In contrast, expression of SG-related tristetraprolin (TTP), a tumor suppressor, decreases in cancer (Anderson et al., 2015). Although G3BP is not considered an oncogene, it promotes cancer survival and its levels are also elevated in many cancers (Alam and Kennedy, 2019). In line with this, G3BP overexpression induces SG formation (Tourrière et al., 2003).

1.6 SGs and neurodegeneration

The high energy demands of the nervous system make it susceptible to pathologies during ageing, which is associated with increased oxidative and ER stresses, and decreased energy production and antioxidant defence (Lin and Beal, 2006; Niedzielska et al., 2016). Neurodegeneration often presents in the late adulthood, and it is progressive, debilitating, fatal and incurable. Neurodegenerative diseases may affect central or peripheral nervous system, or a combination of both, and the most prevalent disorders include Alzheimer's, Huntington's and Parkinson's disease (AD, HD, PD), and ALS/FTD spectrum (Niedzielska et al., 2016). Their shared pathological features are cell death of selected neuronal populations, and the presence of misfolded protein inclusions in affected neurons (Salahuddin et al., 2016). Activation of ISR, and deregulation of SG dynamics is associated with the abovementioned neurodegenerative disorders (Vanderweyde et al., 2013). SG proteins, such as TIA-1, TTP and G3BP, co-localize with phospho-tau inclusions in animal models of AD, and this association increases with disease progression (Vanderweyde et al., 2012). Decreased association of tau with microtubules makes it prone to aggregation, which is promoted further by its interaction with RNA (Kampers et al., 1996), suggesting a seeding mechanism similar to SG formation. Similarly, seeding-prone huntingtin inclusions in HD sequester TIA-1 (Waelter et al., 2001; Furukawa et al., 2009). Furthermore, a PD-related protein DJ-1, which is a redox sensitive chaperone preventing α-synuclein aggregation (Shendelman et al.,

2004), associates with SGs during stress and in models of parkinsonism (Repici et al., 2019).

ALS is characterized by a complex pathophysiology, but a common theme in the spectrum of this disease strongly points to misregulated SG dynamics (Li et al., 2013; Mahboubi and Stochaj, 2017). Many mutated genes causing ALS encode RBPs, several of which are components of SGs, including: ATXN2, C9orf72, EWSR1, FUS, hnRNPA1, SMN, TAF15, TIA-1, TDP-43, UBQLN2 or VCP (ALSoD database, http://alsod.iop.kcl.ac.uk; Vanderweyde et al., 2013). Poly-Ub and hyper-phosphorylated cytoplasmic TDP-43 inclusions containing several SG components became a histopathological hallmark of ALS, and can be detected in degenerating spinal cord, brainstem and brain tissue in the majority of patients (Neumann et al., 2006; Kwong et al., 2007; Liu-Yesucevitz et al., 2010; Dewey et al., 2011; Wolozin, 2012), irrespective of the genetic disease background – with the notable exception of ALS patients carrying mutations in superoxide dismutase 1 (SOD1) (Mackenzie et al., 2007). Mutations in SOD1 are present in approximately 5% of all ALS patients; and the mutant protein promotes oxidative stress (Shaw et al., 1995; Ferrante et al., 1997; Barber and Shaw, 2010). Recently, it was demonstrated that mutant $SOD1^{G93A}$, but not $SOD1^{WT}$, specifically interacts with G3BP and perturbs the formation of SGs during oxidative stress (Gal et al., 2016), suggesting that neuronal cell death could be a result of hypo-regulation of SG dynamics. In contrast, increased SG persistence, potentially giving rise to pathological aggregates, has been correlated with self-aggregation-prone mutant RBPs, such as FUS, TDP-43 or TIA-1 (Wolozin, 2012*;* Protter and Parker, 2016). Interference with their native function and misregulation of RNA processing could be particularly deleterious in neurons. At present, the most common genetic factor underlying ALS (40% of all patients) is intronic hexanucleotide repeat expansion (G4C2) in C9orf72 (DeJesus-Hernandez et al., 2011; Renton et al., 2011), which produces toxic nuclear RNA quadruplexes (Fratta et al., 2012) and toxic aggregation-prone dipeptide proteins due to repeat-associated non-ATG translation (RAN-translation) (Lee et al., 2016b). While normal C9orf72 associates with SGs (Maharjan et al., 2017) and its depletion perturbs SG formation, the toxic dipeptides facilitate seeding of abnormal SGs (Boeynaems et al., 2017; Maharjan et al., 2017), which directly contribute to the deficits in nucleocytoplasmic transport observed in ALS (Boeynaems et al., 2016; Zhang et al., 2018). Inefficient SG clearance due to

mutations in VCP, and other PQC proteins, was also suggested to give rise to pathogenic inclusions (Buchan et al., 2013).

Although it is not fully understood exactly how SGs relate to neurodegeneration, several lines of evidence point towards the impairment of ISR, SG dynamics, stress recovery and perturbed function of RBPs. Interfering with SG-related pathways, such as by blocking eIF2α phosphorylation, targeting components regulating SG assembly or the oxidative defence system, could be promising in tackling devastating diseases such as ALS (Li et al., 2013; Chen and Liu, 2017).

1.7 Neurotrophins and neurodegeneration

NTs are crucial in the early development of the nervous system, during which time they are highly expressed (Kaplan and Miller, 2000). The role of NTs in the developed adult nervous system was demonstrated in studies using a conditional TrkB knockout mouse model (Xu et al., 2000) and antibodies against NGF (Ruit et al., 1990), which showed that chronic downregulation of NT signalling in the mature organism leads to slow neuronal loss, similar to that observed in adult-onset neurodegenerative diseases. In fact, perturbed NT signalling and trafficking has been strongly associated with neurodegenerative and cognitive disorders (Gardiner et al., 2009). In addition, loss of trophic support may directly promote neuronal death by activating the JNK pathway (Le-Niculescu et al., 1999). Because of the beneficial effect of NTs on the overall health of the nervous system, restoring and facilitating NT signalling should in principle improve neuronal fitness in neurological conditions.

NTs, such as BDNF, act indirectly on the mitochondrial respiratory chain, promoting the correct ROS balance (Markham et al., 2004), and inducing the activity of antioxidative enzymes, glutathione reductase and superoxide dismutases (Mattson et al., 1995). In contrast, BDNF withdrawal enhances oxidative stress and cell cycle re-entry (Boutahar et al., 2010), which may promote neuronal death (Copani et al., 2001). Chronic low-level exposure to oxidative stress may also reduce the expression of BDNF, further potentiating the ROS damage (Wu et al., 2004). Interestingly, both oxidative stress and cell cycle re-entry, observed in AD, could be a consequence of dysregulated trophic support, and some studies demonstrated that certain NTs may even further

potentiate the disease (Connor et al., 1996; Zhu et al., 2004). For instance, increased NGF/TrkA and reduced BDNF/TrkB expression is observed in the cortex in AD and motor neurons in ALS (Kruttgen et al., 2003), and expression of both trophic factors and their receptors is reduced in PD, which contributes to the deterioration of dopaminergic neurons (Baquet et al., 2005).

Loss of NT support observed in neurodegeneration could be attributed to the perturbed axonal transport (Kruttgen et al., 2003). In AD, pro-oxidative β-amyloid directly damages the microtubule cytoskeleton (Seyb et al., 2006). Reduced BDNF trafficking is also linked to mutant huntingtin (Htt) in HD. In healthy individuals, Htt promotes BDNF transport by linking BDNF/TrkB endosomes with dynein, thereby protecting neurons against the loss of trophic support and associated toxicity (Gauthier et al., 2004). Interestingly, inhibition of tubulin deacetylation by pharmacological inhibition of HDAC6, restores BDNF transport and neuroprotection in models of HD; and reduced acetylation level of microtubules is observed in brains of HD patients (Dompierre et al., 2007).

Restoration of NT signalling and trafficking had beneficial effects in many animal models of neurodegeneration; however, the use of NTs as therapy in humans has met certain challenges, most notably their short half-life in blood and poor blood-brain barrier (BBB) penetration (Gould and Oppenheim, 2011). Alternative methods are being developed, such as the use of small BBB-permeable molecules acting as agonists/antagonists of NTRs (Tejeda and Díaz-Guerra, 2017). A true ground-breaking clinical trial has now completed for the treatment of PD, in which GDNF is “infused” via small catheters directed into the affected brain region. This study shows promising results, not only in restoring brain function, but also in regenerating the affected neuronal population and reversing the symptoms of PD (Whone et al., 2019a; Whone et al., 2019b).

ALS is rapidly progressing (death usually within 3-5 years of diagnosis), and has a complex pathophysiology, making it difficult to target and develop effective therapies (Turner et al., 2009; Taylor et al., 2016). Misregulation of NT support is also associated with ALS, and could be directly related to the deficits in dynein-mediated transport, implicated in the disease pathogenesis (LaMonte et al., 2002; Hafezparast et al., 2003; Zhang et al., 2007; Bilsland et al., 2010). Although proof-of-principle studies using SOD1 animal models of ALS have shown beneficial effects of NT treatment on motor neuron survival (Federici and Boulis, 2006;

Federici and Boulis, 2012), therapies utilizing NTs such as BDNF, CNTF and IGF-1 shown disappointing results in clinical trials, explained later by poor tissue penetration and high instability of these growth factors (Federici and Boulis, 2006; Sorenson et al., 2008). Use of patient mesenchymal stromal cells (MSCs) holds a greater therapeutic promise, and at the time of writing it entered phase 3 clinical trials. MSCs, which can be obtained from bone marrow and adipocytes, are expanded and reprogrammed *ex vivo* to secrete NTs ("NurOwn"), and re-injected into affected regions, like the lumbar spine. This approach was shown to be well-tolerated, but clinical benefits are yet to be confirmed (Karussis et al., 2016; Madigan et al., 2017; clinicaltrials.gov).

1.8 Aims of the thesis

Correct spatiotemporal regulation of NT signalling and trafficking is essential for neuronal development and homeostasis, and misregulation of support provided by these growth factors is associated with complex neurological disorders. In addition, perturbations in the ISR are strongly implicated in neurodegeneration and cancer, therefore understanding SG dynamics and how diverse biological processes are regulated in neurons undergoing stress is essential to increase the chances of finding effective therapies. This thesis is dedicated to exploring the mechanisms regulating the NT pathway and the ISR.

The main aims of this thesis are:

1. To characterize the interaction between BICD1 and PTPN23 using biochemical approaches and microscopy, thus furthering our understanding of the mechanisms controlling NTR turnover (Chapter 3).
2. To investigate the role of PTPN23 in the endocytic dynamics of NTRs, using an anti-NTR antibody accumulation assay. This approach highlights a novel, neuronal function of PTPN23 and reveals its association with BICD1 and the NT pathway (Chapter 4).
3. To explore the relationship of BICD1 and PTPN23 with SGs, thus contributing to deciphering SG dynamics (Chapter 5).
4. To assess the effect of oxidative stress on NTR trafficking and signalling, which is of significance to future studies implementing NTs as a therapeutic strategy for neurodegeneration (Chapter 6).

2 Materials and methods

2.1 Materials

2.1.1 Chemicals and reagents

Chemicals used in the study were purchased from Sigma, unless stated otherwise. Reagents for mammalian cell culture were from Gibco. Reagents for polymerase chain reaction (PCR) and cloning were from New England BioLabs (NEB). Transfection reagents were from Invitrogen.

2.1.2 Primers

Primers used for PCR, cloning, mutagenesis and sequencing were purchased from Invitrogen; sequences are available in Appendix 2 (9.1).

2.1.3 Antibodies and fluorescent probes

Primary antibodies used for western blotting (WB) and immunocytochemistry (ICC) are available in Appendix 2 (9.3). For WB, horseradish peroxidase (HRP)-conjugated secondary antibodies (Dako) were used at 1:1,000. For IF, fluorescent AlexaFluor® secondary antibodies (Life Technologies) were used at 1:1,000. Fluorescently-labelled phalloidin (AlexaFluor488, 555, 647) was used as actin counterstain at 1:50, added with secondary antibodies (Life Technologies). Fluorescently-conjugated cholera toxin subunit B (CTB; AlexaFluor488) was used for trafficking assay at 1:300 (C34775, Molecular Probes). DAPI (4',6-diamidino-2-phenylindole) was used as DNA stain at 1:5,000.

2.1.4 Buffers and solutions

The composition of all buffers and liquid media is available in Appendix 2 (9.4).

2.1.5 Drugs

Drugs with indicated target and concentration are available in Appendix 2 (9.5). All drugs were tested by confocal microscopy for autofluorescence, with/without secondary antibodies.

2.1.6 Bacterial strains

E. coli strains with indicated use are available in Appendix 2 (9.6).

2.1.7 Mammalian cell lines

Mouse neuroblastoma Neuro-2a (N2A) cell line stably expressing FLAG-tagged TrkB receptor (N2A-FLAG-TrkB) (Terenzio et al., 2014a) and human embryonic kidney 293 (HEK293) cell lines were used for ICC, co-immunoprecipitation (co-IP), pull down, oxidative and endoplasmic reticulum stress, and BDNF signalling assays. Mouse embryonic stem cells (mESc) were derived from hybrid blastocysts generated at the Crick Institute Biological Resource Unit, by mating C57BL6/6J and 129 (S6)SvEv mice, as described previously (Bryja et al., 2006).

2.2 Methods

2.2.1 Nucleic acid techniques

2.2.1.1 Agarose gel electrophoresis

DNA gel electrophoresis was performed on 0.7% agarose gel dissolved in TBE buffer, containing ethidium bromide. MassRuler™ DNA Ladder Mix (ThermoFisher Scientific) was used as molecular weight (MW) marker. Gel was run at 90 V for 1 h and visualised on UV light transilluminator or by ChemiDoc™ Imaging system (BioRad). QIAquick Gel Extraction Kit (Qiagen) was used for DNA extraction according to manufacturer's instructions.

2.2.1.2 Bacterial transformation

An aliquot of 30-80 µl of chemically competent *E. coli* was thawed on ice for 5 min, and 100 ng (0.5-2 µl) of pre-chilled plasmid DNA was added. Mixture was incubated on ice for 30 min, heat-shocked for 45 s in water bath at 42°C and placed back on ice for 2 min. Next, 350-900 µl of SOC medium was added and bacteria were incubated for 1 h at 37°C in a thermal shaker at 225 revolutions per minute (RPM). Bacteria were spread on Luria broth (LB) agar plates containing the appropriate antibiotic (100 µg/ml ampicillin or 50 µg/ml kanamycin), and incubated overnight at 37°C.

2.2.1.3 Plasmid DNA isolation

A single colony was used to inoculate 5 ml of LB, containing an appropriate antibiotic. Culture was grown at 37°C overnight in shaking incubator at 200 RPM.

The following day, plasmid DNA was purified using QIAprep Spin Miniprep Kit (Qiagen) according to manufacturer's instructions.

2.2.1.4 DNA quantification

A nanodrop spectrophotometer (Labtech International) was used to determine DNA concentration by measuring optical density at 280 nm.

2.2.1.5 PCR

DNA fragments, used for FastCloning, were generated by polymerase chain reaction (PCR), using primer pairs (available in Appendix 2, 9.1). Sequences in bold correspond to overhang regions which do not anneal to the template. Annealing temperatures of non-bold sequences were calculated using online Tm Calculator tool (http://tmcalculator.neb.com). All fragments were amplified by Phusion® High Fidelity DNA polymerase (NEB), according to manufacturer's instructions, optimized for specific target DNA sequences. Cycling parameters are summarised in Table 1. PCR products were verified by gel electrophoresis (Figure 2.1).

Table 1 PCR cycling parameters.

Step	**Temperature (°C)**	**Time**	**Number of cycles**
Initial denaturation	98	30 s	1
Denaturation Annealing Extension	98 55-68 72	10 s 30 s 20 s/kb	18-25
Final extension	72	10 min	1
Hold	4	infinite	1

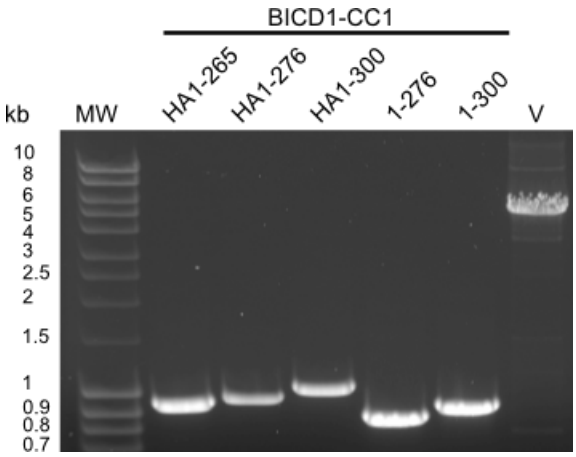

Figure 2.1 Gel electrophoresis of DNA fragments used for FastCloning, amplified by PCR.

Representative DNA gel showing PCR of five BICD1-CC1 fragments, producing bands between 0.8-1 kb. Amplified pGEX-4T-1 vector (V) produced a band of 5 kb. Predicted fragment sizes were calculated using ApE software (Plasmid editor v2.0.49.10).

2.2.1.6 FastCloning

Cloning was based on "FastCloning" method by Li et al. (2011). Briefly, target DNA ("insert") sequence was amplified by PCR using a primer pair containing 9-15 bp overhang (in bold), complementary to desired site on the acceptor vector. The acceptor vector was amplified using primer pair with no overhangs, inclusive of region complementary to overhang sequences on insert primers (total PCR reaction volume: 50 µl). PCR products of corrects size were diluted in water (1:3 PCR product, 1:15 *Dpn*I buffer; total reaction volume: 50 µl) and treated for 2 h at 37°C with *Dpn*I, to eliminate template vector. Next, insert:vector were mixed at ratio 3:1 [µl], incubated for 1 min on ice, transformed into 50-80 µl of XL-10 Gold ultracompetent bacteria and grown in SOC medium for 1 h. Whole reaction was plated on LB agar plates containing appropriate antibiotic for selection (Figure 2.2). Next day, selected colonies were inoculated overnight, and plasmid DNA was isolated. New sequences were assembled using ApE (Plasmid editor v2.0.49.10). Cloning was verified by restriction enzyme digestion (Figure 2.3) and sequencing.

For bacterial protein expression, BICD1 fragments were cloned from mammalian expression vector HA-BICD1-pEGFPN1, containing kanamycin resistance gene (Kan^R) to pGEX-4T-1, containing ampicillin resistance gene (Amp^R), and N-terminal GST-tag. PTPN23 fragments were cloned from HA-PTPN23-pcDNA3.1+ (Amp^R) to pET28a+ (Kan^R), containing an N-terminal His_6-tag. Presence of

different antibiotic resistance genes between insert and target vectors reduces background in FastCloning. HA-BICD1-pEGFPN1 containing human BICD1 cDNA (835 aa, Q96G01-4, NCBI Reference Sequence: NM_001003398) with N-terminal HA-tag, was a kind gift from Prof. Casper Hoogenraad (Utrecht University). HA-PTPN23-pcDNA3.1+ containing human PTPN23 cDNA (1636 aa, Q9H3S7-1, NCBI Reference Sequence: NM_015466.3) with N-terminal HA-tag, was a kind gift from Prof. Philip Woodman (University of Manchester). For mammalian protein expression, GFP-BICD1$^{\Delta 95\text{-}265}$ and GFP-BICD1$^{95\text{-}265}$ were cloned from HA-BICD1-pEGFPN1 into pEGFPC1 plasmid with N-terminal GFP (kindly prepared by David Villarroel-Campos). To generate PTPN23-dsRed2 constructs, sequences were cloned from HA-PTPN23-pcDNA3.1+ into DsRed2-N1 (Kan^{R}) plasmid expressing C-terminal dsRed2 protein. For full list of generated expression constructs refer to Appendix 2 (9.2).

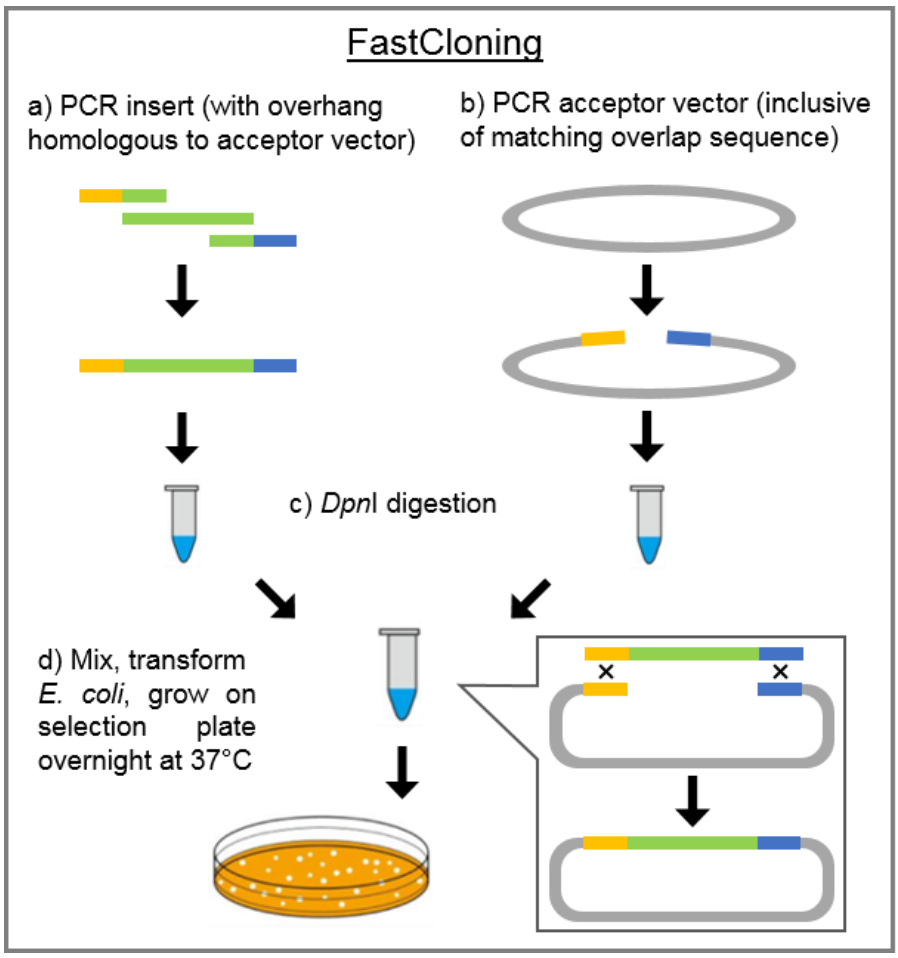

Figure 2.2 Schematic of PCR-based FastCloning procedure.

Insert is amplified by PCR using primer pair with overhangs complementary to a target vector. Vector is amplified inclusive of complementary overhang sequences, present on the insert. Both products are digested in *DpnI* enzyme, mixed, transformed into ultracompetent *E. coli* and grown on selection plate overnight at 37°C.

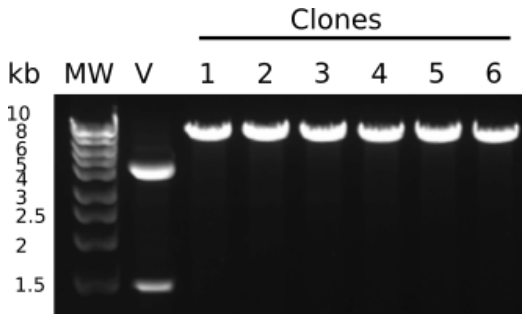

Figure 2.3 Example of cloning verification by restriction enzyme digestion.

Vector (V) produced bands at 1.4 kb and 4 kb, while clones (1-6) produced band at 7.5 kb, when digested with *Xho*I and *EcoR*V, verifying the presence of the insert, which disrupted *Xho*I restriction site. Predicted sizes were calculated using ApE software. Sequences were verified by sequencing.

2.2.1.7 Mutagenesis

To generate a vector expressing shRNA2-resistant PTPN23 (bp351-354, TCTC<CCTG), QuickChange Lightning Site-Directed Mutagenesis Kit was used according to manufacturer's instructions (Cat: 210518; Agilent Technologies). In short, mutagenesis was performed by PCR using a pair of overlapping primers, containing silent changes at two positions in the middle of primer pair. PTPN23$^{8-407}$-dsRed2 vector was used as a template. Mutagenesis was verified by sequencing. To generate vector expressing full length protein, PTPN23$^{408-1636}$ was subcloned from HA-PTPN23-pcDNA3.1+ into PTPN23$^{8-407}$(TCTC<CCTG)-dsRed2 and PTPN23$^{8-407}$-dsRed2 by FastCloning.

2.2.1.8 Restriction enzyme digestion

Two hundred nanograms of DNA was incubated with restriction enzyme (2 units of enzyme per reaction), according to manufacturer's instructions (NEB). DNA was separated by gel electrophoresis.

2.2.1.9 Sequencing

All constructs generated by FastCloning and mutagenesis were sequenced by Source Bioscience, using Sanger sequencing method.

2.2.1.10 Transfection

Mammalian cell lines were transfected using Lipofectamine® 3000 (Invitrogen), according to manufacturer's instructions, and evaluated by WB and ICC.

2.2.1.11 Lentivirus production

Commercially-available shRNA against four distinct regions on mouse PTPN23, and non-targeting shRNA ("scrambled"), were obtained from GeneCopoeia (cat: MSH025913). Targeting sequences are available in

Table 2. shRNA in psiLVRU6GP vector contains targeting short hairpin under U6 promoter, and eGFP reporter under SV40 promoter (Figure 2.4). Lentiviral plasmids were amplified using GCI-5α *E. coli*, and targeting sequences were verified by sequencing. Prior to virus production, knockdown efficiency and GFP expression in N2A-FLAG-TrkB cells were assessed 72 h post-transfection by WB. To produce lentivirus, 70% confluent 15 cm dish of LentiHEK cells of low passage number (P7-9), cultured in regular cell culture medium, was transfected using Lipofectamine3000® according to manufacturer's instructions. In short, 1.25 ml of OptiMem was mixed with 50 µl Lipofectamine3000®Reagent, and 1.25 ml OptiMem was mixed with 31.3 µg DNA (7.8 µg VSV-G [envelope protein-expressing vector pMD.G.2], 11.75 µg PAX [packaging vector pCMVdeltaR8.74] and 11.75 µg shRNA plasmid) and 62.5 µl P3000™. Both solutions were combined, incubated for 15 min and added to LentiHEK cells. Media, containing viral particles, was collected at 48 h and 72 h post-transfection, and concentrated using Lenti-X™ Concentrator (cat: 631231, Clontech), according to manufacturer's instructions. Briefly, cell debris was removed by centrifugation for 10 min at 500 g. Lenti-X™ was added to virus-containing media at 1:3, gently combined, incubated for at least 1 h at 4°C and centrifuged for 45 min at 1,500 g at 4°C. Media was removed and centrifuged again for 10 min at 1,500 g at 4°C. Pellet containing lentivirus was resuspended on ice in OptiMem, aliquoted, snap-frozen and stored at -80°C for future use. Knockdown levels and GFP-reporter expression were assessed 72 h post-transduction by WB and ICC.

Table 2 PTPN23-targetting and scrambled shRNA sequences.

Name	Target sequence
shRNA1	gctacactacctacagagt
shRNA2	ggcctgtattctctacaac
shRNA3	cctggacaagcttaatgaa
shRNA4	gtcctgacatctttgccaa
scrambled	gcttcgcgccgtagtctta

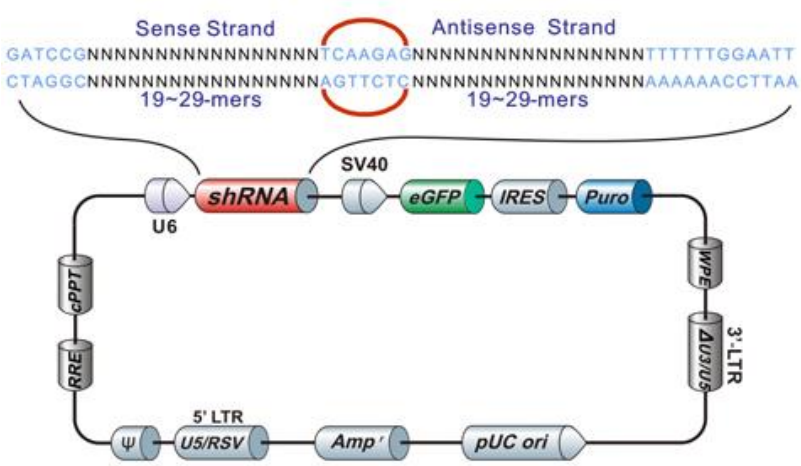

Figure 2.4 Plasmid backbone carrying shRNA used for lentivirus production.

Adapted from GeneCopoeia (www.genecopoeia.com).

2.2.1.12 Mammalian cell transduction

To transduce N2A-FLAG-TrkB cells, lentivirus was added immediately after plating, and cells were assayed after 72 h. For ES-MNs, lentivirus was added either 4 h or 24 h after plating and cells were assayed after 48 h or 72 h. To assess protein levels, samples were extracted in radioimmunoprecipitation assay (RIPA) buffer, and examined by SDS-PAGE and WB. Alternatively, cells were fixed and assessed by ICC. Expression level of GFP-reporter was evaluated in every experiment.

2.2.2 Protein techniques

2.2.2.1 Immunocytochemistry and confocal microscopy

For ICC and confocal microscopy, cells were grown on cat. 1.5 acid-washed glass coverslip with appropriate coating: 0.1 mg/ml poly-L-lysine (N2A-FLAG-TrkB, HEK293), or 1:100 polyornithine and 1:300 laminin (motor neurons). Cells were washed with phosphate-buffered saline (PBS), fixed with 4% paraformaldehyde (PFA) in 1x PBS (4% PFA/PBS) for 15 min at room temperature (RT), permeabilized for 10 min with 0.1% Triton X-100 in PBS (PBSTx) and washed. Next, cells were incubated for 1 h at RT in blocking solution (10% goat serum and 0.5% bovine serum albumin (BSA) in PBS). Cells were then incubated overnight at 4°C with primary antibodies (Appendix 2, 9.3) diluted in reduced blocking

solution (5% goat serum, 0.5% BSA in PBS). Next day cells were washed and incubated for 2 h with secondary fluorescent antibodies in reduced blocking solution. Control staining was performed for primary and secondary antibodies. Coverslips were mounted using Mowiol 4-88 or Fluorescence Mounting Medium (S3023, Dako). Images were taken on LSM510 inverted laser scanning confocal microscope (Zeiss), using 63x/1.40 oil objective, using following acquisition settings: frame mode, 1.28-3.20 µsec pixel dwell time, 12 bit depth, single line direction, mean number of 4-8 averages, <0.8 µm optical slice (pinhole ~1 Airy Units), z-stacks acquired at 0.2-0.5 µm spacing. All image analyses were performed using Fiji (ImageJ, Version: 2.0.0-rc-65/1:51u).

2.2.2.2 Protein extraction and quantification

Cells were washed twice with ice-cold PBS and scraped in NP-40 or RIPA lysis buffer (formulas available in Appendix 2, 9.4), supplemented with HALT protease and phosphatase inhibitor cocktail (1:100) (Thermo Scientific). Cells were incubated on ice for 30 min, and centrifuged for 10 min at 14,900 RPM at 4°C. The supernatant was separated from the pellet, and protein concentration was quantified by BCA assay (BioRad) according to manufacturer's instructions. Bradford assay was used to quantify concentration of purified proteins used in *in vitro* binding assays. Fresh protein standards ranging between 0.05-0.5 mg/ml of BSA were prepared in corresponding lysis buffer.

2.2.2.3 Co-immunoprecipitation

For BICD1 co-immunoprecipitation (co-IP), N2A-FLAG-TrkB/HEK293 cells were grown to 80% confluency in 10 cm dishes, serum-starved for 3-5 h and assayed where indicated. Cells were washed with ice-cold PBS on ice and protein (2-4 mg) was extracted in 0.2-0.4% NP-40 lysis buffer. To perform co-IP, 20 µl of magnetic Dynabeads® Protein G (Novex) were pre-washed with 300 µl of PBS 0.02% Tween-20 (PBST). Next, beads were incubated with 2 µg of primary antibody or species-matched IgGs as control in 200 µl PBST for 20 min – 1 h on a rotator at RT or at 4°C. Unbound antibodies were removed by PBST wash on a magnetic rack. Following that, fresh cell lysate containing 2-4 mg protein was added, and mixture was incubated for 1-3 h at 4°C, rotating end-over-end. Beads were washed 4x with 200 µl (10x bead volume) of lysis buffer, transferred to fresh tubes and washed again. Beads were boiled for 4 min at 95°C in 20 µl 1x Laemmli

sample buffer (LSB) to elute proteins. Whole eluted co-IP sample was used for analysis by SDS-PAGE and WB.

2.2.2.4 GFP-trap

Magnetic green (GFP)-Trap®_M (Chromotek) beads were used to co-IP GFP-tagged recombinant proteins. Briefly, 25 µl of beads were equilibrated in GFP-beads wash buffer on a magnet rack, following manufacturer instructions (washed 3 times in 500 µl wash buffer). Beads were equilibrated in 0.4% NP-40 lysis buffer and incubated for 2 h at 4°C with lysate prepared in the same buffer. Beads were washed 4 times with lysis buffer and proteins were eluted by boiling in 1x LSB.

2.2.2.5 SDS-PAGE

Sodium dodecyl sulfate polyacrylamide gel electrophoresis (SDS-PAGE) was used to separate proteins, using gradient 4-12% NuPAGE Bis-Tris polyacrylamide gel (Novex) or 4–15% Mini-PROTEAN® TGX Stain-Free™ Protein Gel (BioRad), and run according to manufacturer's instructions.

2.2.2.6 Coomassie Blue staining

SDS-PAGE gel was fixed for 10 min in destaining solution. To detect and visualise proteins, gel was submerged in Coomassie Blue staining solution, microwaved for 2 min (with 10 s pause, every 10 s) and incubated for following 20-30 min at RT. Coomassie Blue staining solution was removed and the gel was incubated in destaining solution, which was being replaced until bands were clearly visible. Gel was imaged on ChemiDoc™ (BioRad). *Note: TGX Stain-Free™ BioRad gels do not recognize tryptophan-free proteins.*

2.2.2.7 Western blotting

Protein transfer from SDS-PAGE gel was performed in wet or semi-dry format to either nitrocellulose (Whatman) or methanol-activated polyvinylidene fluoride (PVDF, BioRad) membrane, as previously described (Debaisieux et al., 2016). Membrane was blocked for 1 h with 5% fat-free dry milk dissolved in PBST for detection of all proteins, or with 5% BSA dissolved in TBST for detection of phosphorylated proteins. Next, membrane was incubated for 1 h (at RT) or overnight (at 4°C) with primary antibody (Appendix 2, 9.3), diluted in blocking solution. After washing the membrane 3x 10 min with PBST/TBST, it was

incubated for 1 h with secondary antibody diluted 1:1,000 in appropriate blocking solution. The membrane was washed and incubated with enhanced chemiluminescent (ECL) substrate. Blots were exposed to X-ray film (FUJI medical X-ray film, Super RX, FUJIFILM), developed in medical film processor (SRX-101A, KonicaMinolta) and analysed in FIJI. Alternatively, blots were developed using ChemiDoc™ (BioRad) and analysed in ImageLab (version 5.2.1, build 11; 14th Nov, 2014, BioRad).

2.2.2.8 Protein expression and purification

E. coli SoluBL21™ strain (Appendix 2, 9.6) was used for recombinant protein expression, following manufacturer's instructions. Various expression conditions were tested by Coomassie Blue and/or WB. Most optimal expression condition for majority of recombinant proteins were: induction with 1 mM isopropyl β-D-1-thiogalactopyranoside (IPTG) at 0.4 OD_{600} (OD, optical density), in M9 minimal media, at 21°C overnight, on orbital shaker at 200 RPM. Recombinant protein size prediction was sequence-based, using online ProtParam tool (https://web.expasy.org/protparam). All subsequent steps were performed at 4°C, unless stated otherwise.

2.2.2.8.1 GST-purification

Bacteria expressing glutathione S-transferase (GST)-BICD1 recombinant proteins were harvested by centrifugation for 10 min at 3,000 RPM. Pellet was resuspended and washed twice with 0.05% PBST. Bacteria were then resuspended in GST lysis buffer and lysed by sonication (Soniprep 150 Ultrasonic disintegrator, MSE) with 3 bursts of 20 s and 1 min cooling interval between each cycle. Insoluble material was pelleted by centrifugation for 20 min at 14,900 RPM. The soluble fraction was removed and used for subsequent analysis (protein purification, SDS-PAGE, Coomassie Blue staining or WB) or snap-frozen in liquid nitrogen. Purification of GST-fusion proteins was performed using glutathione (GSH)-agarose affinity resin (Sigma) or GSH-magnetic beads (for *in vitro* pull down assays with His_6-PTPN23 proteins), rotating end-over-end for 2 h at 4°C with fresh bacterial soluble supernatant. Next, resin was washed 3x 10 bead volumes with 0.05% PBST, resuspended in DNAK buffer and incubated in a 37°C water bath for 20 min. Resin was washed with 0.05% PBST containing 0.5 M NaCl.

For elution, resin was incubated 3x 30 min at RT with GST elution buffer. Elution fractions were analysed by SDS-PAGE and Coomassie Blue and selected fractions were pooled together. Buffer formulas are available in Appendix 2 (9.4).

Proteins were dialysed for 5 h and then overnight against 10 mM HEPES and 150 mM NaCl or PBS with 5-10% glycerol using 10 kDa molecular weight cut-off Slide-A-Lyser dialysis cassette, according to manufacturer's instructions (Thermo Fisher).

GST-tag cleavage was performed on GSH-resin or after dialysis (with subsequent GST-tag reabsorption) by 1 h incubation with thrombin (Sigma), at RT or 37°C. Thrombin was inactivated with 0.3 mM phenylmethylsulfonyl fluoride (PMSF) for 15 min at 37°C.

Proteins were concentrated using Amicon® Ultra-4 Centrifugal Filter Units with 10-30 kDa molecular weight cut-off according to manufacturer's instructions (MerckMillipore).

2.2.2.8.2 His_6-tag purification

Bacterial extract was prepared in His_6 lysis buffer, as described above, and His_6-PTPN23 proteins were purified using nickel-charged (Ni-NTA) resin (Qiagen), according to manufacturer's instructions. For purification, resin was washed multiple times with Ni-NTA wash buffer. Buffer formulas are available in Appendix 2 (9.4).

2.2.2.9 *In vitro* pull down assay and BICD1 mapping

GSH-resin, containing equal amounts of different GST-BICD1 recombinant proteins, was incubated for 1-2 h at 4°C with 0.5-1 ml of freshly prepared cell lysate from N2A-FLAG-TrkB cells overexpressing PTPN23 (5 µg plasmid per 10 cm dish of 80% confluent cells), lysed in 0.4% NP-40 lysis buffer or with equal volume of bacterial extracts containing equal amounts of His_6-PTPN23 proteins, in low protein binding microcentrifuge tubes. Next, resin was gently washed 4-6 times with appropriate buffer and pelleted by gravity, transferred to fresh tube and washed again. Bound proteins were eluted by boiling for 4 min at 95°C in 1x LSB, and analysed by SDS-PAGE and WB.

2.2.2.10 Mapping of PTPN23

Ni-NTA resin containing equal amounts of His_6-PTPN23 fragments was incubated with purified GST-BICD1 proteins or with GST as control (20 µg); *in vitro* pull down assay was conducted as above.

2.2.2.11 Cellular fractionation

N2A-FLAG-TrkB cells (one 10 cm dish, 80% confluent) were treated for 1 h with 0.5 mM sodium arsenite or vehicle control (as per oxidative stress assay protocol below). The cell fractionation method was based on Hua and Zhou (2004). Cells were placed on ice, washed twice with ice-cold PBS, and lysed in 500 µl fractionation buffer A (10 mM HEPES-NaOH, pH 7.8, 10 mM KCl, 0.1 mM EDTA, 0.1 mM EGTA, 1 mM DTT, 0.6% NP-40, 1 mM PMSF, protease inhibitor cocktail) for 15 min on ice. Sample was collected as total lysate fraction. Lysate was clarified by centrifugation for 10 min at 4°C at 14,000 RPM. Supernatant was collected as cytoplasmic fraction. Pellet was resuspended in 200 µl of fractionation buffer B (20 mM HEPES-NaOH, pH 7.9, 0.4 M NaCl, 1 mM EDTA, 1 mM EGTA, protease inhibitor cocktail) and incubated on ice for 1 h. Nuclear fraction was clarified by centrifugation for 15 min at 4°C at 14,000 RPM. Obtained supernatant was collected as nuclear fraction. Final pellet was resuspended in 200 µl 1x LSB, while other fractions (total lysate, cytoplasmic and nuclear extracts) were resuspended with 4x LSB. Then, 10 µl of total lysate, 15 µl of cytoplasmic extract, 15 µl of nuclear extract and 10 µl of final pellet were loaded for SDS-PAGE, and protein levels were analysed by WB.

2.2.3 Cell culture techniques

All cells were grown and maintained in humidified incubator at 37°C and supplemented with 5% CO_2. All procedures were performed in sterile laminar flow cabinet. Instruments and equipment were autoclaved and/or sterilized with 70% ethanol. Solutions were autoclaved or filter-sterilized by passing through 0.22 µm filter.

2.2.3.1 N2A-FLAG-TrkB and HEK293 culture

N2A-FLAG-TrkB and HEK293 cell lines were cultured in Dulbecco's modified Eagle's medium (DMEM) supplemented with 10% foetal bovine serum (FBS) and

1% GlutaMAX. Cells were passaged upon reaching 80% confluency. Briefly, cells were rinsed with PBS, to remove any residual medium, and incubated with 0.025% trypsin for 3 min at 37°C. Once detached, cells were collected in fresh complete medium, pelleted by centrifugation for 3 min at 1,000 RPM and re-suspended in 1 ml of fresh medium. Cells were seeded on a new tissue culture-treated dish or coated glass coverslips for ICC and microscopy.

2.2.3.2 Embryonic stem cell maintenance

Mouse embryonic stem (ES)-cells were maintained and differentiated into motor neurons (ES-MNs) as previously described (Wichterle et al., 2002; Debaisieux et al., 2015). In short, cells were grown in 0.2% fish skin gelatinized T25 tissue culture-treated flasks in ES-growth medium (5% ES-treated FBS, 5% KnockOut (KO) serum replacement, 1:100 GlutaMAX, 0.1 mM β-mercaptoethanol, LIF (1000 units/ml), in DMEM/F-12+GlutamMAX). To passage cells, they were washed with PBS and treated for 3 min with Accutase, collected in growth medium, and pelleted for 3 min at 1,000 RPM at RT. Cells were passaged (1:10) every other day.

2.2.3.2.1 Embryonic stem cell differentiation into motor neurons

For differentiation into motor neurons, ES cells were detached with Accutase, pelleted and resuspended in DFNK medium (10% KO serum replacement, 1:100 GlutaMAX, 0.1 mM β-mercaptoethanol, in 1:1 Neurobasal (NB):DMEM/F-12+GlutaMAX). Two million cells were seeded per one 10 cm sterile dish (non-tissue culture treated) in DFNK medium. For following 6 days, embryoid bodies, formed in suspension, were gently collected, pelleted by gravity and seeded in fresh DFNK medium. From third day onwards, DFNK medium was supplemented with 1 μM retinoic acid and 333 nM sonic hedgehog agonist. To dissociate embryoid bodies, they were pelleted by gravity, washed with sterile L-15 medium and incubated for 10 min at 37°C with Accumax (with gentle stirring every 3 min). Next, embryoid bodies were gently disaggregated by 10-15 strokes. Cells were passed through cell strainer to removed debris and incompletely disaggregated embryoid bodies, and then resuspended in motor neuron medium (2% B27, 2% HI-HS, 1:100 GlutaMAX, 25 nM β-mercaptoethanol, 1:200 PenStrep, 10 ng/ml CNTF, 0.1 ng/ml GDNF, 1 μM retinoic acid, in NB). Next, Cells were pelleted for 5 min at 1,000 RPM and seeded at desired density in motor neuron medium.

Motor neurons were assayed at DIV3. For ICC and confocal microscopy, cells were seeded on polyornithine- and laminin-coated glass coverslips.

2.2.3.3 Primary motor neuron culture

Primary ventral horn cultures for oxidative stress and receptor accumulation assays were kindly prepared by David Villarroel-Campos. In short, spinal cords were dissected from E12.5-E14.5 mouse embryos, meninges were removed and the ventral cord was separated, fragmented and then digested for 10 min with 0.025% trypsin at 37°C, followed by 2x trituration in DNase solution (0.1 mg/ml and 0.02 mg/ml). Cells were pelleted into 4% BSA “cushion” by centrifugation for 5 min at 1,500 RPM, and resuspended in motor neuron medium (as for ES-MNs, supplemented with 1 ng/ml BDNF). Extracted cells from one spinal cord were seeded onto 5-6 coated glass coverslips.

2.2.4 Cell-based assays

All assays on live cells were performed in humidified incubator at 37°C and supplemented with 5% CO_2, unless stated otherwise.

2.2.4.1 Receptor internalization and accumulation assay

Cells were washed twice with DMEM (N2A-FLAG-TrkB cells) or NB (motor neuron cultures), and serum-starved for 3-5 h. An antibody targeting extracellular epitope of neurotrophin receptor (1:1000 α-TrkB, #AB9872, Millipore; 1:1000 α-$p75^{NTR}$, stock 0.9 mg/ml, #CRD 5410, CRUK; 1:500 FLAG-M1, #F3040, Sigma) was added to cells for 30 min at 37°C. Next, to facilitate antibody-receptor complex uptake, 100 ng/ml BDNF was added to the cultures for 15-60 min. To remove unbound and cell surface-coating α-TrkB and α-$p75^{NTR}$ antibodies, cells were pre-chilled on ice for 5 min and washed for 1-2 min with ice-cold acid wash solution. For FLAG-M1 antibody, cells were washed on ice with calcium- and magnesium-free PBS, supplemented with 1 mM EDTA. Following that, cells were washed with ice-cold PBS on ice and fixed with 4% PFA/PBS for 15 min at RT. Next, cells were processed by standard ICC protocol. Internalized antibody-receptor complex was visualized by fluorescently-labelled secondary antibodies (1:1000 anti-rabbit for α-TrkB and α-$p75^{NTR}$; 1:500 anti-mouse for FLAG-M1) and

confocal microscopy. Mouse and rabbit immunoglobulins (IgG) were used alone or in combination with fluorescently-conjugated CTB as controls.

Endosomes, containing α-p75^{NTR}, had a distinct morphology in PTPN23 knockdown (KD) cells. For endosome classification and size distribution analysis, five fields were imaged by confocal microscopy at 2.7x magnification using 63x objective. FIJI was used to measure the diameter of randomly chosen 100 endosomes (with selection criteria of 50 “large” and 50 “small”) per genotype (PTPN23 KD and scrambled), in three independent experiments. Endosomes were then classified, with binning every 0.5 µm, as endo-lysosomes (diameter 0-2 µm) or vacuoles (2-5 µm). Diameter frequency graph was generated in GraphPad Prism.

To establish proportion of cells with either endosomal phenotype, 5-7 random fields were imaged per genotype at 1x magnification using 63x objective, and cells containing puncta or vacuole, as well as total number of cells per field (average of 80 cells per field) were counted, in three independent experiments.

2.2.4.1.1 Transmission electron microscopy

To validate the localization of α-p75^{NTR} by transmission electron microscopy (TEM) in N2A-FLAG-TrkB cells transduced with PTPN23 KD or scrambled lentiviruses, anti-p75^{NTR} antibody (#CRD 5410, CRUK) was conjugated to 5 nm colloidal gold nanoparticles (α-p75^{NTR}-gold, stock 0.9 mg/ml). Antibody-gold conjugation was kindly prepared by Prof. Giampietro Schiavo, as described previously (Terenzio et al., 2014a). Accumulation assay using α-p75^{NTR}-gold (1:500) was performed as described above. After acid wash on ice, cells were washed once with PBS, and once with DMEM. Next, cells were fixed for 15 min at RT in 8% PFA in Sorenson’s buffer (133 mM Na_2HPO_4, 133 Mm KH_2PO_4) diluted 1:1 with DMEM (final concentration: 4% PFA). Next, cells were post-fixed with 2.5% glutaraldehyde and 4% PFA in Sorenson’s buffer for the following 20 min. Cells were stored at 4°C in 1% PFA in Sorenson’s buffer. Samples were processed for TEM and imaged by Anne Weston at The Francis Crick Institute (London). Sections and grids were scanned for the presence of gold. Equal number of images was obtained for both genotypes, and all gold-containing internal structures were imaged. Then, gold-containing organelles were classified as tubulo-vesicular/early endosome (membranous or tubular structures, absent

for electron-dense components; <500 nm), late endosome/lysosome (electron-dense structures, including multilamellar bodies and late endo-lysosome fusion organelles), or vacuoles (large bodies absent for internal membranous structures, reminiscent of enlarged early endosome >500 nm) (Bright et al., 1997; Stefan et al., 2017).

2.2.4.2 Inhibition of protein degradation

N2A-FLAG-TrkB cells were transduced with scrambled or PTPN23-targetting shRNA lentivirus for 72 h (DIV3 post-transduction). To prevent proteasomal protein degradation, cells were treated with MG132 for 5 h (15 µM) or overnight (5 µM). To prevent lysosomal degradation, cells were treated with bafilomycin A1 (BafA1) for 5 h (0.5 µM) or overnight (100 nM). For 5 h treatment, drug was added at DIV3 post-transduction. For overnight treatments, drug was added at DIV2 post-transduction. Next, cells were lysed on ice in RIPA buffer, and protein levels were analysed by SDS-PAGE and WB.

2.2.4.3 Oxidative and endoplasmic reticulum stress assay

One hour prior to stress induction, cells were washed once with DMEM (N2A-FLAG-TrkB) or NB (motor neurons). To induce oxidative stress, 0.1-0.5 mM sodium arsenite ($NaAsO_2$), 0.25-1 mM hydrogen peroxide (H_2O_2) or vehicle control was added to cells for 1 h. To induce endoplasmic reticulum (ER) stress, 15 µM thapsigargin (Thap) was added for 1 h. For drug stock concentrations, vehicles and targets refer to Appendix 2 (9.5). Next, cells were placed on ice for 5 min and washed with ice-cold PBS. Cells were fixed with 4% PFA/PBS for 5 min on ice and 10 min at RT. Cells were processed by standard ICC protocol to detect stress granules (using an anti-G3BP and anti-FMRP antibodies as stress granule markers) and co-localizing proteins. To analyse the overlap between G3BP or FMRP and BICD1 or PTPN23, fluorescence intensity of each protein was measured (in separated channels) over 1.5-4 µm line (1-10 pixel thickness), drawn across stress granule in FIJI. Measurements were imported, and intensity plots generated using GraphPad Prism.

To count cells positive for stress granules, 4-5 fields were imaged per condition (with average of 50 cells per field), at 1x magnification using 63x objective, in three independent experiments. Cells bearing multiple (>3) clearly distinguishable foci (>0.5 µm in diameter), visualised using anti-G3BP antibody,

were scored as positive, in line with other reports (Loschi et al., 2009; Fay and Anderson, 2018; Xie et al., 2018). All cells were cross-examined through the Z-plane for the presence of stress granules.

The same methodology was used to analyse stress granule-positive cells after transduction with scrambled/PTPN23 KD lentivirus (72h post-infection), using G3BP or FMRP as stress granule markers, in three independent experiments per marker per genotype. In PTPN23 KD experiments, 10 fields per genotype (with average of 10 cells in total per field) were imaged at 2.7x magnification using 63x objective. To analyse BICD1 intensity in G3BP- or FMRP-positive stress granules, in PTPN23 KD or scrambled cells, G3BP and FMRP channels were thresholded and used as mask, and intensity of both proteins and BICD1 was determined using FIJI. Using mask of G3BP and FMRP, distribution of stress granule areas was determined using 0.2 μm^2 binning (cut-off >0.2 μm^2) in PTPN23 KD and scrambled cells.

2.2.4.4 Time course of stress granule assembly and disassembly

For stress granule assembly, N2A-FLAG-TrkB cells were washed 1 h prior to stress induction, and 0.5 mM $NaAsO_2$ was applied for 10–60 min (with 10 min increments) and 2 h. For stress granule disassembly, cells were treated for 1 h with 0.5 mM $NaAsO_2$, washed with DMEM, and left to recover for 30-60 min (fixation at 10 min increments). Cells were washed and fixed, as described above, and immunostained using anti-G3BP and anti-BICD1 antibodies.

2.2.4.5 Stress granule disassembly by polysome stabilization

One hour prior to stress induction, cells were washed once with DMEM (N2A-FLAG-TrkB) or NB (motor neurons), and treated for 1 h with 0.25 mM $NaAsO_2$, followed by 30 min treatment with 50 µg/ml cycloheximide, added in the presence of $NaAsO_2$. Appropriate vehicle controls were included. Cells were washed and fixed, before processing by ICC, as described above.

2.2.4.6 The Golgi apparatus and cytoskeleton disassembly

To promote disassembly of the Golgi apparatus, N2A-FLAG-TrkB cells were treated for 1 h with 10 µg/ml brefeldin A (BrefA); verified by ICC using anti-GM130 antibody as control. To promote depolymerization of actin cytoskeleton, cells were treated for 1 h with 0.5 µM latrunculin B (LatB); verified by staining with

phalloidin-AlexaFluor488. To promote disassembly of microtubules, cells were treated for 1 h with either 20 µg/ml nocodazole or 5 µM vincristine; verified by ICC using anti-βIII-tubulin antibody (#mms-435p, Covance). To assess the effect of the Golgi apparatus or cytoskeleton disassembly on stress granule formation, cells were treated with abovementioned drugs for 2 h. After 1 h, 0.5 mM $NaAsO_2$ was added. Cells were processed by ICC and analysed by confocal microscopy.

2.2.4.7 $p75^{NTR}$ accumulation assay in oxidative/ER stress

N2A-FLAG-TrkB cells and motor neurons were washed and serum-starved for 2 h as described above. Next, vehicle control, $NaAsO_2$, H_2O_2 or thapsigargin (concentrations indicated in figure legends) or vehicle control was added for 45 min, followed by addition of α-$p75^{NTR}$ (1:1000; #CRD 5410, CRUK). After 15 min, cell were stimulated for the following 1 h with 100 ng/ml BDNF. Drugs were present during receptor accumulation assay. Next, cells were placed on ice, acid-washed, fixed and processed by ICC, as described above.

To analyse the correlation between stress granules and α-$p75^{NTR}$ accumulation, cells were treated with 0.5 mM $NaAsO_2$ or vehicle, and immunostained using an anti-G3BP antibody. Cells were scored for stress granules and accumulated perinuclear α-$p75^{NTR}$ puncta. Five random fields were imaged per condition in three independent experiments (with average of 60 cells per field). Images were acquired at 1x magnification using 63x objective. All cells were cross-examined through the Z-plane for presence of stress granules and internalized α-$p75^{NTR}$.

To analyse the effect of oxidative stress on the endocytic pathway, CTB was added at the same time as α-$p75^{NTR}$, in the presence of abovementioned drugs. Cells positive for internalized CTB, with distinct peri-Golgi accumulation, were counted as positive. Cells with distinct perinuclear α-$p75^{NTR}$ puncta were counted as positive. Cells positive for CTB and α-$p75^{NTR}$ were counted as double-positive. Five random fields were imaged per condition and positive/double-positive cells were counted (with average of 80 cells in total per field), in three independent experiments. Images were acquired at 1x magnification using 63x objective. All cells were cross-examined through the Z-plane for the presence of each probe.

2.2.4.8 Wheat germ agglutinin staining

Following α-$p75^{NTR}$ accumulation assay, cells were placed on ice, acid-washed, and subsequently washed 3x with Hank's balanced salt solution (HBSS, without

phenol red). Next, cells were incubated on ice for 40 min with wheat germ agglutinin (WGA) conjugated to AlexaFluor647 (diluted 1:200 in HBSS). Cells were then washed three times with HBSS and once with PBS, fixed with 4% PFA/PBS for 15 min, and processed by standard ICC.

2.2.4.9 BDNF signalling

Cells were washed and serum-starved for 3-5 h, as described before. Next, cells were stimulated for 2 or 5 min with 100 ng/ml BDNF (in DMEM or NB). In all BDNF signalling assays, timepoint “0” refers to addition of DMEM or NB, not supplemented with BDNF, for the duration equivalent to BDNF stimulation. Cells were immediately placed on ice, and proteins were extracted in RIPA buffer. Lysates were assayed by SDS-PAGE and WB. Densitometry of phosphorylated AKT, ERK1/2 and TrkB was performed using total AKT, ERK1/2 and TrkB as loading controls.

For BDNF signalling under oxidative stress conditions, cells were washed and serum-starved for 3 h. Next, vehicle control, $NaAsO_2$, H_2O_2 or thapsigargin (concentration indicated in figure legends) was added for 1 h, followed by 2 or 5 min stimulation with BDNF. Cells were placed on ice, proteins extracted in RIPA buffer, and lysates analysed by SDS-PAGE and WB.

To determine the effect of $NaAsO_2$ and H_2O_2 on BDNF signalling ability, motor neurons were subjected to oxidative stress or treated with vehicle control for 1 h, washed with NB, and BDNF was applied for 5 min either immediately or after 30 min of stress recovery. Next, proteins were extracted for SDS-PAGE and WB, as described above.

To determine the level of AKT and ERK1/2 activation after BDNF stimulation in motor neurons subjected to oxidative stress, starved cells were stressed for 1 h or treated with vehicle control, and stimulated for 5 min with or without BDNF, as described above. Next, cells were placed on ice, fixed and immunostained using anti-pAKT or anti-pERK1/2 antibodies, and an anti-βIII-tubulin antibody as neuron-specific marker, and analysed by confocal microscopy. Fluorescence intensity of pAKT and pERK1/2 was determined in FIJI, using βIII-tubulin as mask for neuronal cells (pAKT and pERK1/2), or outside of βIII-tubulin mask for non-neuronal cells (pERK1/2 only), in cells stimulated with or without BDNF. Five

fields were imaged per condition at 2.7x magnification using 63x objective. Fluorescence intensity plots were generated in GraphPad Prism.

2.2.5 Statistical analysis

All image analyses were performed using Fiji (ImageJ, Version: 2.0.0-rc-65/1:51u). Prism 6 (GraphPad, La Jolla, CA, USA) was used for all statistical analyses and to visualize the data throughout this thesis. Datasets were analysed using unpaired two-tailed Student's *t*-test, and one- or two-way analysis of variance (ANOVA), with Bonferroni's/Dunnett's multiple comparisons test, where appropriate. X^2 test (chi-square test for trend) was used to analyse the difference in endosome/stress granule size distribution. All graphs show mean values, and error bars show ±standard error of the mean, unless stated otherwise, with significance stated in the legends or main text. "N" numbers represent biological replicates.

3 Exploring the BICD1-PTPN23 interaction

3.1 Aims of this chapter

Our laboratory has previously demonstrated that the dynein adaptor BICD1 is a master regulator of NTR turnover in embryonic stem cell-derived motor neurons (ES-MNs). BICD1 enables the lysosomal degradation of BDNF-activated TrkB/p75^{NTR}, while its depletion leads to increased NTR accumulation in enlarged endocytic compartments in the neuronal soma, as well as increased plasma membrane recycling of dominant-negative TrkB-T1 receptor, an adaptive neuronal response regulating the amplitude and duration of BDNF-mediated signalling (Terenzio et al., 2014a).

A proteomic analysis of BICD1-interacting partners, performed by co-immunoprecipitation from N2A cells stably expressing FLAG-tagged TrkB (N2A-FLAG-TrkB) and ES-MNs, and identified by mass spectrometry (Golding and Schiavo, unpublished), revealed a potential novel BICD1 binding protein, PTPN23, which has an established role in receptor turnover in non-neuronal cells (Kharitidi et al., 2015; Ma et al., 2015; Gahloth et al., 2017). Importantly, the effect of PTPN23 knockdown on epidermal growth factor receptor (EGFR) sorting in HeLa cells (Doyotte et al., 2008) phenotypically resembles BICD1 depletion. PTPN23 depletion leads to an increased accumulation of ubiquitinated EGFR in aberrant early endosomes, subsequently reducing its lysosomal degradation. To better understand the molecular machinery regulating the sorting of NTRs, the initial goal of this work was to explore the BICD1-PTPN23 functional interaction in neuronal cells, using biochemical approaches, such as co-immunoprecipitation and *in vitro* binding assays, as well as fluorescence microscopy.

3.2 Results

3.2.1 PTPN23 co-immunoprecipitates with BICD1

First, I aimed to validate the main findings of the proteomic screen (Appendix 1) by co-immunoprecipitation (co-IP) and western blotting. For co-IPs, all steps, including generation of soluble protein lysates, were performed at 4°C; co-IP beads were washed four times in lysis buffer, prior to elution of antibody-protein

complexes by boiling the beads in the presence of SDS for 4 min at 95°C (see Methods for details).

Initially, GFP-BICD1 and HA-PTPN23 were overexpressed overnight in human embryonic kidney 293 (HEK293) cells. Lysates, extracted in radioimmunoprecipitation assay (RIPA) buffer, were then incubated for 1 h with Dynabeads, pre-bound with an anti-GFP antibody raised in mouse or with mouse immunoglobulins (IgG) as control. Antibody-free beads were used as an additional control. Analysis of co-IP by SDS-PAGE and western blotting, using anti-HA and anti-GFP antibodies, revealed a specific immunoprecipitation of HA-PTPN23 with GFP-BICD1, albeit at a very low level (Figure 3.1A).

BICD1 and BICD2 exist as homodimers in cells (Hoogenraad et al., 2001; Liu et al., 2013; Terawaki et al., 2015) and share high sequence homology, in particular between their C-terminal cargo-binding coiled coil 3 (CC3; Figure 3.1B) (Terenzio and Schiavo, 2010). Identification of BICD2 as a potential BICD1 binding partner (Appendix 1) raised a possibility that these proteins associate with each other and/or share their interactome, as previously demonstrated for Rab6 (Matanis et al., 2002). For these reasons, I assessed whether PTPN23 co-precipitates specifically with BICD1.

HA-PTPN23 was overexpressed overnight, together with GFP-BICD1 or GFP-BICD2, in N2A-FLAG-TrkB cells. Because a relatively low level of HA-PTPN23 was detected in the GFP-BICD1 co-IP when lysates where generated in RIPA buffer (Figure 3.1A), proteins were extracted in a less-stringent lysis buffer (0.4% NP-40) from N2A-FLAG-TrkB cells. Then, lysates containing overexpressed proteins were incubated for 1 h with GFP-trap beads, and eluates were evaluated by immunoblotting using anti-HA and ani-GFP antibodies (Figure 3.1C). As previously (Figure 3.1A), HA-PTPN23 precipitated with GFP-BICD1, but not with GFP-BICD2 (Figure 3.1C), suggesting that the PTPN23-BICD1 interaction is specific.

Crucially, this association using endogenous BICD1 and PTPN23 was validated. Lysates of N2A-FLAG-TrkB cells in 0.4% NP-40 lysis buffer were subjected to co-IP using Dynabeads pre-coated with anti-BICD1 antibody raised in rabbit, or rabbit IgG as control. In line with the above results (Figure 3.1A,C), PTPN23 was

successfully detected by immunoblotting using anti-PTPN23 antibody specifically in the BICD1-immunoprecipitated fraction (Figure 3.1D).

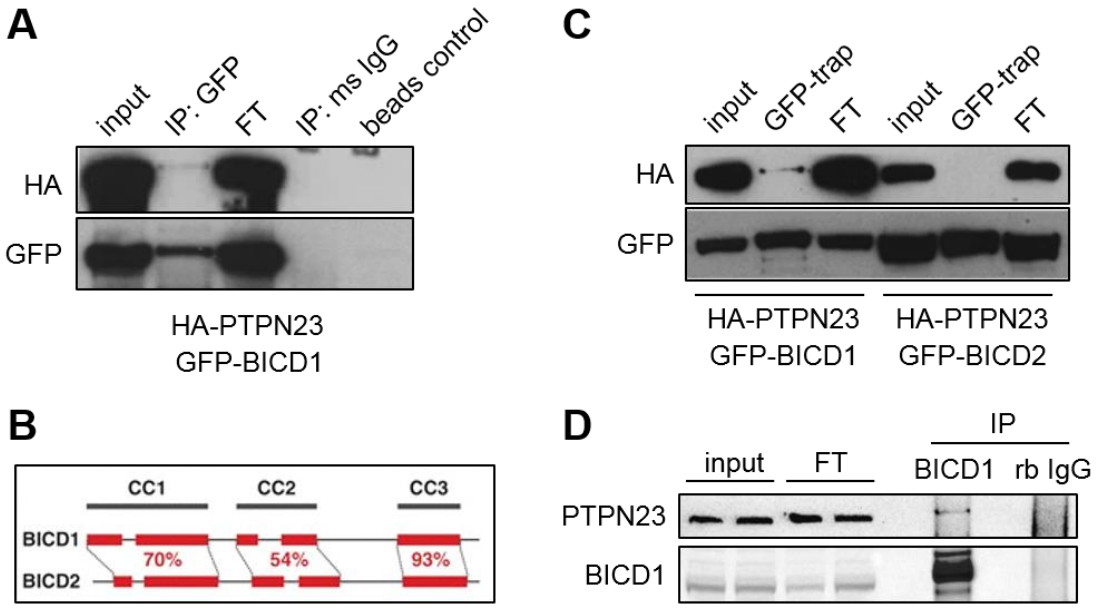

Figure 3.1 PTPN23 co-immunoprecipitates with BICD1 in mammalian cell lysates.

A) HEK293 cells overexpressing HA-PTPN23 and GFP-BICD1 were lysed in RIPA buffer and subjected to co-IP, using Dynabeads pre-coated with an anti-GFP antibody, or mouse IgG as control. Empty beads were used as an additional control. Samples, immunoblotted using anti-HA and anti-GFP antibodies, revealed that a small fraction of HA-PTPN23 immunoprecipitated (IP) with GFP-BICD1 (n=2). B) Schematic representation of BICD1 and BICD2 domain structure, depicting the sequence similarities (as percentage) within each coiled coil (CC) (adapted from Terenzio and Schiavo, 2010). C) N2A-FLAG-TrkB cells, overexpressing HA-PTPN23 and GFP-BICD1 or GFP-BICD2, were serum-starved for 3 h in DMEM. Cell extracts, prepared in 0.4% NP-40 lysis buffer, were subjected to co-IP using GFP-trap beads. HA-PTPN23 associated specifically with GFP-BICD1, but not with GFP-BICD2, as shown by western blotting using anti-HA and anti-GFP antibodies (n=1). D) N2A-FLAG-TrkB cells were serum-starved for 3 h, and proteins extracted in 0.4% NP-40 lysis buffer. Lysates were subjected to co-IP using anti-BICD1 or rabbit IgG as control, bound to Dynabeads. SDS-PAGE and western blotting using anti-BICD1 and anti-PTPN23 antibodies revealed immunoprecipitation of endogenous PTPN23 with BICD1 (n=5). For all SDS-PAGE and western blotting, 1/50 of soluble lysate used for co-IP was loaded as input, 1/50 of post-co-IP lysate as flow through (FT), and whole eluate, extracted by boiling for 3 min at 95°C in 1x Laemmli sample buffer, as IP/GFP-trap fraction (see Methods for details and composition of lysis buffers).

3.2.2 BICD1 and PTPN23 co-distribute in the perinuclear region

To further explore the relationship between BICD1 and PTPN23, the distribution of these proteins was assessed by immunocytochemistry and confocal microscopy in fixed N2A-FLAG-TrkB cells (Figure 3.2). As expected, immunostaining revealed that endogenous BICD1 and PTPN23 had predominantly a punctate cytoplasmic distribution throughout the cell, suggesting

their association with vesicles and membranous organelles. The enrichment of BICD1 was observed at the tips of protrusions, while PTPN23 was highly abundant near the cell surface. Partial co-distribution of both proteins could be detected in these areas (Figure 3.2A,B). Although the highest level of enrichment and co-distribution between BICD1 and PTPN23 was observed in the perinuclear region (Figure 3.2A,B), in line with previous studies reporting the localization of the individual proteins (Matanis et al., 2002; Wanschers et al., 2007; Doyotte et al., 2008; Husedzinovic et al., 2014), their immunostaining was only partially overlapping in this area (Figure 3.2B').

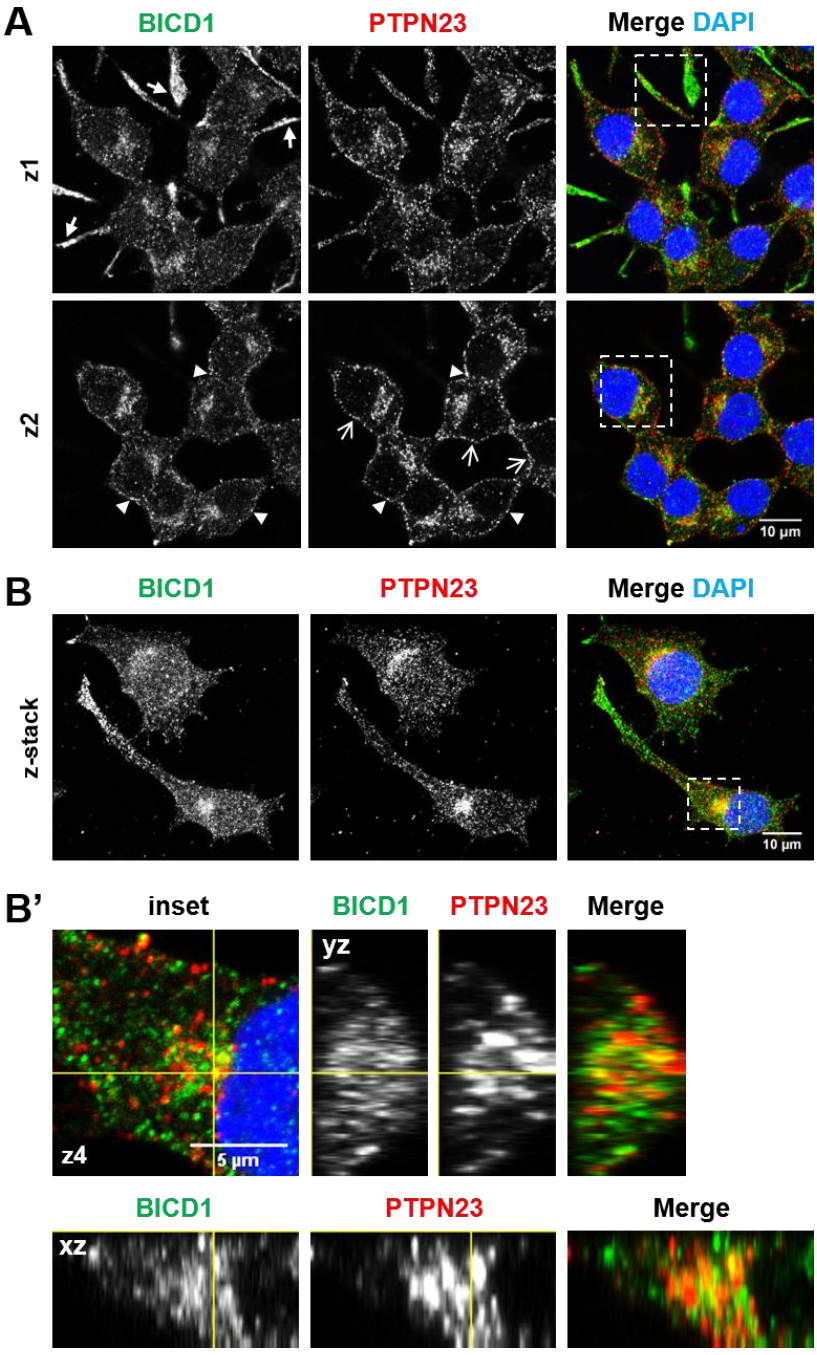

Figure 3.2 BICD1 and PTPN23 partially co-distribute in the perinuclear region of N2A-FLAG-TrkB cells.

A) Representative confocal images of N2A-FLAG-TrkB cells, fixed and immunostained for BICD1 and PTPN23. Both proteins are enriched in the perinuclear region. BICD1 is highly abundant in protrusions (arrows), while PTPN23 is enriched near the cell surface (open arrows), where they partially co-localize (arrowheads; A,B) (n=6). Images show two selected frames (z1 and z2) from a Z-stack projection. B) Z-stack projection, acquired at 0.5 µm spacing, showing BICD1 and PTPN23 immunostaining, partially overlapping in the perinuclear region. B') Magnification of a selected frame from the dashed rectangle area in B, and yz and xz view of BICD1 and PTPN23 co-localization within the dashed rectangle are in the Z-stack in B.

Next, the co-distribution of endogenous BICD1 and PTPN23 was assessed in ES-MNs. At day *in vitro* 3 (DIV3), ES-MNs were fixed and immunostained for BICD1 and PTPN23, as well as the neuronal marker βIII-tubulin (Figure 3.3A,B). BICD1 and PTPN23 exhibited a punctate staining pattern; they were detected in the neuronal soma and in the neurites. Similarly to N2A-FLAG-TrkB cells (Figure 3.2), a significant enrichment of these proteins could be observed in the perinuclear region (Figure 3.3A,B), where fluorescence intensity profiles of both proteins partially overlapped (Figure 3.3C).

Mass spectrometry analysis revealed that BDNF stimulation may influence the interaction of BICD1 with PTPN23 (Appendix 1). To assess whether stimulation with BDNF affects their co-localization, ES-MNs were serum-starved in Neurobasal (NB) for 3 h and stimulated with or without 100 ng/ml BDNF for 1 h. Confocal microscopy revealed that perinuclear enrichment and co-distribution of BICD1 and PTPN23 was independent of BDNF stimulation (Figure 3.3D), verified by co-localization analysis using Manders coefficient (Figure 3.3E). Confocal microscopy (Figure 3.3A,D) and co-localization analysis (Figure 3.3E) was conducted by David Villarroel-Campos, as a part of an experimental project for MSc Neuromuscular Disease, UCL Institute of Neurology (2016).

To summarize, in line with previous reports, BICD1 and PTPN23 exhibit punctate immunostaining in the neuronal cells, suggestive of their interaction with membrane vesicles. Significant enrichment of both proteins is particularly evident in the perinuclear region, where they partially co-localize, due to their association with the endo-lysosomal system (Matanis et al., 2002; Wanschers et al., 2007 Doyotte et al., 2008; Tanase, 2010). However, fluorescence intensity profiles of BICD1 and PTPN23 in the perinuclear region slightly differ (Figure 3.2C; Figure 3.3C), and their co-localization is not further influenced by BDNF stimulation

(Figure 3.3E), implying a partial overlap between these proteins within the endocytic system.

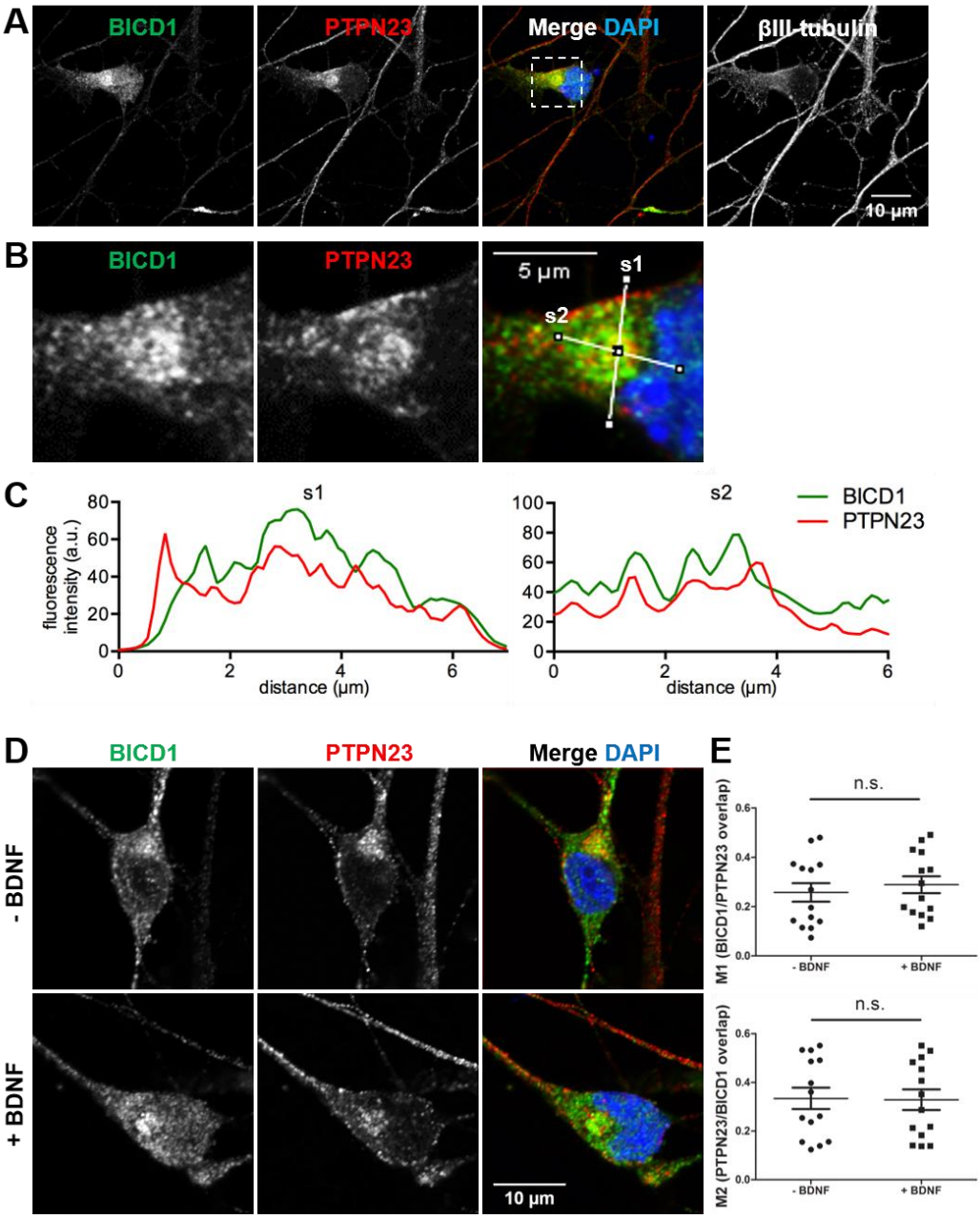

Figure 3.3 BDNF stimulation does not affect BICD1 and PTPN23 co-localization in pMNs.

A) Representative confocal images of ES-MNs, fixed and immunostained for BICD1, PTPN23 and the neuronal marker, βIII-tubulin, in addition to DAPI (n=4). B) Magnification of dashed rectangle area in A. C) Fluorescence intensity profiles of BICD1 and PTPN23 along the lines s1 and s2 (1 pixel wide), visible in merged image in B, showing enrichment and partial overlap of both proteins in the perinuclear region. D) ES-MNs were serum-starved in NB for 3 h and stimulated with or without BDNF for 1 h. Representative confocal images show that perinuclear enrichment of BICD1 and PTPN23 is not significantly affected by BDNF stimulation. E) Quantification of BICD1 and PTPN23 co-localization (from D), using Mander's coefficient, showing no effect of BDNF stimulation on the level of co-localization between these proteins in ES-MNs. Analysis of 14 neurons per condition; not significant (n.s.) $p>0.05$, Student's *t*-test.

In neuronal cells, BICD1 and PTPN23 exhibit a characteristic enrichment in the perinuclear region (Figure 3.2; Figure 3.3); a subcellular compartment where the Golgi apparatus resides and endo-lysosomal organelles are highly abundant (Huotari and Helenius, 2011). While the role of BICD1 in the *trans*-Golgi network (TGN)-related transport is well-documented (Matanis et al., 2002; Wanschers et al., 2007), the association of PTPN23 with this organelle has not been extensively characterized (Doyotte et al., 2008; Husedzinovic et al., 2014). Interestingly, a study identifying novel mammalian proteins mediating the endosome-to-TGN retrieval of cation-independent mannose 6-phosphate receptor (CIMPR) suggested a potential involvement of PTPN23 in this process. Although its role was not extensively explored, a pilot screen of PTPN23 knockdown showed a reduced CD8-CIMPR reporter retrieval at the Golgi (Breusegem and Seaman, 2014).

To explore the relationship between PTPN23 and the TGN, I assessed the effect of brefeldin A (BrefA) on the co-distribution of the Golgi apparatus resident proteins, BICD1 (Figure 3.4A) and Rab6 (Figure 3.4B), with the *cis*-Golgi network (CGN) marker GM130, and between PTPN23 and TGN46 (Figure 3.4C). Due to lack of antibody species compatibility, the distribution of PTPN23 relative to GM130, and BICD1 relative to TGN46, could not be demonstrated. Brefeldin A inhibits transport from the endoplasmic reticulum (ER) back to the Golgi apparatus, leading to the progressive disassembly of the Golgi apparatus (Fujiwara et al., 1988).

In vehicle-treated N2A-FLAG-TrkB cells, BICD1 and Rab6 immunostaining highly overlapped with GM130 (Figure 3.4A,B). However, both proteins could be detected in the proximal structures lacking GM130 staining, suggestive of the TGN. Treatment with brefeldin A led to disassembly of the CGN, and dispersal of BICD1 and Rab6 immunostaining.

Although PTPN23 partially co-localized with TGN46 in vehicle-treated ES-MNs, treatment with brefeldin A had no effect on the perinuclear accumulation of PTPN23, whilst peripheral redistribution of TGN46 was observed, as expected (Figure 3.4C). These preliminary results suggest that while PTPN23 partially co-localizes with the Golgi components, its perinuclear accumulation is independent of the integrity of the Golgi apparatus and the presence of BICD1.

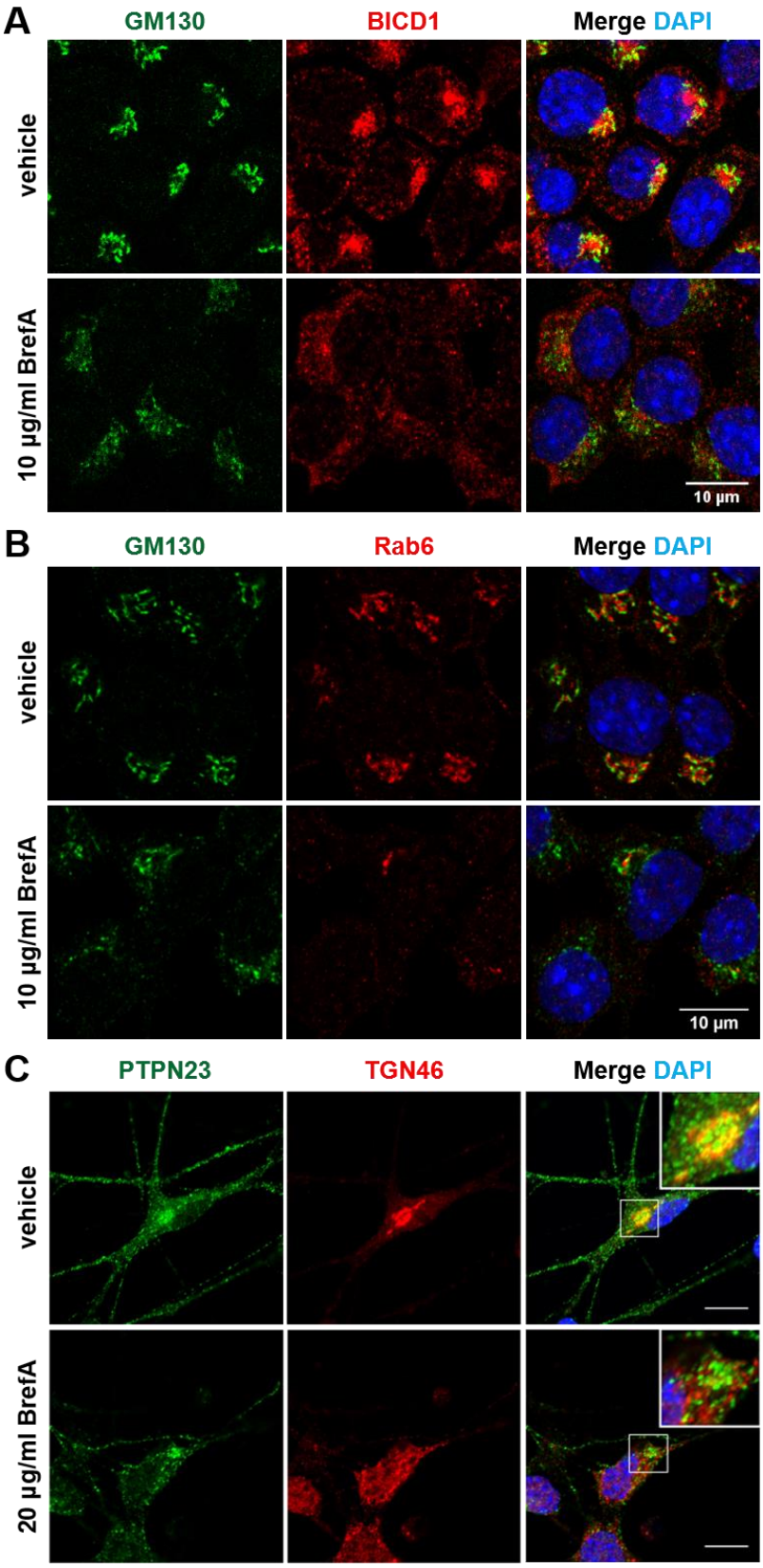

Figure 3.4 BICD1, but not PTPN23, resides in the Golgi apparatus.

A,B) Representative confocal images of N2A-FLAG-TrkB cells treated for 1 h with 10 µg/ml brefeldin A (BrefA) or vehicle control. Cells were fixed and immunostained for GM130 and BICD1 (B) or Rab6 (C) (n=2). C) Confocal images of ES-MNs treated for 1 h with 20 µg/ml brefeldin A or vehicle control, fixed and immunostained for PTPN23 and TGN46 (experiment kindly performed by David Villarroel-Campos; n=1). Scale bar: 10 µm.

3.2.3 PTPN23 interacts with the first coiled coil domain ($CC1^{95-265}$) of BICD1

Following successful validation of the BICD1-PTPN23 interaction by co-IP (Figure 3.1) and their partial co-distribution by microscopy (Figure 3.2; Figure 3.3), I next addressed the determinants of the BICD1-PTPN23 binding at the molecular level. To start, I focused my attention on BICD1, and hypothesized that its C-terminal CC3, which is responsible for binding to cargoes such as Rab6 and RanBP2 (Matanis et al., 2002; Terawaki et al., 2015), may also promote the recruitment of PTPN23. To explore the BICD1-PTPN23 interaction, a series of *in vitro* pull downs was set up, summarized below (see Methods for details on cloning, protein purification and pull down assays).

First, different regions of BICD1 were subcloned into an N-terminal glutathione S-transferase (GST)-expressing vector (Figure 3.5A). Then, GST-BICD1 fusion proteins and GST control were expressed in SoluBL21 *E. coli* (Amsbio), a strain which improves the solubility of mammalian proteins. After assessing the expression level and solubility of GST-BICD1 fusion proteins by SDS-PAGE and western blotting using an anti-GST antibody, proteins were purified from soluble bacterial extracts using glutathione (GSH) agarose affinity resin. Next, proteins were eluted from equal volume of GSH resin by boiling for 4 min at 95°C, and assessed by Coomassie Blue and immunoblotting. For pull downs, beads containing equal amounts of GST fusion proteins was incubated for 2 h at 4°C with N2A-FLAG-TrkB cell lysate, prepared in 0.4% NP-40 lysis buffer, containing overexpressed HA-PTPN23. Then, samples were assessed by SDS-PAGE, Ponceau S and immunoblotting using an anti-HA antibody (Figure 3.5B-D).

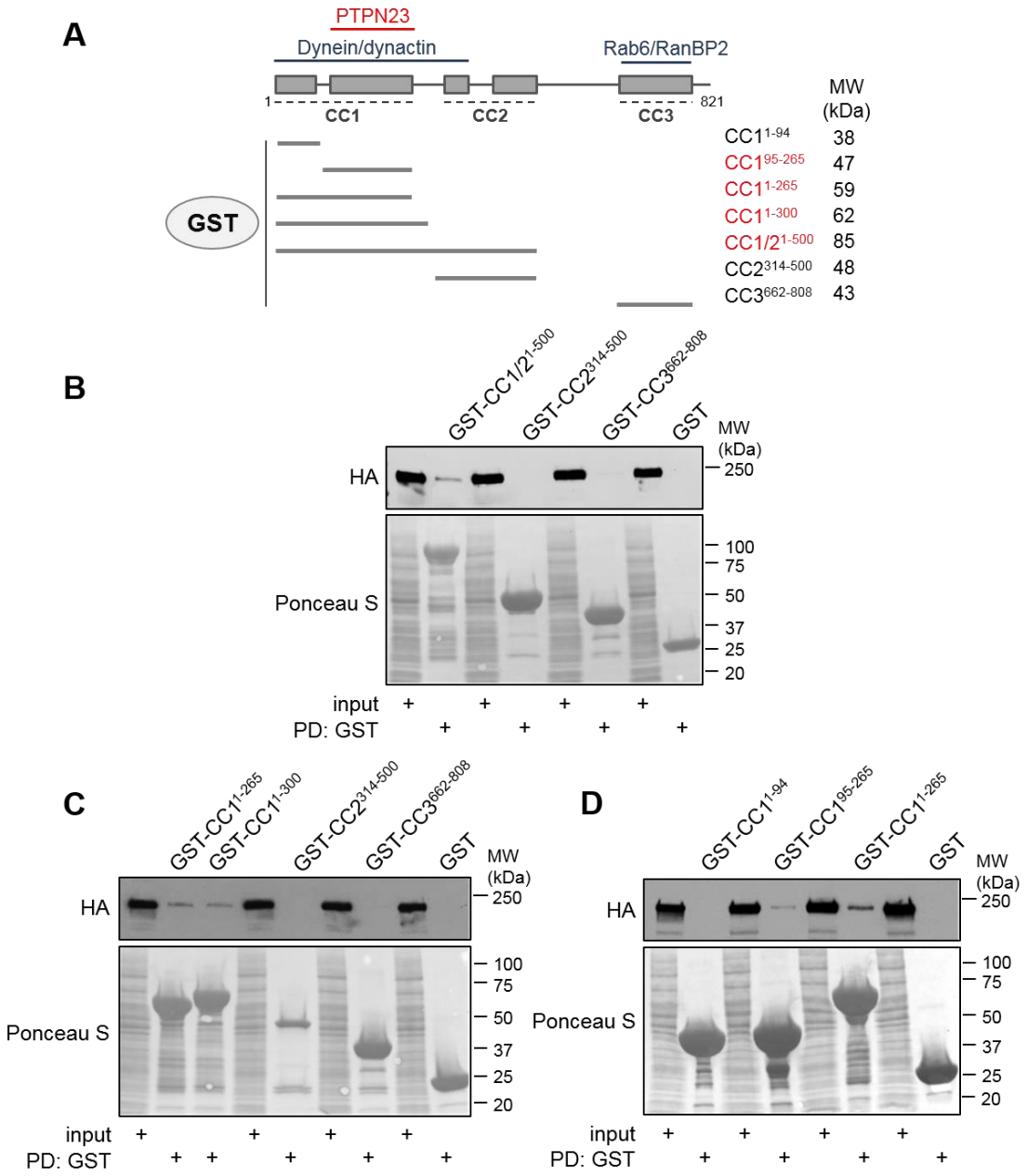

Figure 3.5 BICD1 interacts with PTPN23 via CC1$^{95-265}$.

A) Schematic representation of BICD1 domain architecture, showing coiled coil (CC) domains and highlighting the known binding regions for dynein, Rab6 and RanBP2. Below, a schematic of GST-BICD1 fusion proteins, with predicted molecular weight (MW), used for *in vitro* pull down assays. GST-BICD1 fragments in red bind PTPN23. B,C,D) GST-BICD1 proteins were expressed in bacteria and purified using GSH resin. Then, resin containing equal amounts of GST-BICD1 proteins was incubated with N2A-FLAG-TrkB cell lysates, containing overexpressed HA-PTPN23. Pulled down (PD) proteins were eluted by boiling, and assessed by SDS-PAGE and immunoblotting using an anti-HA antibody. BICD1-CC1$^{95-265}$ co-precipitates HA-PTPN23 (n=6). For input, 1/50 of N2A-FLAG-TrkB lysate was loaded; for pull down, whole eluted fraction. Ponceau S shows whole lysates and GST-BICD1 fragments used in pull downs.

To assess which BICD1 region associates with PTPN23, recombinant GST-BICD1 fusion proteins spanning the N-terminal CC1/2$^{1-500}$, middle CC2$^{314-500}$ or C-terminal CC3$^{662-808}$ were generated (Figure 3.5A). Surprisingly, GST-CC1/2$^{1-500}$ precipitated HA-PTPN23 from N2A-FLAG-TrkB lysates (Figure 3.5B). Because it was absent in GST-CC2$^{314-500}$, it suggested that the N-terminal CC1 may mediate this interaction. HA-PTPN23 was not detected in pull downs using other GST-BICD1 fragments or GST control (Figure 3.5B).

To test whether PTPN23 binds to CC1, I generated two recombinant fusion proteins spanning the N-terminal CC1: GST-CC1$^{1-265}$ and GST-CC1$^{1-300}$. Both proteins interacted with HA-PTPN23, whilst other fragments did not display any significant binding (Figure 3.5C).

To further narrow down the PTPN23 binding region on BICD1, CC1 was divided, making use of the low complexity region spanning amino acids (aa) 86-103 within CC1 (https://www.expasy.org/resources/search/keywords:coiled-coils), subsequently generating GST-CC1$^{1-94}$ and GST-CC1$^{95-265}$. The C-terminal portion of CC1, GST-CC1$^{95-265}$, was still able to pull down HA-PTPN23 from cell lysates, albeit with a lower efficiency than the full GST-CC1$^{1-265}$ (Figure 3.5D).

Those results were unexpected, since the N-terminal CC1/2 of BICD proteins is a well-characterized region responsible for the binding and activation of the dynein motor complex (Hoogenraad and Akhmanova, 2016), raising several questions on the potential role of PTPN23 in the BICD1-dynein interaction and suggesting that PTPN23 is not a classical BICD1 cargo, binding to its C-terminus.

3.2.4 Expression of BICD1-CC1$^{\Delta 95-265}$ drives Rab6 out of the Golgi apparatus

In the previous chapter, I demonstrated that GST-CC1$^{95-265}$ associates with PTPN23. To validate this finding in mammalian cells, BICD1-CC1$^{95-265}$ was subcloned into a plasmid expressing N-terminal GFP-tag, and the PTPN23-binding deficient mutant, GFP-BICD1$^{\Delta 95-265}$, was generated (Figure 3.6A).

To test the behaviour of this mutant, HA-PTPN23 and either GFP-BICD1^{WT} or GFP-BICD1$^{\Delta 95-265}$ were overexpressed overnight in N2A-FLAG-TrkB cells. Then, lysates were generated in 0.2% NP-40 lysis buffer, and incubated overnight with

GFP-trap beads. Proteins associated with the beads were eluted by boiling in SDS-containing sample buffer and assessed immediately by SDS-PAGE and western blotting, using anti-HA and anti-GFP antibodies. HA-PTPN23 was detected in the IP fraction ("GFP-trap") when co-expressed with GFP-BICD1^{WT}, while PTPN23-binding deficient mutant, GFP-BICD1$^{\Delta 95\text{-}265}$, exhibited a much reduced affinity for PTPN23 (Figure 3.6B). As BICD proteins exist as homodimers (Terawaki et al., 2015), it is possible that GFP-BICD1$^{\Delta 95\text{-}265}$ interacts with endogenous BICD1, leading indirectly to PTPN23 co-precipitation.

Next, the co-distribution of overexpressed HA-PTPN23 with GFP-BICD1 proteins was assessed in N2A-FLAG-TrkB cells. Proteins were overexpressed overnight, and cells were fixed and processed by immunocytochemistry using an anti-HA antibodies. Similarly to the endogenous proteins (Figure 3.2), HA-PTPN23 and GFP-BICD1^{WT} exhibited punctate staining and were enriched in the perinuclear region (Figure 3.6C). I did not detect co-distribution of HA-PTPN23 with GFP-BICD1$^{\Delta 95\text{-}265}$, which was prone to aggregation and redistribution to the cell periphery, similarly to previous reports testing dominant-negative BICD2-CC3 constructs (Matanis et al., 2002). In contrast, GFP-BICD1$^{95\text{-}265}$ displayed a diffused distribution in the cytoplasm, which resembled that of GFP alone. However, in several cells I detected GFP-BICD1$^{95\text{-}265}$ co-distributing with HA-PTPN23 in a diffuse perinuclear region, rather than in puncta (Figure 3.6C), suggesting that these proteins accumulate together but do not associate with membrane organelles. Whether GFP-BICD1$^{95\text{-}265}$ is able to interact with dynein is not known.

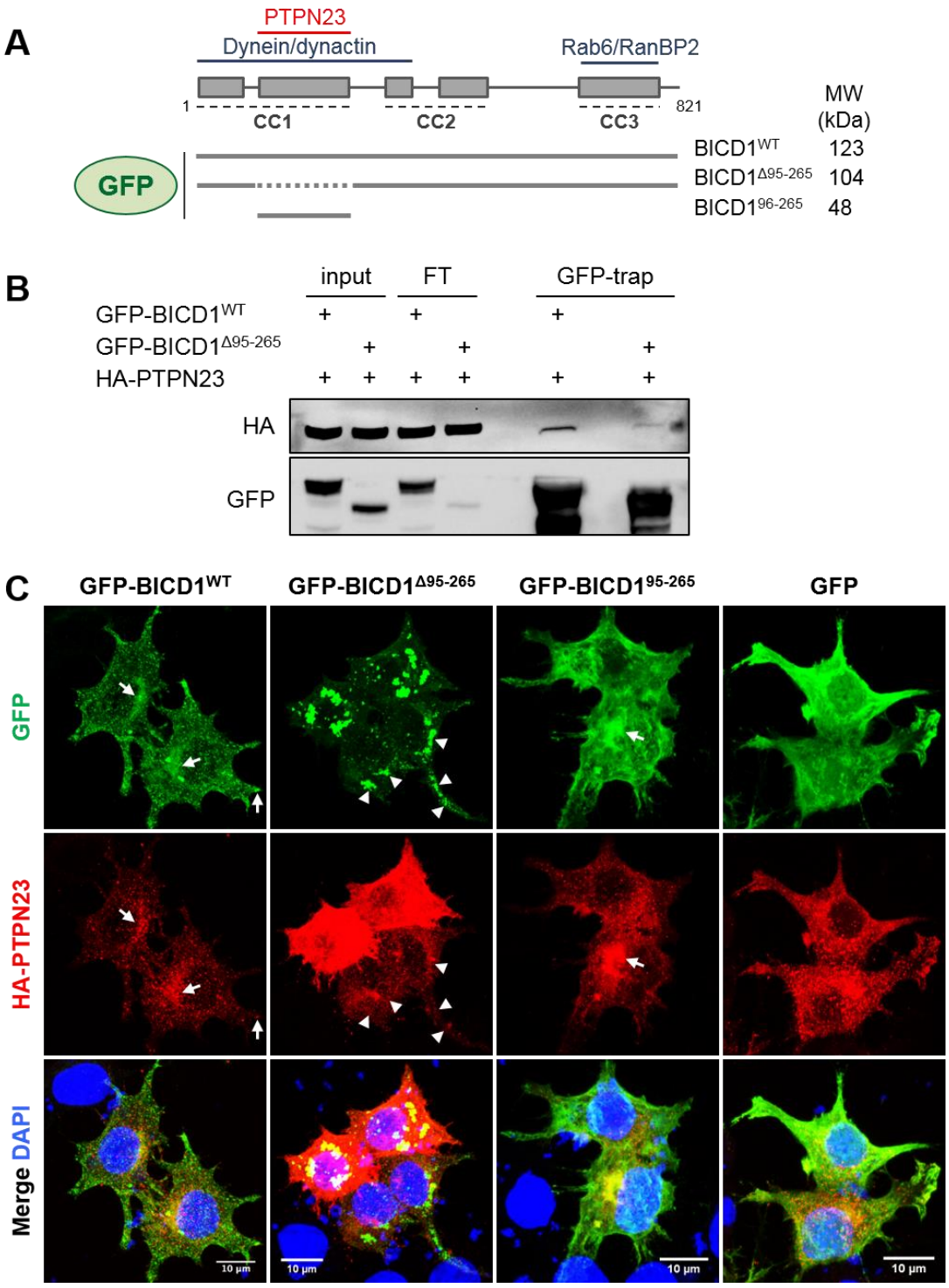

Figure 3.6 GFP-BICD1$^{\Delta 95\text{-}265}$ displays reduced association with PTPN23.

A) Schematic of GFP-BICD1 proteins used for co-IP and confocal microscopy in mammalian cells. B) N2A-FLAG-TrkB cells were transfected with plasmids encoding HA-PTPN23 and GFP-BICD1^{WT} or GFP-BICD1$^{\Delta 95\text{-}265}$. The following day, proteins were extracted in 0.2% NP-40 lysis buffer and incubated overnight with GFP-trap beads for co-IP. Input, FT (1/50 of lysate) and co-IP ("GFP-trap"; whole eluate) fractions were immunoblotted using anti- HA and anti-GFP antibodies, revealing a reduced association of mutant BICD1 and PTPN23 (n=1). C) Representative confocal images of N2A-FLAG-TrkB cells overexpressing HA-PTPN23 and GFP-BICD1 proteins, or GFP alone as control. Cells were fixed and immunostained using anti-HA antibody. Only GFP-BICD1^{WT} and GFP-BICD1$^{95\text{-}265}$ co-distributed with HA-PTPN23 (arrows), while aggregation-prone GFP-BICD1$^{\Delta 95\text{-}265}$ partially translocated to the cell periphery and did not significantly co-distribute with HA-PTPN23 (arrowheads) (n=2). Images show maximum intensity Z-stack projections, acquired at 0.5 µm spacing.

Previously, it was demonstrated that overexpression of BICD2-CC3 exerts a dominant-negative effect, leading to increased accumulation of BICD2-CC3 and its C-terminal binding partner Rab6 at the Golgi apparatus, as well as extensive peripheral redistribution of BICD2-CC3/Rab6 (Matanis et al., 2002). Due to a distinct localization of GFP-BICD1$^{\Delta 95\text{-}265}$ in N2A-FLAG-TrkB cells (Figure 3.6C), I asked next whether this PTPN23-binding deficient mutant elicits a similar phenotype on Rab6-positive vesicles.

To this end, N2A-FLAG-TrkB cells overexpressing different GFP-BICD1 mutant proteins were fixed and immunostained for Rab6. In addition, I assessed whether overexpression of GFP-BICD1$^{\Delta 95\text{-}265}$ affects the structural integrity of the Golgi apparatus, although this phenotype was not observed for BICD2-CC3 (Matanis et al., 2002). Interestingly, Rab6 highly co-localized with GFP-BICD1$^{\Delta 95\text{-}265}$, which drove it towards the cell periphery, while the Golgi apparatus staining appeared intact (Figure 3.7). These results confirmed the findings of Matanis et al. (2002), suggesting that GFP-BICD1$^{\Delta 95\text{-}265}$, lacking only a small portion of its dynein-binding domain, acts as a dominant-negative mutant of BICD1 function.

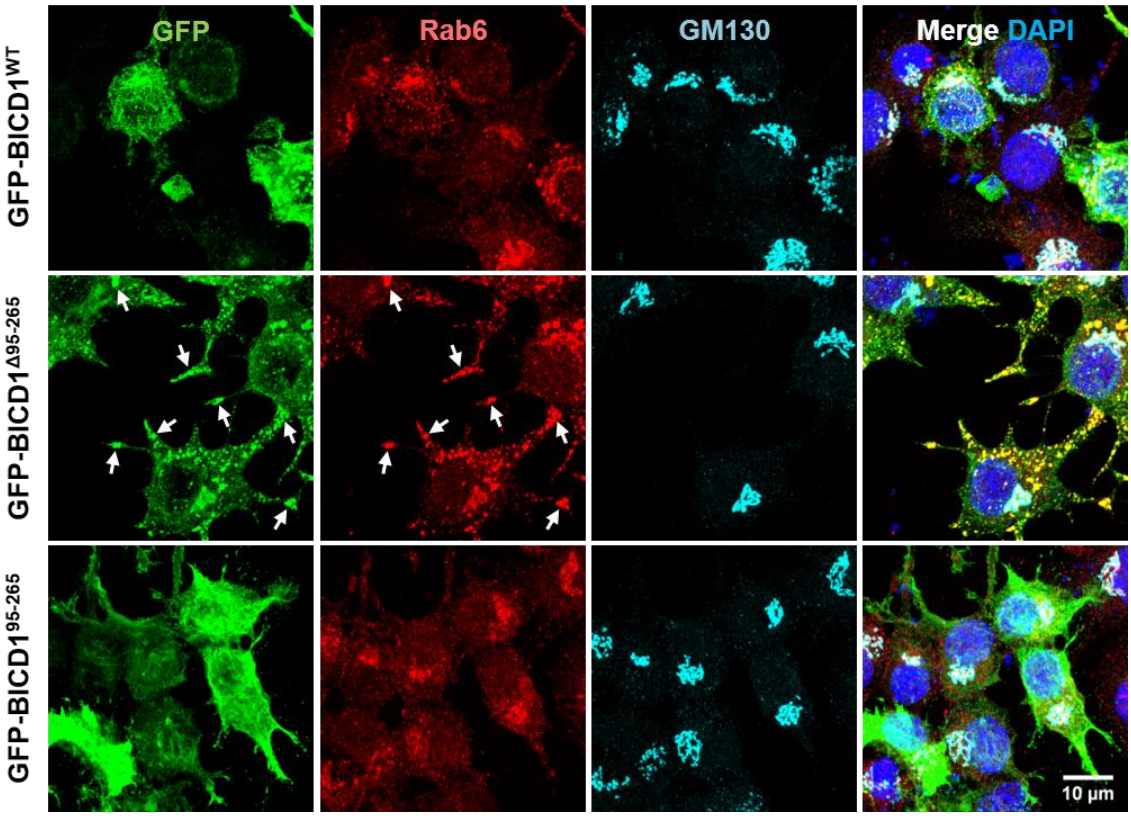

Figure 3.7 Expression of GFP-BICD1$^{\Delta 95\text{-}265}$ mutant drives Rab6-positive organelles to the cell periphery.

N2A-FLAG-TrkB cells, overexpressing different GFP-BICD1 constructs, were fixed and immunostained for Rab6 and GM130. While overexpression of GFP-BICD1$^{\Delta 95\text{-}265}$ results in Rab6

translocation towards the cell periphery (arrows), it does not affect the integrity of the Golgi apparatus (n=2). Images show maximum intensity Z-stack projection, acquired at 0.5 µm spacing.

3.2.5 PTPN23 interacts with BICD1 via its V/CC domain

So far, I demonstrated that the $CC1^{95-265}$ domain of BICD1 is likely to mediate the interaction with PTPN23 (Figure 3.5; Figure 3.6). Because mammalian cell lysates containing overexpressed PTPN23 were used in the initial screen, it leaves the possibility that the association between recombinant BICD1 and PTPN23 might be indirect. To assess if this interaction is instead direct, the domains of interest of PTPN23 were subcloned into a plasmid containing N-terminal poly-histidine tag (His_6; Figure 3.8A) and expressed in bacteria (see Methods for details). His_6-PTPN23 proteins were then used for *in vitro* pull downs.

I set out to map the BICD1-PTPN23 interaction using GST-$CC1^{95-265}$ bound to GSH beads (Figure 3.8B) or GSH magnetic beads (Figure 3.8C), incubated with bacterially-expressed His_6-PTPN23 proteins. As shown in Figure 3.8B, only His_6-Bro-V/CC co-precipitated with resin-bound GST-$CC1^{95-265}$. However, a small amount of His_6-Bro-V/CC could also be detected in the control pull down using GST. Because His_6-Bro-V/CC was enriched in pull down of GST-$CC1^{95-265}$ in comparison to GST control, and His_6-Bro did not significantly interact with GST-$CC1^{95-265}$, these results suggest that BICD1 might associate with the V/CC domain of PTPN23. Indeed, isolated His_6-V/CC co-precipitated specifically with GST-$CC1^{95-265}$ (Figure 3.8C), confirming this hypothesis. As previously shown (Figure 3.8B), His_6-Bro-V/CC was significantly enriched in GST-$CC1^{95-265}$ pull down (Figure 3.8C). These findings suggested not only that PTPN23-$V/CC^{401-653}$ mediates the interaction with BICD1-$CC1^{95-265}$ (n=3), but also that these proteins may bind directly.

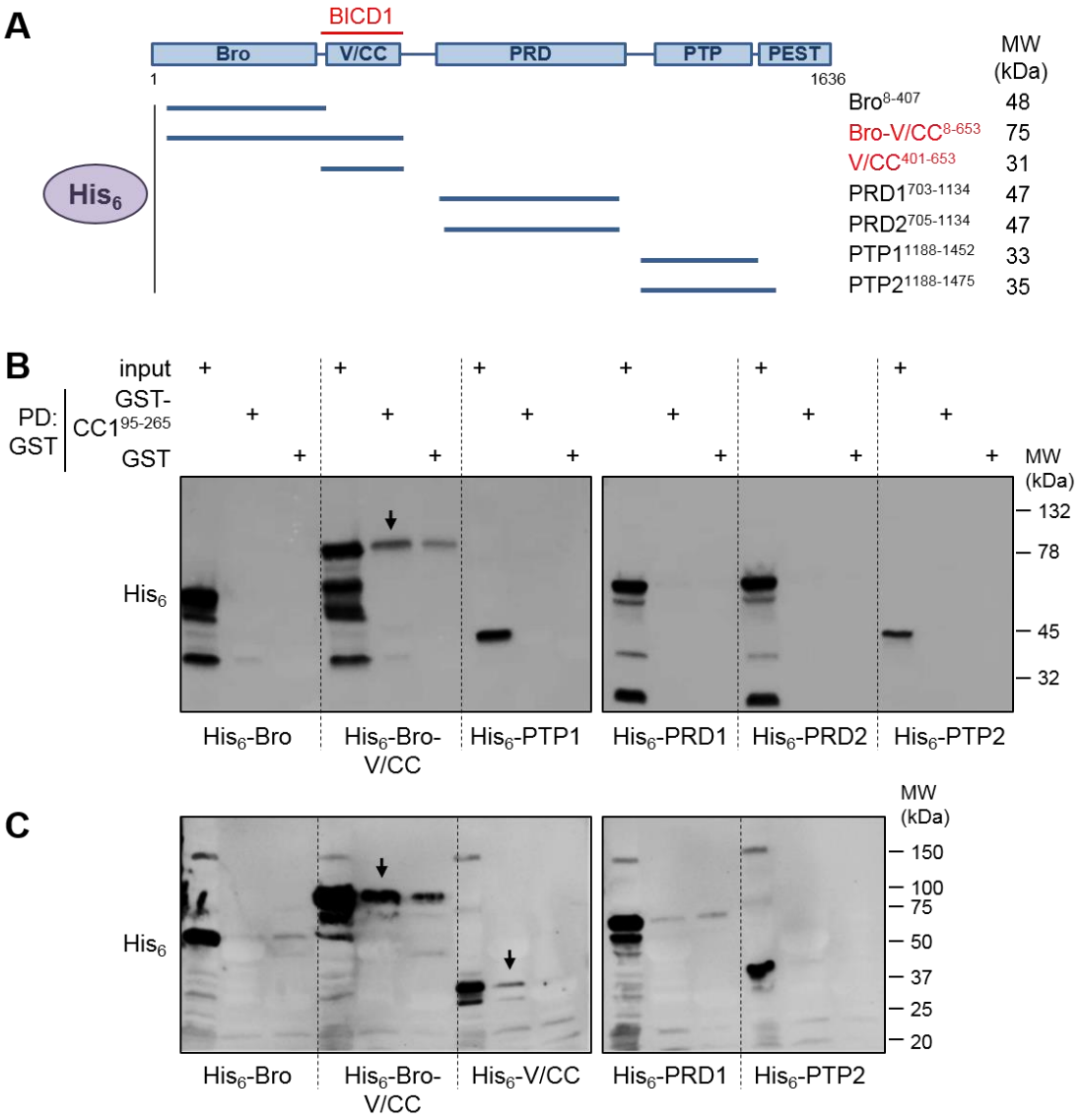

Figure 3.8 PTPN23-V/CC$^{401-653}$ interacts with BICD1-CC1$^{95-265}$.

A) Schematic representation of PTPN23 domain architecture and His$_6$-PTPN23 fragments, with their predicted MW, used in *in vitro* pull down assays. His$_6$-PTPN23 fragments in red bind BICD1. GST-CC1$^{95-265}$ or GST control, pre-bound to GSH resin (B; n=2) or GSH magnetic beads (C; n=4), were incubated for 2 h with soluble bacterial extracts containing equal amounts of His$_6$-PTPN23 proteins. Pulled down (PD) proteins were eluted from GSH beads by boiling, and assessed by SDS-PAGE and immunoblotting, using an anti-His$_6$ antibody. Bacterial extracts containing His$_6$-PTPN23 fragments were loaded as input (approximately 1/25-1/50 of lysate used for pull downs). His$_6$-Bro-V/CC and His$_6$-V/CC co-precipitated with GST-CC1$^{95-265}$ (arrows; B,C).

While His$_6$-Bro-V/CC and His$_6$-V/CC bound to GST-CC1$^{95-265}$, several His$_6$-PTPN23 fragments appeared to non-specifically interact with GST beads (Figure 3.8C). I therefore attempted the purification of His$_6$-PTPN23 proteins, using nickel-nitrilotriacetic acid (Ni-NTA) resin, which binds His$_6$-tagged proteins with high affinity. Although His$_6$-PTPN23 fragments exhibited high affinity for Ni-NTA resin (Figure 3.9A), a sufficient purity of these proteins could not be obtained, as

shown by Coomassie Blue staining (Figure 3.9B), in which several bacterial contaminants were detected.

I attempted pull downs using impure Ni-NTA-bound His_6-PTPN23 fragments, incubated with GST, GST-$CC1^{1-265}$ or GST-$CC1^{95-265}$. However, all GST proteins co-precipitated equally with each of His_6-PTPN23 proteins (Figure 3.9C), and conditions in which a significant enrichment could be achieved, could not be found. Regrettably, I was not able to establish optimal His_6-PTPN23 purification conditions prior to pull down assay.

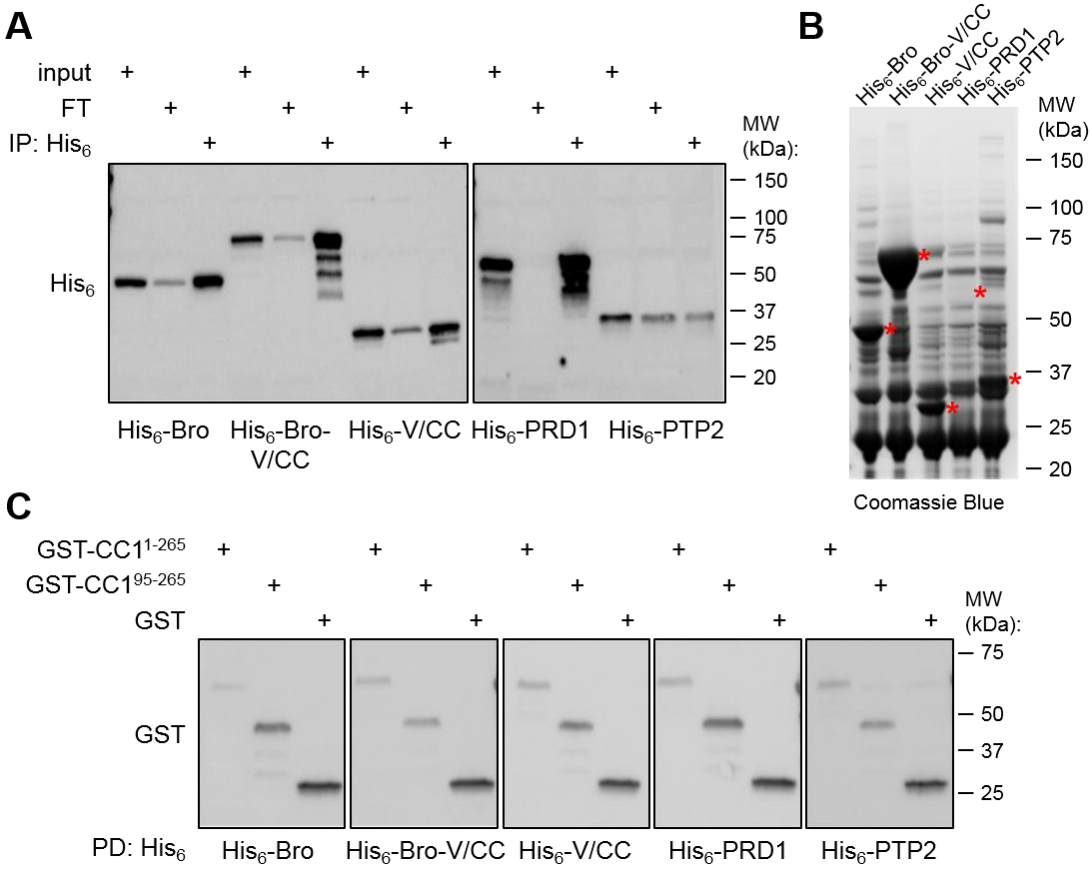

Figure 3.9 Purified His_6-PTPN23 show high degree of unspecific interactions.

A) His_6-PTPN23 fragments were expressed in bacteria and purified using Ni-NTA resin. Inputs, FT and His_6-PTPN23 eluted from 20 µl of resin were analysed by SDS-PAGE and immunoblotting with an anti-His_6 antibody. B) Purity of His_6-PTPN23 fragments eluted from Ni-NTA resin (red asterisk) was additionally assessed by SDS-PAGE and Coomassie Blue staining, showing several contaminating bacterial proteins. C) Ni-NTA resin containing equal amounts of His_6-PTPN23 fragments was incubated for 1 h with 20 µg of GST-BICD1 fusion proteins. Samples were assessed by SDS-PAGE and immunoblotting using an anti-GST antibody. GST proteins co-precipitated with all His_6-PTPN23 fragments, without specificity or enrichment (n=2).

3.3 Discussion and future directions

Correct balance between receptor degradation and recycling ensures a precise response of downstream signalling effectors to extracellular cues. This is tightly regulated at several levels, starting from receptor endocytosis, through endocytic transport and finally sorting of activated receptors to an appropriate cellular destination, such as the plasma membrane, via the recycling route or for degradation in lysosomes (Huotari and Helenius, 2011). Accurate spatiotemporal regulation of the signalling elicited by neurotrophins and their receptors (NTRs) is particularly important for neurons, and ensures proper development and maintenance of the nervous system (Bronfman et al., 2007). While NTR endocytosis and retrograde transport from distal nerve terminals to the soma has been extensively characterized (Barford et al., 2017; Villarroel-Campos et al., 2018), the molecular machinery regulating the somatic sorting of ligand-activated NTRs is not completely understood. Following the discovery of BICD1 as a main regulator of NTR turnover (Terenzio et al., 2014a; Terenzio et al., 2014b) and later identification of PTPN23 in a mass spectrometry proteomic screen of BICD1 interacting partners, I was prompted to investigate the molecular interaction between BICD1 and PTPN23 in neuronal cells, which was not characterized to date. This analysis may reveal important insights on the mechanism controlling sorting of cargoes, such as NTRs.

3.3.1 BICD1-CC1$^{95\text{-}265}$ interacts with PTPN23

To investigate the relationship between BICD1 and PTPN23, I employed biochemical assays and confocal microscopy. I demonstrated that both endogenous and overexpressed PTPN23 can be identified by western blotting in complexes with BICD1 in mammalian cell lysates (Figure 3.1). PTPN23 was detected consistently in co-IPs performed using lysates prepared in buffers of varying stringency, and when using two different types of magnetic beads, pre-coated with antibodies against BICD1 or GFP, suggesting that PTPN23 stably associates with BICD1. However, the level of PTPN23 was relatively low in BICD1-immunoprecipitates, which correlated well with the rather sparse co-localization between these proteins, observed predominantly in the perinuclear region (Figure 3.2; Figure 3.3). Because BICD1 and PTPN23 associate with the

highly dynamic endocytic pathway, it would be tempting to speculate that they interact transiently along the endocytic pathway.

BICD1 and BICD2 are highly homologous and share certain cargoes, such as Rab6 and RanBP2 (Matanis et al., 2002; Splinter et al., 2010; Terawaki et al., 2015; Hoogenraad and Akhmanova, 2016). In addition, the proteomic screen revealed that BICD1 and BICD2, which are known to exist predominantly as homodimers (Terawaki et al., 2015), may interact (Appendix 1). Here, the association with PTPN23 appeared to be specific to BICD1 and not BICD2, suggesting a distinct function of BICD proteins (Figure 3.1C).

I designed *in vitro* binding assays to map the interaction between BICD1 and PTPN23. As a starting point, I used N2A-FLAG-TrkB cell lysates containing overexpressed PTPN23, incubated with the GST-BICD1 baits expressed and purified from bacteria (Figure 3.5). Using this approach, I was able to narrow down the PTPN23 binding region on BICD1 to the C-terminal half of the first coiled coil, $CC1^{95\text{-}265}$ (Figure 3.5D), and validated these findings using mutant BICD1 lacking the PTPN23-binding region (Figure 3.6). Association of PTPN23 with the N-terminus of BICD1 was not anticipated, since this region participates in the recruitment of the dynein complex, while its C-terminal CC3 appears in literature predominantly as “the cargo-binding domain” (Hoogenraad and Akhmanova, 2016). In fact, binding of cargoes such as Rab6 or RanBP2 releases the autoinhibition state of BICD1, exhibited by the interaction between CC3 and CC1, leading to recruitment of the dynein complex by CC1 (Carter et al., 2016). Besides the dynein complex, there is currently no published evidence of other proteins binding to BICD1-CC1. These findings highlight that PTPN23 is not a canonical, C-terminal BICD1 cargo and suggest that PTPN23 does not release the autoinhibition state of BICD1; instead, its association with BICD1 might be context- and cargo-dependent. At present, it is not known whether PTPN23 and the dynein complex can bind BICD1 simultaneously or whether their binding is competitive. Deciphering this mechanism should be the primary focus of future studies, as it may reveal the principles of cargo sorting towards degradation.

3.3.2 PTPN23-V/$CC^{401\text{-}653}$ interacts with BICD1-$CC1^{95\text{-}265}$

Using *in vitro* pull downs, I demonstrated that BICD1-$CC1^{95\text{-}265}$ directly interacts with PTPN23, and this binding relies on the V-domain of PTPN23 (Figure 3.8;

Figure 3.10), a region characterized by the presence of coiled coils (V/CC) (Gahloth et al., 2017a). Although this interaction was consistently detected in pull down assays, where GST-BICD1-CC1$^{95-265}$ was used as a bait for bacterially-expressed His$_6$-PTPN23 fragments (Figure 3.8D), I was not able to demonstrate it in reverse, such as by using immobilized PTPN23-V/CC and BICD1 fragments expressed in bacteria (Figure 3.9C). A possible cause was the co-elution of several contaminating bacterial proteins, which bound to Ni-NTA resin used for His$_6$-PTPN23 purification (Figure 3.9B). To overcome this problem, several washing conditions for His$_6$-PTPN23 purification were tested. Increasing the concentration of imidazole, from initial 10 mM to 20-50 mM, was the most efficient in reducing the binding of bacterial proteins. Imidazole competes with His$_6$ binding to Ni-NTA resin, thereby facilitating protein purification and elution (Bornhorst and Falke, 2000). However, I was not able to reduce the contamination of bacterial proteins. Because bacterially-expressed mammalian proteins are prone to misfolding (Schein, 1989), recombinant PTPN23 proteins, although soluble, may have been incompletely folded, subsequently leading to their co-aggregation with bacterial proteins. In future work, His$_6$-PTPN3 proteins could be co-expressed with a larger protein tag facilitating protein folding, such as maltose-binding protein (MBP) (Kapust and Waugh, 1999).

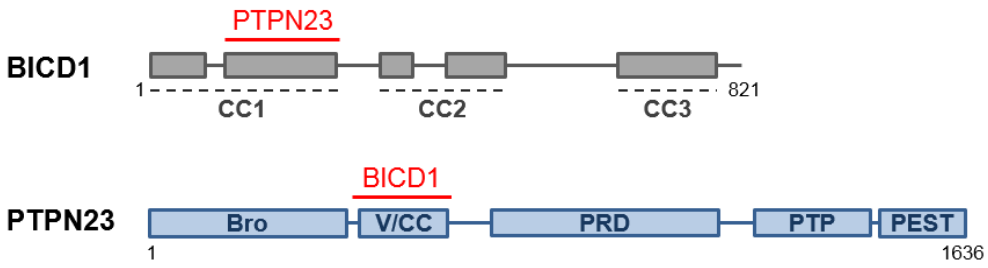

Figure 3.10 Proposed model of BICD1-PTPN23 interaction regions.

Schematic representation of BICD1 and PTPN23 domain architecture, with proposed binding regions on both proteins as a result of *in vitro* mapping.

Nevertheless, the association of PTPN23-Bro-V/CC domains with BICD1 appears the most logical, since these domains are the minimal functional unit of PTPN23 supporting cargo sorting towards the degradative pathway via multivesicular body (MVB) biogenesis (Doyotte et al., 2008; Tabernero and Woodman, 2018). Expression of these two domains together boosts their stability and supports PTPN23 function in cargo sorting and ESCRT recruitment (Gahloth

et al., 2017a), potentially explaining why increased binding of His_6-V/CC to BICD1 was observed when co-expressed with the Bro domain (Figure 3.8). In addition, Bro-V/CC of PTPN23 is structurally and functionally related to mammalian Bro-containing protein Alix (called also PDCD6IP), and a yeast Bro1 protein, both of which mediate protein sorting and MVB formation (Bissig and Gruenberg, 2014). While PTPN23 contains a catalytically-inactive phosphatase (PTP) domain (Gingras et al., 2009b), it is likely to mediate processes not directly related to receptor sorting, such as maintenance of the high phosphorylation level of the survival motor neurons (SMN) complex, necessary for its nuclear translocation and association with Cajal bodies (Husedzinovic et al., 2014; Smigiel et al., 2018).

3.3.3 PTPN23 dynamics are independent of TGN

Because of the close association of BICD1 with the TGN (Matanis et al., 2002), as well as extensive co-distribution of BICD1 and PTPN23 in the vicinity of this organelle (Figure 3.2; Figure 3.4), I was prompted to investigate whether PTPN23 associates with the TGN. Although it was not extensively explored (Doyotte et al., 2008), in particular in neurons, PTPN23 may play a role in the late endosome-to-TGN retrieval pathway (Breusegem and Seaman, 2014). In addition, mammalian PTPN23 and its *Drosophila* homolog Myopic support early endosome-to-Golgi sorting and plasma membrane recycling of Wnt/Wls (Pradhan-Sundd and Verheyen, 2014), suggesting that PTPN23 may facilitate sorting of cargoes beyond MVBs. ESCRT proteins also mediate the sorting of the newly synthesized degradative enzymes from the Golgi apparatus to MVB and lysosomes (Hurley, 2010; Kim et al., 2005), raising the possibility that PTPN23 and BICD1 participate in cargo sorting within this platform.

Here, PTPN23 and TGN46 partially co-localized in ES-MNs (Figure 3.4C). Interestingly, while disruption of the Golgi complex by brefeldin A led to dispersal of BICD1 (Figure 3.4B), the perinuclear distribution of PTPN23 was not affected. This preliminary finding suggests that the perinuclear accumulation of PTPN23 is independent of BICD1 and of the Golgi apparatus integrity, although it may facilitate the retrieval of certain cargoes to and from TGN. Unsurprisingly, as the subcellular distribution of BICD1 and PTPN23 strongly depends on their trafficking within the endo-lysosomal system, interfering pharmacologically with

microtubule stability, which causes peripheral redistribution of organelles localized near microtubule minus ends (Matteoni and Kreis, 1987), such as MVBs, lysosomes and the Golgi apparatus (Matteoni and Kreis, 1987; Huotari and Helenius, 2011; Von Bartheld and Altick, 2011), led to a loss of perinuclear enrichment of both proteins (not shown).

3.3.4 BICD1$^{\Delta 95\text{-}265}$ exerts dominant-negative effect

Unlike BICD2 and BICDR1 (Grigoriev et al., 2007; Schlager et al., 2010; Splinter et al., 2010), it is not presently known whether BICD1 supports anterograde transport of cargoes by binding to kinesin motors. Interestingly, PTPN23-, and potentially dynein-binding deficient mutant GFP-BICD$^{\Delta 95\text{-}265}$ extensively translocated to the cell periphery, where it co-accumulated with Rab6-positive vesicles (Figure 3.7). These results are consistent with a report describing the effect of dominant-negative BICD2-CC3 overexpression, which resulted in extensive Rab6 trafficking to the cell periphery (Matanis et al., 2002). In future experiments, binding of BICD1 to a kinesin motor should be investigated, as well as the transport kinetics and localization of GFP-BICD$^{\Delta 95\text{-}265}$/Rab6 upon inhibition of conventional kinesin or depolymerization of microtubules. It was previously shown that BICD2 strongly associates with kinesin-1 (Kif5a) via a region within CC2 spanning amino acids 336-595 (Splinter et al., 2010). For a BICD2-kinesin interaction to occur, the release of BICD2 from autoinhibited state by cargo binding is required (Grigoriev et al., 2007). In addition, CC1 of BICDR1 (amino acids 1-353) binds Kif1C (Schlager et al., 2010). While association of these BICD proteins with kinesins depends on the cellular context, such as during the early developmental stage of a neuron (Schlager et al., 2010), or during the late G2 phase in mitotic cells (Splinter et al., 2010), it would be interesting to explore whether similar molecular interaction between BICD1 and kinesins exist. In addition, the interaction between dynein and GFP-BICD$^{\Delta 95\text{-}265}$ or GFP-BICD$^{95\text{-}265}$ should be clarified, although a previous report mapping the association of BICD2 with dynein suggest that only CC1 spanning amino acids 1-271 immunoprecipitates dynein from cell lysates (Hoogenraad et al., 2001).

3.3.5 Final conclusions

In this chapter, I demonstrated that BICD1-CC1$^{95\text{-}265}$ interacts with PTPN23-V/CC$^{401\text{-}653}$, an association which is likely to occur in the perinuclear region. In

addition, PTPN23 partially co-localizes with components of the TGN, although its perinuclear accumulation in neuronal cells is independent of BICD1 and the Golgi complex integrity. In addition, I observed that mutant BICD1 lacking PTPN23- and a portion of dynein-binding domain potentially exerts a dominant-negative effect, leading to strong peripheral redistribution of Rab6-positive vesicles.

4 Investigating the role of PTPN23 in the NTR sorting in neuronal cells

4.1 Aims of this chapter

In the previous chapter, I explored the interaction between BICD1 and PTPN23. These proteins co-localize predominantly in the vicinity of the Golgi apparatus in N2A-FLAG-TrkB cells and ES-MNs, and PTPN23 co-immunoprecipitates with BICD1 from mammalian cell lysates. In addition, *in vitro* mapping analyses revealed a direct interaction between BICD1-CC1$^{95\text{-}265}$ and PTPN23-V/CC$^{401\text{-}653}$. These findings, together with the previously reported role of PTPN23 in turnover of transmembrane receptors, such as EGFR, PDGFR, α5β1 integrin or MHC class I (Doyotte et al., 2008; Kharitidi et al., 2015; Ma et al., 2015; Parkinson et al., 2015) and multivesicular body (MVB) biogenesis in non-neuronal cells (Ali et al., 2013; Gahloth et al., 2017), suggested that PTPN23, together with BICD1 (Terenzio et al., 2014b; Terenzio et al., 2014a), may contribute to NTR sorting towards lysosomal degradation. As the role of PTPN23 in receptor turnover in neuronal cells has not been addressed to date, the aim of this chapter was to explore the effect of PTPN23 silencing on TrkB and p75^{NTR} turnover, utilizing an anti-receptor antibody accumulation assay (Terenzio et al., 2014a).

4.2 Results

4.2.1 PTPN23 co-localizes with internalized TrkB

To investigate the relationship between PTPN23 and NTRs, I utilized an anti-receptor antibody accumulation assay (as outlined in Figure 4.1A,b). In short, neuronal cells expressing TrkB and p75^{NTR} receptors were incubated with an antibody raised against an extracellular epitope of a receptor. Importantly, these antibodies should not alter the trafficking or activity of these receptors and were previously validated in trafficking and accumulation assays. To facilitate the uptake of antibody-receptor complexes, cells were serum-starved for 3 h prior to the accumulation assay, incubated with the specific antibody for 30 min, and for the following 30 min with 100 ng/ml BDNF, the ligand for TrkB and p75^{NTR} (Sasi et al., 2017). In this work, anti-FLAG (M1; #F3040, Sigma) or anti-TrkB (#9872, Merck Millipore) antibodies were used to label TrkB (Chen et al., 2005), or anti-

p75^{NTR} antibody (#5410, CRD, CRUK) to label p75^{NTR} (Deinhardt et al., 2006; Terenzio et al., 2014a). To validate that antibodies labelling NTRs are internalized specifically, cells were incubated under the same experimental conditions with mouse immunoglobulins G (IgG) or rabbit IgG as controls (Figure 4.1B). Following antibody accumulation, cells were pre-chilled on ice and washed with ice-cold acid (pH 2.4; for anti-TrkB and anti-p75^{NTR} antibodies) or magnesium- and calcium-free PBS supplemented with 1 mM EDTA (for anti-FLAG), to facilitate the dissociation of surface-bound antibodies, which did not enter the cell by endocytosis. Following wash with PBS and fixation with 4% PFA/PBS, internalized antibody-receptor complexes (α-FLAG; α-TrkB; α-p75^{NTR}) were visualized by immunocytochemistry using an appropriate secondary antibody. For co-localization analyses with a protein of interest, cells with internalized probes were first immunostained with appropriate secondary antibodies (Figure 4.1B).

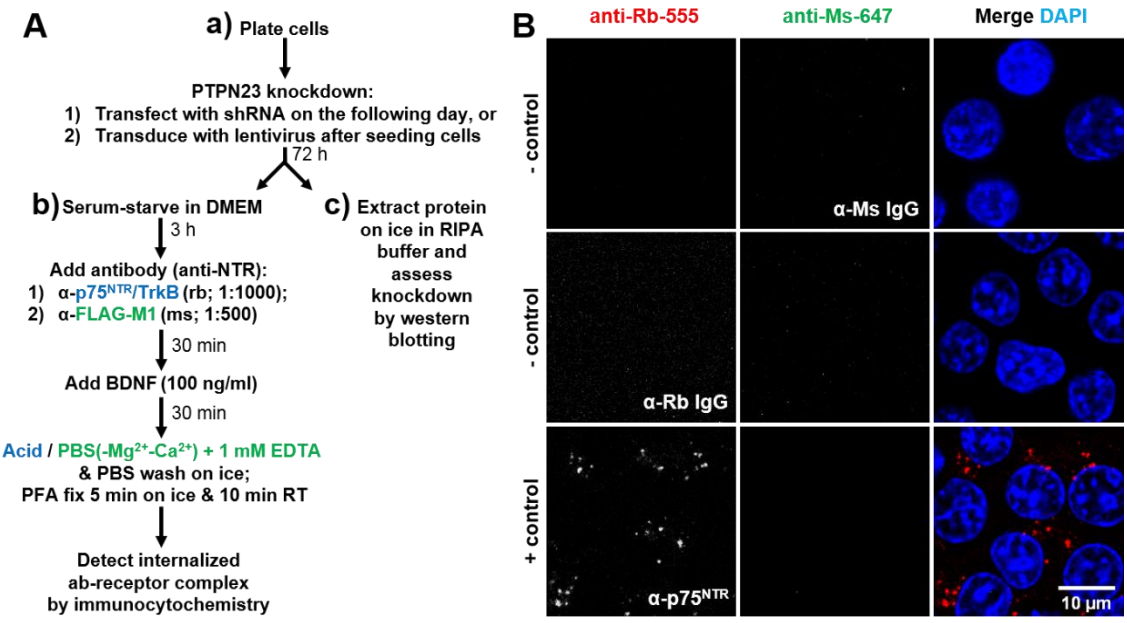

Figure 4.1 Outline of workflow and examples of accumulation assay controls.

A) A flow diagram outlining the workflow in this chapter. In short, following PTPN23 silencing by shRNA (72 h) (a), an antibody accumulation assay was performed (b) and/or protein levels were assessed by western blotting (c). B) Examples of negative (-) and positive (+) controls for antibody accumulation assays performed in N2A-FLAG-TrkB cells. To validate that the uptake of an antibody raised against an extracellular portion of the membrane receptor is specific, cells were incubated with normal IgG derived from relevant species, and secondary antibody cross-reactivity was assessed following the antibody accumulation assay.

First, the co-localization between PTPN23 or BICD1 and internalized TrkB was assessed in N2A-FLAG-TrkB cells. Following accumulation assays, using anti-

TrkB or anti-FLAG antibodies, cells were immunostained for PTPN23 (Figure 4.2A) or BICD1 (Figure 4.2B), respectively. Internalized α-TrkB and α-FLAG exhibited punctate staining, observed predominantly in the perinuclear region, which partially overlapped with PTPN23 and BICD1, suggesting that endogenous PTPN23 and BICD1 associate with endosomes carrying internalized NTRs in neuronal cells. However, the overall detection rate of internalized antibody-receptor complexes was relatively low. Analysis of the surface and total FLAG immunostaining in non-permeabilized and permeabilized cells, respectively, revealed that a relatively small number of cells displayed FLAG-TrkB on their surface (Figure 4.2C).

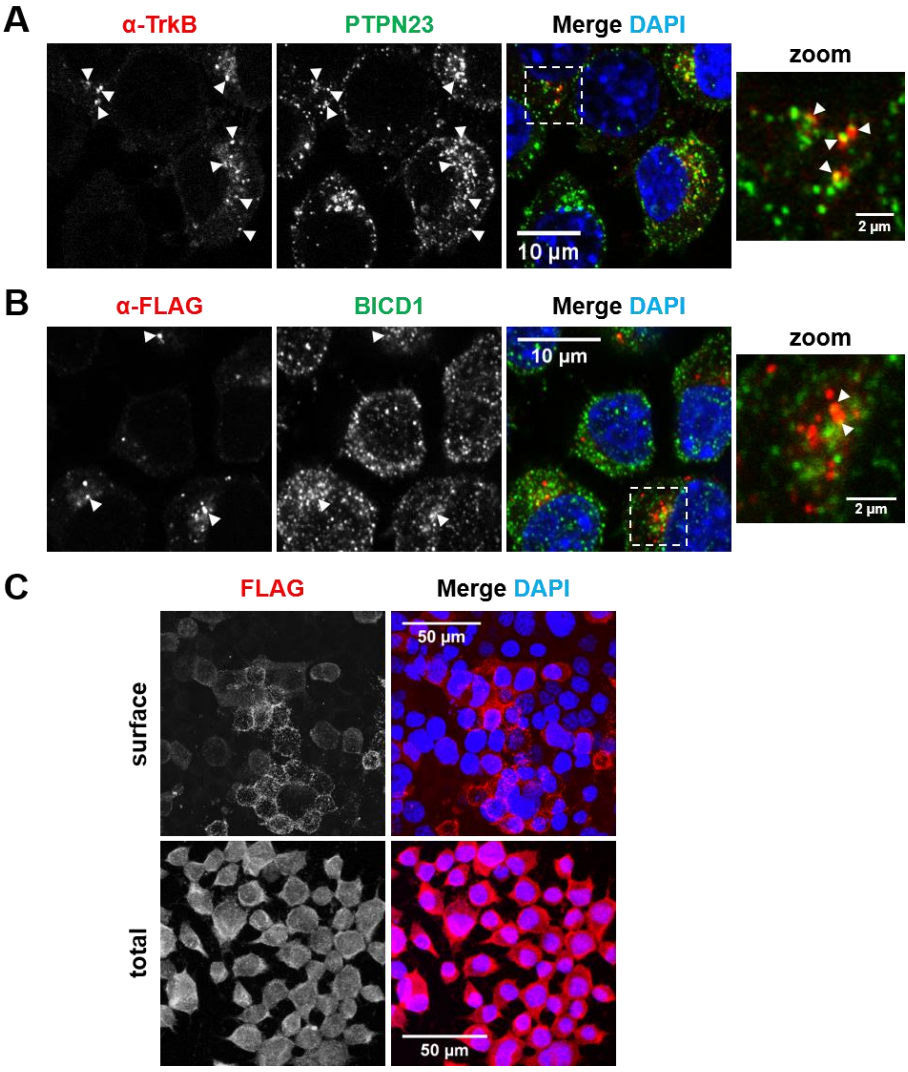

Figure 4.2 PTPN23 and BICD1 co-localize with internalized TrkB receptor.

Representative confocal images of α-TrkB (A; #9872) or α-FLAG (B) accumulation assay in N2A-FLAG-TrkB cells. Following acid/PBS-EDTA wash and fixation, cells were immunostained for PTPN23 (B) or BICD1 (B). PTPN23 and BICD1 partially co-localized with internalized antibody-receptor complexes (arrowheads; n=1). C) Representative confocal images showing anti-FLAG immunostaining in non-permeabilized (surface; maximum intensity Z-stack projection) or permeabilized cells (total).

4.2.2 PTPN23 is efficiently depleted by shRNA

To investigate whether PTPN23 plays a role in endocytic sorting of internalized NTRs, PTPN23 expression was silenced using a commercially-available short hairpin RNA (shRNA) pool (Figure 4.3A; #MSH025913, GeneCopoeia; www.genecopoeia.com). First, N2A-FLAG-TrkB cells were transfected with individual plasmids expressing PTPN23-targeting shRNA or scrambled control, and a GFP reporter. After 48 h, the levels of PTPN23 and GFP were assessed by immunoblotting (Figure 4.3B). The most effective silencing of PTPN23 was achieved by shRNA1, 2 and 4, while cells transfected with scrambled control exhibited PTPN23 levels comparable to non-transfected cells. Next, to facilitate shRNA delivery and PTPN23 silencing in neuronal cells, lentiviral particles were produced using shRNA1, 2, 3 (sh1,2,3) and scrambled (scr). To test the efficacy of lentiviruses, two different volumes of lentiviral suspension (2.5 and 6 µl per well in 24-well plate) were incubated with N2A-FLAG-TrkB cells for 72 h, and the level of PTPN23 knockdown was assessed by immunoblotting. ShRNA2 lentivirus ("sh2") was more potent than sh1 in silencing PTPN23. In contrast, sh3 was less efficient than sh1 and 2, only mildly reducing PTPN23 levels despite exhibiting the highest levels of GFP expression (Figure 4.3C).

Sh2 lentivirus was chosen for further work, because it was the most efficient in depleting PTPN23. Hereafter, PTPN23 silencing was conducted over 72 h, unless specified otherwise. First, N2A-FLAG-TrkB cells were transduced immediately after seeding with sh2 or scrambled control. I observed that sh2, but not scrambled-transduced cells, tended to easily detach from the surface of a glass coverslip. After 72 h, cells were fixed and immunostained for PTPN23 and GFP, and analysed by confocal microscopy. Relative to scrambled, the level of PTPN23 immunofluorescence was significantly reduced by sh2 (Figure 4.3D). However, residual protein could be detected, which, as expected, inversely correlated with the level of GFP reporter expression.

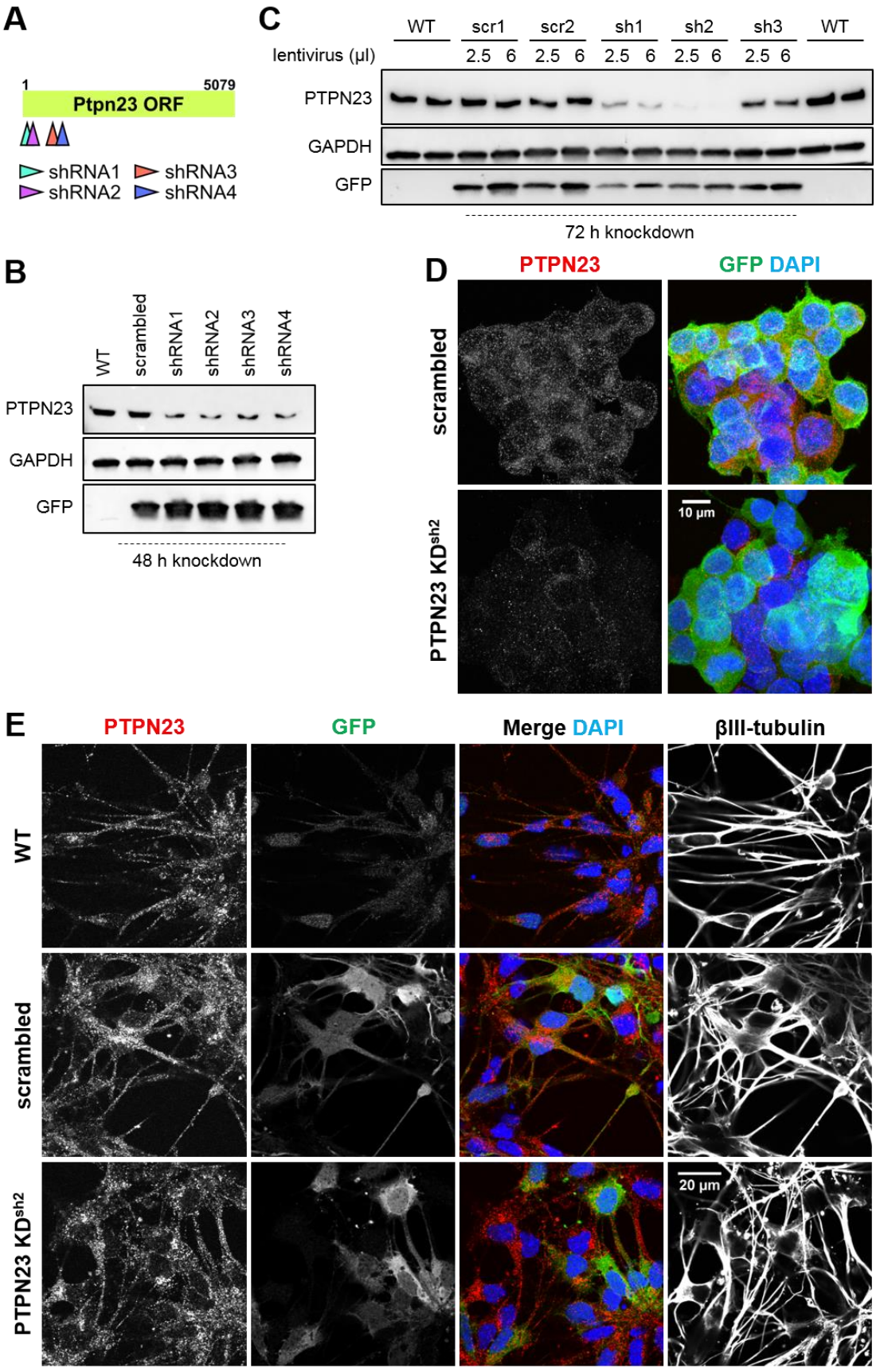

Figure 4.3 PTPN23 expression is effectively silenced using shRNA.

A) Map of shRNA targeting regions on Ptpn23 transcript (ORF – open reading frame; NCBI accession number: NM_001081043.1). B) N2A-FLAG-TrkB cells were transfected with plasmids expressing PTPN23-targetting shRNA (1-4) or scrambled shRNA (scr) and reporter GFP. After 48 h, the level of PTPN23 and GFP was assessed by western blotting. GAPDH was used as a

loading control (n=3). C) Cell lysates of N2A-FLAG-TrkB cells, transduced for 72 h with two different volumes of a lentivirus, were immunoblotted for PTPN23, GFP and GAPDH. The level of PTPN23 knockdown was the most efficient with sh2. D) Representative confocal images of N2A-FLAG-TrkB cells, transduced for 72 h with sh2 or scrambled lentiviruses (2.5 µl per well in 24 well plate), fixed and immunostained for PTPN23 and GFP. Sh2 efficiently depleted PTPN23. Images show maximum intensity Z-stack projection, acquired at 0.5 µm spacing. E) ES-MNs were transduced at DIV1 (0.75 µl per well in 24 well plate). At DIV3, cells were fixed and immunostained for PTPN23, GFP and neuronal marker βIII-tubulin.

Next, I assessed the efficacy of sh2 delivery into ES-MNs. After 7 days of ES cell differentiation in suspension, embryoid bodies were disaggregated and plated (see Methods for details). Next, sh2 or scrambled lentiviruses were added 5 h after seeding cells, and ES-MNs were fixed on day *in vitro* 3 (DIV3; 72 h transduction). Alternatively, ES-MNs were transduced at DIV1, and fixed at DIV3 or DIV4. In addition, several doses of the lentivirus were tested. ES-MN transduction was challenging. The addition of a lentivirus 5 h after seeding led to a significantly higher transduction of non-neuronal cells, whereas very few GFP- and βIII-tubulin-positive cells could be detected. A greater number, although still relatively low, of GFP-positive neurons could be detected when ES-MNs were transduced at DIV1 and fixed at DIV3, however the silencing of PTPN23 after 48 h was insufficient (Figure 4.3E). Incubation of ES-MNs until DIV4 resulted in cultures of poor health. Overall, treating ES-MN with sh2 led to clustering of neuronal cell bodies, cable-like alignment of neurites, neuronal blebbing and detachment from the surface of glass coverslips, making them a challenging model to study PTPN23 knockdown and NTR accumulation. While it was possible to retain a number of neurons on the coverslip for further analyses, I suspected that these cells retained higher levels of PTPN23 expression, and therefore were not representative for our study (Figure 4.3E).

4.2.3 PTPN23 knockdown leads to TrkB accumulation in vacuoles

Similarly to ES-MNs, N2A-FLAG-TrkB cells were prone to detachment after PTPN23 knockdown. Although these neuroblastoma-derived cells undergo mitosis and morphologically do not share the unique features of neurons, such as the highly polarized cell compartmentalization into axonal and somato-dendritic domains (Terenzio et al., 2017), I was able to significantly reduce the levels of PTPN23 (Figure 4.3B-D). In addition, these cells stably express FLAG-

tagged TrkB (Terenzio et al., 2014a), as well as endogenous p75^{NTR}, allowing to explore the general features of NTR sorting upon PTPN23 downregulation.

To begin with, the anti-FLAG accumulation assay was performed on PTPN23 KD^{sh2} or scrambled N2A-FLAG-TrkB cells, as outlined in Figure 4.1A. Confocal microscopy revealed punctate and predominantly perinuclear localization of antibody-receptor complex (α-FLAG) in scrambled cells (Figure 4.4), as observed previously (Figure 4.2). However, in PTPN23 KD^{sh2} cells, enlarged vacuole-like structures were detected, in addition to cells with punctate perinuclear staining (Figure 4.4). Because this observation aligned with previous reports of the enlarged receptor-containing endosome morphology (Doyotte et al., 2008; Kharitidi et al., 2015), this finding suggested that PTPN23 may play a role in NTR sorting in neuronal cells.

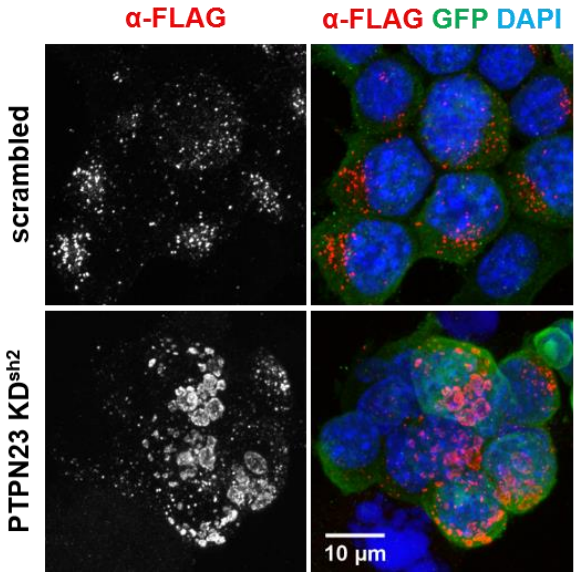

Figure 4.4 PTPN23 knockdown by sh2 leads to TrkB accumulation in vacuoles.

Representative confocal images of α-FLAG accumulation assay in scrambled or PTPN23 KD^{sh2} N2A-FLAG-TrkB cells. In addition to α-FLAG perinuclear puncta, PTPN23 depletion results in accumulation of the FLAG-TrkB receptor in vacuole-like organelles. Images show maximum intensity Z-stack projection (n=3).

4.2.4 PTPN23 knockdown downregulates expression of NTRs and NTR scaffold Kidins220

While a significant accumulation of α-FLAG was observed in N2A-FLAG-TrkB cells upon PTPN23 knockdown (Figure 4.4), I next assessed whether its

downregulation affects the total level of NTRs. Immunoblotting of cell lysates revealed that PTPN23 silencing for 72 h led to a decrease of TrkB full length receptor (TrkB-FL) and p75^{NTR} levels (Figure 4.5A,B).

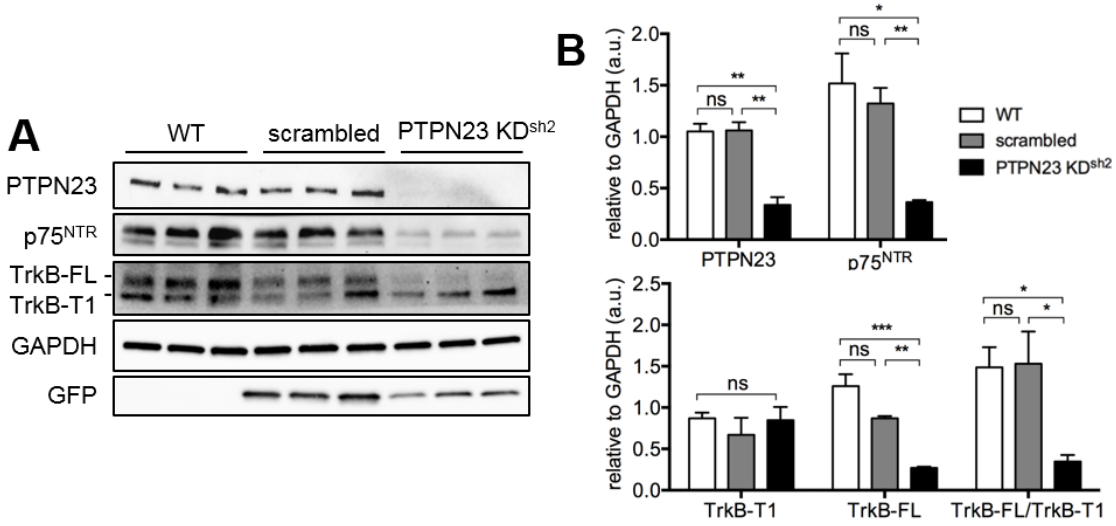

Figure 4.5 PTPN23 KD leads to reduction of the total levels of NTRs.

A) Immunoblotting of wild type (WT), scrambled and PTPN23 KD^{sh2} N2A-FLAG-TrkB cell lysates for NTRs (n=3). GAPDH was used as a loading control, and the level of GFP reporter was assessed. B) Densitometric analysis of NTR levels, normalized to GAPDH (n=3). *P<0.05, **P<0.01, ***P<0.001, one-way ANOVA with Bonferroni's multiple comparison test.

A significant reduction of TrkB and p75^{NTR} levels (Figure 4.5) prompted me to investigate whether PTPN23 silencing had an effect on kinase-D-interacting substrate of 220 kDa (Kidins220; or ankyrin repeat-rich membrane spanning – ARMS). Kidins220 is a large scaffolding protein interacting with NTRs in response to NT stimulation, and is involved in regulation of NTR signalling, amongst its many functions (Neubrand et al., 2012). Importantly, Kidins220 was also identified in a large high-throughput proteomic study as a potential binding partner of PTPN23 (Hein et al., 2015), further suggesting that PTPN23 is involved in the NT signalling and trafficking.

First, a previously established co-immunoprecipitation (co-IP) assay (Figure 3.1) was used to explore the potential association between Kidins220, PTPN23 and BICD1. Anti-BICD1 or rabbit IgG control were used to co-IP protein complexes from N2A-FLAG-TrkB cell lysates, extracted in 0.2% NP-40 lysis buffer. Immunoblotting of co-IP fractions revealed that Kidins220, in addition to PTPN23, co-precipitated with BICD1-protein complexes (Figure 4.6A). These proteins were not detected in control co-IP. Although the significance of this potential

novel interaction is yet to be established, this preliminary finding strongly suggests that PTPN23 associates with protein complexes related to NTRs.

Next, I examined whether PTPN23 downregulation affects the level of Kidins220, as observed for TrkB and $p75^{NTR}$. In line with the results reported in Figure 4.5, silencing of PTPN23 led to a significant reduction of Kidins220 levels (Figure 4.6B,C). Furthermore, a loss of the characteristic membrane distribution of Kidins220 at cell-cell contact sites was detected upon PTPN23 silencing in N2A-FLAG-TrkB cells (Figure 4.6D).

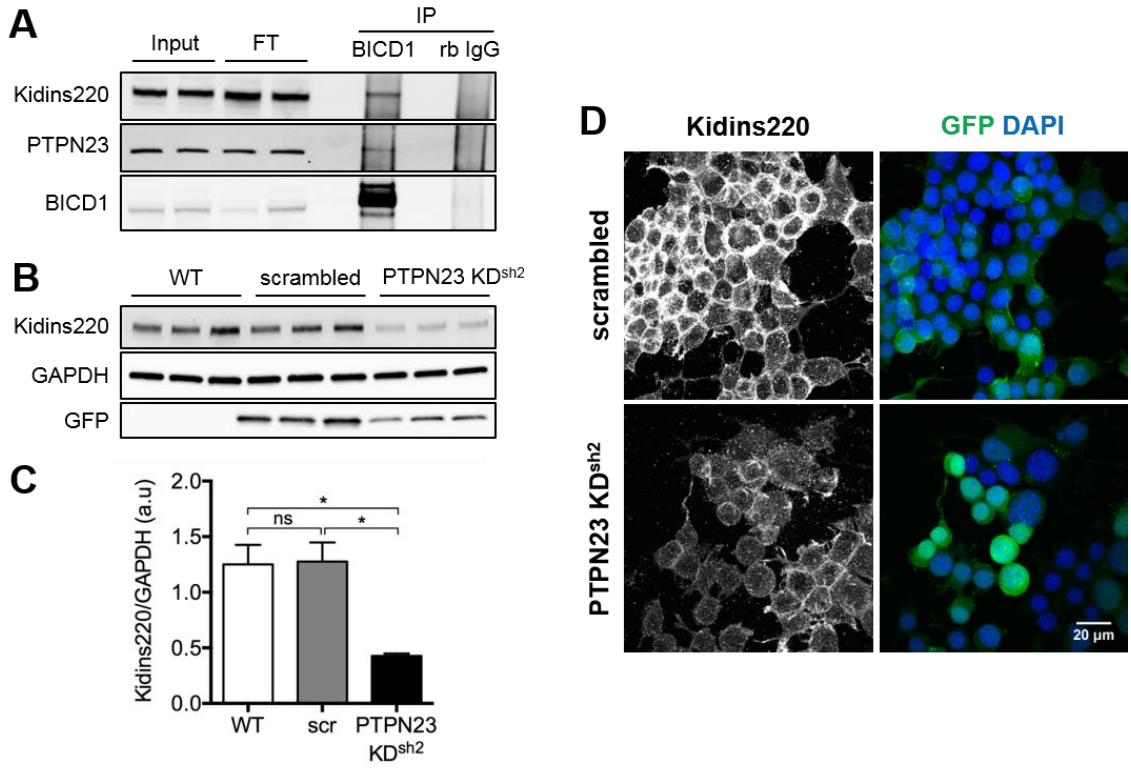

Figure 4.6 PTPN23 KD reduces levels of Kidins220

A) N2A-FLAG-TrkB cells were lysed in 0.2% NP-40 lysis buffer, and protein extracts were subjected to co-IP using magnetic Dynabeads pre-coated with anti-BICD1 antibody or rabbit IgG as control. Input, flow through (FT) and eluted fractions (IP) were immunoblotted using anti-BICD1, -PTPN23 and -Kidins220 (#KNA, CRUK) antibodies. For SDS-PAGE and western blotting, 1/40 of soluble lysate used for co-IP was loaded as input, and 1/40 of post-co-IP lysate as FT. Whole eluted fraction was loaded in the IP lane (n=1). B) Immunoblotting of proteins extracted from WT, scrambled or PTPN23 KD^{sh2} N2A-FLAG-TrkB cells, showing reduced Kidins220 levels upon PTPN23 knockdown (n=3). GAPDH was used as a loading control, and GFP as the lentiviral reporter. C) Densitometric analysis of Kidins220 levels, normalized to GAPDH (n=3). *P<0.05, one-way ANOVA with Bonferroni's multiple comparison test. D) Representative confocal images showing Kidins220 (#GSC16; CRUK) and GFP immunostaining in scrambled and PTPN23 KD^{sh2} N2A-FLAG-TrkB cells. Images show maximum intensity Z-stack projections (n=3).

Because of such prominent decrease in the levels of NTRs (Figure 4.5) and Kidins220 (Figure 4.6), I then assessed whether PTPN23 silencing leads to

increased proteasomal or lysosomal degradation of these proteins. The knockdown of BICD1 elicited a similar phenotype, where increased proteasomal degradation of TrkB was detected as an adaptive response to increased receptor recycling to the plasma membrane (Terenzio et al., 2014a).

To test whether loss of PTPN23 leads to increased degradation of NTRs and Kidins220, PTPN23 KD^{sh2} and scrambled cells were incubated for 5 or 24 h with a proteasome inhibitor, MG132 (15 or 5 µM) or a vacuolar (V)-ATP-ase inhibitor, which impairs lysosome function, bafilomycin A1 (BafA1; 0.5 or 0.1 µM). To assess proteasomal and lysosomal inhibition, cell lysates were immunoblotted for p62 and LC3. Inhibition of proteasome and lysosome function leads to an increase of p62 levels, as well as the increased ratio of LC3-II to LC3-I (Choe et al., 2014; Bao et al., 2016; Yoshii and Mizushima, 2017). These changes were observed after addition of MG132 or bafilomycin A1 to scrambled and PTPN23 KD^{sh2} cells, suggesting that both degradative pathways are functional and can be inhibited in these cells. Importantly, the level of several proteins of interest remained comparable with and without the drug treatments in PTPN23 KD^{sh2} cells, suggesting that the decrease in protein levels was not due to increased protein degradation. Interestingly, the overnight application of DMSO led to an increase in BICD1 levels, which should be taken into consideration in future studies using this vehicle. Furthermore, 5 h proteasome inhibition in scrambled cells resulted in an increase of PTPN23 levels, suggesting that PTPN23 is rapidly degraded by the proteasome, in line with previous reports (Mariotti et al., 2006; Castiglioni and Maier, 2012). Inhibition of proteasomal of lysosomal activity suggested that PTPN23 silencing did not drive the increased degradation of TrkB, p75^{NTR} or Kidins220.

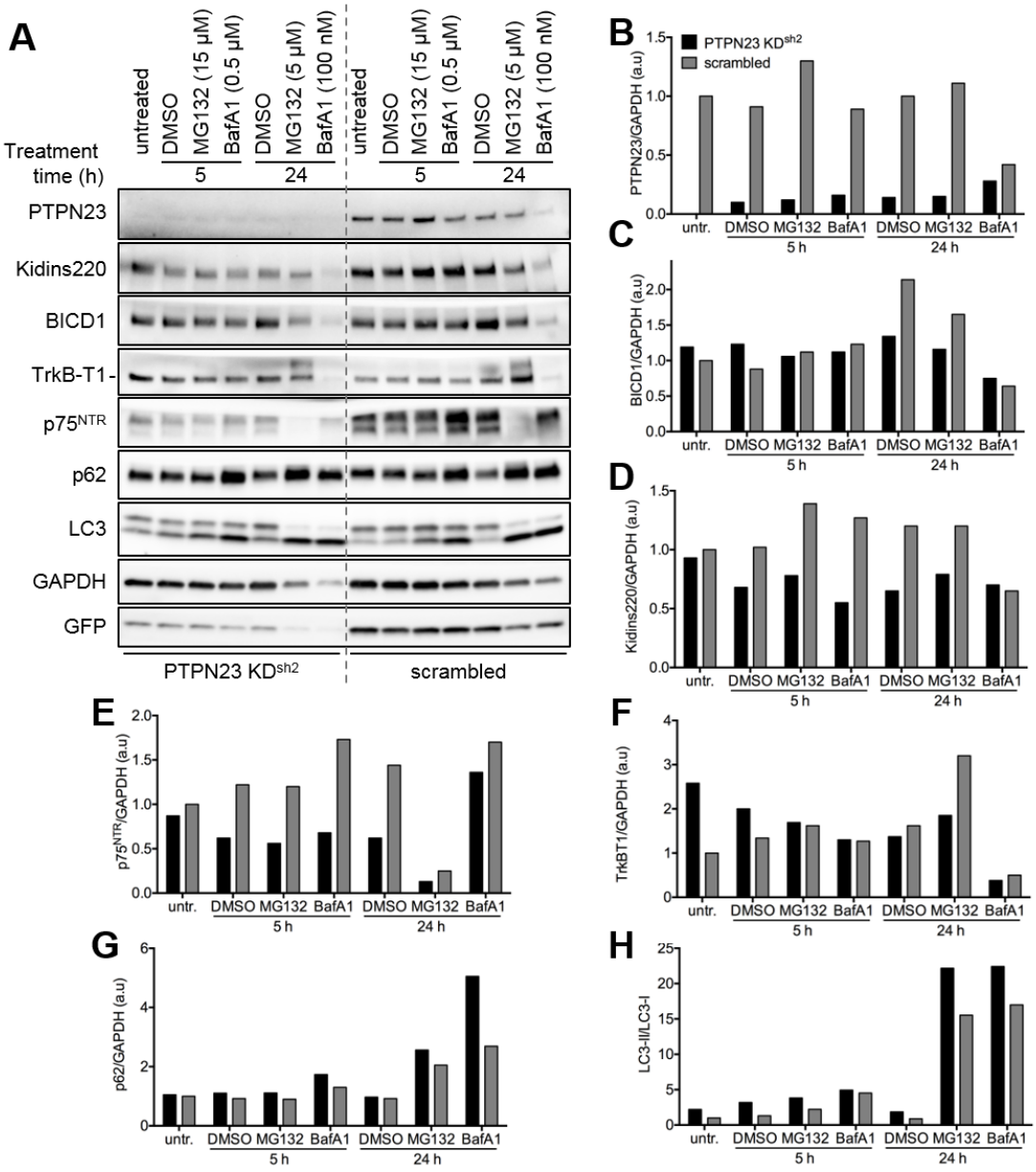

Figure 4.7 Reduced receptor levels is not a consequence of increased protein degradation.

A) Scrambled or PTPN23 KD^{sh2} cells were incubated for 5 h or overnight with MG132 (15 µM or 5 µM), bafilomycin A1 (BafA1; 0.5 µM or 100 nM) or vehicle control (DMSO). Proteins were extracted and immunoblotted for proteins of interest (n=1). B-G) Densitometric analyses of protein levels, normalized to GAPDH. H) Densitometric analysis of LC3-II/LC3-I ratio (n=1).

4.2.5 Sh2-resistant PTPN23 does not rescue the phenotype induced by endogenous PTPN23 downregulation

To control whether the decrease in protein levels was directly associated with the downregulation of PTPN23, a plasmid expressing shRNA2-resistant PTPN23 was generated. Due to technical challenges, the mutagenesis using previously characterized HA-PTPN23-pcDNA3.1 plasmid could not be performed (Doyotte

et al., 2008). Hence, using HA-PTPN23-pcDNA3.1 as a template, a sequence encoding amino acids 8-407 was subcloned into a plasmid expressing C-terminal dsRed2 fluorescent protein. Following succesful mutagenesis, a sequence encoding amino acids 408-1636 was then subcloned into the dsRed2 plasmid containing the sh2 resistant portion of PTPN23. I anticipated that using this approach I would be able to to easily detect the overexpressed protein by microscopy, following dsRed2 expression, without further need for immunocytochemistry with anti-PTPN23 antibodies.

PTPN23^{sh2Res}-dsRed2 was overexpressed overnight in wild type, scrambled or PTPN23 KD^{sh2} N2A-FLAG-TrkB cells, as well as in cells transduced with sh1. Sh1 is directed against a 3' site of PTPN23 sequence and hence it should silence the expression of PTPN23^{sh2Res}-dsRed2, due to the lack of sh1 resistance. First, cell lysates were immunoblotted to assess the levels of proteins of interest. Not only did PTPN23^{sh2Res}-dsRed2 not restore the the level of TrkB, p75^{NTR} and Kidins220, this plasmid was expressed at the lowest level in PTPN23 KD^{sh2} cells (Figure 4.8A). Because expression of PTPN23^{sh2Res}-dsRed2 was detected in PTPN23^{sh1} cells, albeit slightly lower than in scrambled or wild type cells, the observed decrease in TrkB, p75^{NTR} and Kidins220 levels, and potentially many other proteins, was most likely a result of off-target and expression-limiting effects of shRNA2 rather than specific PTPN23 silencing. Intriguingly, PTPN23^{sh2Res}-dsRed2 overexpression further decreased levels of NTRs and Kidins220 (Figure 4.8A). In addition, off-target effects of sh2 may be responsible for caspase-3 activation and induction of apoptosis in PTPN23 KD^{sh2} cells (Figure 4.8C,D).

Analysis of PTPN23^{sh2Res}-dsRed2 expression by microscopy revealed the odd behaviour of the mutant and the potential reason behind its effect on protein levels. In PTPN23 KD^{sh2} (Figure 4.8B) and scrambled cells (not shown), severe aggregation of PTPN23^{sh2Res}-dsRed2 was observed, suggesting that it was not likely to rescue the α-FLAG accumulation phenotype. Whether due to mutagenesis or chosen protein tag, it was not explored further.

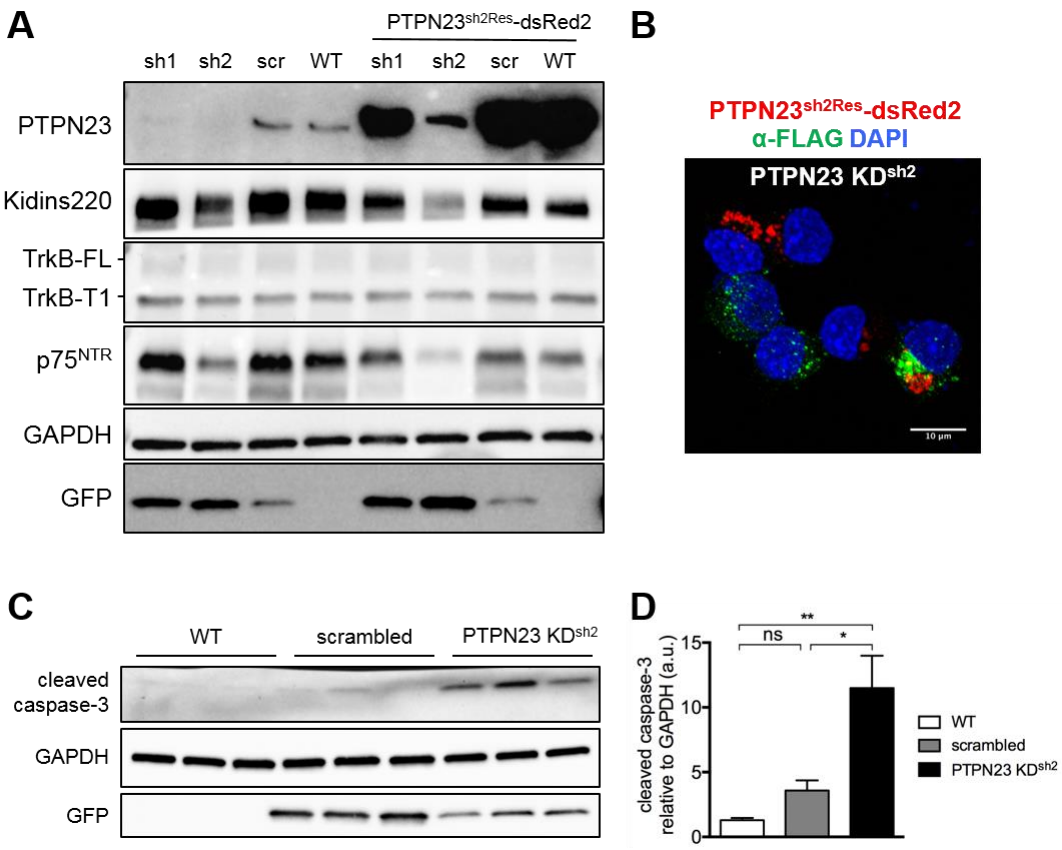

Figure 4.8 Sh2 is toxic to cells.

A) Immunoblotting of lysates from sh1, sh2, scrambled (scr) or wild type (WT) cells, containing overexpressed PTPN23^{sh2Res}-dsRed2, for proteins of interest. GAPDH was used as a loading control, and GFP as reporter for viral transduction (n=2). B) Representative merged image of PTPN23 KD^{sh2} cells overexpressing PTPN23^{sh2Res}-dsRed2. PTPN23^{sh2Res}-dsRed2 exhibited high levels of aggregation and did not rescue the vacuole-like α-FLAG accumulation phenotype. Scale bar: 10 µm. C) Immunoblotting of WT, scrambled and PTPN23 KD^{sh2} N2A-FLAG-TrkB cell lysates for cleaved caspase-3, GAPDH and GFP (n=3). D) Densitometric analysis of cleaved caspase-3 levels, normalized to GAPDH (n=3). *P<0.05, **P<0.01, one-way ANOVA with Bonferroni's multiple comparison test.

4.2.6 PTPN23 depletion by sh1 phenocopies NTR vacuole accumulation

In the last set of experiments, a toxic effect of sh2 was detected, which resulted in significant depletion of NTRs (Figure 4.5), Kidins220 (Figure 4.6), and potentially several other proteins. Because the levels of these proteins did not appear significantly perturbed in cells transduced with sh1 (Figure 4.8A), PTPN23 KD phenotype was re-evaluated using this shRNA.

First, the level of NTRs, Kidins220, BICD1 and cleaved caspase-3 was re-assessed by immunoblotting. Unlike sh2, the silencing of PTPN23 by sh1 was not accompanied by a decrease in protein levels, nor did it induce an increase in

cleaved caspase-3 (Figure 4.9A,B). Being able to study the deficit of PTPN23 using sh1 additionally meant that HA-PTPN23-pcDNA3.1 plasmid could be used for rescue experiments without further need for mutagenesis, as it encodes the human protein, the sequence of which slightly differs from the mouse transcript. However, as with sh2-mediated PTPN23 silencing, sh1 treatment also caused a significant detachment of cells from plates and coverslips, suggesting a role of PTPN23 in neuronal cell adhesion. These findings align with previous reports, which demonstrated that PTPN23 directly regulates cell adhesion proteins, such as integrins, E-cadherin and focal adhesion kinase (FAK) (Lin et al., 2011; Kharitidi et al., 2015; Castiglioni et al., 2007). In line with this, loss of PTPN23 is associated with increased metastatic potential in cancer (Manteghi et al., 2016; Zhang et al., 2017).

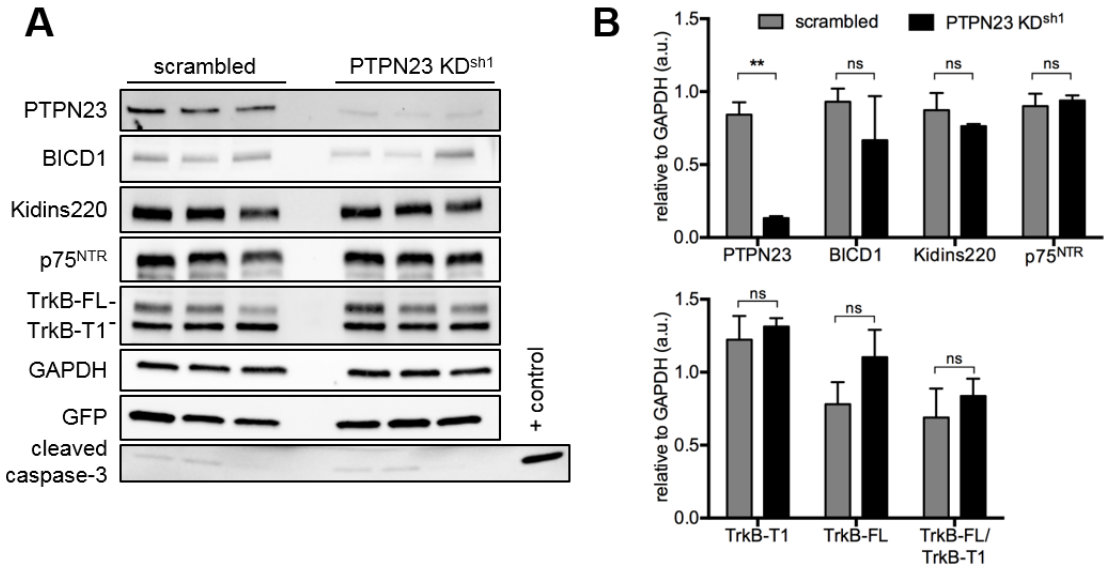

Figure 4.9 Sh1 does not reduce NTR-related protein levels.

A) Lysates of N2A-FLAG-TrkB cells, transduced with scrambled or sh1, were immunoblotted for the proteins of interest (n=3). While silencing PTPN23 expression, no decrease in other protein levels was observed in cells transduced with sh1. B) Densitometric analysis of protein levels, normalized to GAPDH. Not significant (ns) P>0.05; **P<0.01, unpaired Student's *t*-test.

Next, an anti-receptor antibody accumulation assay was repeated to establish whether silencing of PTPN23 using sh1 leads to NTR accumulation in vacuole-like compartments, as previously observed with sh2-mediated PTPN23 knockdown (Figure 4.4). First, using anti-FLAG antibody, previous observations were confirmed (Figure 4.4), and several cells with the vacuole-like phenotype were detected (not shown). However, a relatively small number of cells

internalized anti-FLAG antibody due to its low plasma membrane localization (Figure 4.2C). Hence, the abundance of cell surface and total p75^{NTR} levels was assessed in scrambled and PTPN23 KD^{sh1} cells, to establish whether it would be beneficial to use the anti-p75^{NTR} antibody in accumulation assays. The number of cells displaying p75^{NTR} on their surface was much higher than that of FLAG-TrkB (Figure 4.2C), and comparable between scrambled and PTPN23 KD^{sh1} cells (Figure 4.10). Similarly, no overt differences in the total receptor levels were observed in permeabilized cells (Figure 4.10), which correlated well with immunoblotting (Figure 4.9).

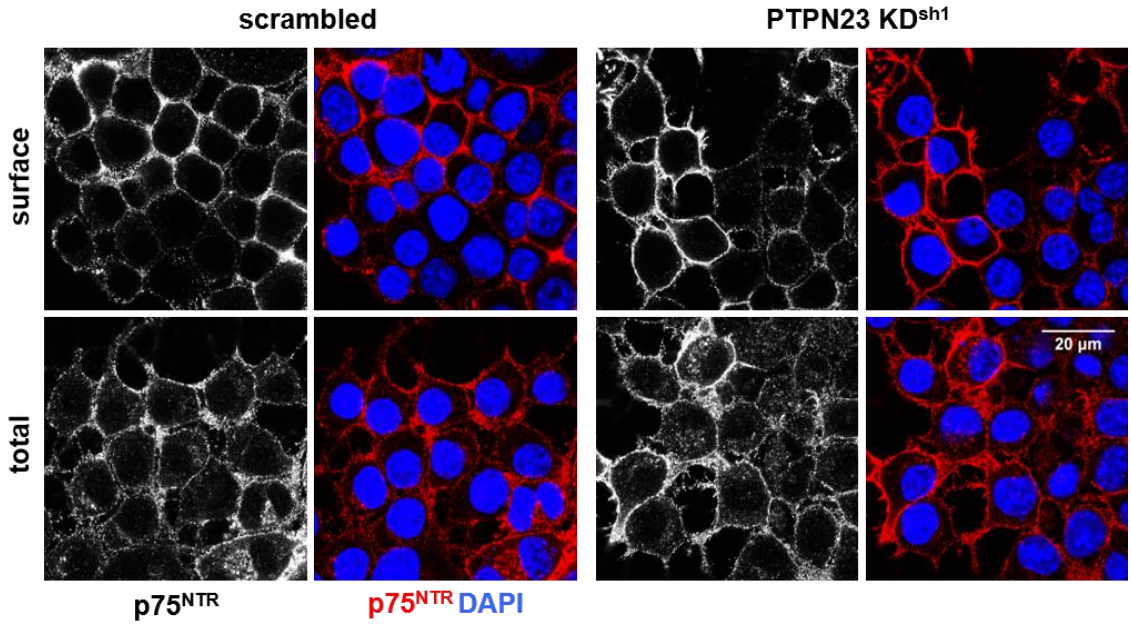

Figure 4.10 PTPN23 KD does not affect p75^{NTR} levels at the plasma membrane.

Representative confocal images showing surface (non-permeabilized cells) and total (permeabilized cells) p75^{NTR} immunostaining in scrambled and PTPN23 KD^{sh1} N2A-FLAG-TrkB cells (n=2).

Next, α-p75^{NTR} accumulation assay was performed in scrambled and PTPN23 KD^{sh1} cells. Similarly to α-FLAG, α-p75^{NTR} exhibited a vacuole-like immunostaining in cells with downregulated PTPN23 expression, although the perinuclear punctate phenotype of α-p75^{NTR} was dominant (Figure 4.11A). To assess the effect of PTPN23 depletion on endosome morphology, the diameters of endosomes were measured. To assess the relative frequency of endosome populations, endosome diameters were categorized using 0.5 µm binning, and further classified into two populations: <1.5 µm in diameter as “endo-lysosome”, and >1.5 µm as vacuolar compartments. As two distinct populations of

endosomes could be observed, further analysis revealed that depletion of PTPN23 led to a significant difference in the endosome diameters (Figure 4.11B; ****P<0.0001; two-tailed chi-square test for trend). Lastly, the proportion of cells bearing an endo-lysosome or a vacuole-like phenotype was determined. While the majority of scrambled cells with internalized α-p75^{NTR} exhibited punctate endo-lysosome pattern, PTPN23 knockdown resulted in a significant decrease of cells with this staining pattern, and significant increase of cells with a vacuolar phenotype. Because only 20% of PTPN23 KD^{sh1} cells exhibited the vacuolar phenotype, it suggests that residual PTPN23 or an alternative mechanism contributes to p75^{NTR} sorting. Nevertheless, these results suggested that PTPN23 downregulation leads to an accumulation of internalized NTRs into vacuole-like structures.

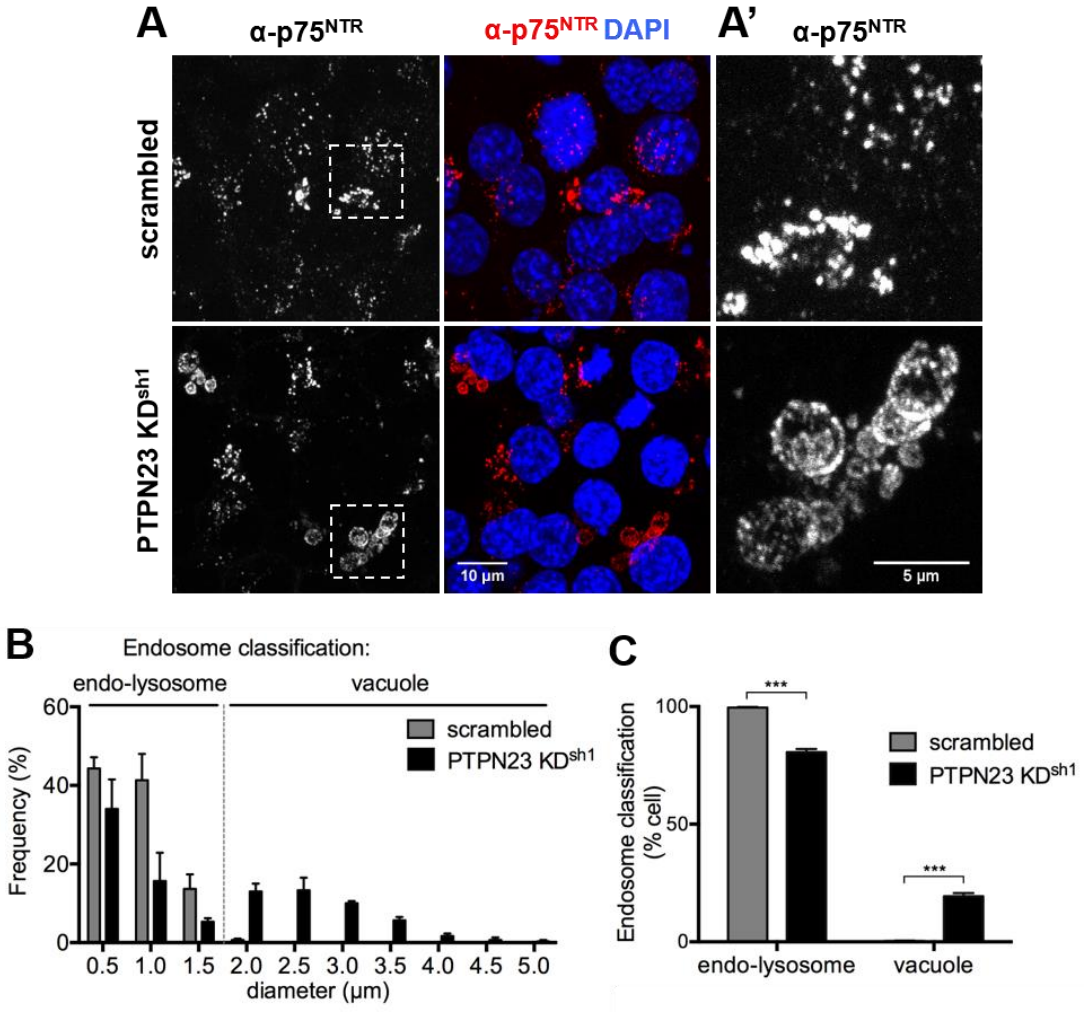

Figure 4.11 PTPN23 KD leads to accumulation of p75^{NTR} in vacuolar-like compartments.

A) Representative confocal images of α-p75^{NTR} accumulation assay in scrambled and PTPN23 KD^{sh1} cells. Images show maximum intensity Z-stack projections (n=5). A') Magnification of dashed rectangle area in A. B) Diameters of 100 endosomes (per n) were measured and grouped using 0.5 µm binning, in three independent experiments. Because of two distinct endosome

populations, the diameters of 50 puncta and 50 vacuoles were measured. As no vacuoles were detected in scrambled, the diameters of 50 large endosomes were measured, such as that visible in the centre in A (grayscale/scrambled). Endosomes were classified as endo-lysosomes (<1.5 μm) or vacuoles (>1.5 μm). C) Cells with endo-lysosome or vacuole phenotype were counted; overall approximately 50% of cells displayed clearly internalized α-p75^{NTR}. To demonstrate the proportion of either phenotype, cells lacking α-p75^{NTR} were not included in the analysis. Here, percentages of α-p75^{NTR}-positive cells with either phenotype are shown. For quantification, approximately 80 cells per field were counted, in 5 fields, in three independent experiments. ***P<0.001, unpaired Student's *t*-test.

Prior to evaluating the identity of vacuoles, I wanted to establish whether reintroducing PTPN23 expression would rescue this phenotype. Using the α-p75^{NTR} accumulation assay in N2A-FLAG-TrkB cells, overexpressing overnight the HA-PTPN23 construct, revealed a mixed phenotype. The vacuoles could be detected in cells lacking HA-PTPN23 expression (Figure 4.12A), as well as in cells with a very high expression level (not shown). However, punctate α-p75^{NTR} immunostaining was detected in several cells with an intermediate HA-PTPN23 expression level (Figure 4.12B), suggesting that the vacuole-like phenotype of α-p75^{NTR} in PTPN23 KD^{sh1} cells is a result of PTPN23 downregulation.

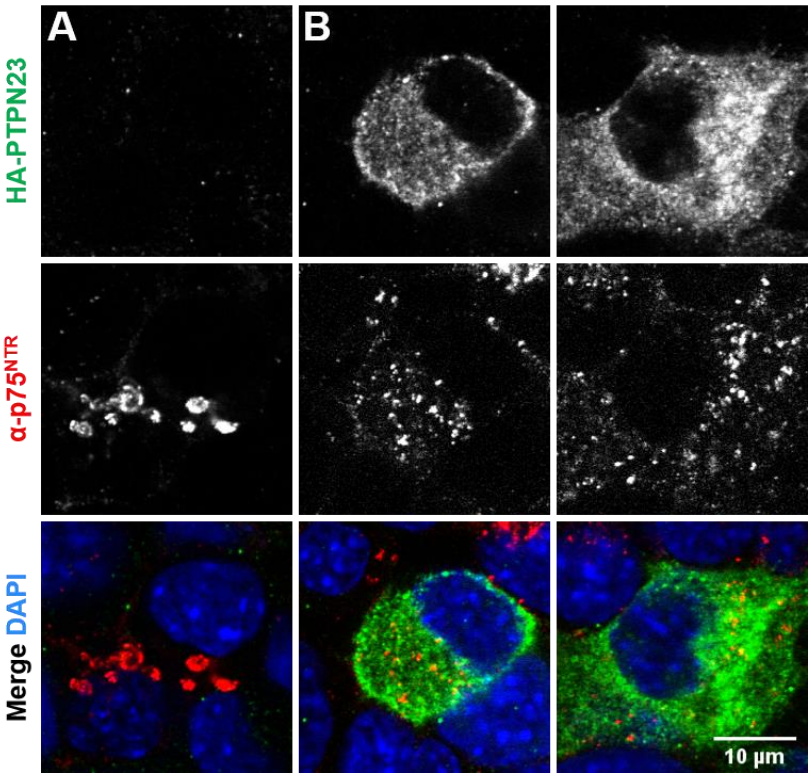

Figure 4.12 PTPN23 KD^{sh1} cells with intermediate HA-PTPN23 expression do not accumulate α-p75^{NTR} in vacuoles.

Representative confocal images of α-p75^{NTR} accumulation assay in PTPN23 KD^{sh1} cells, overexpressing HA-PTPN23. Cells were fixed and immunostained using anti-HA antibody. α-p75^{NTR} vacuolar phenotype could be detected in N2A-FLAG-TrkB cells lacking HA-PTPN23 expression (A). However, punctate α-p75^{NTR} immunostaining was detected in cells with an intermediate level of HA-PTPN23 expression (B; n=2).

4.2.7 Exploring the vacuole identity

Silencing of PTPN23 expression in N2A-FLAG-TrkB cells caused the an accumulation of NTRs in large endosomes of unique morphology, referred to as vacuoles, which were detected in a significant proportion of cells (Figure 4.11). These results correlated with previous studies, reporting the localization of internalized receptors, such as EGFR (Doyotte et al., 2008) and PDGFR (Ma et al., 2015), as well as α5β1 integrin (Kharitidi et al., 2015) in similar compartments upon PTPN23 downregulation. In these reports, these receptor-containing large organelles often co-labelled with markers of early and recycling endosomes. Furthermore, deficit of PTPN23 usually caused an increased receptor recycling to the plasma membrane. Past studies revealed not only that PTPN23 facilitates lysosomal degradation of activated transmembrane receptors, but also directly controls endosomal maturation and MVB biogenesis (Doyotte et al., 2008).

To further explore the nature of α-p75^{NTR} vacuoles, the accumulation assay was performed using the same anti-p75^{NTR} antibody labelled with 5 nm gold nanoparticles (α-p75^{NTR}-gold), in scrambled and PTPN23 KD^{sh1} N2A-FLAG-TrkB cells. After acid wash and appropriate fixation, cells were processed as previously described (Terenzio et al., 2014a), and the identity of α-p75^{NTR}-gold-containing organelles were revealed by transmission electron microscopy. Internalized α-p75^{NTR}-gold was detected in a number of different structures/organelles, which were classified into three categories, based on their morphology. Those included: 1) organelles of low electron density, resembling early endosomes, tubules or vesicles; 2) electron-dense organelles resembling late endosomes and lysosomes; 3) swollen vacuoles with a diameter >500 nm. Examples of these organelles, taken from representative images, are shown in Figure 4.13. All organelles containing gold particles were imaged, and a comparable number of images was acquired per genotype, with approximately 80 organelles (per genotype per total number of images) counted. Whilst gold particles were detected to a similar degree in tubulo-vesicular and late endo-lysosomal organelles in both genotypes, vacuoles were observed exclusively in cells lacking PTPN23. These swollen compartments did not contain internal membranous structures, and accumulated α-p75^{NTR}-gold near their surrounding membrane, suggesting that loss of PTPN23 resulted in defective sorting of NTRs and potentially other cargoes.

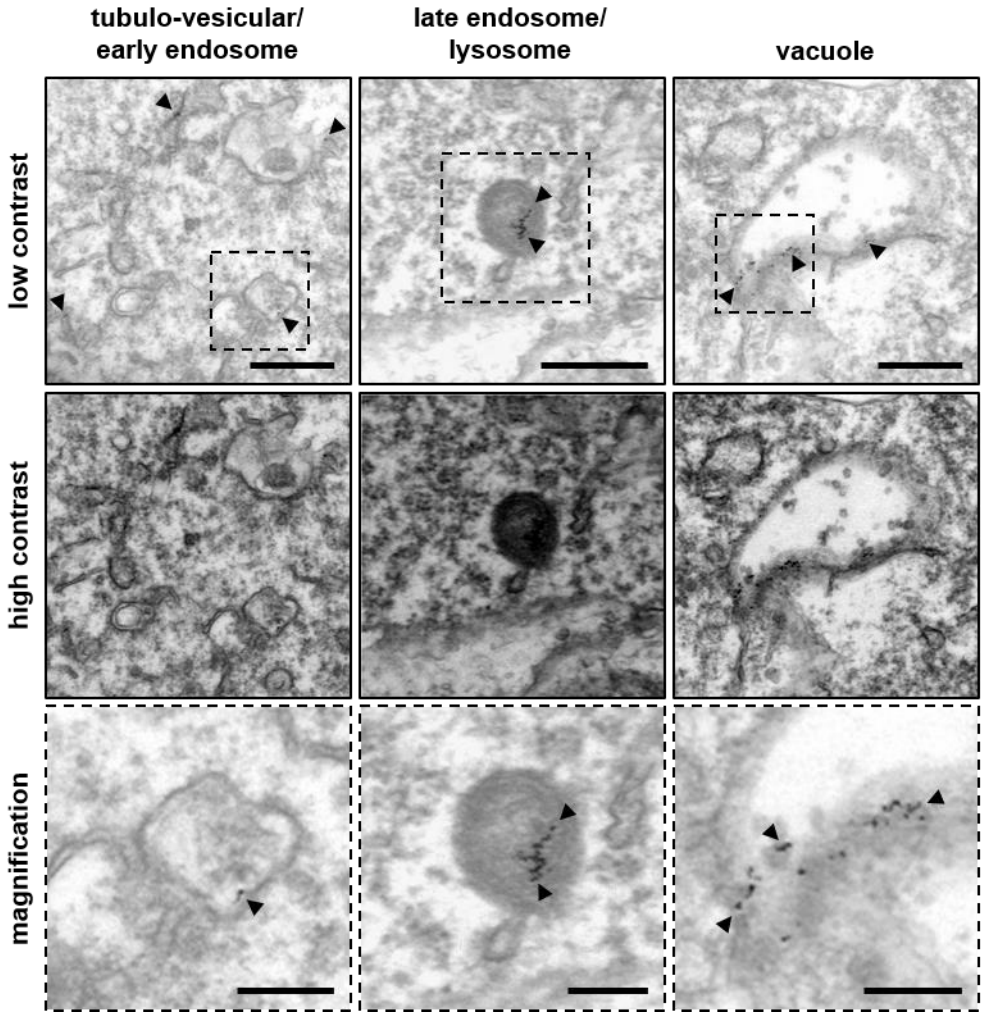

Figure 4.13 Identification of α-p75^{NTR}-gold organelles by transmission electron microscopy.

Representative transmission electron microscopy images showing the three classes of organelles containing α-p75^{NTR}-gold (arrowheads; n=1; approximately 37 images acquired per genotype). Vacuole-like compartments were detected exclusively in N2A-FLAG-TrkB cells depleted of PTPN23. Scale bars: 500 nm (low contrast); 200 nm (magnification).

Next, I investigated the co-localization of α-p75^{NTR} with markers labelling early endosomes (early endosome antigen 1; EEA1) and late endosomes (Rab7), in scrambled and PTPN23 KD^{sh1} N2A-FLAG-TrkB cells.

The EE1 immunostaining was predominantly punctate in all cells. In scrambled cells, very little co-localization between EEA1 and α-p75^{NTR} endo-lysosomes was detected. In contrast, EEA1 co-labelling with α-p75^{NTR} vacuoles was consistently observed in cells with downregulated PTPN23 expression. However, EEA1 usually exhibited a punctate staining on the periphery of the vacuoles, rather than fully co-localizing with it, and several of these EEA1 puncta, associating with the same vacuole scanned across the Z-plane, could be observed. In most of the

vacuoles, assessed across the Z-plane, peripheral punctate EEA1 immunostaining was detected (Figure 4.14A,A').

Unlike EEA1, Rab7 immunostaining was heavily clustered. In scrambled and PTPN23 KD^{sh1} cells, Rab7 co-localized with α-p75^{NTR} puncta (Figure 4.14B). With regards to α-p75^{NTR} vacuoles in PTPN23 KD^{sh1} cells, a mixed phenotype was observed. Some of the vacuoles fully co-localized with Rab7, while others almost lacked Rab7 immunostaining. Lack of Rab7 co-localization was especially evident in the largest vacuoles, although some Rab7 puncta-like association was detected, similarly to EEA1, as shown on the example in Figure 4.14B' (middle panel). Taken together, these findings suggest that α-p75^{NTR} vacuoles in PTPN23 KD^{sh1} cells correspond to organelles of mixed identity, originating from early endosomes and partially co-labelling with late endosome markers, suggestive of an intermediate endocytic compartment. Vacuole morphology implies that PTPN23 plays a role in α-p75^{NTR}-containing endosome maturation and α-p75^{NTR} retrieval, and its deficit results in the disruption of the overall endocytic flow.

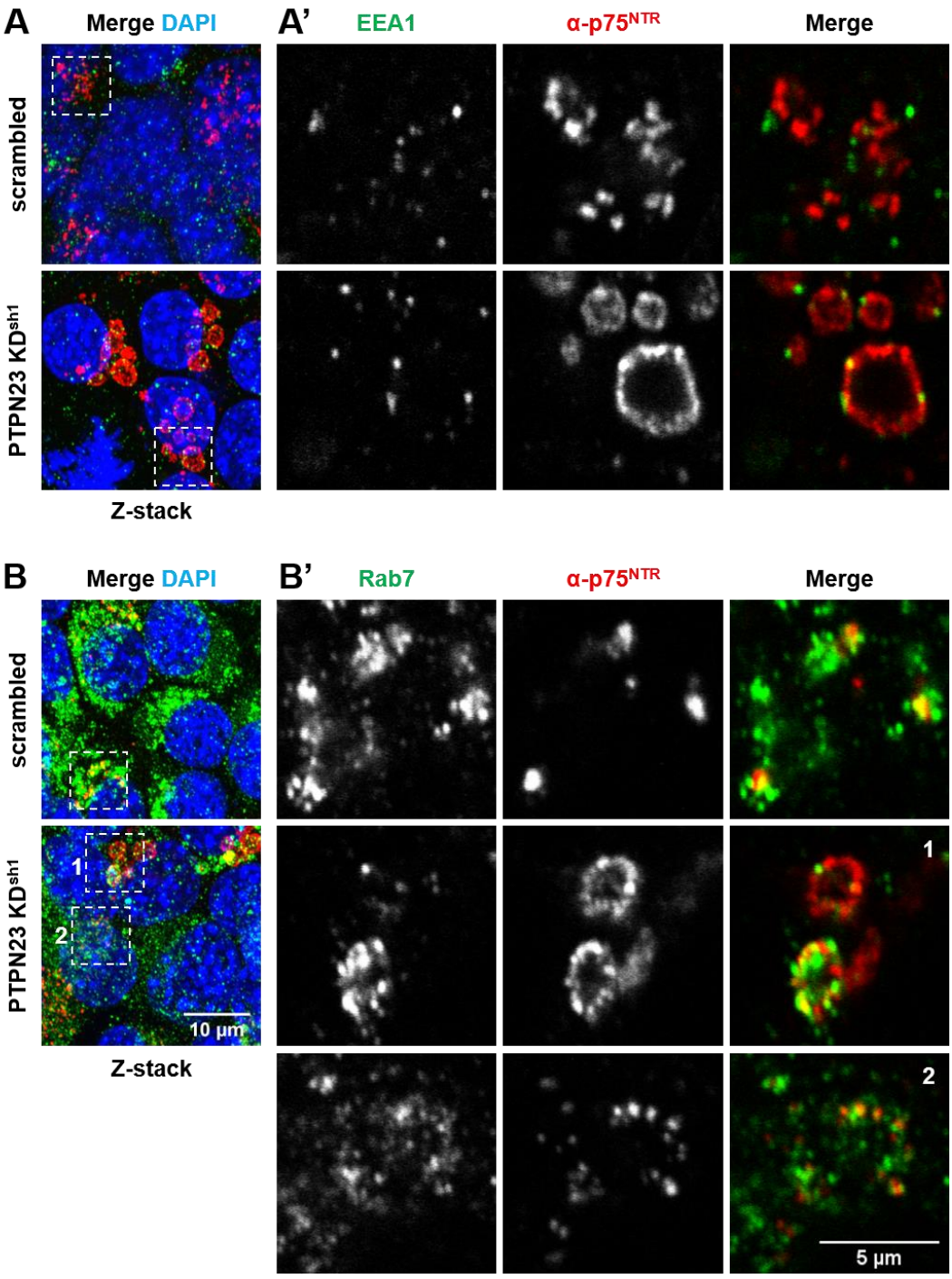

Figure 4.14 α-p75^{NTR} vacuoles exhibit mixed identity.

Representative confocal images of α-p75^{NTR} accumulation assay in scrambled and PTPN23 KD^{sh1} cells. Following acid wash and fixation, cells were immunostained using anti-EEA1 (A,A') or anti-Rab7 (B,B') antibodies (n=3). A,B) Merged images showing maximum intensity Z-stack projections. Dashed rectangles depict area used to show magnification of a representative single Z-plane (A'B').

Lastly, I investigated whether α-p75^{NTR}-containing vacuoles were positive for ubiquitin. Although p75^{NTR} ubiquitination has not been extensively explored (Sanchez-Sanchez and Arevalo, 2017), it was previously demonstrated that in

hippocampal neuronal cell line HT-22, stimulation with NGF leads to p75^{NTR} phosphorylation-dependent ubiquitination by the ubiquitin ligase TRAF6 (Geetha et al., 2012). Interestingly, PTPN23 mediates EGFR deubiquitination by recruiting USP8 onto EGFR, and this ubiquitin recycling step is necessary to downregulate EGFR-mediated signalling and its sorting into MVBs for subsequent lysosomal degradation (Ali et al., 2013). In line with this, EGFR-vacuoles in cells depleted of PTPN23 show increased co-labelling with ubiquitin (Doyotte et al., 2008). Furthermore, increased TrkB ubiquitination was also detected in cells lacking BICD1 (Terenzio et al., 2014a).

As previously, scrambled and PTPN23 KD^{sh1} cells were immunostained upon α-p75^{NTR} internalization using the anti-ubiquitin antibody FK2, which recognizes mono- and poly-ubiquitin chains. Interestingly, nearly all α-p75^{NTR} vacuoles in PTPN23 KD^{sh1} cells, but not α-p75^{NTR} puncta in either scrambled and PTPN23 KD^{sh1} cells, fully co-localized with ubiquitin (Figure 4.15). These results suggest that PTPN23 mediates ubiquitin recycling from NTR-containing endosomes. However, as a relatively small population of cells exhibited the vacuolar phenotype (Figure 4.11D), direct p75^{NTR} ubiquitination, such as by immunoprecipitation, was not explored further.

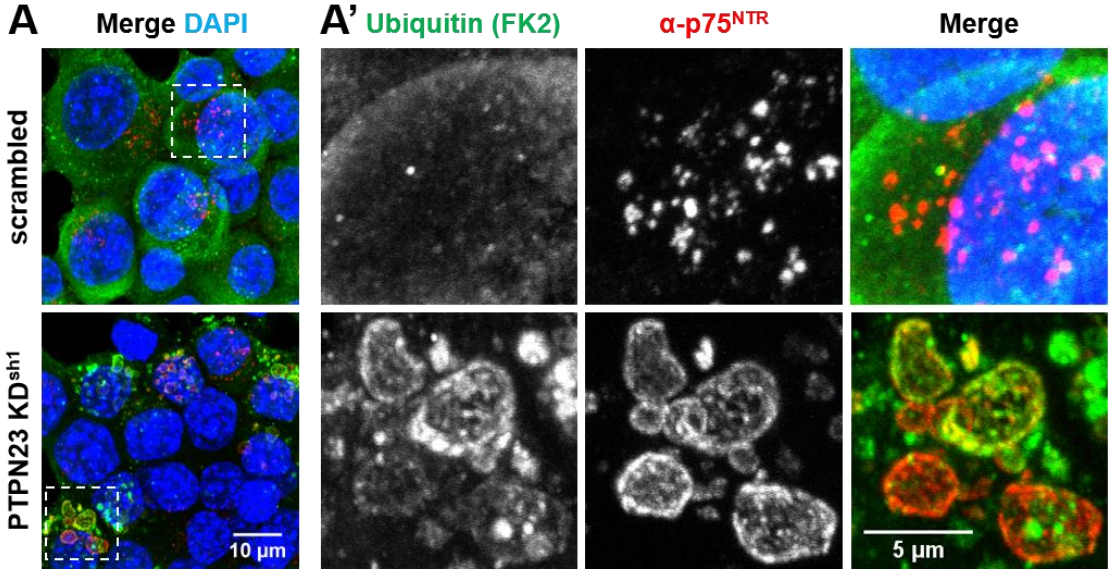

Figure 4.15 α-p75NTR vacuoles are heavily ubiquitinated.

Representative confocal images showing α-p75^{NTR} accumulation assay in scrambled and PTPN23 KD^{sh1} cells, immunostained using anti-ubiquitin antibody (FK2; n=3). Merged images (A) and magnified dashed rectangle area (A') show maximum intensity Z-stack projections.

4.3 Discussion and future directions

Endocytosis, trafficking and degradation of cargoes, such as transmembrane signalling receptors, are some of the most important biological processes in all cells (Scott et al., 2014). Signalling by ligand-activated transmembrane receptors directly regulates cellular growth, differentiation, proliferation or survival. Because these process are highly complex, their tight regulation on several levels is essential for cellular health and homeostasis (Huotari and Helenius, 2011), and their misregulation may lead to changes in cellular behaviour, often observed in tumorigenesis (Hanahan and Weinberg, 2011). Unlike other cell types, differentiated neurons do not undergo cell division, and appropriate control over receptor signalling is crucial. As such, signalling mediated by neurotrophins and their receptors (NTRs) is pivotal for neuronal health and survival, but most of all it plays an integral role in the development and correct wiring of the nervous system (Huang and Reichardt, 2001). Our laboratory demonstrated that BICD1 participates in the downregulation of activated NTRs, ultimately regulating the signalling elicited by these receptors (Terenzio et al., 2014b; Terenzio et al., 2014a). This finding led to the identification of its new binding partner PTPN23. This non-canonical member of the ESCRT machinery mediates the turnover of several distinct receptors by facilitating their forward transition from an early endosome, through MVBs and late endosomes, to the lysosomes, which consequently downregulates the signalling capacity of these receptors (Tabernero and Woodman, 2018). In the previous chapter, I explored the basis of the BICD1-PTPN23 interaction, which could provide some clues to deciphering their role in receptor fate decisions. To further our understanding of this novel molecular interaction, the association of PTPN23 with the NTR pathway was investigated. Here, I demonstrated that PTPN23 co-localized with BDNF-activated TrkB receptor in neuronal cells, and its downregulation led to the accumulation of TrkB and $p75^{NTR}$ receptors in aberrant ubiquitinated organelles, providing the first functional evidence of the role of PTPN23 in mammalian neuronal cells.

4.3.1 PTPN23 mediates sorting of NTRs

To study the association between PTPN23 and NTRs, I utilized an antibody-mediated receptor accumulation assay, a popular tool used to follow the lifecycle

of transmembrane receptors. Using this approach, I demonstrated that PTPN23 co-localized with internalized TrkB receptors in N2A-FLAG-TrkB cells (Figure 4.2). Silencing of PTPN23 expression using shRNA lentivirus, and subsequent PTPN23 downregulation, resulted in increased accumulation of internalized TrkB and $p75^{NTR}$ receptors in enlarged vacuole-like compartments, which were up to 5 µm in diameter (Figure 4.4; Figure 4.11; Figure 4.13). Although shRNA2 was toxic and caused a global decrease of NTRs and Kidins220, and activated apoptosis (Figure 4.5-Figure 4.8), the same vacuole-like receptor accumulation phenotype (Figure 4.4) was detected when PTPN23 silencing was driven by shRNA1 (Figure 4.11), and was rescued by expression of shRNA-resistant human PTPN23 (Figure 4.12). In addition, a potential novel interaction between BICD1, PTPN23 and Kidins220 was uncovered (Figure 4.6A), further highlighting the involvement of PTPN23 in the neurotrophin-related pathway. Subsequent analysis of the aberrant $p75^{NTR}$-containing compartments by transmission electron microscopy revealed the characteristics of a swollen early endocytic compartment (Figure 4.13), which morphologically correlated with previous studies reporting such structures (Bright et al., 1997; Stefan et al., 2017). In these vacuole-like organelles, gold particles conjugated to $p75^{NTR}$ antibody were detected near the surrounding membrane, suggesting that membrane loss of PTPN23 resulted in defective lumenal sorting of NTRs and potentially other cargoes. Then, co-localization analysis of vacuoles revealed that they contain markers of early endosome (EEA1), and some of them exhibited an extensive Rab7 staining (Figure 4.14). These results suggest that this compartment has mixed features of sorting or intermediate endocytic organelles in N2A-FLAG-TrkB cells. As EEA1 immunostaining was very weak in N2A-FLAG-TrkB cells, further analysis using a more general early endosome marker, such as Rab5, should be performed in future studies (Deinhardt et al., 2006). The association of these organelles with Rab5 effector protein APPL1 should also be investigated, as it was found on a sub-population of early sorting endosomes mostly negative for EEA1 (Kalaidzidis et al., 2015). APPL1 associates with diverse transmembrane receptors (Diggins and Webb, 2017), including TrkA (Lin et al., 2006), TrkB (Fu et al., 2011) and EGFR (Miaczynska et al., 2004a), and couples early ligand-induced receptor trafficking and MAPK/AKT signalling events (Diggins and Webb, 2017; Goto-Silva et al., 2019). In particular, it would be interesting to explore whether loss of PTPN23 leads to changes in NTR association with EEA1 and

APPL1 endosomes, and the ESCRT make-up of these organelles, to establish whether a deficit in PTPN23 potentially induces the preferential sorting of receptors into the recycling rather than the degradation route (Kalaidzidis et al., 2015). Interestingly, a study conducted in HeLa cells found that the early endocytic route of EGFR, marked by the presence of the ESCRT-0 components, is largely APPL1-independent and instead EGFR associates with an early endocytic vesicle positive for SNX15 (Flores-Rodriguez et al., 2015). In contrast, BDNF-activated TrkB in hippocampal neurons extensively colocalizes with APPL1 signalling endosomes, which exhibit retrograde motility (Fu et al., 2011; Goto-Silva et al., 2019), suggesting that the association of different signalling receptors with distinct endosomal populations could be context- and cell type-specific.

Consistent with reports of PTPN23-mediated recruitment of the deubiquitinating enzyme USP8 to EGFR prior to its sorting and subsequent lysosomal degradation (Doyotte et al., 2008; Ali et al., 2013), $p75^{NTR}$-containing vacuoles were heavily ubiquitinated in cells depleted of PTPN23 (Figure 4.15). Regrettably, a direct analysis of $p75^{NTR}$ ubiquitination was not performed in this work and should be addressed in future studies, as an activity-dependent post-translational modification of $p75^{NTR}$ was previously reported (Geetha et al., 2012). Whether PTPN23 recruits deubiquitinating enzymes such as USP8 to $p75^{NTR}$, and potentially TrkB, prior to their sorting, should be investigated in future studies, which would contribute to current knowledge about the NTR fate-regulation by this post-translational modification and PTPN23 (Sanchez-Sanchez and Arevalo, 2017). Indeed, the interaction between NGF-activated TrkA and USP8 on early endosome, necessary for NGF-TrkA degradation, was demonstrated in PC12 cells (Ceriani et al., 2015), providing a potential further link between PTPN23 and NTRs. Furthermore, several USP family members, including USP3 and 5, localize on axonal signalling endosomes containing Trks (Debaisieux et al., 2016).

4.3.2 BICD1-PTPN23 receptor sorting hypothesis

Linking mechanistically the function of PTPN23 and BICD1 to cargo sorting, taking into account the current understanding of these proteins and the sorting process, is conceptually challenging. What makes it even more complicated, are

the differences between trafficking and sorting processes in neurons and mitotic cells (Terenzio et al., 2017), as well as the documented heterogeneity of signalling endosomes in different cells and locations within a neuron (Villarroel-Campos et al., 2018). Although further work is necessary to fully characterize PTPN23 downregulation phenotype, the role of PTPN23 in cargo sorting process is easier to understand than that of BICD1, due to massive ground work in the characterization of PTPN23 function in the sorting of EGFR (Woodman, 2016; Gahloth et al., 2017; Tabernero and Woodman, 2018). In addition, PTPN23 binds endophilin A1 (Ichioka et al., 2007), and endophilins participate in endocytic sorting of TrkB in hippocampal cultures (Burk et al., 2017). Interestingly, depletion of endophilins leads to accumulation of TrkB in endosomes marked by EEA1 and Rab7 (Burk et al., 2017), which perfectly align with observations documented in this work (Figure 4.14).

To elucidate the potential mechanism by which BICD1 and PTPN23 regulate endocytic sorting of NTRs, lets summarize the collective receptor sorting phenotype, observed upon the knockdown of these proteins in neuronal and mitotic cells, assuming PTPN23 plays the same role in NTR sorting in neuronal cells as demonstrated for EGFR and other receptors (Doyotte et al., 2008; Kharitidi et al., 2015; Ma et al., 2015; Parkinson et al., 2015). The shared features include: 1) receptor accumulation in enlarged vacuole-like compartments; 2) perturbed endosome maturation and deficit in MVB biogenesis; 3) increased receptor ubiquitination; 4) increased receptor recycling to the plasma membrane. These features generally align with perturbed function of the ESCRT machinery (Frankel and Audhya, 2018), and suggest that BICD1 may contribute to this process. In neurons, BICD1 is likely to exert this function in the somatic compartment, where its perinuclear enrichment (Figure 3.2; 3.3), and NTR accumulation upon its depletion is observed (Terenzio et al., 2014a). Furthermore, while BICD1 was initially detected on purified signalling endosomes (Terenzio et al., 2014a), that was not the case when these organelles were isolated at different time points from ES-MNs using a similar approach (Debaisieux et al., 2016), suggesting that BICD1 may transiently associate with this organelle, within a specific time window. In line with this, BICD1 depletion in motor neurons does not significantly alter the transport kinetics of signalling endosomes *in vitro* (Terenzio et al., 2014b). However, recent results by Fellows et.al. suggests that upregulation of axonal BICD1 boosts the transport of

signalling endosomes upon modulation of IGF1 receptor (Fellows and Schiavo, submitted). The general consensus is that the interaction between the components of ESCRT-II complex (VPS22 and VPS36), Rab-interacting lysosomal protein (RILP) and dynein facilitate late endosome transport towards lysosomes (Progida et al., 2006; Wang and Hong, 2006; Reck-Peterson et al., 2018). Interestingly, both overexpression (Wang and Hong, 2006) and depletion (Progida et al., 2007) of RILP cause the prolonged EGFR retention in enlarged early endosomes and perturbed MVB biogenesis in HeLa cells.

What is the potential function of BICD1 in this process, in light of its association with PTPN23? There are a few possibilities, which could be explored further in future studies. First of all, the exact identity of different ESCRT components associated with NTR-containing signalling endosomes should be established. As demonstrated for MHC class I, its sorting does not require ESCRT-II (Parkinson et al., 2015), and PTPN23 bridges the interaction between ESCRT-I and ESCRT-III machinery. Due to phenotypic similarities, this finding raises the possibility that upon signalling endosome delivery to the soma, BICD1 may play a role similar to that of RILP (Progida et al., 2007), via the association with PTPN23 rather than ESCRT-II.

In the previous experimental chapter, I demonstrated that PTPN23 associates with the C-terminus of BICD1-CC1 (Figure 3.5), which binds dynein with high affinity. Therefore, establishing whether PTPN23 and dynein can bind BICD1 simultaneously represents an important priority for the future, as it might reveal the potential role of BICD1 in the cargo sorting process. In addition, based on our findings using mutant BICD1 lacking the PTPN23- and dynein-binding region, it is crucial to explore whether BICD1, activated by binding of a cargo to its C-terminus, can associate with kinesin. Simultaneous binding of BICD2 to dynein and kinesin was previously shown to allow centrosome and nuclear positioning before mitotic entry (Splinter et al., 2010). The concerted actions of dynein and kinesin are important for endosome maturation and “tug of war” endosome fission-fusion events (Driskell et al., 2007; Soppina et al., 2009). Therefore, an interesting hypothesis, based on the fact that swollen endosomes are observed after BICD1 and PTPN23 knockdowns, is that the association between dynein-kinesin-BICD1 and PTPN23 may contribute to this process. To date, the kinesin adaptors involved in this process have not been fully identified (Granger et al.,

2014). In line with this, early endosome fission is necessary for cargo sorting to the degradative and recycling pathways, and extensive endosome tubulation was previously observed in PTPN23 and BICD1-depleted cells, a sign of perturbed endosome fission (Huotari and Helenius, 2011). In contrast, BICD1-dynein may oppose the action of kinesin, as increased action of kinesin-3 (KIF16B) at early endosomes leads to a decrease in cargo degradation and increased recycling (Hoepfner et al., 2005).

It is unlikely that BICD1 is the main determinant for the recruitment of PTPN23 onto endosomes, as several lines of evidence suggests that PTPN23 can directly associate with transmembrane receptors, such as EGFR, and their adaptors. PTPN23 recruitment onto early endosome membranes is also facilitated by ESCRT-0 and -I, which directly polymerize on the surface of these organelles. It would be important to assess whether BICD1 depletion elicits a similar perturbed sorting phenotype for receptors, such as EGFR, the sorting of which is regulated by PTPN23.

4.3.3 Challenges with studying PTPN23 function in neurons

The primary goal of this chapter was to explore the function of PTPN23 in NTR sorting in motor neurons. To date, its function in the mammalian nervous system has not been extensively explored, yet its high expression in the nervous tissue during early development suggests it plays an important role in this process (Gingras et al., 2009a). Furthermore, studies on the *Drosophila* orthologue of PTPN23, Myopic, suggest that its function in the nervous system extends beyond receptor sorting. In fact, a recent studies demonstrated that Myopic may play a role in neurotransmission at neuromuscular junction, by downregulating the activity-dependent release of *Drosophila* insulin-like peptide 2 (Dilp-2) neuropeptide from dense core vesicles at the synapse (Bulgari et al., 2018), as well as in synaptic pruning during development (Loncle et al., 2015).

Regrettably, I was not able to explore the function of PTPN23 in NTR sorting directly in ES-MNs. Although I overcame the challenges of shRNA delivery into these cells, their extensive detachment from the culture plates and coverslips made it infeasible to perform reliably antibody-receptor accumulation and BDNF signalling assays. In the future, an alternative approach should be explored for this purpose, such as the use of microfluidic chambers (MFC) (Park et al., 2006),

or change of the growth substrate to a more advanced matrix, such as growth factor-reduced Matrigel. In MFCs, neurons projecting their axons along the microgrooves are essentially “trapped” between a dish and polymer surfaces, which could potentially share forces on their surface contributing to the decrease of the observed neuronal detachment. A three-dimensional (3D) neuronal culture could be another alternative to study the function of PTPN23 (Lin et al., 2011; Frimat et al., 2015). However, as PTPN23 controls turnover of proteins involved in cell adhesion (Castiglioni et al., 2007; Kharitidi et al., 2015), changing the culturing system may not necessarily overcome this problem. Indeed, loss of PTPN23 is associated with increased cell migration, tumorigenesis and invasiveness in cancer (Manteghi et al., 2016; Gingras et al., 2017). What would be the physiological consequence of PTPN23 loss with respect to neuronal adhesion is not known. However, a number of reports have recently recognized a link between mutations within *PTPN23*, encephalopathies and global developmental delay (Alazami et al., 2015; Sowada et al., 2017; Smigiel et al., 2018), suggesting that fully functional PTPN23 is vital for the development of a functional mammalian nervous system, which would align well with its role in NTR sorting demonstrated in this work. Interestingly, it is during mammalian embryonic development when the expression of the neurotrophins and their receptors (Huang and Reichardt, 2001), BICD1 (Terenzio et al., 2014a) and PTPN23 (Gingras et al., 2009a) is the highest in the nervous system. Both BICD1 and PTPN23 knock out animal models are embryonic lethal (Gingras et al., 2009; Fridolfsson et al., 2010), suggesting that both proteins play vital roles in early developmental processes, making them challenging candidates to study.

4.3.4 Final conclusions

In summary, I provided the first evidence that PTPN23 mediates the sorting of NTRs in neuronal cells. However, the receptor accumulation phenotype was detectable in a relatively small proportion of cells, suggesting alternative mechanisms of NTR sorting or that residual levels of PTPN23 were sufficient to mediate maturation of NTR-containing endosomes. Because of the challenges of studying PTPN23 function in ES-MNs, and the heterogeneity of the NTR accumulation phenotype in N2A-FLAG-TrkB cells, an alternative model should be developed, such as an inducible PTPN23 knockdown, to study the trafficking and sorting of endogenous NTRs. In addition, plasma membrane recycling and

BDNF-mediated signalling in neuronal cells depleted of PTPN23 needs to be explored to determine whether PTPN23 knockdown causes a similar phenotype to that reported with BICD1 depletion.

5 BICD1 and PTPN23 in stress granule dynamics

5.1 Aims of this Chapter

The main aim of Chapter 5 is to explore novel aspects of stress granule (SG) biology. This will broadly contribute to the current understanding of cellular stress responses and regulation of SG dynamics, which may facilitate the development of therapeutic targets for treating devastating neurological disorders and cancer. Following up on the findings of Loschi et al. (2009), I wanted to investigate whether BICD1 is a *bona fide* component of SGs and if so, establish the determinants of its targeting to these membrane-less organelles. Next, using our PTPN23 knockdown model, I assessed whether PTPN23 plays a role in stress granule dynamics.

5.2 Results

5.2.1 Establishing an oxidative stress assay

Oxidative stress plays a central role in many chronic disorders, including neurological conditions, cancer and cardiovascular diseases (Uttara et al., 2009). Exposure of cells to oxidative, endoplasmic reticulum (ER) and other environmental stresses exhibits in formation of SGs – a membrane-free organelles comprising complex ribonucleoprotein particles (RNPs) (Anderson and Kedersha, 2006).

Immortalized cell lines are a popular model to study SG composition and dynamics (Tourrière et al., 2003; Kedersha et al., 2005; Loschi et al., 2009; Markmiller et al., 2018; Zhang et al., 2018). To investigate the role of BICD1 in oxidative stress response, I first set out to establish the assay in N2A-FLAG-TrkB, outlined in Figure 5.1A. Changing to fresh basic media for an hour before stress induction was suggested to improve the reproducibility of SG-related assays (Jain et al., 2016, Wheeler et al., 2017); full media contains antioxidants and other components likely to influence a response to oxidative stress (Halliwell, 2014). For oxidative stress assays in neurons, it may not be advisable to use full motor neuron medium, supplemented with B27™, rich in antioxidants and vitamins (Brewer and Cotman, 1989; Brewer et al., 1993). For these reasons, all stress assays in N2A-FLAG-TrkB cells and primary motor neurons (pMNs) were

performed in plain Dulbecco's modified Eagle's medium (DMEM) or Neurobasal (NB), respectively, unless stated otherwise.

To induce oxidative stress, N2A-FLAG-TrkB cells were treated for one hour at 37°C with vehicle or 0.5 mM sodium arsenite ($NaAsO_2$) – a well-characterized oxidative stress inducer commonly used to study SG biology (Yang and Bloch, 2007; Kato et al., 2012; Jain et al., 2016). To preserve SGs, cells were immediately placed on ice and fixed for 5 min, followed by 10 min fixation at room temperature (RT) with 4% paraformaldehyde in phosphate-buffered saline (PFA/PBS). Next, cells were immunostained for a canonical SG marker, Ras GTPase-activating protein-binding protein 1 (G3BP) (Tourrière et al., 2003; Kedersha et al., 2005) (Figure 5.1B). Cells bearing >3 SG, of >0.5 μm in diameter, were then scored as SG-positive, in line with previous studies (Aulas et al., 2017; Fay et al., 2017; Fay and Anderson, 2018; Xie et al., 2018). While SGs were detected in 80% of cells treated with sodium arsenite (Figure 5.1C), no SGs were observed in vehicle-treated cells cultured in these conditions. Treatment with sodium arsenite had no effect on cell density, however it caused a drastic change in cellular morphology, exhibited by cell rounding, blebbing of the plasma membrane and retraction of protrusions, observed by light microscopy (not shown) and staining of actin cortex with phalloidin (arrows, Figure 5.1B). SGs are protective against cell death (Eisinger-Mathason et al., 2008), yet oxidative stress may ultimately lead to apoptosis (Zou et al., 2011). Hence, cells with fragmented nuclei, although not more prevalent in treated cells compared to controls, were excluded from quantification.

Having successfully elicited and detected SGs, I then wanted to examine whether BICD proteins and PTPN23 associate with SGs in N2A-FLAG-TrkB cells and primary motor neurons (pMN) during oxidative and ER stresses.

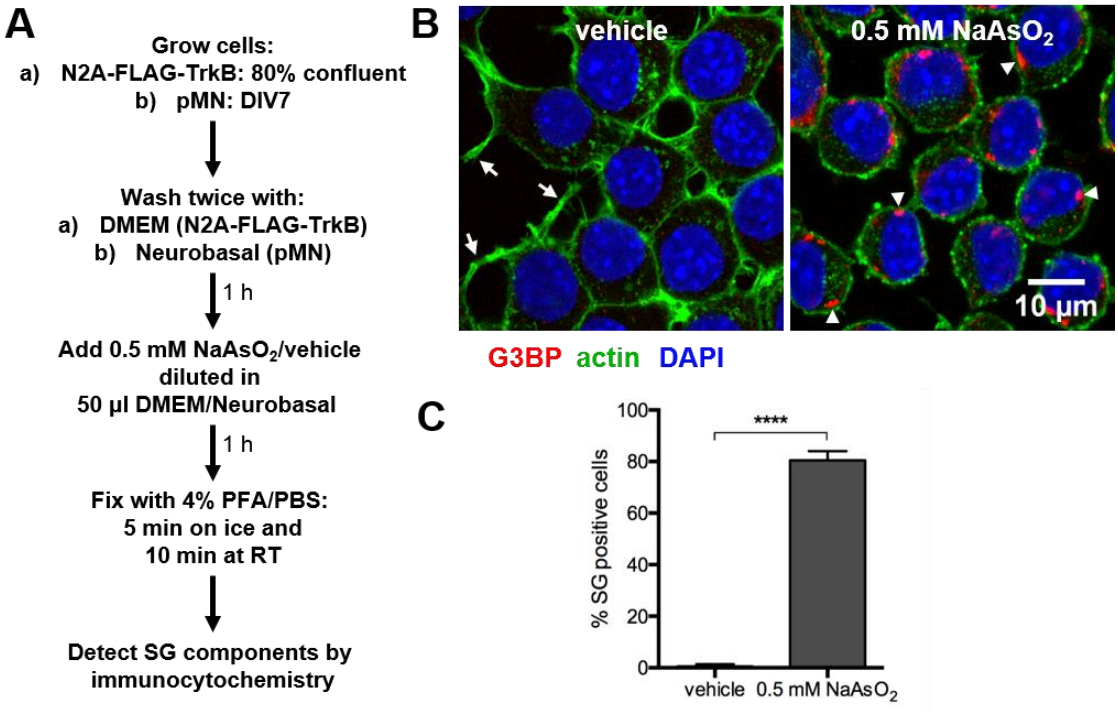

Figure 5.1 Oxidative stress in N2A-FLAG-TrkB cells.

A) Flow diagram outlining the steps of oxidative stress assay. In short, cells were grown to desired confluency, and cultured in serum-free fresh medium for an hour. Next, vehicle or 0.5 mM sodium arsenite was applied for the following hour to induce oxidative stress. To preserve SGs, cells were pre-chilled and fixed on ice for 5 min followed by standard fixation and immunocytochemistry. B) Cropped representative confocal images showing successful detection of SGs (arrowheads) using anti-G3BP antibody in N2A-FLAG-TrkB cells treated with sodium arsenite, but not in vehicle control. Oxidative stress leads to retraction of protrusions, visible in vehicle-treated cells (arrows). Actin filaments were stained with fluorescently-labelled phalloidin and nuclei with DAPI (n=3). C) Cells with healthy nuclei containing >3 SGs (>0.5 µm in diameter) were counted as SG-positive. No SGs were present in vehicle-treated cells. For each condition, four fields were imaged and an average of 50 cells per field were counted in three independent experiments. ****P<0.0001, unpaired Student's *t*-test.

5.2.2 Mammalian BICDs as novel components of SGs

Next, I investigated the association of BICD proteins with SGs. In their work, Loschi et al. (2009) deciphered the role of anterograde and retrograde trafficking machinery in SG formation. Using siRNA, they revealed that dynein heavy chain 1 (DHC1) and BICD1 (but not DHC2 or BICD2) are essential for SG formation, whereas kinesin heavy chain (KHC, KIF5B) and light chain (KLC1, but not KLC2) for SG disassembly. In addition, DHC1, dynein intermediate chain (DIC), KHC and KLC directly co-localize with SG components (TIAR, PABP and STAU1) in fibroblast cell lines (COS-7 and NIH3T3). However, co-localization of BICD1 and BICD2 with SG markers was not explored. Interestingly, dynein adaptors, including BICDs, Hooks or Spindly, were not identified to date in proteomic

screens of SG-related and -interacting proteins (Jain et al., 2016; Markmiller et al., 2018; Youn et al., 2018), raising the question on how SGs recruit molecular motor complexes for their transport in mammalian cells.

The association of BICD1 with SGs in N2A-FLAG-TrkB cells was examined first. Following the previously established oxidative stress assay, cells were fixed and immunostained for BICD1 and G3BP. Confocal microscopy revealed punctate cytoplasmic distribution of both proteins in vehicle-treated cells, with BICD1 being predominantly localized to the Golgi apparatus and protrusion tips (Figure 5.2A,A'), as previously shown (Figure 3.2; 3.4A). No obvious co-localization was observed between these proteins in control cells, as shown by fluorescence intensity profiles (Figure 5.2B). After sodium arsenite treatment, G3BP was recruited to SGs (Figure 5.2A,A'), as previously reported (Tourrière et al., 2003). These G3BP-positive stress granules (G3BP$^+$ SGs) were positive for BICD1, and this was verified by fluorescence intensity profiles (Figure 5.2B). An increased accumulation of BICD1 in the perinuclear region was also apparent after oxidative stress induction (Figure 5.2A).

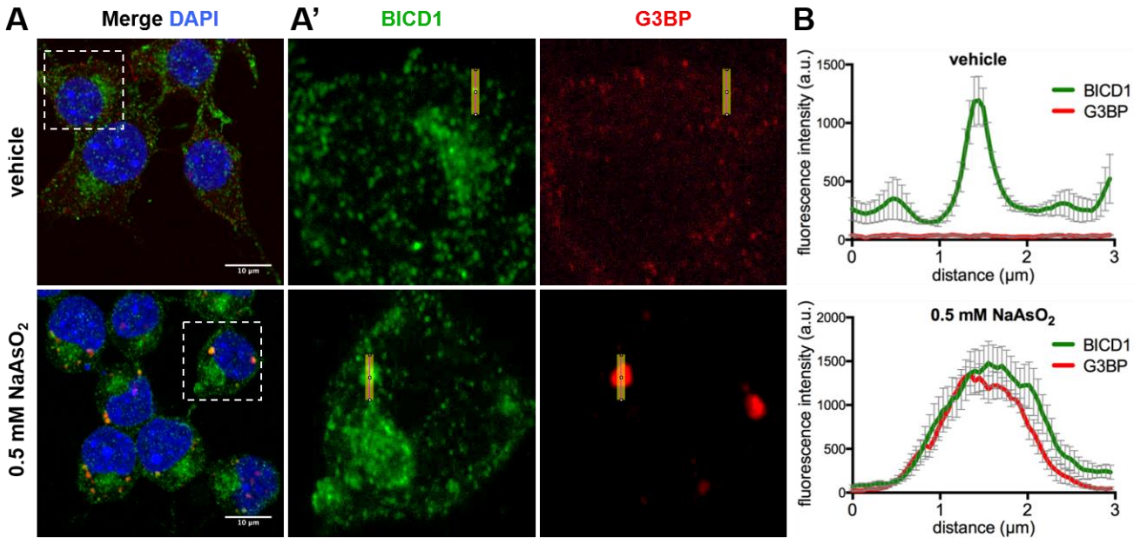

Figure 5.2 BICD1 co-localizes with SGs in N2A-FLAG-TrkB cells.

A) Representative confocal images of N2A-FLAG-TrkB cells treated with vehicle or 0.5 mM sodium arsenite, and immunostained for BICD1 and G3BP (n=3). Images show maximum intensity Z-stack projections, acquired at 0.5 µm spacing. Dashed rectangle indicates magnified area. Scale bar: 10 µm. A') Magnification of A. B) Fluorescence intensity profiles across the line (10 pixel wide, 3 µm long) drawn through six different puncta/SGs, as shown in an example in A', were plotted per treatment. Error bars: SEM. Fluorescence intensity profiles of both proteins overlap after treatment with sodium arsenite.

SG composition strongly depends on the stress stimuli (Kedersha et al., 1999), metabolic state (Buchan et al., 2011), cell type and cellular localization (Tsai et al., 2009; Markmiller et al., 2018). To verify whether BICD1 is present in somatic SGs in pMNs, the oxidative stress assay (as outlined in Figure 5.1A) was conducted on embryonic ventral horn cultures at DIV7.

Cells were fixed and immunostained for BICD1, G3BP and neuron-specific marker, βIII-tubulin (Figure 5.3). In control cells, G3BP was localized particularly in the somatic compartment and less-so in the neurites, while BICD1 was abundant throughout the cell with an enrichment in the perinuclear region. As previously observed (Figure 5.2), acute oxidative stress resulted in formation of $BICD1^{+}$ SGs in motor neurons and surrounding cells (ventral horn fibroblasts and glia cells) (Figure 5.3A). $G3BP^{+}$ SGs were observed predominantly in pMN's somatic compartment, and their size and morphology were more heterogenous when compared to these in surrounding non-neuronal cells or N2A-FLAG-TrkB cells. Although recent evidence suggests the presence of SGs in the neurites (Tsai et al., 2009; Markmiller et al., 2018; Sahoo et al., 2018), due to lack of distinct foci, no further analysis was performed and I focussed on the neuronal soma. Unlike in N2A-FLAG-TrkB cells, no striking morphological changes or membrane blebbing in motor neurons treated with sodium arsenite were observed. Abundance of BICD1 in somatic SGs was further examined by confocal microscopy. BICD1 clearly co-localized with G3BP (Figure 5.3B), which was verified by fluorescence intensity profiles of both proteins (Figure 5.3C).

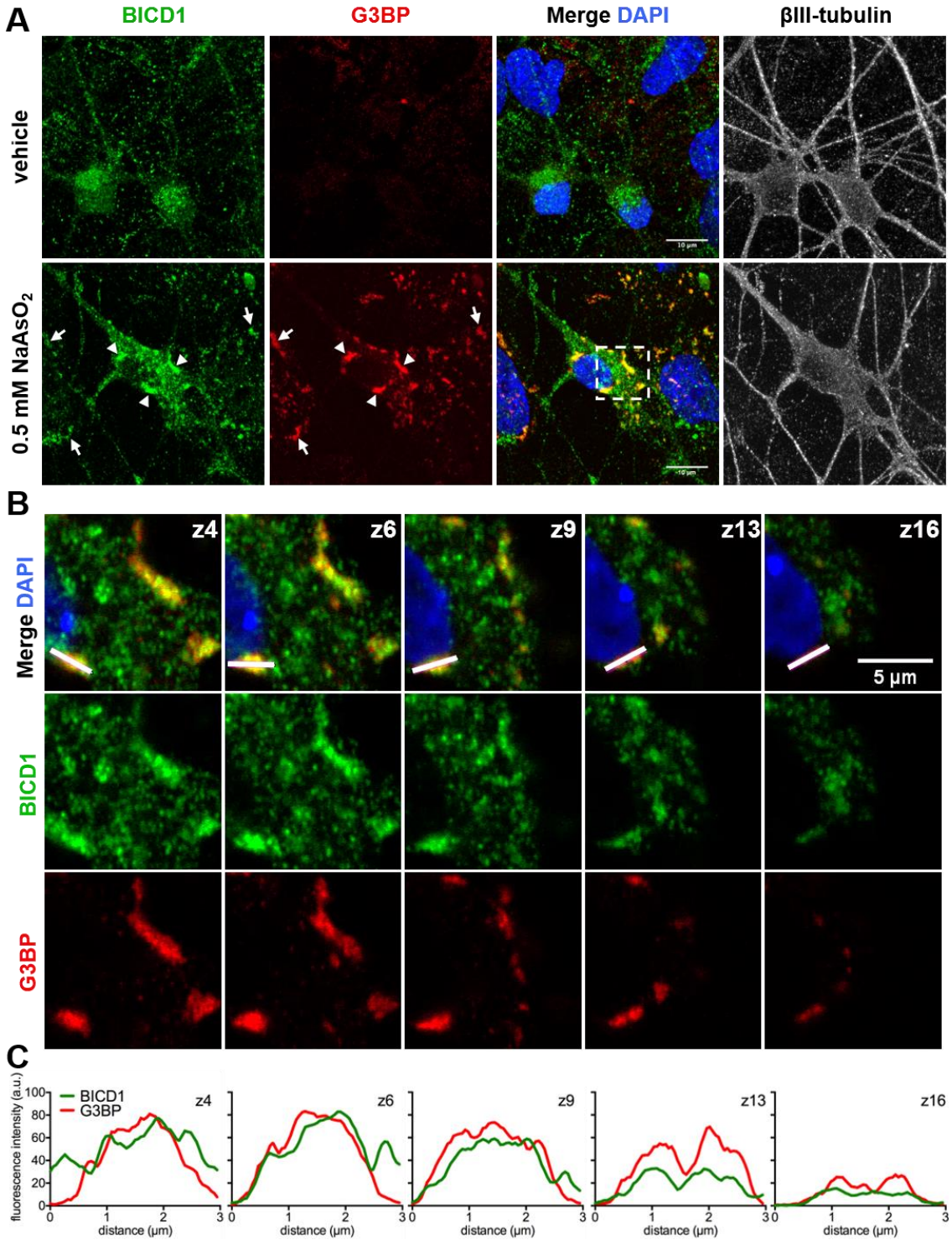

Figure 5.3 BICD1 is a novel SG component in pMNs.

A) Confocal images of pMNs treated with vehicle or 0.5 mM sodium arsenite, and immunostained for BICD1, G3BP and βIII-tubulin (n=3). The presence of SGs was evident in pMN soma (arrowheads) as well as in surrounding cells (arrows) cultured from mouse ventral horn. Images show maximum intensity Z-stack projections, acquired at 0.2 µm spacing. Dashed rectangle in sodium arsenite treatment depicts area used to shown magnification, through selection of Z-planes, in B. B) Confocal slicing of βIII-tubulin-positive (not shown) motor neuron soma. White line visible in merged images was used to acquire fluorescence intensity profiles of both proteins, in separate channels. C) Fluorescence intensity profiles of BICD1 and G3BP along the white line (3 µm long, 10 pixels wide) in merged images (B), drawn at different angles across SG, showing large overlap between both proteins.

Currently, no link between BICD2 and SGs has been previously established. Unlike BICD1, it is not essential for SG assembly (Loschi et al., 2009). To explore this further, I assessed by confocal microscopy the co-localization of BICD1 (Figure 5.4A) and BICD2 (Figure 5.4B) with another well-established stress granule marker, fragile X mental retardation protein (anti-FMRP antibody; #sc-101058, Santa Cruz), in N2A-FLAG-TrkB cells and pMN cultures. Interestingly, the *Drosophila* orthologue BicD regulates expression of FMRP, its bi-directional transport and dendritic branching (Bianco et al., 2010), as well as mRNA localization and transport in oogenesis and embryogenesis (Bullock and Ish-Horowicz, 2001).

In vehicle-treated cells, FMRP was diffused in the cytoplasm and largely absent in the nucleus. In pMNs, FMRP was particularly abundant in the soma and nearly absent in neurites (Figure 5.4), similarly to G3BP. BICD1 (Figure 5.4A) and BICD2 (Figure 5.4B) were present throughout neurons and N2A-FLAG-TrkB cells, and perinuclear enrichment was more evident for BICD1. Both proteins were enriched at the tips of N2A-FLAG-TrkB protrusions. In pMNs, FMRP-positive SGs ($FMRP^+$ SGs) formed nearly exclusively in the soma, similarly to $G3BP^+$ SGs (Figure 5.3). Importantly, $FMRP^+$ SGs were positive for BICD1 (Figure 5.4A) and BICD2 (Figure 5.4B) in examined cells. Interestingly, accumulation of BICD1 in the perinuclear region after exposure to sodium arsenite, as seen previously (Figure 5.4A), was observed to less extend for BICD2 in both cell types (Figure 5.4B).

Overall, oxidative stress evoked by sodium arsenite triggered the redistribution of BICD1 and BICD2 in N2A-FLAG-TrkB cells and pMNs, and both dynein adaptors co-localized with SG markers, G3BP and FMRP. Next, I wanted to verify whether this response is unique to oxidative stress or a feature of a more general response to stress.

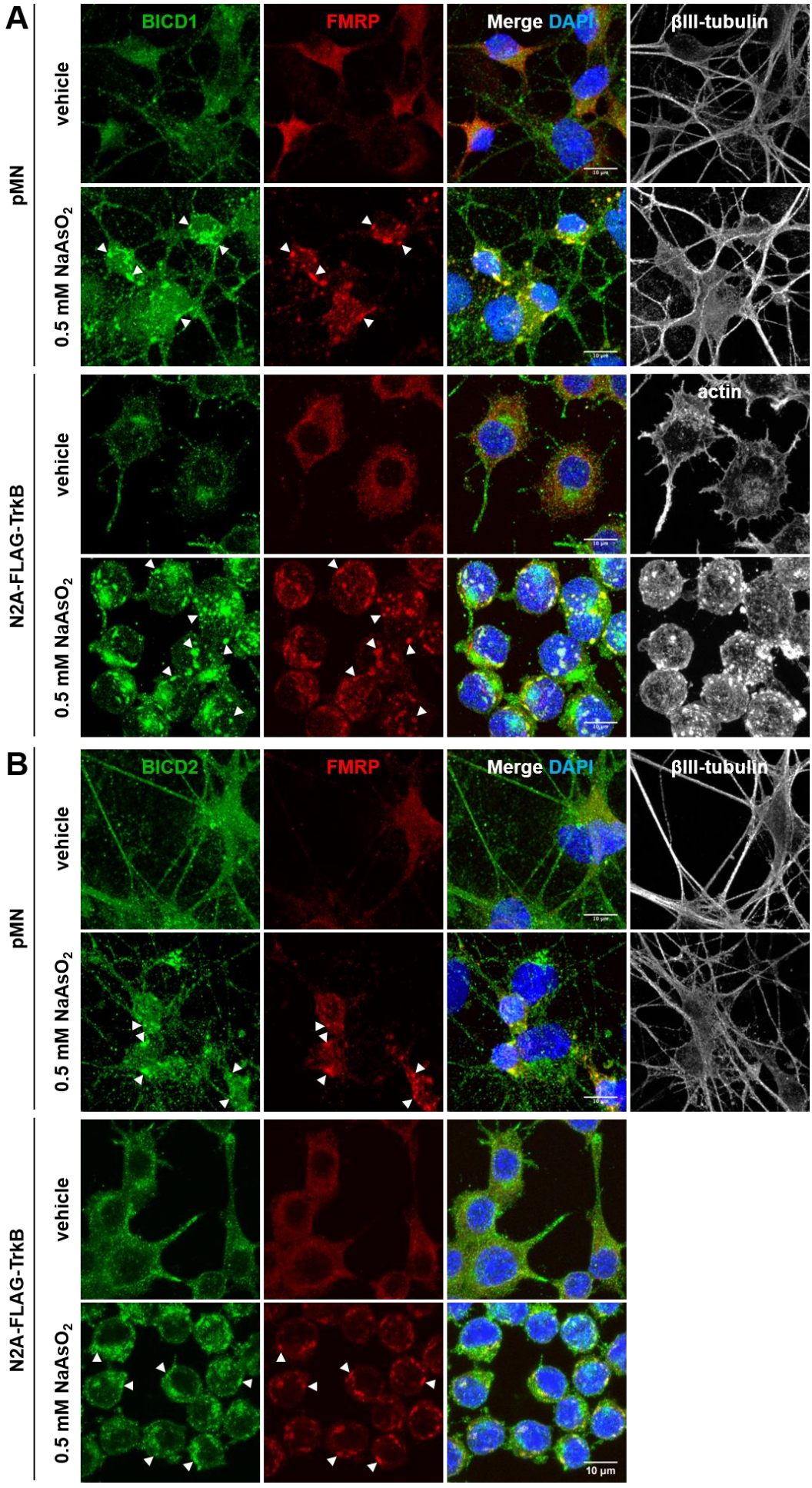
A
pMN
vehicle
0.5 mM NaAsO2
N2A-FLAG-TrkB
vehicle
0.5 mM NaAsO2
BICD1
FMRP
Merge DAPI
βIII-tubulin
actin
B
pMN
vehicle
0.5 mM NaAsO2
N2A-FLAG-TrkB
vehicle
0.5 mM NaAsO2
BICD2
FMRP
Merge DAPI
βIII-tubulin
10 μm

Figure 5.4 BICDs co-localize with FMRP$^+$ SGs.

Confocal images of pMNs and N2A-FLAG-TrkB cells treated with vehicle or 0.5 mM sodium arsenite and immunostained for FMRP and BICD1 (A) or BICD2 (B). Neurons were immunostained for βIII-tubulin (#ab41489, Abcam); actin was stained with phalloidin. BICD1 (A) and BICD2 co-localize with FMRP$^+$ SGs (arrowheads). Images show maximum intensity Z-stack projections, acquired at 0.2 µm (pMN; n=1) or 0.5 µm (N2A-FLAG-TrkB; n=2) spacing. Scale bar: 10 µm.

5.2.3 BICD1 colocalizes with ER stress-induced SGs

Next, I wanted to determine whether ER stress also induces BICD1$^+$ SGs and its increased perinuclear accumulation, or if this occurs solely due to oxidative stress. Compositionally-diverse SGs form in response to drugs and different environmental stresses (Kedersha and Anderson, 2007; Kedersha et al., 2013; Aulas et al., 2017). These stimuli evoke a distinct detection mechanism, via one of four stress-sensing kinases, which leads to eIF2α phosphorylation, translational arrest and SG formation (Kedersha et al., 2013). The aging mammalian nervous system is particularly susceptible to endoplasmic reticulum (ER) stress. There is a strong association between ER stress and incurable and fatal neurodegenerative disorders, including Parkinson's disease (PD), Alzheimer's disease (AD), Huntington's disease (HD) and amyotrophic lateral sclerosis (ALS) (reviewed by Hetz and Saxena, 2017). One of the best characterized functions of BICD proteins is Golgi-ER membrane trafficking in the COPI-independent pathway (Matanis et al., 2002). In addition, Loschi et al. (2009) demonstrated that BICD1 is required for SG formation in response to ER stress.

To induce ER stress, N2A-FLAG-TrkB cells were treated for 1 h with vehicle or 15 µM thapsigargin (Thap) and analysed by confocal microscopy for co-localization of BICD1 with two SG markers, G3BP (Figure 5.5A) and FMRP (#sc-101058, Santa Cruz) (Figure 5.5B). Thapsigargin inhibits sarco/endoplasmic reticulum Ca^{2+} ATPase (SERCA) (Lytton et al., 1991), leading to unfolded protein response (UPR) and ER-stress (Bertolotti et al., 2000). Similarly to oxidative stress (Figure 5.3; Figure 5.4), preliminary analysis of G3BP$^+$ and FMRP$^+$ SGs revealed that they contained BICD1 (Figure 5.5A,B). Interestingly, cell morphology appeared largely unaffected by ER stress, but, like oxidative stress,

it resulted in increased accumulation of BICD1 in the perinuclear region (Figure 5.5C,D).

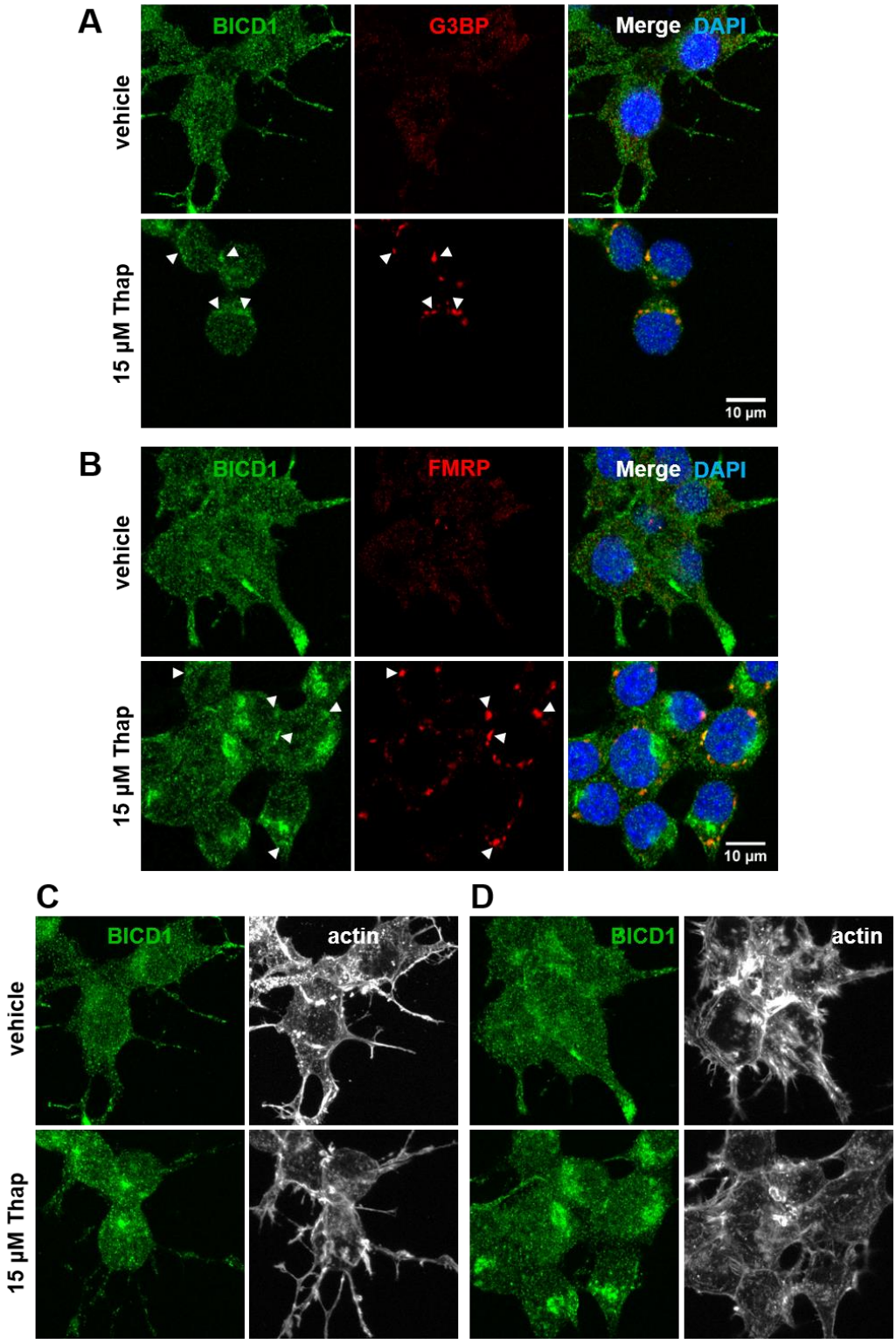

Figure 5.5 BICD1 co-localizes with SG markers during ER stress.

Confocal images of N2A-FLAG-TrkB cells treated with vehicle or 15 µM thapsigargin and immunostained for BICD1 and G3BP (A) or FMRP (B). SGs induced by ER stress are positive for BICD1 (arrowheads; n=1). Images show representative fields selected from Z-stack projections. C,D) Z-stack projections, corresponding to A,B respectively, showing immunostaining of BICD1 and actin filaments in cells treated with vehicle or thapsigargin.

5.2.4 Time course of BICD1 recruitment and release from SGs

I next wanted to follow BICD1 recruitment to SGs and its release. Depending on the type of stress and cell, SGs form within 5-30 min of stress exposure. The mechanism of SG assembly can be divided into a few distinct steps, which comprise SG nucleation, initial growth, and active, microtubule-dependent SG maturation (Wheeler et al., 2016). As SGs mature, they enrich for many messenger ribonucleoprotein particles (mRNPs) and other protein species, and merge together, leading to increase in their size, while their overall number in cells decreases (Ohshima et al., 2015). Mechanistically, SG disassembly follows reverse chronology to their formation (Wheeler et al., 2016).

To follow the recruitment of BICD1 into SGs, N2A-FLAG-TrkB cells were treated with 0.5 mM sodium arsenite for 10-60 min and fixed every 10 min, and up to 120 min. Cells were immunostained for BICD1 and G3BP (Figure 5.6). Small foci appeared at 10-20 min of treatment, but majority were devoid of BICD1, as verified by fluorescence intensity profiles (not shown). Between 20-30 min an increased recruitment of BICD1 was observed and majority of larger SGs were BICD1-positive from that 20 min onwards. Between 30-40 min of oxidative stress application, numerous small foci were detected to a lesser extent, and appearance of larger SGs was observed. Increased accumulation of BICD1 in the perinuclear region was evident from 30 min onwards, which correlated with the first changes in cell morphology. The perinuclear accumulation of BICD1 significantly decreased after two hours treatment with sodium arsenite.

To follow the release of BICD1 from SGs, N2A-FLAG-TrkB cells were treated for 1 h with 0.5 mM sodium arsenite and washed with DMEM. Next, cells were allowed to recover in full media for 30-60 min and were fixed every 10 min. At 30-50 min of recovery, SGs persisted; they varied in size and were positive for BICD1 (Figure 5.7A). However, at 50-60 min of stress recovery, although larger granules were positive for BICD1 (Figure 5.7B), there was an increased number of small foci that were either partially or fully devoid of BICD1 (Figure 5.7B), as revealed by fluorescence intensity profiles (Figure 5.7C). In the perinuclear region, BICD1 was condensed into clusters at all timepoints during stress recovery.

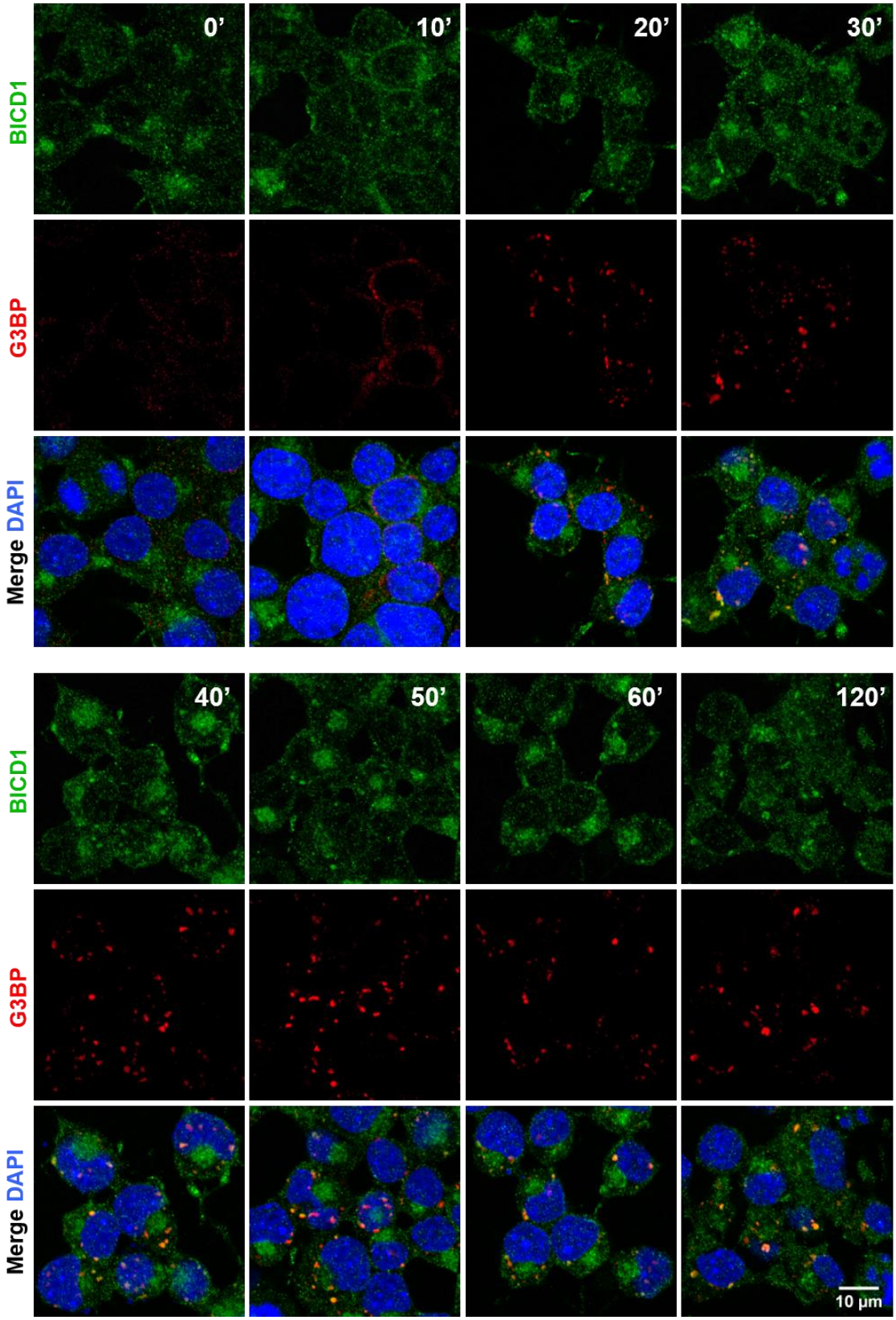

Figure 5.6 Time course of BICD1 recruitment to SGs.

Confocal images of N2A-FLAG-TrkB cells treated with 0.5 mM sodium arsenite for 10-120 min and immunostained for BICD1 and G3BP to monitor time course of stress granule assembly and BICD1 recruitment. Stress granules appear from 10-20 min of drug treatment and increase in size with time. Stress granules are positive for BICD1 from 30 min onwards (n=2).

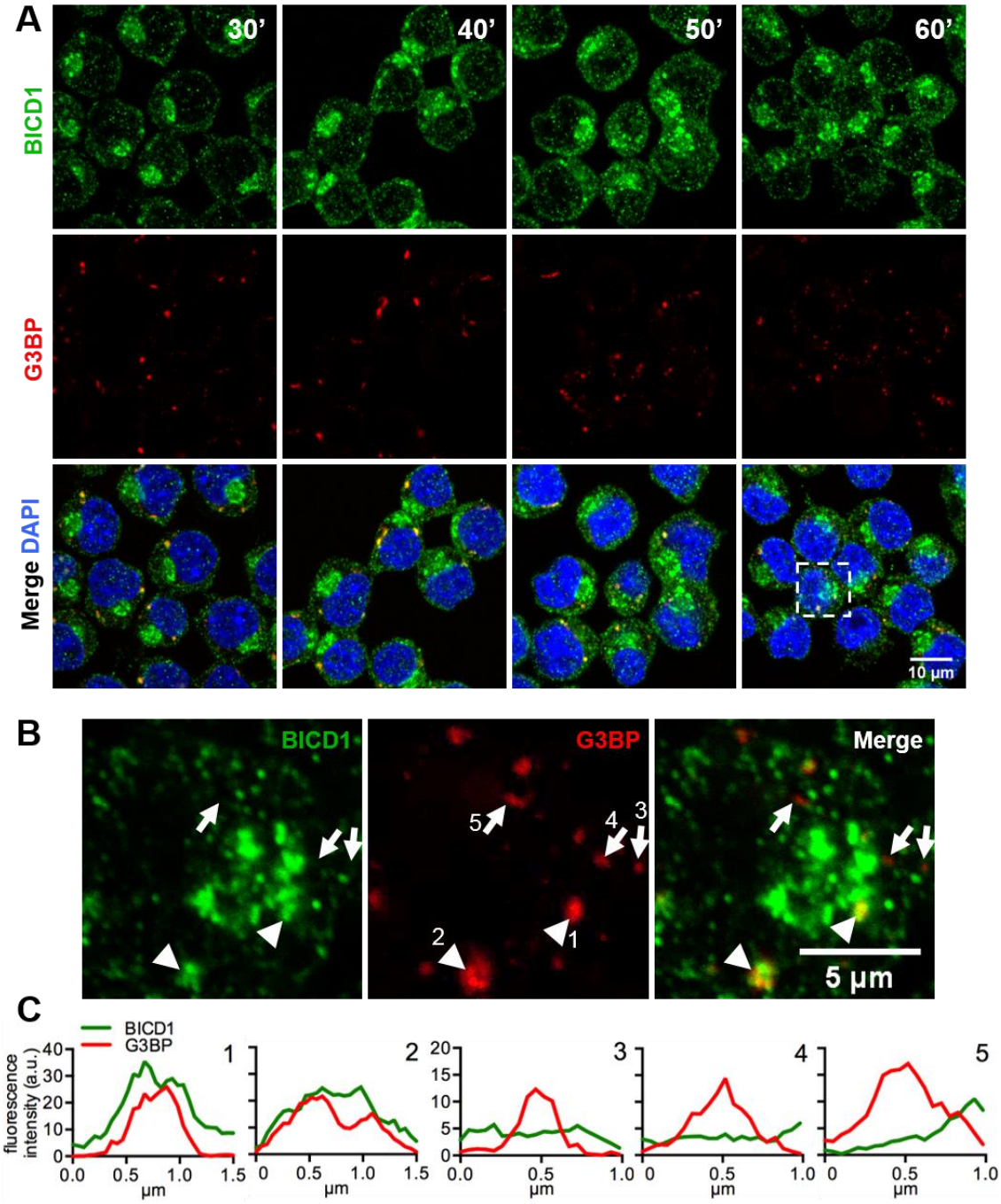

Figure 5.7 Time course of BICD1 release from SGs during stress recovery.

A) Confocal images of N2A-FLAG-TrkB cells treated for 1 h with 0.5 mM sodium arsenite, washed and recovered (30-60 min) in full media. Cells were immunostained for BICD1 and G3BP (n=2). SGs persist at all time points and are positive for BICD1. SGs decrease in size between 50-60 min of stress removal. Dashed rectangle in merged image at 60 min indicates cropped area in (B). B) Magnified view of the cropped area in (A). White arrows indicate foci mostly negative for BICD1, while arrowheads indicate SG positive for BICD1. C) Fluorescence intensity profiles of G3BP-foci (1-5) from (B). To measure fluorescence intensity, a 1-1.5 µm line (1 pixel wide) was drawn across the longest axis of a foci, from left to right.

5.2.5 Golgi apparatus integrity is not essential for BICD1 targeting to SGs

Thus far, I showed that oxidative and ER stresses altered the subcellular localization of BICD1. BICD1 not only localized to SGs, but its increased accumulation in the perinuclear region became apparent under these conditions. One of the best characterized functions of mammalian BICD proteins is regulation of COPI-independent Golgi-to-ER trafficking, via direct interaction of their C-termini with Rab6 on *trans*-Golgi membranes (Matanis et al., 2002). In earlier work, I showed that the cellular localization of Rab6 is dependent on BICD1 (Figure 3.7), in line with previous reports (Moorhead et al., 2007; Wanschers et al., 2007; Schlager et al., 2010; Splinter et al., 2010; Matsuto et al., 2015; Terawaki et al., 2015). Recently, it has been demonstrated that Golgi apparatus-resident proteins, such as AKAP350A and PARP12, translocate from the Golgi apparatus into SGs (Kolobova et al., 2009; Catara et al., 2017). For these reasons, I next sought to investigate whether Golgi apparatus integrity is necessary for BICD1 recruitment to SGs, and if the BICD1 interaction partner and Golgi-resident protein, Rab6, also transitions to these organelles during stress.

To achieve this, N2A-FLAG-TrkB cells were treated with vehicle, 0.5 mM sodium arsenite (1 h) or 10 µg/ml brefeldin A (BrefA; 2 h), either alone or in combination. Treatment with brefeldin A inhibits the ER-to-Golgi transport, thereby redistributing Golgi apparatus proteins to the ER, and disassembling the Golgi complex (Fujiwara et al., 1988). After fixation, cells were immunostained for the SG markers G3BP or FMRP (#17722, Abcam), in combination with BICD1, BICD2, Rab6 or the *cis*-Golgi marker GM130 (Figure 5.8). Treatment with brefeldin A alone led to loss of the perinuclear localization of BICD proteins, Rab6 and GM130-cisternae, as well as loss of BICDs and Rab6 from the tips of protrusions. It did not affect the localization of FMRP, cellular morphology or induce SGs. Interestingly, anti-FMRP antibody (#17722, Abcam), recognizing the C-terminus of the protein (around 550 aa), revealed its localization to protrusion tips in vehicle-treated N2A-FLAG-TrkB cells (Figure 5.8; Figure 5.13D), reminiscent of BICD1's localization in this area. Staining with anti-FMRP antibody (#sc-101048, Santa Cruz), recognizing N-terminal 100-225 aa (UniProt ref: Q06787; www.uniprot.org), was strikingly different, as no FMRP was observed in protrusions (Figure 5.4; Figure 5.5B). Unfortunately, due to antibody species incompatibility, it was not possible to verify whether BICD1 and FMRP co-localize

in protrusion tips prior to stress induction. As shown before (Figure 5.4), BICDs localized to SGs during oxidative stress, but this was not the case for Rab6 and GM130. All Golgi apparatus-related proteins, however, were clustered in the perinuclear region and characteristic GM130-ribbons were lost after treatment with sodium arsenite, as previously reported (Kolobova et al., 2009; Catara et al., 2017). Pre-treatment with brefeldin A did not affect formation of SGs in the presence of sodium arsenite and recruitment of BICD proteins to these membrane-less organelles (Figure 5.8).

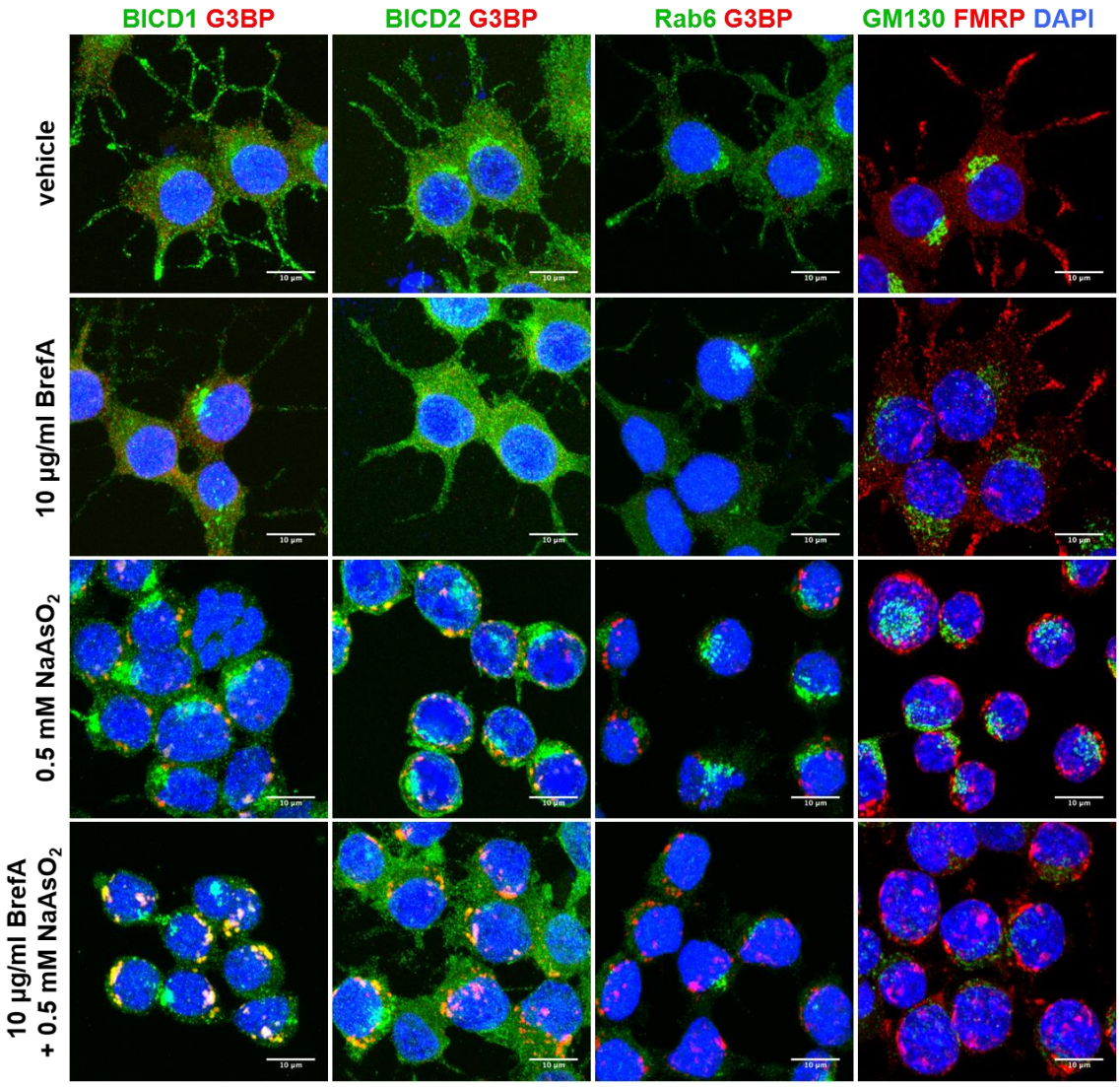

Figure 5.8 Golgi apparatus integrity is not essential for targeting of BICDs to SGs.

Confocal images of N2A-FLAG-TrkB cells treated with vehicle, 10 µg/ml brefeldin A (2 h) or 0.5 mM sodium arsenite (1 h), alone or in combination. Cells were immunostained for BICD1, BICD2, Rab6 and GM130, and a SG marker, G3BP or FMRP. Brefeldin A does not impair SG formation and BICDs recruitment in oxidative stress. Images show maximum intensity Z-stack projections acquired at 0.5 µm spacing (n=1). Scale bar: 10 µm.

5.2.6 BICD1 recruitment to SGs is not altered by cytoskeleton disruption

Next, I wanted test whether cytoskeletal integrity is crucial for targeting of BICD1 to SGs. During oxidative stress, structural changes as well as accumulation of Golgi apparatus-related proteins were observed in N2A-FLAG-TrkB cells (Figure 5.8) – a phenomenon which may be attributed to perturbations of the cytoskeletal network (Copeland et al., 2016) or alteration of membrane trafficking dynamics (Vega et al., 1999; Catara et al., 2017). Although, initially, SGs nucleate near ER-associated and translationally-stalled polysomes, the microtubule network promotes their transport, as well as formation of complex assemblies and fusion-fission events (Chernov et al., 2009; Kolobova et al., 2009; Nadezhdina et al., 2010).

To achieve this, N2A-FLAG-TrkB cells were first treated for 2 h with either latrunculin B (LatB) to promote depolymerization of actin filaments, or with nocodazole (Noc) or vincristine (Vinc) to facilitate microtubule disassembly. The effect of the drug on the cytoskeleton was verified using corresponding markers (Figure 5.9A-C). Although latrunculin B perturbed the organization of the actin network and integrity of protrusions (Figure 5.9A), cells depleted of microtubules were morphologically reminiscent of cells treated with sodium arsenite, i.e. they were rounded, swelled and lacked protrusions. In addition, tubulin assembled into characteristic paracrystals after treatment with vincristine (Figure 5.9C) (Nas and Timasheff, 1982), but not nocodazole (Figure 5.9B). Treatment with the above mentioned drugs alone did not induce SG formation (not shown).

Next, cells were treated for 2 h with a combination of a cytoskeleton-targeting drug and sodium arsenite for 1 h, or with sodium arsenite alone. Cells were fixed and immunostained for BICD1 and G3BP (Figure 5.9D). In line with previous reports, disruption of microtubule cytoskeleton had a more profound effect on SG dynamics than actin filaments depolymerization: there were increased numbers of smaller foci relative to cells treated with sodium arsenite alone or in combination with latrunculin B. This phenomenon appeared more accentuated in the cells pre-treated with vincristine, relative to nocodazole (Figure 5.9D). As expected, oxidative stress-induced perinuclear accumulation of BICD1 was dependent on microtubule network. Visual inspection revealed that the microtubules, but not actin, might be crucial for targeting of BICD1 to SGs.

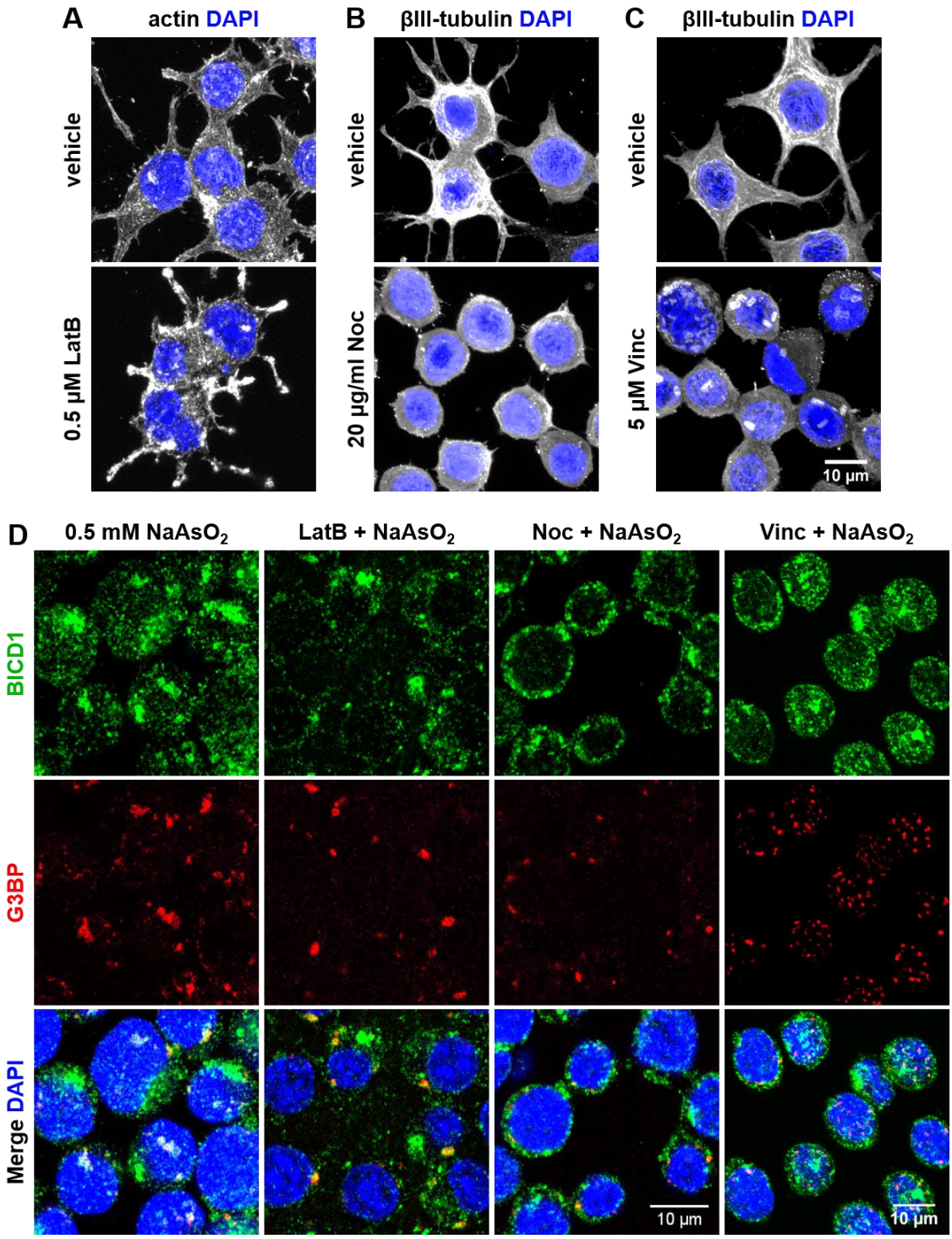

Figure 5.9 Microtubules but not actin network are essential for complex SG formation.

Confocal images of control N2A-FLAG-TrkB cells treated for 2 h with drugs targeting the actin (A – latrunculin B; stained with phalloidin) or microtubule cytoskeleton (B – nocodazole; C – vincristine; revealed by βIII-tubulin immunostaining). Images show maximum intensity Z-stack projections (n=1). D) Cells were treated with sodium arsenite (1 h) alone or in combination with latrunculin B, nocodazole or vincristine (2 h), fixed and immunostained for BICD1 and G3BP. Both microtubule-targeting drugs affected SG dynamics (n=2).

Next, representative SGs were further analysed for the relative abundance of BICD1 upon disruption of the cytoskeletal elements. Surprisingly, fluorescence intensity profiles revealed that the localization of BICD1 to SGs was not affected by disruption of actin filaments (Figure 5.10A,A'), nor the microtubule network (Figure 5.10B-C'). In all cases, BICD1 and G3BP fluorescence intensity profiles were comparable in SGs induced by sodium arsenite and when additionally pre-treated with drugs targeting the cytoskeleton.

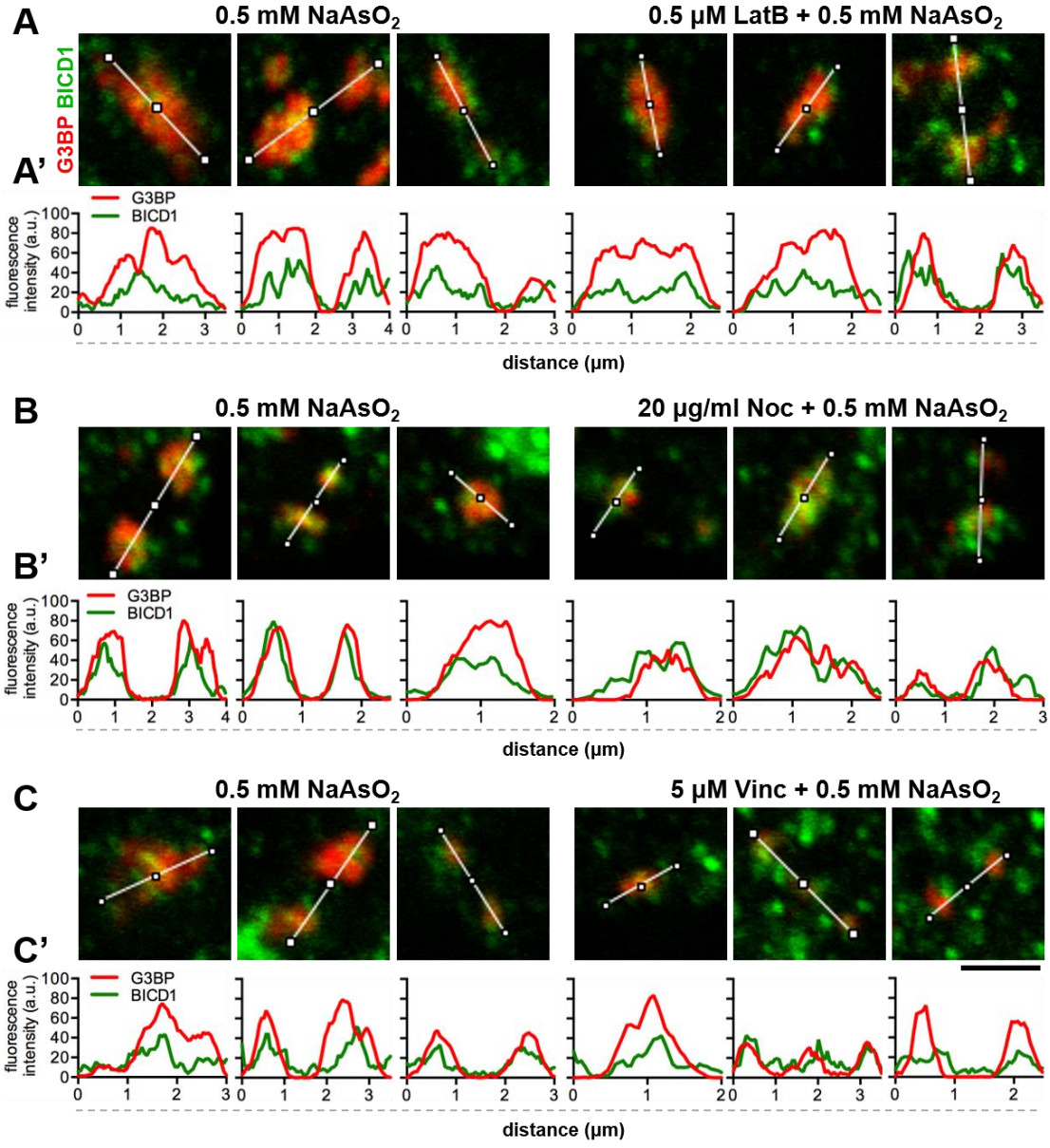

Figure 5.10 Cytoskeletal interference does not affect BICD1 recruitment to SGs.

Merged confocal images of selected SGs from N2A-FLAG-TrkB cells pre-treated with latrunculin B (A), nocodazole (B) and vincristine (C) and stressed with sodium arsenite, in combination or alone (n=2). Cells were immunostained for BICD1 and G3BP. Scale bar: 2 µm. Corresponding fluorescence intensity profiles (A', B', C' respectively) of BICD1 and G3BP were determined across the white line visible in merged images. Lines (1 pixel wide, 2-4 µm) were drawn through the centre of 1-3 SGs per image, from left to right.

5.2.7 BICD1 is a component of SGs, but not of P-bodies

Next, I wanted to verify the *bona fide* nature of BICD1/G3BP$^+$ SGs. Oxidative stress halts mRNA translation and leads to mRNA translocation to SGs. Sodium arsenite elicits this response at low concentrations, which may not result in detectable SG formation (Kedersha et al., 2000). Because of the dynamic nature of mRNA and RNA-binding proteins within SGs, as demonstrated by fluorescence recovery after photobleaching (FRAP) (Anderson and Kedersha, 2006; Buchan and Parker, 2009; Jain et al., 2016; Wheeler et al., 2016), drugs stabilizing polysomes, such as cycloheximide (CHX), lead to slow disassembly of SGs, in the presence of a stress or after stress recovery, due to continuous exchange of SG material (Kedersha et al., 2000). Cycloheximide acts by freezing translation and blocking polysome disassembly, subsequently preventing mRNA exiting from polysomes to SGs (Obrig et al., 1971). On the contrary, drugs de-stabilizing polysomes, such as puromycin, promote SG formation (Kedersha et al., 2000).

To disassemble SGs, an oxidative stress assay was adapted as outlined in Figure 5.11A. Primary motor neurons were treated for one hour with a lower concentration of sodium arsenite – 0.25 mM rather than 0.5 mM – which permits, although reduced relative to vehicle controls, mRNA translation as well as SG formation (Kedersha et al., 2000). Cycloheximide was then added for the following 30 min, in the presence of sodium arsenite. Used at 50 µg/ml, cycloheximide was within its higher recommended concentration range. It was proposed that cycloheximide treatment should lead to full stress granule disassembly when used at 20-50 µg/ml for 1-2 h (Kedersha and Anderson, 2007).

Cells were fixed and immunostained for BICD1, G3BP, and neuronal marker βIII-tubulin (#ab41489, Abcam) (Figure 5.11B). Combined cycloheximide treatment led to approximately 65% reduction in SG$^+$-pMNs relative to sodium arsenite treated cells (Figure 5.11C), verifying the true nature of these BICD1-positive organelles. No SGs were observed in vehicle- or cycloheximide-only controls, in line with previous reports (Kedersha et al., 2000, Kedersha and Anderson, 2007).

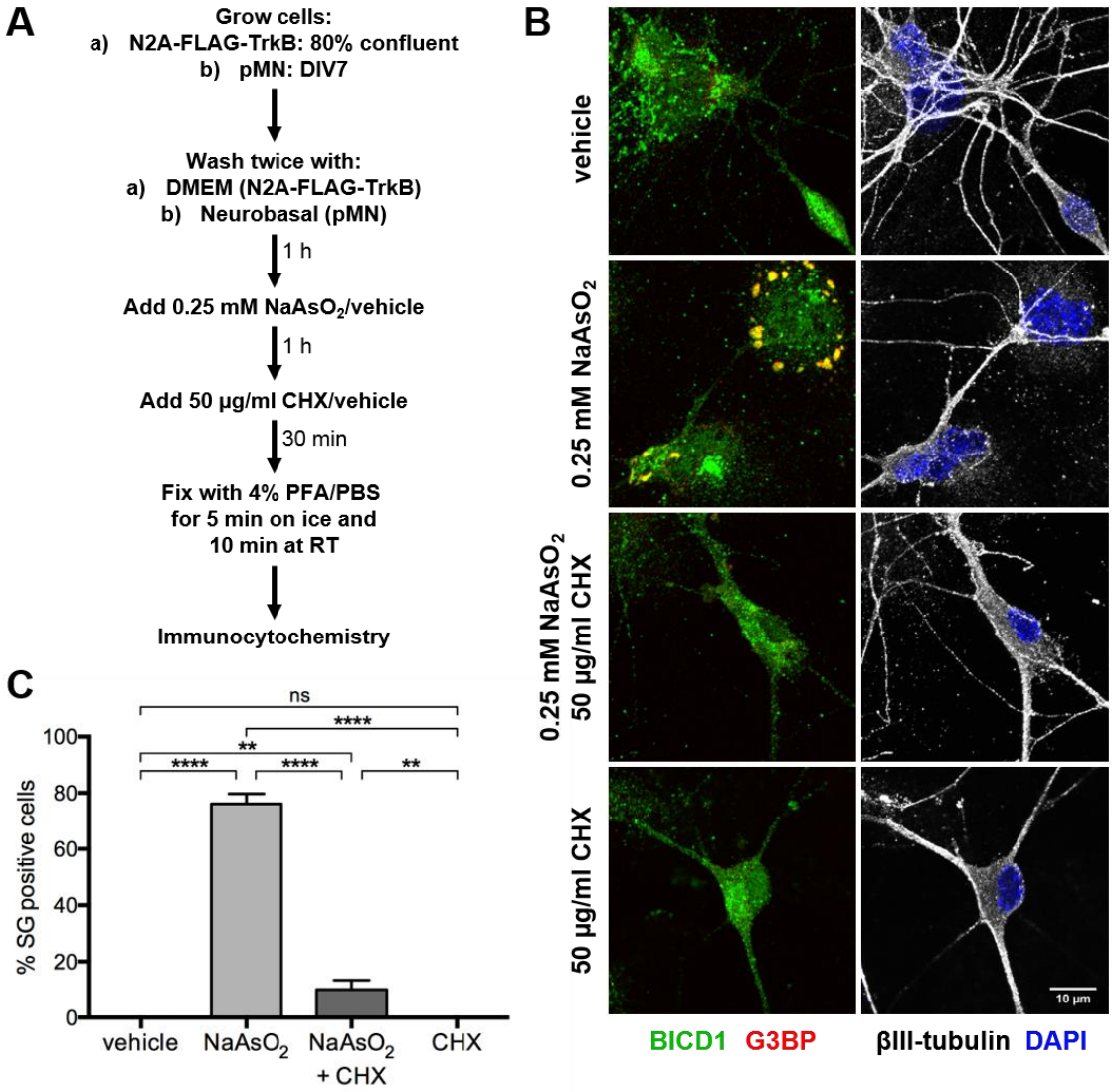

Figure 5.11 BICD1⁺ SGs in pMNs are cycloheximide-sensitive.

A) Flow diagram outlining the steps of SG disassembly assay. In short, after 1 h treatment with 0.25 mM sodium arsenite, 50 µg/ml cycloheximide was added for following 30 min under stress conditions. B) Confocal images showing pMNs in all treatment groups, immunostained for BICD1, G3BP and βIII-tubulin (#ab41489, Abcam). Addition of cycloheximide during stress resulted in SG disassembly (n=3). Scale bar: 10 µm. C) Quantification of (B). Treatment with cycloheximide in addition to sodium arsenite results in reduction of SG⁺ pMNs from ~75% to ~10%. At least 100 motor neurons were counted per condition in three independent experiment. **P<0.01, ***P<0.001, ****P<0.0001, one-way ANOVA with Bonferroni's multiple comparisons test.

Next, I determined whether BICD1 localizes to a distinct type of ribonucleoprotein particle (RNP)-granule, a processing body (P-body) (Anderson and Kedersha, 2006). Although overlap in content and crosstalk between SGs and P-bodies has been demonstrated, they differ in function and can be identified by their unique markers (Kedersha and Anderson, 2007). Both organelles trap translationally-stalled mRNA. While SGs protect mRNA, are abundant in translation initiation

factors and allow the return of mRNA to the translation machinery, the role of P-bodies is less well-defined, although it is generally accepted that they are a site of mRNA storage en route to degradation (Kedersha et al., 2005; Perez-Pepe et al., 2018). SGs and P-bodies are closely associated, and prolonged stress may promote their fusion (Eisinger-Mathason et al., 2008). Drugs stabilizing or blocking polysomes modulate the assembly and dissolution of SGs and P-bodies, but with distinct kinetics (Kedersha et al., 2005).

To assess whether BICD1 is associated with P-bodies, the cycloheximide assay was performed on N2A-FLAG-TrkB cells, as outlined previously (Figure 5.11A). Cells were immunostained for BICD1 and an RNP-specific marker: G3BP for SGs (Figure 5.12A) or mRNA-decapping enzyme 1A (Dcp1a) for P-bodies (Figure 5.12B). Both types of RNA-foci arose in response to oxidative stress. An additional 30 min treatment with cycloheximide resulted in almost complete dispersal of SGs, with very few cells bearing SGs (Figure 5.12A), without any obvious effect on P-body dynamics (Figure 5.12B). No RNP-granules were observed in cells treated with cycloheximide alone. Fluorescence intensity profiles were generated to establish the relationship of BICD1 with both organelles. As shown previously (Figure 5.2; Figure 5.3; Figure 5.10), there was an overlap between BICD1 and G3BP across SG in sodium arsenite-treated cells, alone or in combination with cycloheximide. Fluorescence intensity of both proteins across disassembling stress granules decreased after cycloheximide treatment, relative to these formed in response to oxidative stress alone (Figure 5.12A'). P-bodies were proximal to several BICD1-positive puncta, potentially SGs, but no co-localization of BICD1 and Dcp1a was observed in any treatment group in this preliminary work (Figure 5.12B), as verified by fluorescence intensity profiles (Figure 5.12B'). Dispersal of stress granules by cycloheximide (Figure 5.12A,A') preceded any P-body disassembly (Figure 5.12B,B'), in line with previous reports (Kedersha et al., 2005). Unfortunately, I was not able to verify the apposition of SGs and P-bodies in N2A-FLAG-TrkB cells due to lack of antibody species compatibility.

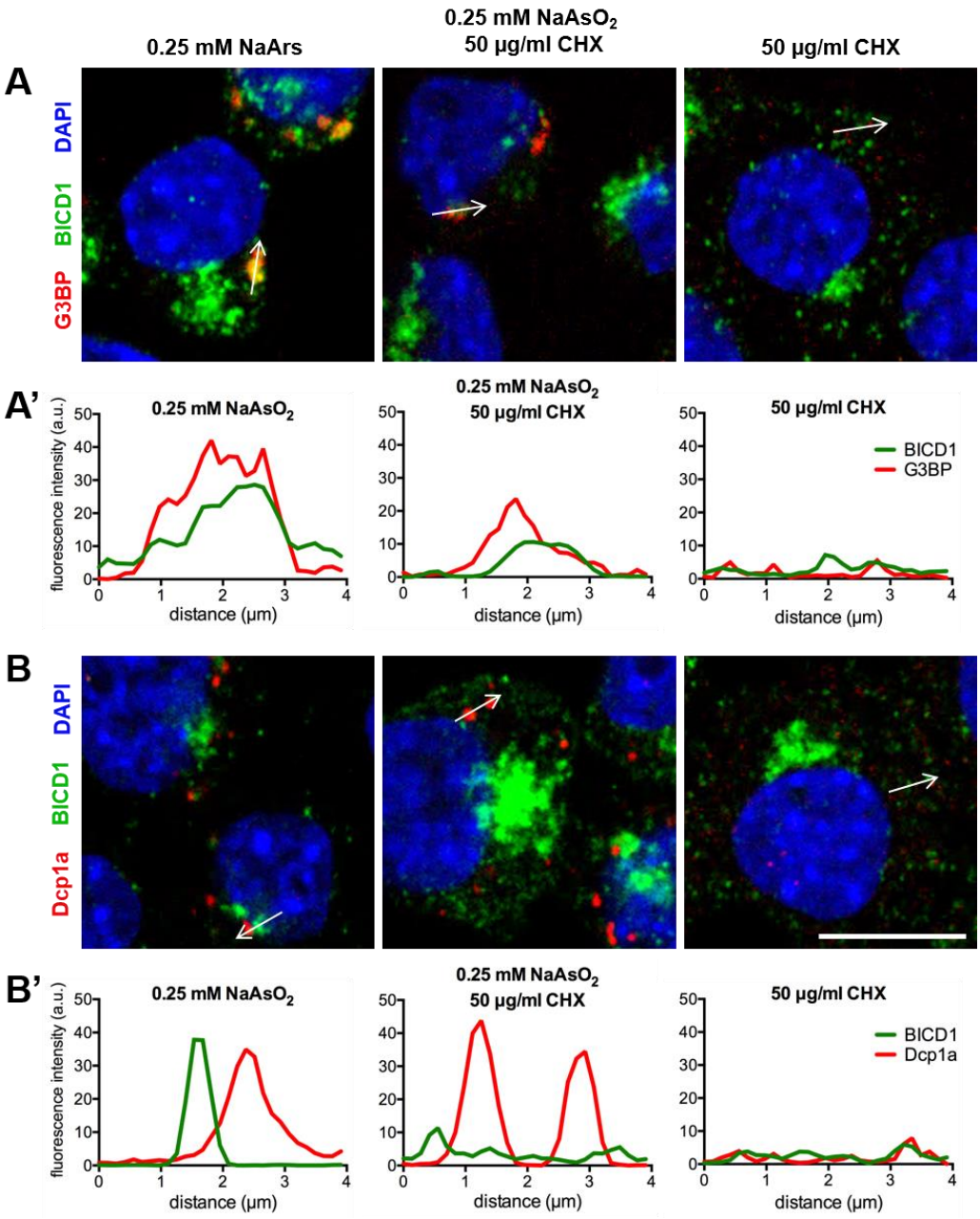

Figure 5.12 BICD1 is not a component of P-bodies.

A,B) Confocal images of N2A-FLAG-TrkB cells treated with 0.5 mM sodium arsenite or 50 µg/ml cycloheximide, alone or in combination. Cells were immunostained for BICD1 and SG marker, G3BP (A) or the P-body marker, Dcp1a (B; n=1). Scale bar: 10 µm. A'B') Fluorescence intensity profiles of selected protein overlap along and in direction of white arrow (4 µm long, 10 pixel wide line in FIJI) in corresponding merged images. BIDC1 intensity profiles differ from Dcp1a (B'), whilst showed a remarkable correspondence in correlation to G3BP (A').

5.2.8 PTPN23 activity does not influence SG dynamics

Having established the relationship between BICD1 and PTPN23 (Chapter 3), and BICD1 and SGs, I investigated the potential role of PTPN23 in SG dynamics, and in the recruitment of BICD1 to these membrane-less organelles. Previously

published data indirectly link PTPN23 to SGs. PTPN23 is necessary for the hyper-phosphorylation state of survival motor neuron 1 (SMN1), which is essential for the shuttling of SMN complex into nuclear Cajal bodies (Narayanan et al., 2004; Shaw et al., 2008; Husedzinovic et al., 2014). In addition, PTPN23 prevents the hyperphosphorylation of focal adhesion kinase (FAK), therefore regulating cell migration (Castiglioni et al., 2007). SMN1 and FAK localize to SGs, however they mediate distinct dynamic processes. While SMN1 is crucial for SG assembly (Hua and Zhou, 2004; Zou et al., 2011), FAK mediates their clearance (Tsai et al., 2008).

Analysis of SGs in pMNs (Figure 5.13A-C) and N2A-FLAG-TrkB cells (Figure 5.13D-F) treated with 0.5 mM sodium arsenite suggests that PTPN23 is not a component of $FMRP^+$ SGs in either cell type, although it appeared to localize closely to these organelles (Figure 5.13C,F). As observed previously, oxidative stress elicited changes in N2A-FLAG-TrkB cell morphology, yet the overall distribution of PTPN23 was not significantly affected by sodium arsenite (Figure 5.13D).

Next, exploiting our PTPN23 knockdown model in N2A-FLAG-TrkB cells, I wanted to verify whether PTPN23 plays an indirect role in SG dynamics, and affects their formation, size or the recruitment of BICD1. N2A-FLAG-TrkB cells, transduced for 72 h with PTPN23 KD^{sh1} or scrambled lentiviruses, were treated for 1 h with 0.5 mM sodium arsenite or vehicle control. Cells were immunostained for GFP reporter (not shown), BICD1 and G3BP (Figure 5.14A) or BICD1 and FMRP (Figure 5.14B). No SGs were detected in transduced cells in the absence of stress (not shown). Unfortunately, lentiviral knockdown combined with oxidative stress resulted in many cells detaching from the coverslips, thus greatly limiting the pool of cells available for analysis. Depletion of PTPN23 resulted in a significant decrease of cells containing $G3BP^+$ SGs (P=0.0074), but not $FMRP^+$ SGs (P=0.8008), relative to scrambled controls (Figure 5.14C), suggesting that PTPN23 may indirectly regulate the dynamics of selected SG-related proteins. Next, the fluorescence intensities of BICD1 and G3BP in $G3BP^+$ SGs (Figure 5.14D) and BICD1 and FMRP in $FMRP^+$ SGs (Figure 5.14F) were measured (see Methods for details). PTPN23 is not required for the recruitment of BICD1 to SGs (Figure 5.14D,F), although a slight tendency for a decrease in G3BP (Figure 5.14D), and BICD1 fluorescence intensities (in $FMRP^+$ SGs; Figure 5.14F) after

PTPN23 depletion was observed. Consistently, further analysis of G3BP^{+} and FMRP^{+} SG area distribution revealed that PTPN23 is not likely to be playing a role in SG assembly and maturation (Figure 5.14E,G).

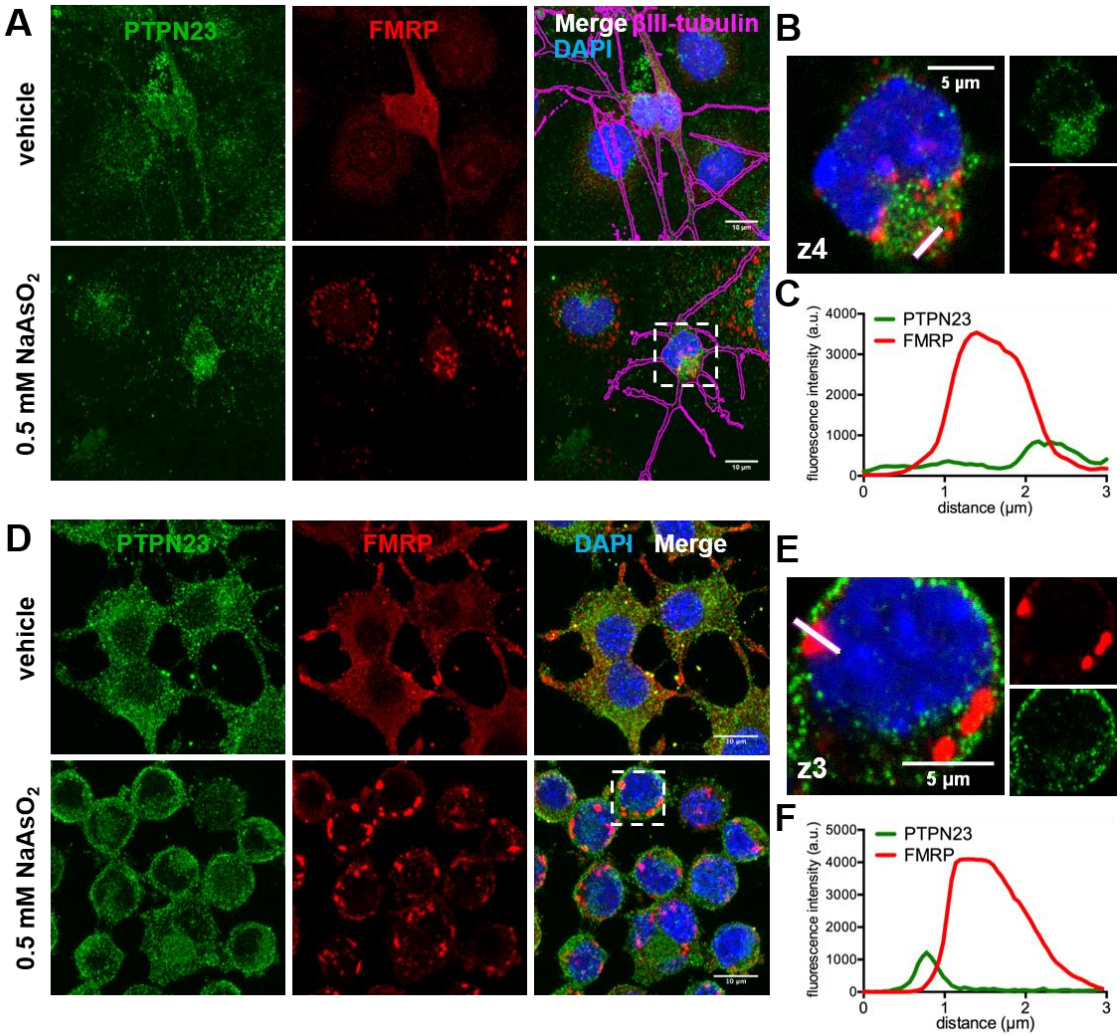

Figure 5.13 PTPN23 does not co-localize with SGs.

Confocal images of pMNs (A,B) and N2A-FLAG-TrkB cells (D,E) treated with vehicle or 0.5 mM sodium arsenite, and immunostained for βIII-tubulin (A, magenta outline; #ab41489, Abcam), PTPN23 and FMRP (#17722, Abcam) (n=2). Images show maximum intensity Z-stack projections, acquired at 0.2 µm (A) or 0.5 µm (D) spacing. Dashed rectangles indicate the area used to show magnification of a representative Z-plane. Scale bar: 10 µm. B,E) Magnified images showing immunostaining in respective fields. C,F) Fluorescence intensity profiles of PTPN23 FMRP were determined along the white line (10 pixel wide, 3 µm long) visible in respective merged images.

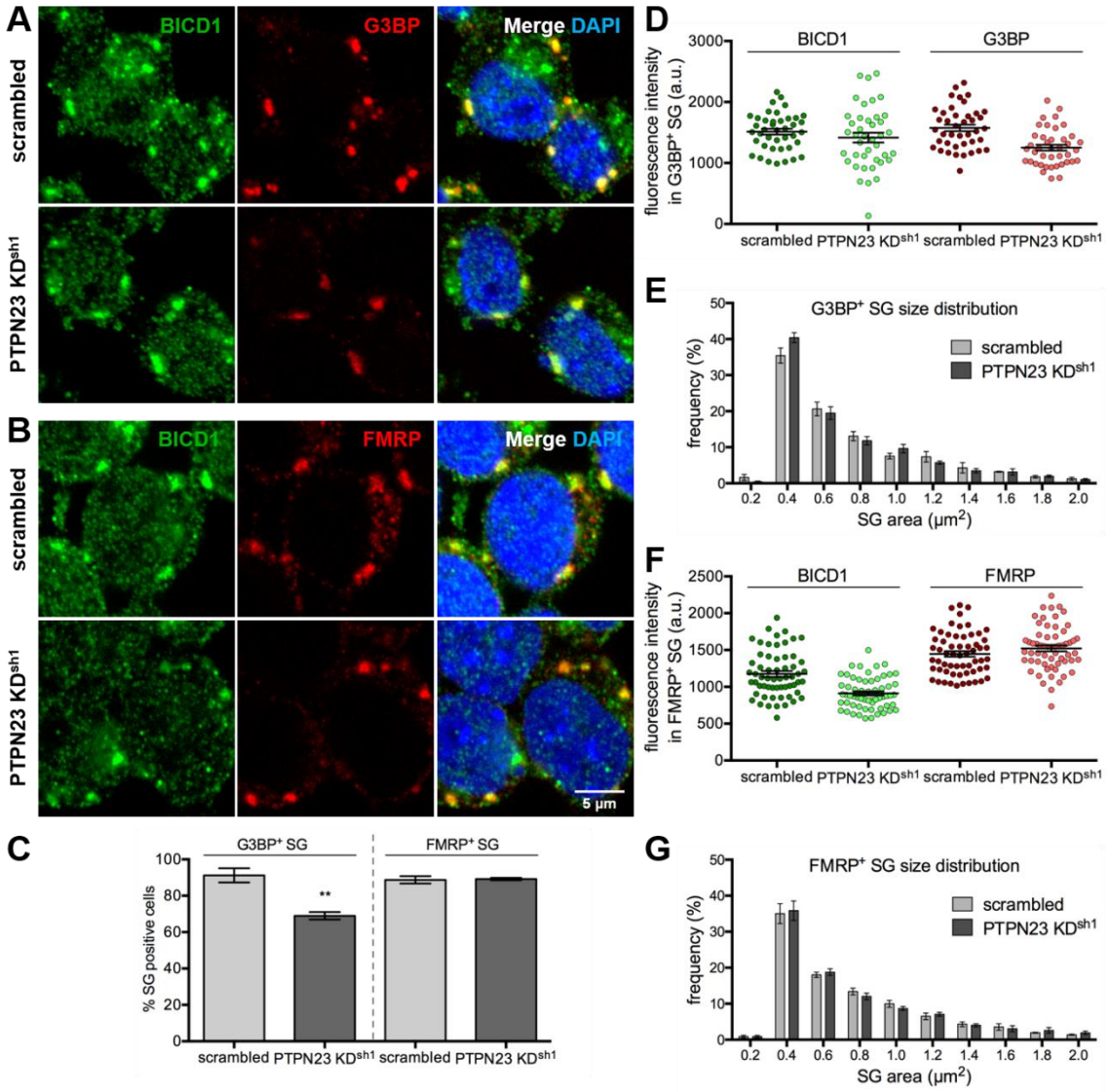

Figure 5.14 PTPN23 knockdown does not affect SG assembly dynamics.

A,B) Confocal images of N2A-FLAG-TrkB cells transduced for 72 h with PTPN23 KD^{sh1} or scrambled lentiviruses, and treated for 1 h with 0.5 mM sodium arsenite. Next, cells were immunostained for reporter GFP (not shown), BICD1 and G3BP (A; n=3) or BICD1 and FMRP (B; #sc-101058, Santa Cruz; n=3). C) Quantification of SG$^+$ cells, showing a 20% reduction of cells positive for G3BP$^+$, but not FMRP$^+$ SGs, after PTPN23 depletion. For each condition, an average of 100 cells were counted in three independent experiments. **P<0.01, unpaired Student's *t*-test. D,F) Fluorescence intensities of BICD1, G3BP and FMRP were measured in scrambled and PTPN23 KD^{sh1} cells, using G3BP$^+$ SGs (D) or FMRP$^+$ SGs (F) as a mask. Ten fields across matched 2-3 Z-planes per condition were imaged in three independent experiments. All datapoints are plotted; mean values were used for statistical analyses (n=3). Error bars show SEM; not significant, P>0.05, unpaired Student's *t*-test. E,G) Masks of G3BP$^+$ (E) or FMRP$^+$ SG (G) were used to measure the areas of SGs in scrambled and PTPN23 KD^{sh1} cells, with >0.2 µm^2 cut-off and 0.2 µm^2 binning (range 0.2-2 µm^2). There was no change in SG sizes following PTPN23 depletion (n=3). Error bars show SEM, not significant, E) P=0.8532, G) P=0.9104, two-tailed chi-square test for trend (using mean values).

5.2.9 BICD1 co-pellets with SG components

To assess the association of BICD1 with SGs biochemically, cellular fractionation was performed as outlined in Figure 5.15A, based on the methodology by Hua and Zhou (2004). Although the shell of SGs is highly dynamic due to its liquid-liquid phase separation (LLPS)-like properties, SG cores are held by complex interactions between its proteins and mRNAs, and withstand lysis in buffers containing up to 1 M NaCl, 50 mM EDTA, 2 M urea or RNase, but not >2% SDS (Jain et al., 2016). Because SGs are not enclosed by a membrane, the integrity of SG cores is not affected by commonly-used non-ionic detergents, such as NP-40 (Jain et al., 2016; Mahboubi and Stochaj, 2017). SG cores, similarly to inclusion bodies (De Bernardez Clark, 1998), can be pelleted by centrifugation from cell lysates (Jain et al., 2016; Wheeler et al., 2016; Wheeler et al., 2017). Several studies demonstrated that SG components can be specifically enriched within the insoluble pellet fraction using cellular fractionation upon induction of stress, and identity of several new SG components, in particular of SG cores, was identified using this approach (Mazroui et al., 2002; Gilks et al., 2004; Mazroui et al., 2007; Tsai et al., 2008; Liu-Yesucevitz et al., 2010; McDonald et al., 2011; Jain et al., 2016; Mahboubi and Stochaj, 2017; Omer et al., 2018). As BICD1 has not been previously identified in the proteomic screens (Markmiller et al., 2018), including that of isolated SG cores (Jain et al., 2016), this raised a question whether BICD1 localizes to the dynamic SG shell, rather than the core. I therefore attempted to purify SGs using a nucleo-cytoplasmic fractionation as a preliminary approach, for three reasons: 1) I expected to find SG core-associated proteins in the pellet fraction after sodium arsenite treatment; 2) I aimed to investigate the changes in protein levels in cytoplasmic and nuclear extracts after application of stress; 3) and to reduce cytoplasmic and nuclear contaminants in the SG core-containing pellet.

To explore the potential association of BICD1 with SG cores, N2A-FLAG-TrkB cells were treated for 1 h with vehicle or 0.5 mM sodium arsenite, and subjected to fractionation in lysis buffers designed to facilitate the extraction of cytoplasmic and nuclear components, and which should not affect the integrity of SG cores, in line with studies above (see Methods for details; Figure 5.15A). Soluble cytoplasmic and nuclear extracts were obtained by centrifugation in fractionation buffers A (10 mM HEPES-NaOH, pH 7.8, 10 mM KCl, 0.1 mM EDTA, 0.1 mM

EGTA, 1 mM DTT, 0.6% NP-40, 1 mM PMSF, protease inhibitor cocktail) and B (20 mM HEPES-NaOH, pH 7.9, 0.4 M NaCl, 1 mM EDTA, 1 mM EGTA, protease inhibitor cocktail), respectively. Those buffers were not supplemented with sodium arsenite. All obtained fractions were analysed by western blotting (Figure 5.15B). The presence of α-tubulin and GAPDH predominantly in the cytoplasmic soluble fraction, and of TDP-43 in the nuclear extracts, verified the reliability of the fractionation protocol. Although I expected to find α-tubulin, BICD1, FMRP and G3BP predominantly in the soluble cytoplasmic fraction, a significant amount of these proteins was detected in the nuclear extracts. Whether these were contaminants from the cytoplasmic pool eluted during lysis in fractionation buffer B, or eluted with nuclear components due to their interaction with these proteins, as previously demonstrated for BICD1 (Terawaki et al., 2015), remains to be investigated in future experiments. On the other hand, the increased detection of GAPDH in the soluble nuclear extract after sodium arsenite treatment is in line with previous reports from neuroblastoma cells, where it was demonstrated that GAPDH translocates to the nucleus during stress prior to induction of the cell death cascade (Dastoor and Dreyer, 2001). This suggests that identification of the other proteins in the nuclear extracts might be specific.

The decrease of TDP-43 in the nuclear and cytoplasmic fractions after sodium arsenite treatment corresponded with its increased detection in the insoluble pellet, in line with previous report (Liu-Yesucevitz et al., 2010), suggesting a successful isolation of SG components. Likewise, in the same fraction obtained from stressed cells I observed the enrichment of other SG proteins, G3BP and FMRP, as well as α-tubulin (Jain et al., 2016). Importantly, I observed a specific association of BICD1 with the insoluble pellet after sodium arsenite treatment (Figure 5.15B), suggesting that BICD1 may associate with the SG core rather than the shell. However, as cellular fractionation was an exploratory approach, it needs to be further validated by increasing the number of repeats.

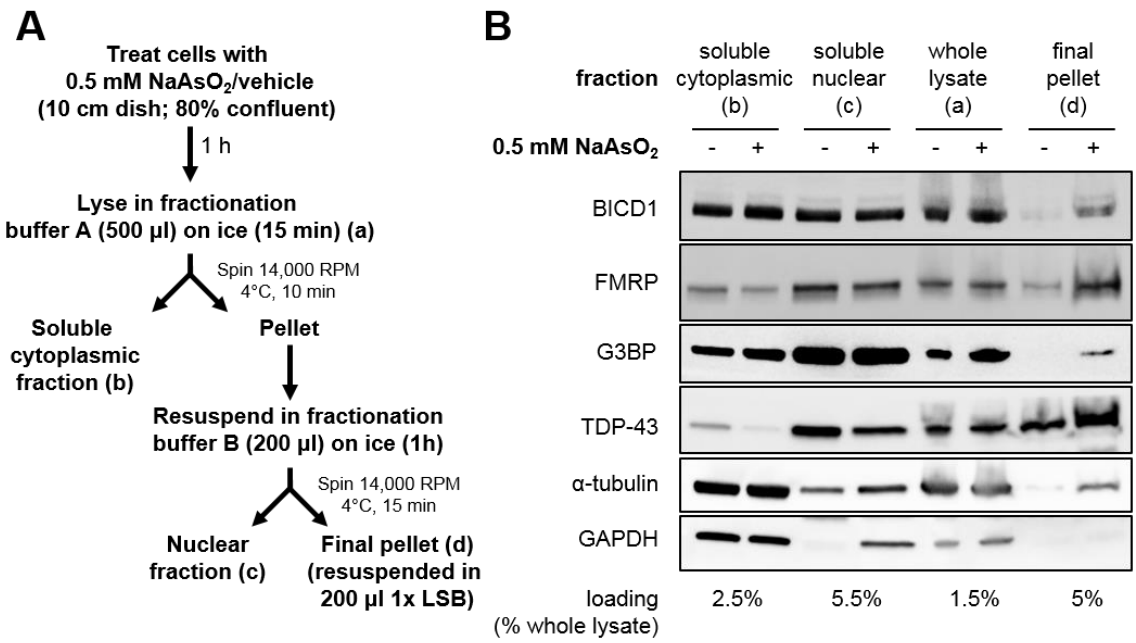

Figure 5.15 BICD1 precipitates with SG-related proteins following oxidative stress.

A) Flow diagram outlining steps of cellular fractionation. In short, cells were treated with vehicle or 0.5 mM sodium arsenite and lysed on ice in buffer A. After centrifugation, the soluble fraction was collected and the pellet was resuspended in buffer B for an hour, before extraction of the soluble nuclear fraction by centrifugation. B) All fractions from cells treated with vehicle or 0.5 mM sodium arsenite were immunoblotted for BICD1, SG markers, α-tubulin and GAPDH. Most SG-related proteins, including BICD1, were enriched in the final insoluble pellet fraction, extracted from cells treated with sodium arsenite (n=1).

5.3 Discussion and future directions

The goal of the work described in this chapter was to characterize the recruitment of BICD1 to SGs, and to explore the potential involvement of PTPN23 in SG dynamics. The last few years have been particularly successful in decrypting the composition of SGs, and as a consequence, in revealing more about their role during stress and their involvement in the pathogenesis of neurodegenerative diseases (Markmiller et al., 2018; Youn et al., 2018). Particular progress has been made since the development of the SG core purification technique, which shed light not only on the composition of SGs but also the principles of SGs formation and function (Jain et al., 2016; Wheeler et al., 2016; Khong et al., 2017).

Although many components of the dynein motor machinery were found associated with SG fractions (dynein heavy, light and intermediate chains, and dynactin), none of the known canonical dynein adaptors, including mammalian BICDs, Hooks or Spindly, were detected by proteomic approaches. However, a

study investigating the role of selected motor components in SG dynamics by siRNA-mediated knockdown revealed the importance of the specific components of the retrograde machinery, including BICD1, in SG assembly, and anterograde machinery in their clearance (Loschi et al., 2009). The importance of dynein in both SG dynamic processes was demonstrated in an independent study using a pharmacological approach (Tsai et al., 2009). Inhibition of dynein by erythro-9-(2-hydroxy-3-nonyl)adenine (EHNA), but not kinesin motors by 5′-adenylylimido-diphosphate (AMP-PNP), blocked SG formation as well as SG disassembly during stress recovery, emphasizing the role of cytoplasmic dynein in SG maturation and clearance (Tsai et al., 2009). A caveat of this approach is that EHNA is known to inhibit other protein complexes, such as phosphodiesterase type 2 (Podzuweit et al., 1995). The specific inhibitors of cytoplasmic dynein, such as ciliobrevins, should be tested in future studies (Roossien et al., 2015).

Taken together, these studies provided the groundwork for regulation of SG dynamics and for our research, with Loschi et al. (2009) being the first group reporting the importance of BICD1 in SG formation. My main goal was to verify the presence of BICD1 in SGs, as it has not been conclusively demonstrated to date. Indeed, BICD1 was consistently detected in SGs in N2A-FLAG-TrkB cells and, more importantly, in pMNs as well as non-neuronal cells cultured from mouse embryonic spinal cord.

5.3.1 BICD1 is a component of neuronal SGs

Four primary stress-sensing kinases drive SG formation through phosphorylation of eIF2α (Kedersha and Anderson, 2007). In addition, SGs may also form in an eIF2α-independent manner (Mahboubi and Stochaj, 2017). Because different types of stresses may evoke the production of SGs of distinct composition (Kedersha et al., 1999; Aulas et al., 2017), and BICD1 depletion perturbs SG formation in response to oxidative and ER stresses (Loschi et al., 2009), our goal was to verify the presence of BICD1 in SGs induced in these conditions. Indeed, BICD1 was detected specifically in G3BP$^+$ (Figure 5.2; Figure 5.3) and FMRP$^+$ SGs (Figure 5.4A) induced by sodium arsenite (oxidative stress) and thapsigargin (ER stress; Figure 5.5). In contrast, BICD1 was not detected in related RNP foci (P-bodies; Figure 5.12B) in preliminary experiments. By treating cells with the polysome-stabilizing drug, cycloheximide, I verified the *bona fide* nature of

BICD1$^+$ SGs and demonstrated that BICD1 and G3BP dissociate from SGs with similar kinetics (Figure 5.11; Figure 5.12A). I could therefore speculate that, similarly to G3BP, BICD1 shuttles in and out of SGs, and/or between SGs and polysomes. This phenomenon could be further explored in future work by treating cells with microtubule depolymerizing drug, in addition to sodium arsenite and cycloheximide, an approach used in previous studies (Kedersha et al., 2000; Nadezhdina et al., 2010). In addition, analysis of BICD1 dynamics within SGs by FRAP should be addressed in future studies (Van Treeck and Parker, 2019).

To explore whether BICD1 plays a central role in SG formation, its recruitment in response to stresses such as heat-shock or amino-acid starvation should also be investigated, as well as its localization to non-G3BP/FMRP$^+$ SGs (Aulas et al., 2017). Whilst only BICD1 is crucial for SG formation (Loschi et al., 2009), BICD2 also appears to localize to neuronal SGs (Figure 5.4; Figure 5.8). For that reason, it would be worth investigating whether other known dynein adaptors (e.g. Hook and Spindly) are recruited to these organelles, and to determine whether they mediate transport of a particular type of SG cargo.

5.3.2 BICD1 associates with SGs after nucleation and until their clearance

After the initial nucleation of mRNPs and liquid-liquid phase separation (LLPS)-mediated growth of core/shell foci, their fusion and maturation is facilitated by microtubule-dependent transport; SG disassembly occurs in a reverse order (Wheeler et al., 2016). Here, I followed the recruitment of BICD1 during oxidative stress (Figure 5.6) as well as its release during stress recovery (Figure 5.7), which is summarized in Figure 5.16. Using N2A-FLAG-TrkB cells, I showed that although SGs nucleated rapidly, within 10-20 min of sodium arsenite treatment, only larger and heterogenous RNP foci contained BICD1 at 20 min. A significant increase of BICD1 was observed at 30 min, with the majority of SGs being positive for BICD1. Therefore it seems that BICD1 recruitment occurs approximately after 10 min from initial SG formation. While it is possible that BICD1 is recruited at an earlier timepoint, its detection using standard microscopy may not be possible due to the nanoscopic nature of nucleating SGs. However, I observed that BICD1 remained associated with SGs throughout the duration of stress, and lasted well beyond two hours (Figure 5.6). Since mature SGs are less mobile (Kedersha et al., 2005), it would be tempting to speculate that the

presence of BICD1 within established SGs goes beyond its proposed role in SG assembly (Loschi et al., 2009), and suggest that BICD1 may participate in SG clearance.

Indeed, during stress recovery, persistent SGs were positive for BICD1 (Figure 5.7). SG dispersal was observed after 50-60 min from stressor removal, and whilst the majority of larger granules contained BICD1, the small RNP droplets were devoid of it (Figure 5.7B,C). Future studies should explore the potential involvement of BICD1 in active SG clearance, further diversifying this largely unexplored area of BICD1 biology, as well as elucidate whether different molecular motor components localize to SGs during this process.

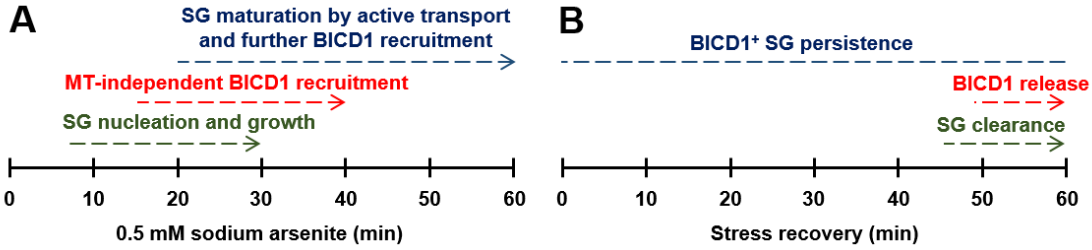

Figure 5.16 Summary of BICD1 recruitment and release from SGs.

Proposed time course of SG formation and clearance, and BICD1 recruitment and release, based on observations in this work (Figure 5.6; Figure 5.7; Figure 5.9; Figure 5.10) and previous reports (Chernov et al., 2009; Kolobova et al., 2009; Nadezhdina et al., 2010). A) SG nucleation is observed as early as 10 min after addition of 0.5 mM sodium arsenite (Figure 5.6). Microtubule (MT)-independent appearance of SG and their growth was previously observed between 15-40 min (Kolobova et al., 2009), during which time BICD1 is recruited to SGs (Figure 5.10). At 30 min, fewer but larger SGs are already detectable, and massive increase of large SGs is observed from 40 min onwards, suggesting MT-based maturation and SG clustering, and potentially further BICD1 engagement due to its presence in the majority of large SGs (Figure 5.6). B) During 1 h stress recovery, large SG, positive for BICD1, are observed at all timepoints. At 50 and 60 min, appearance of smaller foci lacking BICD1 becomes more apparent, suggesting SGs are disassembled and BICD1 is released from that timepoint onwards (Figure 5.7).

Using GFP-BICD1^{WT} as well as the dynein-binding deficient mutant, GFP-BICD1$^{\Delta 95\text{-}265}$, I aimed to illustrate the temporal recruitment and release of BICD1 from SGs by live cell imaging, and determine whether GFP-BICD1$^{\Delta 95\text{-}265}$ has a dominant negative effect on SG formation, as I observed previously that this mutant sequesters Rab6 and translocates to the cell periphery (Figure 3.7). However, both probes were prone to aggregation, and although I was able to track individual puncta in control cells, treatment of N2A-FLAG-TrkB cells with sodium arsenite resulted in cells rapidly changing their morphology (as seen in Figure 5.1B), hence making them unsuitable for live cell imaging (not shown).

This could be addressed in future studies using a cell model does not undergo such rapid morphological changes under stress.

5.3.3 Targeting of BICD1 to SGs is independent of the Golgi apparatus integrity and Rab6

Oxidative and ER stresses affected the intracellular localization of BICD1 (Figure 5.4A; Figure 5.5). I observed not only recruitment of BICD1 to SGs but also its increased accumulation around the Golgi apparatus. I demonstrated that the *cis*-Golgi ribbon-like structure was perturbed by sodium arsenite treatment (Figure 5.8), in line with previous reports (Vega et al., 1999; Kolobova et al., 2009; Catara et al., 2017). In addition, certain Golgi apparatus-associated proteins translocate to SGs in a stress-dependent manner (Kolobova et al., 2009; Catara et al., 2017).

Here, I demonstrated that the Golgi-associated proteins GM130, Rab6 as well as BICD1 and BICD2 accumulated in the perinuclear region in response to sodium arsenite treatment (Figure 5.8), suggesting a perturbed global membrane trafficking to/from Golgi apparatus (Vega et al., 1999). Interestingly, Rab6, a well-studied BICD1 and BICD2 interaction partner, localization of which is highly dependent on BICDs (Figure 3.7; Matanis et al., 2002; Moorhead et al., 2007; Wanschers et al., 2007; Schlager et al., 2010; Splinter et al., 2010; Matsuto et al., 2015; Terawaki et al., 2015), was not recruited to SGs. These preliminary results show a novel BICD1 and BICD2 function, which does not correlate with Rab6-mediated membrane trafficking, and suggest that a Rab6-independent pool of BICD1 and BICD2 is recruited to SGs. Because BICDs and Rab6 mediate coat protein I (COPI)-independent transport of Golgi vesicles to the ER, this finding suggests that the Rab6-free and the ER-associated pool of BICDs could be recruited to SGs, with ER being a site near which SGs form (Kayali et al., 2005).

Indeed, brefeldin A treatment did not impair SG formation or recruitment of BICDs – in fact, SGs appeared larger (Figure 5.8), which might be a result of an increased availability of certain Golgi apparatus- and SG-related proteins, such as BICDs, on the ER-Golgi collapse organelles formed by brefeldin A. The effect of brefeldin A on SG size, however, needs to be explored further in future studies. Similarly to blocking the ER export by brefeldin A, it would be interesting to assess whether inhibition of transport out of the Golgi apparatus can lead to defects in SG formation and/or BICDs recruitment.

5.3.4 SGs require microtubules for maturation, but not for BICD1 recruitment

Next, I demonstrated that SG maturation relies on microtubule integrity, in line with previous studies (Ivanov et al., 2003; Kwon et al., 2007; Loschi et al., 2009; Chernov et al., 2009). Although microtubule network facilitates the recruitment of certain cargos to SGs (Kolobova et al., 2009), this was not the case for BICD1 (Figure 5.9C; Figure 5.10), although it is possible that microtubule-based transport facilitates further targeting of BICD1 to these organelles.

Undoubtedly, it would be necessary to explore the composition of SGs in cells with depolymerized microtubules (Figure 5.10), in particular to verify the association with dynein and kinesin motor components. Unfortunately, I was not able to demonstrate the co-localization of these molecular motors with SGs in sodium arsenite-stressed cells using standard immunocytochemistry (not shown). Although I used antibodies listed in the study by Loschi et al. (2009), live cell-permeabilization step was omitted, which could be the reason behind the lack of detection of the motor components in SGs in N2A-FLAG-TrkB cells and pMNs. Interestingly, Tsai et al. (2009) demonstrated the presence of small RNP foci, comparable to those observed after additional microtubule depolymerization (Figure 5.9), in response to sodium arsenite treatment and block of dynein activity by EHNA. It would be interesting to verify whether BICD1 and other motor machinery components localize to RNP foci formed in similar conditions.

5.3.5 Proposed model of BICD1 recruitment to SGs

The SG nucleating factor recruiting BICD1 is currently unknown. It would be tempting to speculate that there is a candidate protein, which binds BICD1 with high affinity and in a manner similar to that of Rab6 (Matanis et al., 2002). The role of two hypothetical candidates in this process should be explored further: FMRP and histone deacetylase 6 (HDAC6).

In *Drosophila*, BicD regulates the expression and localization of FMRP, in an RNA-dependent manner (Bianco et al., 2010). In addition, BicD and dynein interact with mRNA via Egalitarian (Dienstbier et al., 2009), which is involved in *Drosophila* SG formation (Perez-Pepe et al., 2018). However, a mammalian orthologue of Egalitarian has not yet been identified.

HDAC6 is a microtubule deacetylase (Hubbert et al., 2002), which plays an essential role in SG dynamics (Kwon et al., 2007), similar to its role in aggresome formation (Kawaguchi et al., 2003). In SGs, HDAC6 binds polyubiquitinated proteins and G3BP. It also recruits dynein, and this interaction allows microtubule-based transport of SGs. At present, two studies demonstrated the HDAC6-dynein interaction; it is however based on co-IPs from mammalian cell extracts, raising a question whether HDAC6 can directly bind the dynein complex (Kawaguchi et al., 2003; Kwon et al., 2007). As HDAC6 has not been identified as a dynein adaptor to date, it would be interesting to investigate whether BICD1 mediates HDAC6-dynein interaction.

A hypothetical novel binding partner identified in our BICD1 interactome (Appendix 1) is a related, class II family member, HDAC4 (Harada et al., 2016). However, HDAC4 is not related to aggresomes (Kawaguchi et al., 2003) and SGs (Kwon et al., 2007). Furthermore, mass spectrometry of BICD1-interacting proteins was performed using cell extracts from unstressed cells. Interestingly, comparing our dataset (Appendix 1), the BICD1 dataset on BioGRID (www.thebiogrid.org) and those from studies identifying novel SG components (Jain et al., 2016; Markmiller et al., 2018; Youn et al., 2018), a number of overlapping proteins was found. These include FMRP, NUP153, PRRC2A/B/C, ANKRD17/GTAR, DPYSL2/3, WDR62, granulin, PAWR, CCDC21/CEP85, CIT, DISC1, RanBP2; however, many of these hits await experimental validation.

5.3.6 BICD1 precipitates with SG proteins

The lack of BICD1 detection in proteomic screens suggests that BICD1 may associate with SG dynamic shell, rather than the stable core (Jain et al., 2016). This, however, does not agree with the detection of dynein components in the core fraction (Jain et al., 2016). Here, I used cellular fractionation, which allows the precipitation of SG components (Jain et al., 2016; Wheeler et al., 2016; Wheeler et al., 2017), as a biochemical approach to verify the association of BICD1 with SGs. I detected a stress-specific association of BICD1 and other known SG components, including G3BP, FMRP and TDP-43, to the SG pellet (Figure 5.15B); however, the number of repeats needs to be increased to validate this finding. Although this approach is semi-quantitative and does not allow to determine conclusively whether BICD1 associates with the shell or with the core

of SGs, its detection strongly implies the latter, as SG shell is susceptible to disruption upon cell lysis (Jain et al., 2016).

Because of the abundance of RBPs and mRNAs within SGs (Chantarachot and Bailey-Serres, 2017), as well as recent evidence that BICD2 transports mRNA *in vitro* when co-expressed with the *Drosophila* mRNA co-factor Egalitarian (McClintock et al., 2018), one could further validate the interaction of BICD1 with SG proteins by co-IP of a selected SG protein from control and stressed cells (Tsai et al., 2008), in the presence or absence of RNase, although antigen accessibility by an antibody could be the major caveat using this approach.

5.3.7 PTPN23 does not contribute to SG dynamics

I investigated the role of PTPN23 in SG dynamics. Similarly to BICD1, there are links connecting PTPN23 to several SG cargo, including BICD1, SMN1 (Husedzinovic et al., 2014), FAK (Castiglioni et al., 2007), and ubiquitin-related proteins (Ali et al., 2013; Gahloth et al., 2016). Unlike BICD1, PTPN23 was not detected in neuronal SGs (Figure 5.13). Then, using PTPN23 knockdown model, I demonstrated that PTPN23 is not likely to be playing a role in SG dynamics (Figure 5.14), as there was no statistically significant difference in BICD1, G3BP and FMRP recruitment (Figure 5.14D,F), or change in SG size distribution upon PTPN23 depletion (Figure 5.14E,G). Whilst I observed a statistically significant decrease of cells positive for $G3BP^{+}$, but not $FMRP^{+}$ SGs after depletion of PTPN23 (Figure 5.14C), this was potentially related to the poor health of these cells, as severe cell detachment after combined lentiviral transduction and oxidative stress was observed.

Alternatively, PTPN23 may play an indirect role in regulating the dynamics of individual SG components, such as G3BP. Previously, distinct dynamics of G3BP and FMRP within SGs were demonstrated using FRAP; while G3BP rapidly shuttles in and out of SGs (Kedersha et al., 2005), FMRP is more stable and does not exit SGs as readily (Gareau et al., 2013). In addition, I have not explored the effect of PTPN23 depletion on SG clearance and ubiquitination, this should be addressed in future studies. This approach is potentially interesting, since PTPN23 mediates degradation of ubiquitinated membrane receptors (Doyotte et al., 2008; Ali et al., 2013; Kharitidi et al., 2015; Ma et al., 2015), and the high ubiquitination status of SGs has been shown to play a role in their transport (Kwon

et al., 2007), stability (Xie et al., 2018) and clearance by granulophagy (Buchan et al., 2013).

5.3.8 Final conclusions

In summary, in this work I demonstrated that BICD1 is a novel component of neuronal SGs. However, additional work is necessary to fully decipher the mechanism of BICD1 targeting to these membrane-less organelles. Here, I showed that BICD1 was recruited to SGs approximately 10 min after initial nucleation, in a microtubule-independent manner, and associated with SGs until their clearance (Figure 5.16). This result, together with previous evidence that BICD1 deficit leads to defective SG formation (Tsai et al., 2009; Loschi et al., 2009), suggest that this dynein adaptor plays an instrumental role in SG maturation. Investigating the direct interaction between BICD1 and selected SG components to reveal the principles of its recruitment to nucleating SGs, as well as the role of BICD1 is SG clearance, should be the primary focus of futures studies.

6 The effect of oxidative stress on NTR trafficking and signalling in neuronal cells

6.1 Aims of this chapter

Components of the microtubule-based trafficking machinery are essential for the formation of mature SGs in response to environmental stresses, as well as SG clearance. Proteins, such as dynein and kinesin, co-localize with SGs, and their depletion or pharmacological inhibition perturbs SG dynamics (Kwon et al., 2007; Loschi et al., 2009; Tsai et al., 2009). In addition, oxidative stress (Chen and Liu, 2017) and cellular transport defects (Bilsland et al., 2010) contribute to the pathomechanism in neurodegeneration. Because NT signalling is essential for neuronal health and survival (Bronfman et al., 2007), in this final capter I aimed to explore the relationship between NTR trafficking and signalling in acute oxidative stress conditions.

6.2 Results

6.2.1 Sodium arsenite perturbs α-p75^{NTR} accumulation and BDNF signalling in N2A-FLAG-TrkB cells

The most striking finding in Chapter 5 was the effect of cellular stress on the distribution of BICD proteins – they localized to SGs and accumulated around condensed Golgi apparatus, suggesting a potential alteration to the membrane traffic under stress (Vega et al., 1999; Gougeon et al., 2002; Catara et al., 2017). Retrograde trafficking machinery is required for an effective stress response (Loschi et al., 2009), and there is evidence linking oxidative stress and perturbed cellular trafficking to neurodegeneration (Bilsland et al., 2010; De Vos and Hafezparast, 2017; Zhang et al., 2018). Because the same components of retrograde trafficking machinery, including dynein and BICD1, are essential for the homeostasis of NT signalling in MNs (Yano et al., 2001; Terenzio et al., 2014), I hypothesized that signalling mediated by NTs might be affected in cells responding to stress.

To investigate the effect of oxidative stress on the NT signalling platform in neuronal cells, I utilized a previously established NTR accumulation assay, and

assessed the activation of PI3K/AKT and Ras/ERK1/2 signalling, downstream of BDNF/TrkB, as outlined in Figure 6.1A.

For the NTR accumulation assays, cells were serum-starved for 2 h, and treated for 1 h with vehicle or a stress-inducing drug (specified in the figure legends). Next, I added anti-$p75^{NTR}$ (α-$p75^{NTR}$; #5410, CRD, CRUK) antibody for 15 min, and 100 ng/ml BDNF for the following 45 min, in the presence of a stressor. Species and isotype matched immunoglobulins (IgG) were used as a control in the antibody accumulation assays (Figure 4.1). Following acid wash, the internalized antibody-receptor complex, α-$p75^{NTR}$, was detected by a fluorescent secondary anti-rabbit antibody. See Methods for details and quantification.

For BDNF signalling assays, cells were serum starved for 2 h. Vehicle or stress-inducing drug was applied for the following hour. Next, cells were stimulated with 100 ng/ml BDNF for various time points, in the presence of stress/vehicle. In all experiments, timepoint “0” refers to the incubation with unsupplemented DMEM or NB, for the duration equivalent of BDNF application. Proteins were extracted in RIPA buffer, directly after BDNF stimulation, for later analysis by SDS-PAGE and western blotting. In all experiments, detection of phosphorylated AKT (pAKT) refers to the recognition of phosphoserine-473 (S473; #4060, Cell Signaling).

I first analysed the effect of 0.5 mM sodium arsenite ($NaAsO_2$) treatment on α-$p75^{NTR}$ accumulation. In approximately 60% of control cells, I detected a punctate perinuclear accumulation of α-$p75^{NTR}$. On contrary, detection of this probe was nearly absent in stressed N2A-FLAG-TrkB cells, approximately 40% of which were bearing detectable SGs, suggesting that sodium arsenite may perturb NTR internalization and/or NTR trafficking (Figure 6.1B,C).

In line with α-$p75^{NTR}$ accumulation deficit in stressed cells, I observed no increase in AKT phosphorylation in response to BDNF stimulation in stressed N2A-FLAG-TrkB cells (Figure 6.1D-G), and a decreased basal levels of AKT activation in cells cultivated in full medium (Figure 6.1F,G). This preliminary finding suggests that acute oxidative stress may hinder the sensitivity of cells to NTs, and potentially downregulate the pro-survival signalling in neuronal cells.

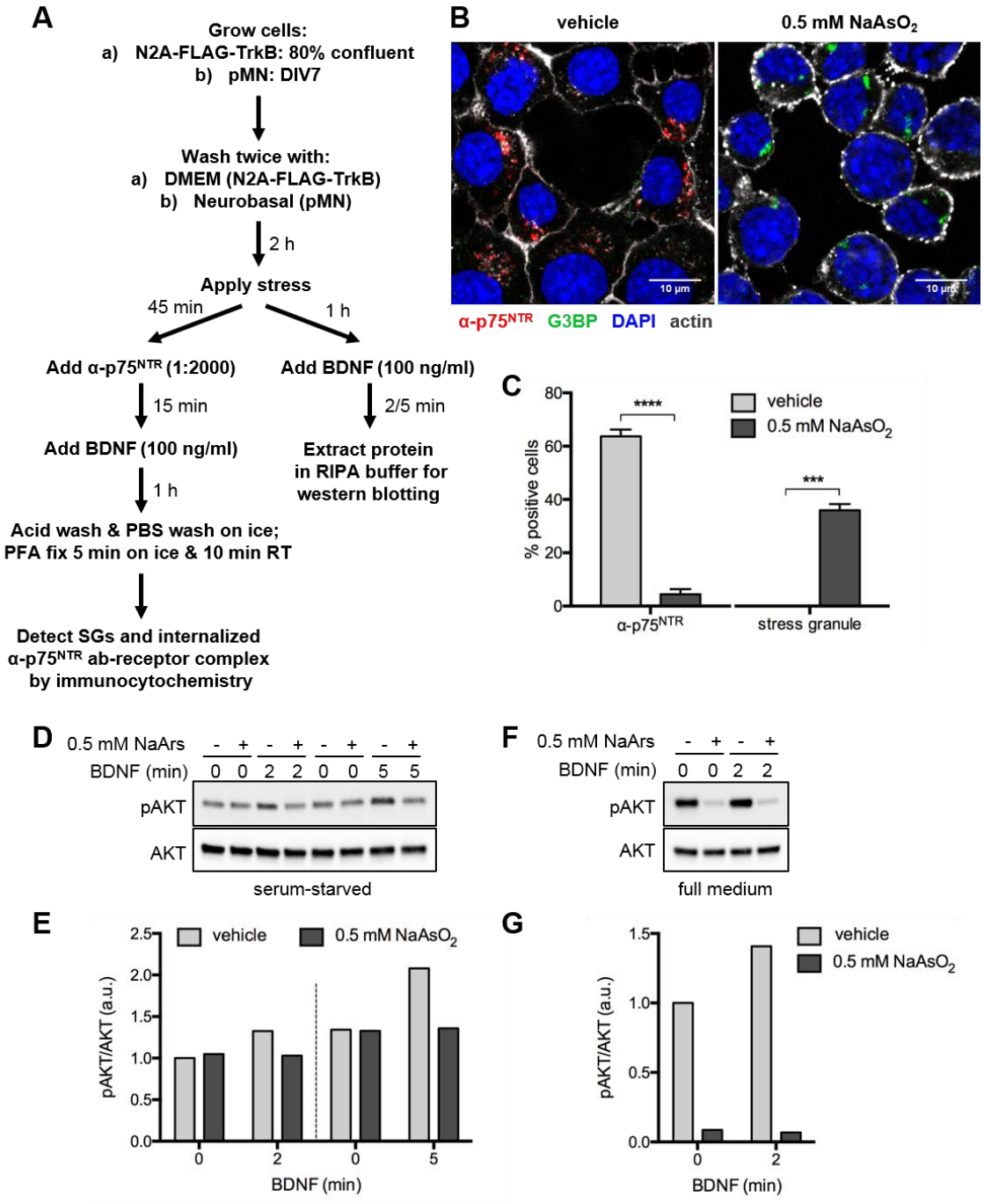

Figure 6.1 Sodium arsenite perturbs α-p75^{NTR} accumulation and AKT signalling.

A) A work flow of α-p75^{NTR} accumulation (left) and BDNF signalling (right) assays under oxidative or ER stress. B) Magnified representative confocal images of N2A-FLAG-TrkB cells showing lack of characteristic perinuclear accumulation of α-p75^{NTR} after treatment with 0.5 mM sodium arsenite, and presence of SGs, immunostained for G3BP, following acid wash and fixation (n=3). Scale bar: 10 µm. C) Quantification of cells positive for α-p75^{NTR}, and SGs (see Methods). Percentages were calculated for each replicate per treatment group (n=3). ***P<0.001, ****P<0.0001, unpaired Student's *t*-test. D,F) Vehicle or 0.5 mM sodium arsenite-treated (1 h) N2A-FLAG-TrkB cells were stimulated without or with BDNF for 2 and 5 min under starved conditions (D) or in full medium (F). Cell extracts were immunoblotted for pAKT and total AKT. E,G) Densitometric analysis of pAKT, normalized to total AKT, of the corresponding blots in D and F, respectively (n=1).

6.2.2 Oxidative stress affects retrograde trafficking and NT signalling selectively, and in a dose-dependent manner

Next, I investigated whether observed α-p75^{NTR} accumulation and BDNF signalling deficits are drug- and dose-dependent. Both preliminary assays were conducted in N2A-FLAG-TrkB cells treated with two concentrations of sodium arsenite (0.25 mM and 0.5 mM) or hydrogen peroxide (H_2O_2; 0.5 mM and 1 mM), another well-characterized oxidative stress inducer (Emara et al., 2012); or under acute ER stress, evoked by 15 μM thapsigargin (Figure 6.2).

In all treatment groups, SGs were detected; their size appeared to correlate with increasing stressor concentration (Figure 6.2A). Relative to control cells, a reduction in α-p75^{NTR} accumulation was observed in cells pre-treated with oxidative stress inducers. In cells exposed to ER stress, α-p75^{NTR} accumulation appeared slightly reduced, yet several cells positive for SGs and perinuclear α-p75^{NTR} were detected (Figure 6.2A). While all tested stressors induce stress response via a distinct sensing mechanism, which exhibits in SG formation (Anderson and Kedersha, 2008; Emara et al., 2012), our preliminary results suggest that oxidative, but not ER stress may perturb NTR trafficking.

Next, I assessed AKT and ERK1/2 signalling, acting downstream of BDNF stimulation, under the same stressed conditions (Figure 6.2B,C). Silencing of these signalling kinase cascades by serum starvation was inefficient in control cells; AKT activation was comparable to that in the cells cultured in full medium (Figure 6.1F,G), and the level of AKT and ERK1/2 phosphorylation was relatively unchanged by BDNF stimulation in control and stressed cells, hence the number of repeats could not be increased. However, approximately 50% reduction in AKT, and 30% in ERK1/2 total activation in cells pre-treated by thapsigargin was observed. Interestingly, while both inducers of oxidative stress appeared to inhibit the activation of AKT, they had a distinct effect on the ERK1/2 signalling. While 0.25 mM sodium arsenite slightly decreased ERK1/2 phosphorylation, 0.5 mM sodium arsenite increased it by approximately 20%, relative to vehicle. In contrast, both concentrations of hydrogen peroxide inhibited the activation of ERK1/2. In all tested conditions, I did not detect activation of apoptosis, demonstrated by the lack of cleaved caspase-3 detection. These observations

suggest that while oxidative stressors may block AKT signalling, they differently affect the signalling of ERK1/2.

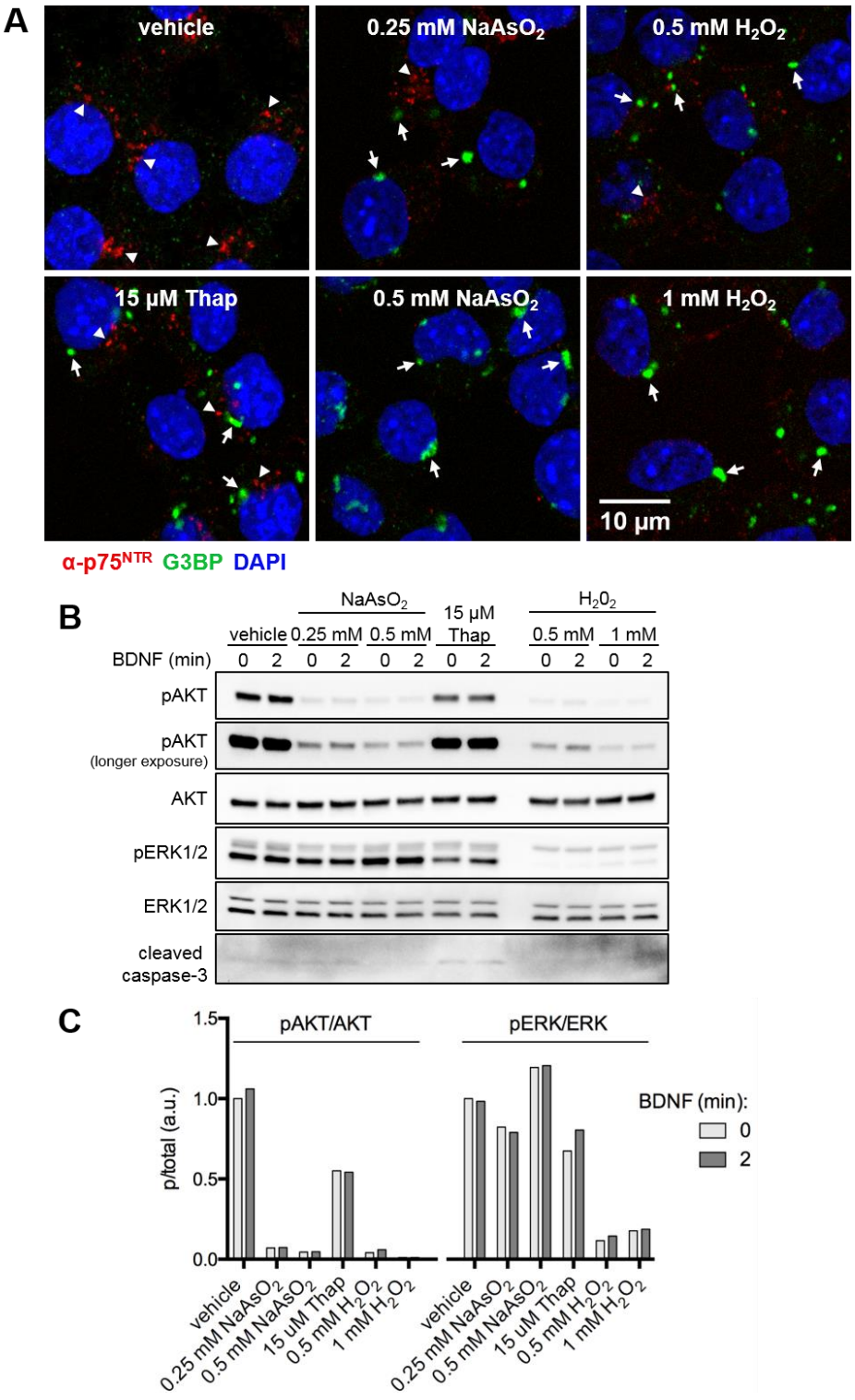

Figure 6.2 Oxidative stress affects NTR signalling cascade in a dose-dependent manner.

A) Representative confocal images showing α-p75^{NTR} accumulation (arrowheads) in N2A-FLAG-TrkB cells exposed to ER or oxidative stress (n=2). Following acid wash, SGs were immunostained for G3BP (arrows). B) Cells were treated for 1 h with selected stresses, as in A, and stimulated for 2 min with or without BDNF. Cell extracts were immunoblotted for phosphorylated and total AKT and ERK1/2, and cleaved caspase-3. C) Densitometric analysis of phosphorylated proteins was normalized to total protein, as shown in (B) (n=1).

Oxidative stress affected the morphology of N2A-FLAG-TrkB cells and visibly reduced their surface area. Having observed perturbed α-p75^{NTR} accumulation (Figure 6.2A), I considered that oxidative stress may lead to a decreased surface localization or total expression of the endogenous p75^{NTR}. However, levels of p75^{NTR} in sodium arsenite treated cell were comparable to control (Figure 6.3A). Similarly, our observations of perturbed NTR accumulation, and AKT and ERK1/2 signalling (Figure 6.2A,B), were not related to apoptosis, as demonstrated by the relative to vehicle cleaved caspase-3 detection by immunocytochemistry in all stressed conditions (Figure 6.3B).

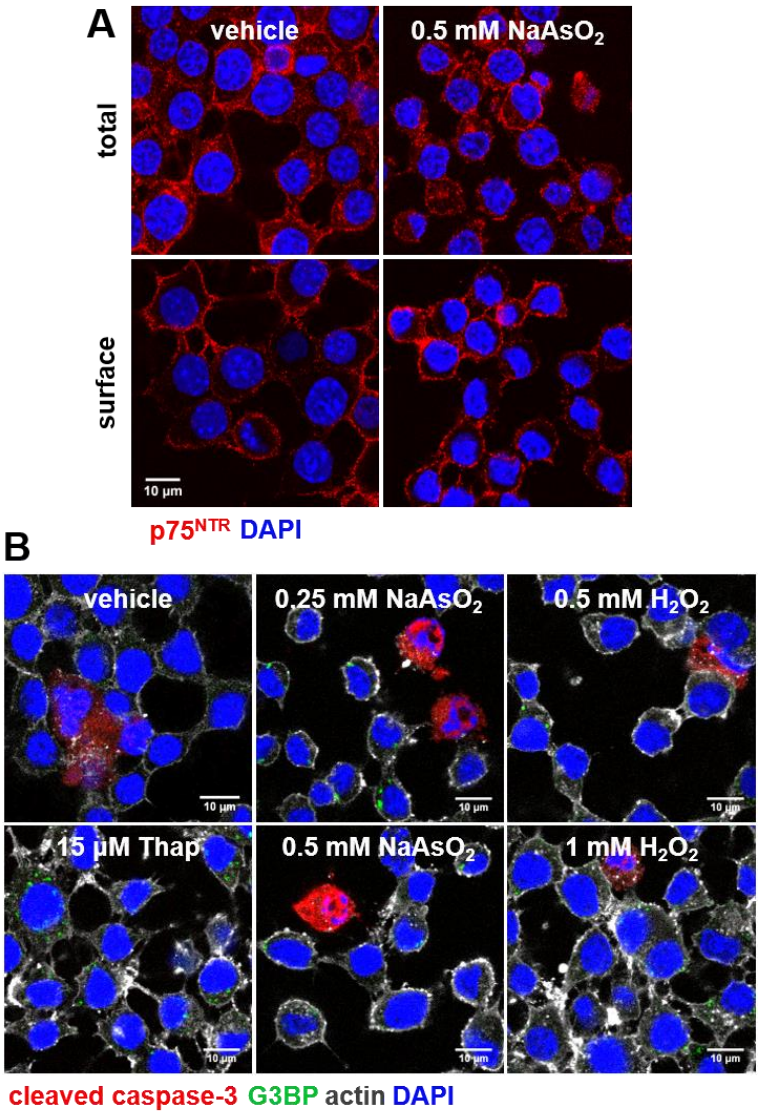

Figure 6.3 Oxidative stress does not affect α-p75^{NTR} levels or induce cell death.

A) Representative confocal images showing the distribution of endogenous p75^{NTR} in fixed and permeabilized (total) or non-permeabilized (surface) N2A-FLAG-TrkB cells, treated for 1 h with vehicle or 0.5 mM sodium arsenite (n=1). B) Images of treated cells (2 h), immunostained for cleaved caspase-3 (n=2).

While no difference in p75^{NTR} localization at the plasma membrane was detected (Figure 6.3A), oxidative stress severely affected perinuclear accumulation of α-p75^{NTR} (Figure 6.2), suggesting that stress may perturb trafficking along the endocytic pathway, which is driven by cytoplasmic dynein (Fang et al., 2012; Catara et al., 2017). To test this hypothesis, I performed the α-p75^{NTR} accumulation assay with the addition of a non-toxic retrograde label, cholera toxin subunit B (CTB; Figure 6.4A) (Von Bartheld, 2004). CTB partially shares the trafficking route of NTRs, by binding to Trk/p75^{NTR}-associated ganglioside GM1 (Butowt and Von Bartheld, 2003), but unlike NTR, it travels to the TGN, rather than towards the degradative or recycling pathways (Schmieg et al., 2014).

Under acute stress, CTB accumulated in clusters (Figure 6.4B), which resembled previously observed dysmorphic Golgi apparatus (Figure 5.8). Detection of cells positive for both probes, CTB and α-p75^{NTR}, was comparable between vehicle- and 0.5 mM hydrogen peroxide-treated cells (Figure 6.4C). Retrograde traffic, however, was significantly reduced by oxidative stress, with up to 50% fewer cells bearing perinuclear CTB when a high-dose oxidative stress was applied, and this reduction was comparable between sodium arsenite and hydrogen peroxide.

Sodium arsenite treatment had a more profound effect on α-p75^{NTR} accumulation than hydrogen peroxide, with very few cells displaying perinuclear puncta. In the majority of α-p75^{NTR}-positive cells, CTB was also detected. While only higher concentration of hydrogen peroxide significantly reduced the accumulation of α-p75^{NTR} (Figure 6.4B,C), both tested concentrations were previously shown to affect AKT and ERK1/2 signalling (Figure 6.2B,C), suggesting hydrogen peroxide may selectively affect the downstream signalling of NTRs, without perturbing their trafficking. These results imply that although there is some overlap in the mode of action of sodium arsenite and hydrogen peroxide, they may affect the NTR trafficking and signalling in a distinct manner.

In addition, unlike in control cells, a plasma membrane-like coating by α-p75^{NTR} was observed in stressed cells, in which perinuclear CTB was detected, particularly in cells pre-treated with a lower dose of each stressor (Figure 6.2B). Although surface-bound ligands were removed prior to fixation by acid wash, it appears that oxidative stress induces receptor retention near the plasma membrane and makes them insensitive to acid-wash, in addition to the perturbed

retrograde traffic. It also suggests that the deficit in α-p75^{NTR} accumulation was not due to a decrease in membrane apposition of the receptor.

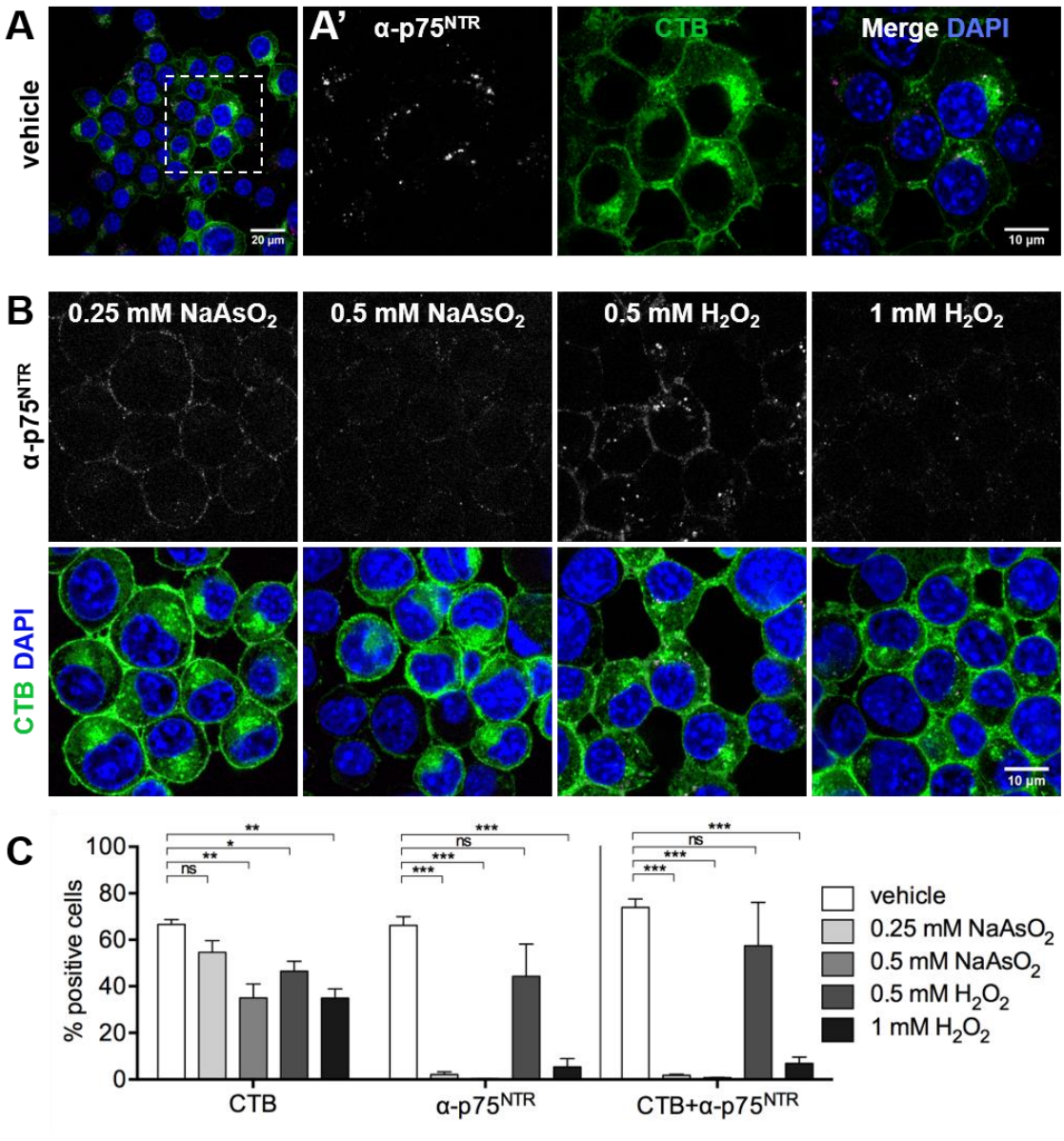

Figure 6.4 Oxidative stress affects retrograde traffic selectively, and in a dose-dependent manner.

A-B) Representative confocal images of α-p75^{NTR} and CTB accumulation assay in N2A-FLAG-TrkB cells treated with vehicle (A; A' – magnified view) or two different doses of sodium arsenite or hydrogen peroxide (B). Cells were acid-washed prior to fixation (n=3). C) Quantification of A-B. For each condition, cells with perinuclear α-p75^{NTR} or CTB were counted as positive (percentage calculated as a fraction of all cells), or cells positive for both probes (percentage calculated as a fraction of CTB-positive cells). For each condition, five fields were imaged and an average of 70 cells per field were counted (n=3). *P<0.05, **P<0.01, ***P<0.001, one-way ANOVA, with Dunnett's multiple comparisons test.

Because of the distinct peripheral localization of α-p75^{NTR} in stressed cells, I verified whether it localized closely to the plasma membrane. The accumulation

assay was performed in vehicle- or 0.25 mM sodium arsenite-treated cells, as described previously (Figure 6.1A). Here, following acid wash and before fixation, the plasma membrane of live cells was labelled on ice with a lectin – fluorescently-labelled wheat germ agglutinin (WGA) (Von Bartheld, 2004). Next, cells were processed by immunocytochemistry to reveal the localization of the internalized receptor, and the actin cortex (Figure 6.5A). The distribution of WGA and actin was overlapping. While in control cells α-p75^{NTR} was predominantly perinuclear, fluorescence intensity plots revealed an overlap of α-p75^{NTR} with WGA and actin in stressed cells (Figure 6.5B), suggesting that oxidative stress potentially affects NTR retrograde trafficking rather than endocytosis, and leads to receptor retention near cell surface after its internalization. Alternatively, these receptors could be trapped in plasma membrane invaginations such as caveolae, which may prevent ligand removal by acid wash.

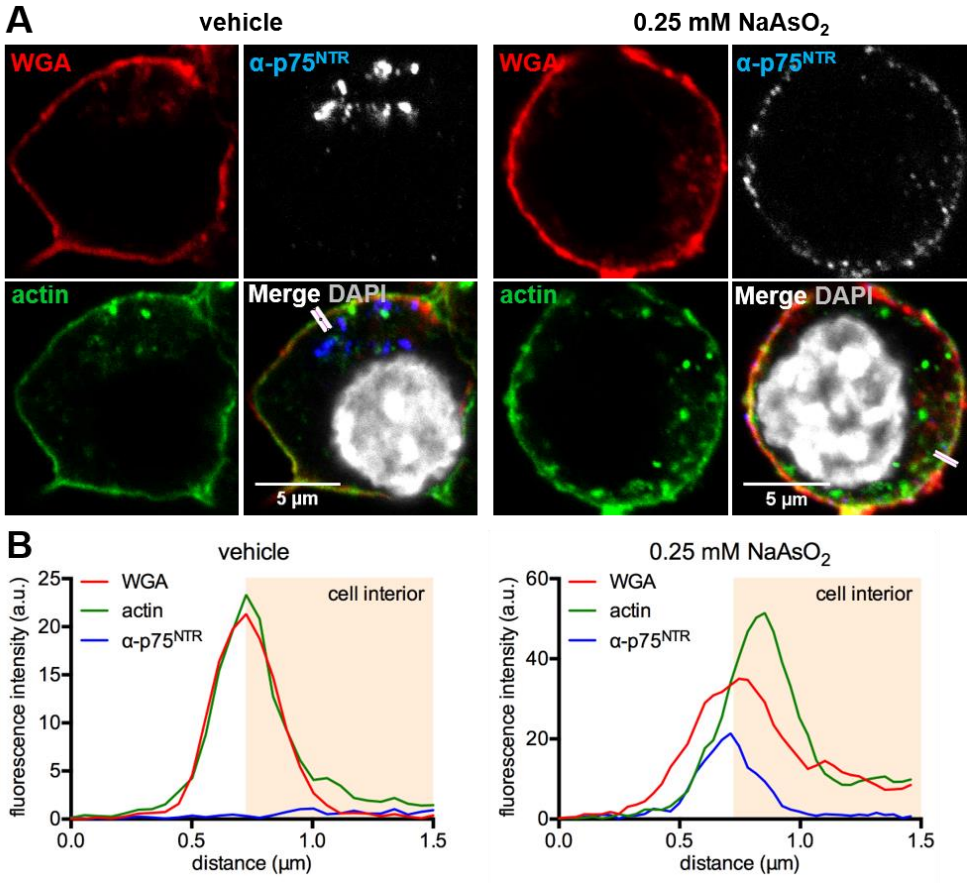

Figure 6.5 Internalized α-p75^{NTR} is retained near the plasma membrane during oxidative stress.

A) Cropped representative images of α-p75^{NTR} accumulation assay in vehicle- or 0.25 mM sodium arsenite-treated N2A-FLAG-TrkB cells. Following acid wash, the plasma membrane was stained with WGA. After fixation, actin was stained with phalloidin. The white lines in merged images indicate the areas used to measure fluorescence intensity of each probe (n=2). B) Fluorescence intensity plots along the line (1.5 µm, 10 pixel wide) drawn across the membrane (from outside-to-inside of the cell).

6.2.3 Oxidative stress perturbs NTR trafficking in pMNs

To investigate whether the oxidative stress-related retrograde trafficking deficit is cell type-specific, I conducted preliminary accumulation assays in pMNs, treated with vehicle or 0.1-0.5 mM sodium arsenite, as outlined in Figure 6.1A. Similarly to our findings in N2A-FLAG-TrkB cells, I observed that oxidative stress likely affects the trafficking of α-p75^{NTR} in pMNs (Figure 6.6). Detection of α-p75^{NTR} puncta in the soma and neurites of pMNs decreased with the increasing concentration of sodium arsenite, which inversely correlated with the detection of SGs (Figure 6.6).

Next, I assessed whether oxidative stress, elicited with 0.25 or 0.5 mM sodium arsenite or hydrogen peroxide, affects retrograde membrane traffic in pMNs. As before, a reduced detection of α-p75^{NTR} in neuronal soma and neurites was observed in pMNs pre-treated with sodium arsenite. However, a decrease in CTB trafficking was observed only with the higher dose of sodium arsenite, although in several cells perinuclear CTB could be detected, suggesting a dose-dependent and selective effect of this drug on retrograde traffic in pMNs (Figure 6.7). In contrast to our findings in N2A-FLAG-TrkB cells (Figure 6.4) and pMNs, α-p75^{NTR} and CTB accumulation assay revealed that hydrogen peroxide perturbed general retrograde membrane traffic in pMNs (Figure 6.7). In addition, hydrogen peroxide induced pronounced membrane blebbing, whereas only mild blebbing was detected when a highest dose of sodium arsenite was applied on pMNs (Figure 6.7). While oxidative stressors elicited an apparent submembrane retention of α-p75^{NTR} in N2A-FLAG-TrkB cells (Figure 6.4; Figure 6.5), it was not easily detected in pMNs grown on coverslips.

Taken together, these preliminary experiments suggest that oxidative stress may perturb NTR trafficking in pMNs. While the effect of sodium arsenite on retrograde traffic appeared more selective, hydrogen peroxide affected the structural integrity of pMNs as well as the retrograde traffic as a whole. Nevertheless, these data imply that both drugs may affect the BDNF/TrkB signalling in pMNs, similarly to the previous observations in N2A-FLAG-TrkB cells (Figure 6.2B,C).

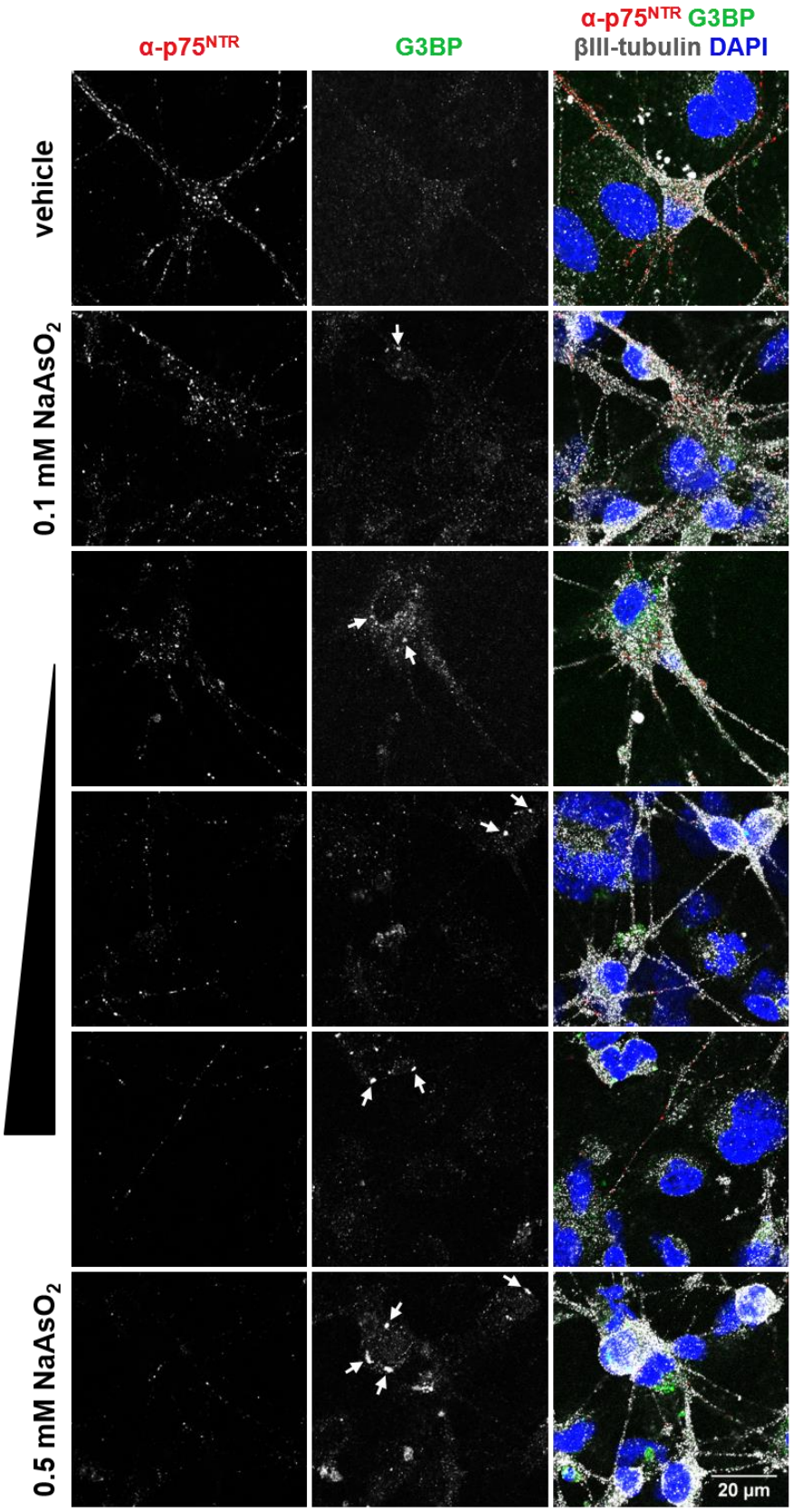

Figure 6.6 Oxidative stress perturbs α-p75^{NTR} trafficking in pMNs.

Representative confocal images showing α-p75^{NTR} accumulation assay in pMNs, pre-treated with vehicle or 0.1-0.5 mM sodium arsenite. Following acid wash, fixed cells were immunostained for SG marker, G3BP (white arrowheads – SGs), and neuronal marker, βIII-tubulin (#ab41489, Abcam) (n=1).

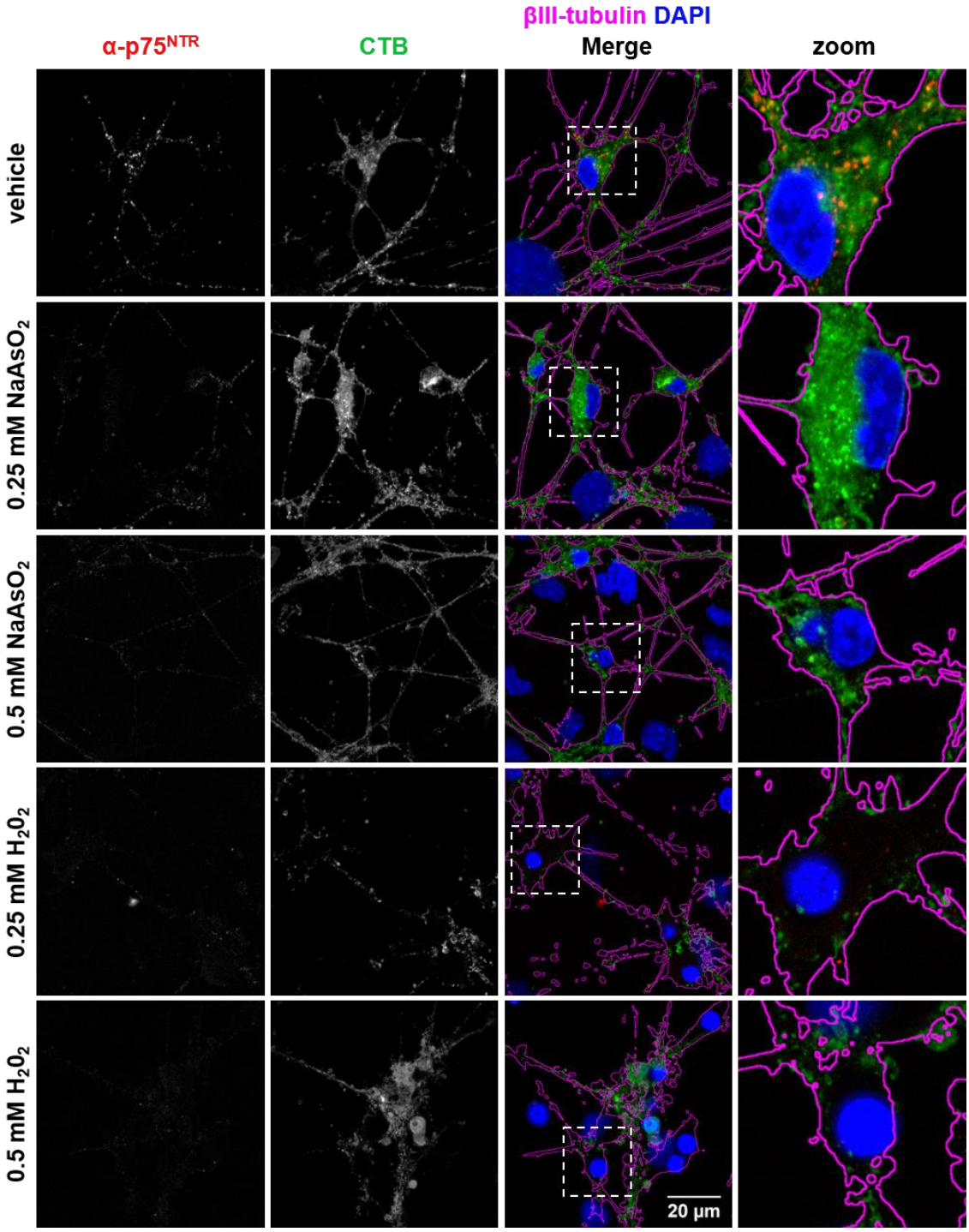

Figure 6.7 Hydrogen peroxide inhibits retrograde membrane traffic in pMNs.

Confocal images showing α-p75^{NTR} and CTB accumulation assay in pMNs treated with vehicle or 0.25-0.5 mM sodium arsenite or hydrogen peroxide. Following acid wash and fixation, cells were immunostained for βIII-tubulin (magenta outline; # mms-435p, Covance) (n=1).

6.2.4 Oxidative stress reduces neuronal sensitivity to NTs and promotes NTR-independent signalling

The preliminary analysis of α-p75^{NTR} accumulation and retrograde traffic in pMNs exposed to oxidative stress (Figure 6.6; Figure 6.7) implied that BDNF/TrkB-mediated signalling in pMNs might also be affected (Figure 6.2B,C).

To test the effect of oxidative stress on PI3K/AKT and Ras/ERK1/2 signalling cascades, BDNF signalling assay was conducted as outlined in Figure 6.1A, in pMNs pre-treated for 1 h with vehicle, 0.5 mM hydrogen peroxide or 0.5 mM sodium arsenite. Next, obtained cell lysates were immunoblotted for phosphorylated and total TrkB, AKT and ERK1/2 (Figure 6.8A).

Since pMNs do not express TrkA, anti-pTrkA/pTrkB antibody (pY706/707; #4621, Cell Signalling) was used for the detection of phosphorylated TrkB in pMNs. The most striking observation was the effect of hydrogen peroxide on BDNF-mediated TrkB activation. While the level of pTrkB was comparable between vehicle- and sodium arsenite-treated pMNs, stress induced by hydrogen peroxide abolished the activation of TrkB by BDNF (Figure 6.8B). Hydrogen peroxide treatment also led to loss of a non-specific band around 240 kDa, however at present it is not known what is detected by this antibody at this molecular weight (red arrow; Figure 6.8A). A significant increase in AKT and ERK1/2 activation was observed upon BDNF stimulation in control cells, however it remained unchanged in pMNs treated with both stressors, which was expected after hydrogen peroxide treatment due to the lack of TrkB activity. Furthermore, while desensitizing cells to BDNF, both stressors induced mild activation of AKT, and sodium arsenite treatment alone led to a significant increase in ERK1/2 activation in pMNs, relative to control unstimulated cells (Figure 6.8B).

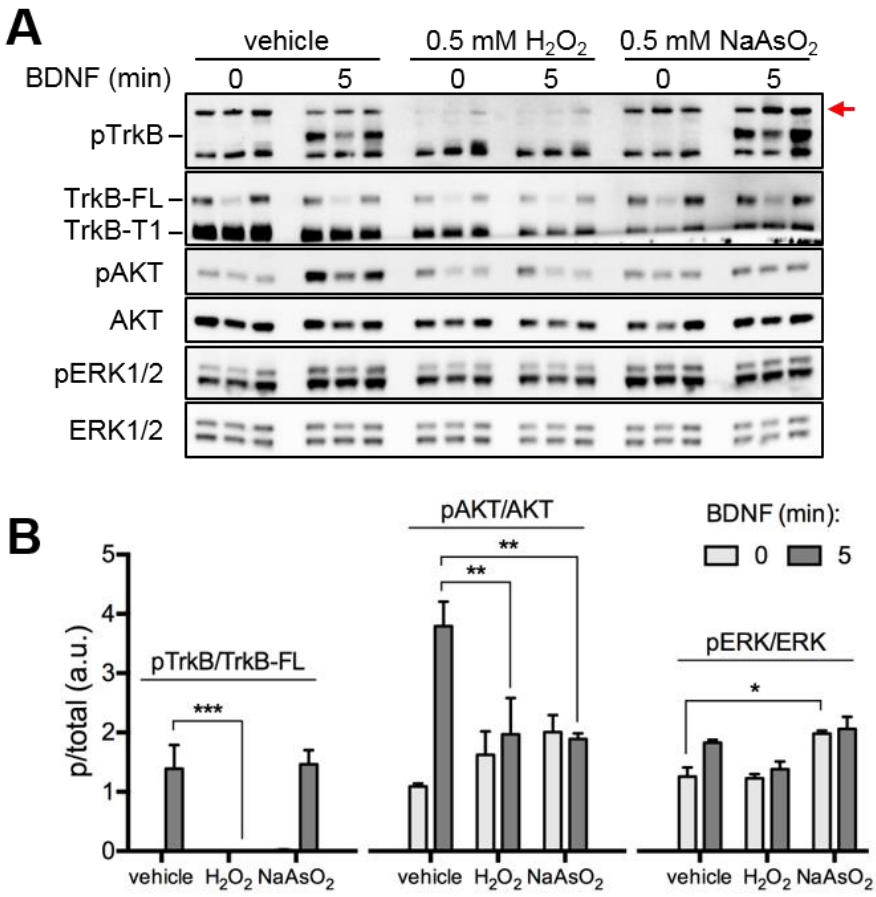

Figure 6.8 Hydrogen peroxide and sodium arsenite affect the NT signalling in a distinct manner.

A) Cells were treated for 1 h with vehicle, 0.5 mM hydrogen peroxide or 0.5 mM sodium arsenite and stimulated for 5 min with or without BDNF, in the presence of stress. Cell lysates were immunoblotted for phosphorylated and total TrkB, AKT and ERK1/2 (n=3, biological replicates). B) Densitometric analysis of phosphorylated proteins was normalized to total protein, as shown in (A; n=3). *P<0.05, **P<0.01, ***P<0.001, two-way ANOVA with Dunnett's multiple comparison test.

Next, to eliminate the potential interference of the stressors with BDNF signalling, and to assess the recovery rate, I performed preliminary BDNF signalling assays in the following conditions: 1) in the presence of stressors in the medium or immediately after a single wash with NB (Figure 6.9A,B); 2) in the presence of stressors or after a single wash and 30 min recovery in NB (Figure 6.9C,D).

While replacing the media evoked the activation of AKT and ERK1/2, further response to BDNF stimulation was observed in control cells. Media change only slightly affected the phosphorylation of these proteins in stressed cells. No response to BDNF was observed and, in particular, no TrkB activation in hydrogen peroxide-treated pMNs (Figure 6.9A,B). These results suggest that the

presence of drugs in the media was unlikely to interfere with the BDNF signalling capacity, and perturbed signalling was an outcome of a stress response in pMNs.

On the other hand, 30 min recovery significantly increased the phosphorylation of AKT and ERK1/2 in sodium arsenite-treated cells, and restored the BDNF-mediated signalling. While increased phosphorylation of AKT and ERK1/2 was detected in hydrogen peroxide-treated cells after recovery, the effect of stress on BDNF/TrkB-mediated signalling in pMNs was not reversed after stress withdrawal (Figure 6.9C,D). Whether pMNs are able to recover from hydrogen peroxide-induced stress, has to be further investigated.

As previously (Figure 6.2; Figure 6.3), I did not detect cleaved caspase-3 (Figure 6.9C,D), suggesting apoptosis was not likely to be playing a role in the perturbed NT-mediated signalling. In addition, this phenotype was unlikely to be a result of the TrkB isoform switching, as relatively comparable ratio of full length (TrkB-FL) and truncated (TrkB-T1) receptors were observed by western blotting in all conditions (Figure 6.9). Whether hydrogen peroxide increases levels of the dominant negative splice variant, TrkB-T1, at the plasma membrane, remains to be investigated.

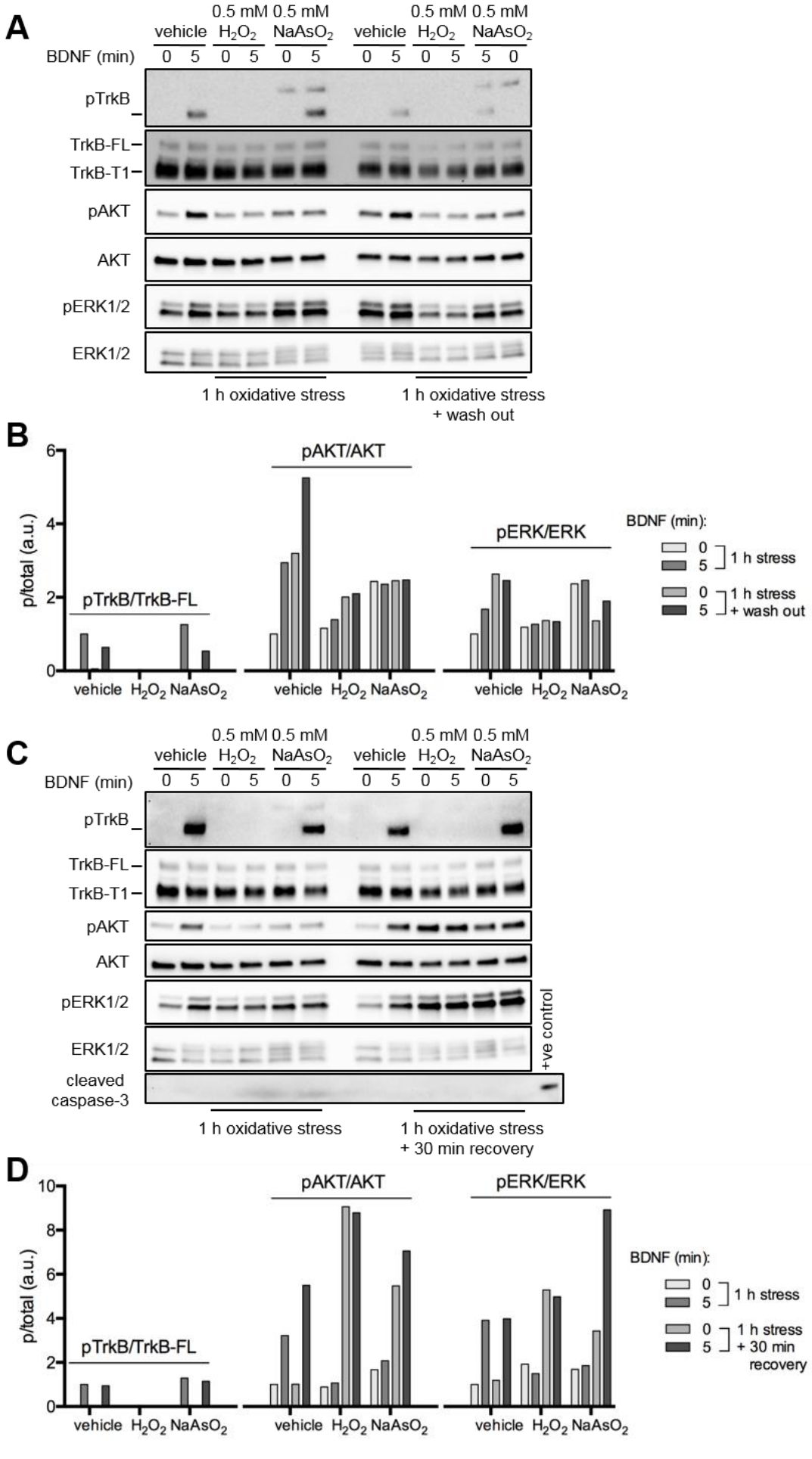
A
vehicle
0.5 mM H2O2
0.5 mM NaAsO2
BDNF (min)
pTrkB
TrkB-FL
TrkB-T1
pAKT
AKT
pERK1/2
ERK1/2
1 h oxidative stress
1 h oxidative stress + wash out
B
p/total (a.u.)
pAKT/AKT
pERK/ERK
pTrkB/TrkB-FL
BDNF (min):
1 h stress
1 h stress + wash out
C
cleaved caspase-3
+ve control
1 h oxidative stress
1 h oxidative stress + 30 min recovery
D
1 h stress + 30 min recovery

Figure 6.9 Recovery from sodium arsenite-induced stress restores BDNF signalling in pMNs.

pMNs were treated for 1 h with vehicle, 0.5 mM hydrogen peroxide or 0.5 mM sodium arsenite. Cells were stimulated for 5 min with or without BDNF, in the presence of stressor or in fresh Neurobasal (NB; A,B), or after 30 min of stress recovery in NB (C,D). Lysates were immunoblotted for total and phosphorylated TrkB, AKT and ERK1/2 (A,C). Lysates, including a positive control, were additionally probed for cleaved Caspase-3 (C). Note: in A, the last two samples are loaded correctly, as annotated. B,D) Densitometric analysis of phosphorylated proteins was normalized to total protein, as in A,C, respectively (n=1).

6.2.5 Exploring the distribution and origin of TrkB, pAKT and pERK1/2 in pMNs and non-neuronal cells

Here, I demonstrated that the TrkB autophosphorylation in response to BDNF treatment was perturbed in pMNs pre-treated with hydrogen peroxide, but not sodium arsenite (Figure 6.8), and the hydrogen peroxide-induced phenotype was not reversed by 30 min stress recovery (Figure 6.9C,D). Analysis of pMN lysates by western blotting revealed no TrkB isoform switching (Figure 6.9), however the potential increased localization of TrkB-T1 to the plasma membrane, due to oxidative stress, remains to be investigated. In earlier experiments, I demonstrated a relatively unperturbed $p75^{NTR}$ dynamics at the plasma membrane of stressed N2A-FLAG-TrkB cells (Figure 6.3A). To better understand the mechanism by which oxidative stress affects NT signalling in pMNs, the total and plasma membrane TrkB levels were assessed by immunocytochemistry.

To reveal the total and cell surface receptor levels, fixed pMNs were immunostained using anti-TrkB antibody (#9872, Merck Millipore), recognizing an extracellular domain, with or without permeabilization, respectively (Figure 6.10A). Next, fluorescence intensity of TrkB was measured within the βIII-tubulin mask (Figure 6.10B). Although in non-permeabilized cells I observed enriched TrkB signal proximal to plasma membrane, fixation with PFA led to partial permeabilization of pMNs and some cytoplasmic staining was observed. However, while oxidative stress appeared to slightly reduce the total receptor levels, a comparable level of TrkB was detected at the plasma membrane in all treatment groups. In addition, a trend towards a slightly increased TrkB fluorescence at the plasma membrane was observed in sodium arsenite-treated cells, relative to vehicle. However, this has to be further validated by increasing the number of repeats.

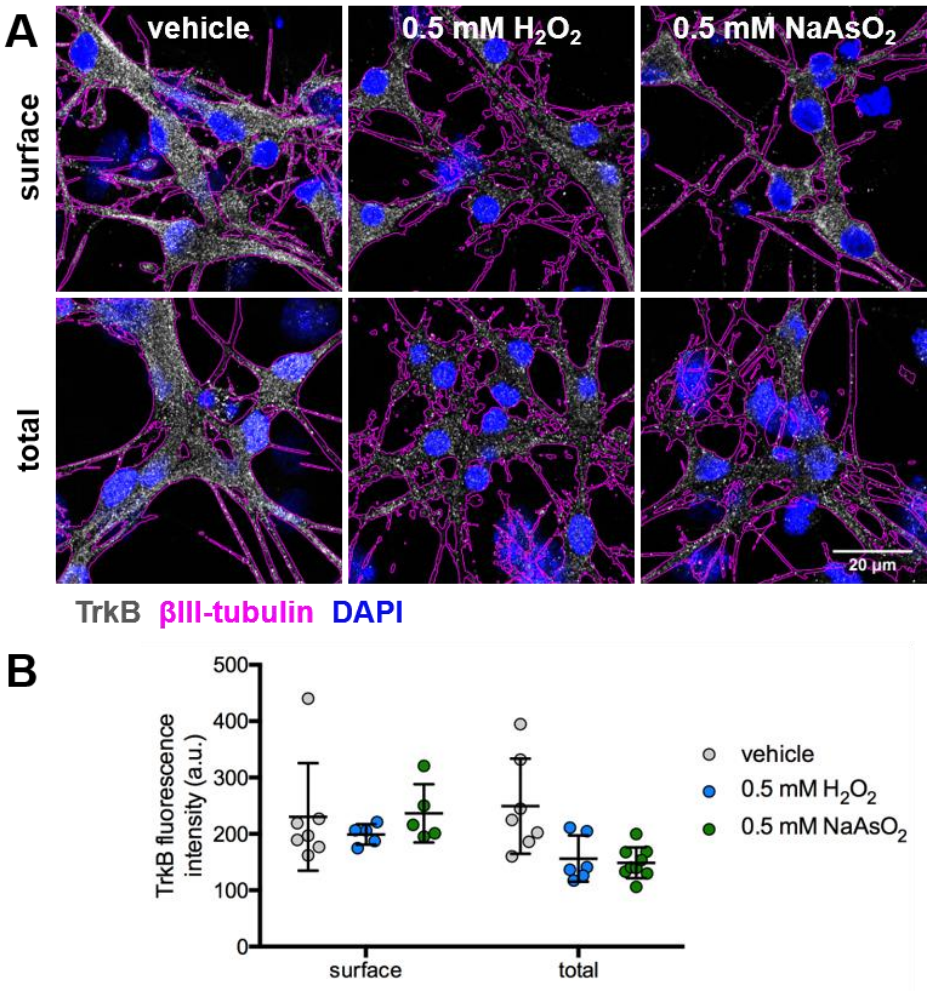

Figure 6.10 Oxidative stress slightly reduces the total receptor levels, but not membrane localization, of TrkB in pMNs.

A) Representative confocal images showing TrkB immunostaining in fixed and non-permeabilized ("surface") or permeabilized ("total") pMNs, after 1 h treatment with vehicle, 0.5 mM hydrogen peroxide or 0.5 mM sodium arsenite. Immunostaining of βIII-tubulin (#mms-435p, Covance) was used as a mask (here shown as magenta outline) for quantification of TrkB levels in pMNs. B) Quantification of TrkB fluorescence intensity within the βIII-tubulin mask. Between 5-9 fields were imaged per condition (n=1). All datapoints were plotted. Error bars show ±SD.

Oxidative stress affected the phosphorylation of AKT and ERK1/2 in mouse ventral horn cultures, and appeared to abolish the response to BDNF stimulation (Figure 6.8). Besides MNs, these primary cultures contain non-neuronal cells such as fibroblasts and glia, which contribute to the source of AKT and ERK1/2, detected by western blotting. Because I observed relatively unperturbed localization of TrkB to the plasma membrane of pMNs (Figure 6.10), I performed preliminary immunocytochemistry experiments to investigate the distribution of phosphorylated AKT and ERK1/2 in pMNs and non-neuronal cells in the cultures, and validated the perturbed response to BDNF stimulation in pMNs.

The activation of AKT in response to BDNF in pMNs was assessed first (Figure 6.11A,B). In vehicle-treated pMNs, a robust increase in pAKT fluorescence intensity was observed upon BDNF stimulation. While pAKT levels in hydrogen peroxide-treated pMNs appeared slightly lower than in control unstimulated cells, it was mildly elevated in pMNs pre-treated with sodium arsenite, which correlated with our findings from western blotting (Figure 6.8). In both treatment groups, however, neuronal pAKT remained relatively unchanged by BDNF stimulation, suggesting that oxidative stress specifically perturbs the NT-mediated activation of pro-survival signalling in these cells.

On the other hand, assessment of the underlying non-neuronal cells revealed a distinct effect of both stressors on the localization of pAKT and the organization of the actin cortex (Figure 6.11C). In vehicle-treated cells, pAKT was detected proximal to the cell boundary and co-localized with the actin. Cells treated with hydrogen peroxide showed increased pAKT immunoreactivity in the nuclei (arrows), in addition to the signal at the plasma membrane, suggesting these cells may be the source of slightly elevated pAKT in western blotting (Figure 6.8). While the actin cortex appeared relatively unperturbed by hydrogen peroxide, sodium arsenite induced a change in its organization, and a loss of the proximal-to-plasma membrane cable-like structure of filamentous actin (F-actin). The presence of perturbed actin cortex in sodium arsenite-treated cells correlated with a perturbed pAKT distribution at the plasma membrane, where it appeared more dispersed when compared with control cells, as well as partial loss of co-localization with the actin cortex. Some nuclear pAKT immunoreactivity was also detected, albeit to a lower degree than in cells treated with hydrogen peroxide (arrows; Figure 6.11).

Detailed analysis of pAKT, AKT and actin distribution in pMNs undergoing oxidative stress has not yet been performed. Since the actin network plays a crucial role in AKT activation in response to extracellular stimuli (Zhao et al., 2015), as well as early endosome trafficking events (Granger et al., 2014), exploring the distribution of the actin network in pMNs is necessary to better understand the significance of our findings.

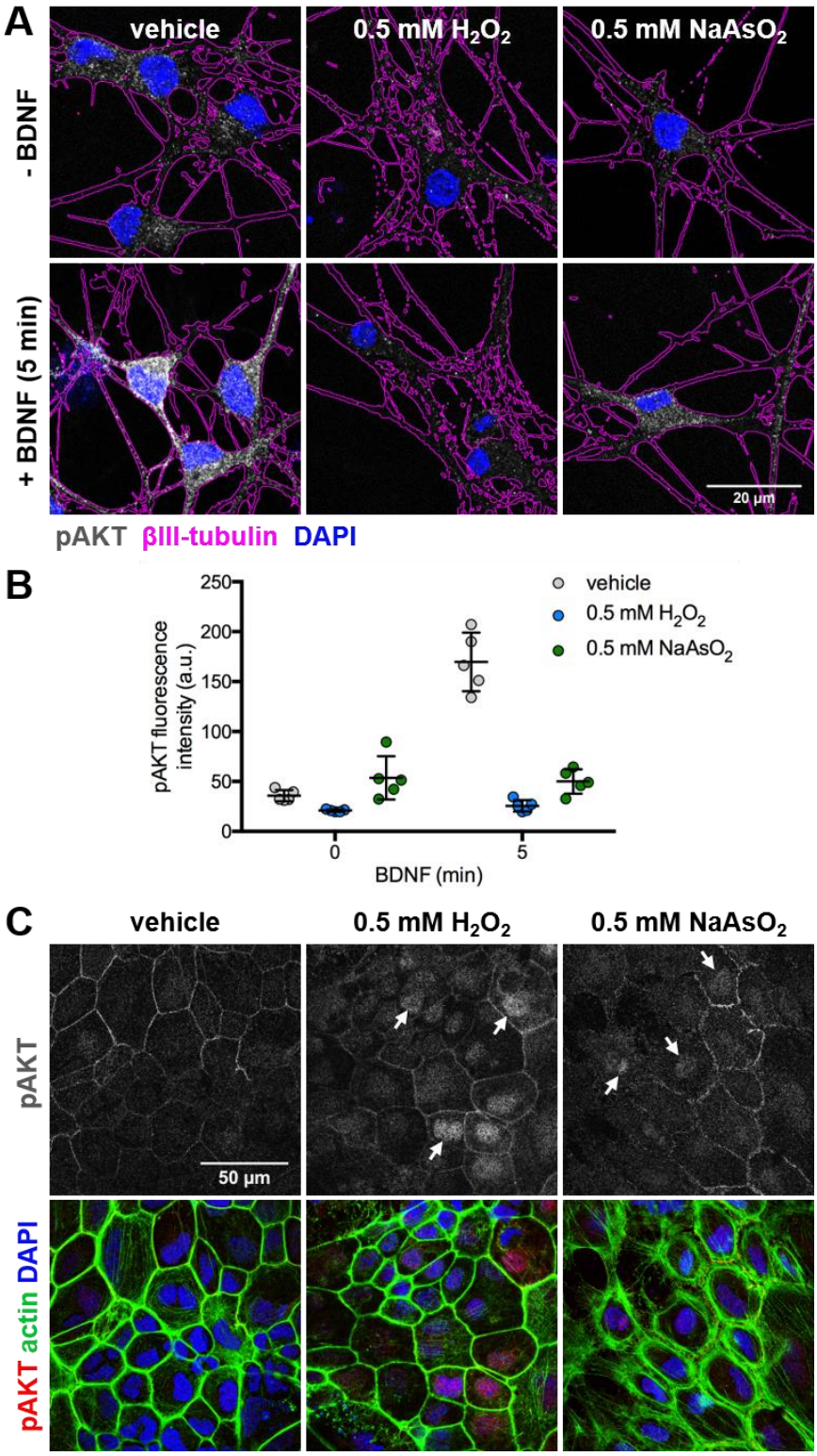

Figure 6.11 Oxidative stress affects the activation and localization of pAKT.

A) pMNs were treated for 1 h with vehicle, 0.5 mM hydrogen peroxide or 0.5 mM sodium arsenite. Next, cells were stimulated for 5 min with or without BDNF, immediately fixed and immunostained for pAKT and βIII-tubulin (magenta outline). B) Quantification of pAKT fluorescence intensity within the βIII-tubulin mask. Five fields were imaged per condition (n=1). All datapoints were plotted. Error bars show ±SD. C) Underlying non-neuronal cell layer from treated ventral horn cultures, fixed and immunostained for pAKT and actin, showing a stress-dependent localization of pAKT, and perturbed actin organization after sodium arsenite treatment.

Similarly to pAKT (Figure 6.11A,B), BDNF stimulation led to a significant increase in pERK1/2 only in vehicle-treated pMNs (Figure 6.12). Sodium arsenite elicited ERK1/2 activation in neurons and non-neuronal cells to a similar degree, suggesting these cells equally contribute to the elevated pERK1/2, detected by western blotting. In contrast, a slight increase in pERK1/2 was observed only in non-neuronal cells treated with hydrogen peroxide. Activation of ERK1/2 is often accompanied by its nuclear translocation (Roskoski, 2012), which was observed in control pMNs stimulated with BDNF. Some nuclear staining was also detected in sodium arsenite-, but not hydrogen peroxide-treated pMNs, irrespective of BDNF treatment. While in vehicle and sodium arsenite-treated non-neuronal cells pERK1/2 was predominantly cytoplasmic, it was significantly enriched in the nuclei of hydrogen peroxide-treated cells (Figure 6.12A).

Further work and increasing the number of repeats is necessary to explore the mechanism by which oxidative stress affects the NT-mediated signalling in pMNs. Through imaging (Figure 6.10; Figure 6.11; Figure 6.12), I partially validated our western blotting results (Figure 6.8). I demonstrated that stressed pMNs did not respond to BDNF stimulation, as no increase in AKT and ERK1/2 activation was detected. In addition, I showed that two oxidative stressors, sodium arsenite and hydrogen peroxide, affected AKT and ERK1/2 signalling in a distinct way, and that this effect was cell-type specific.

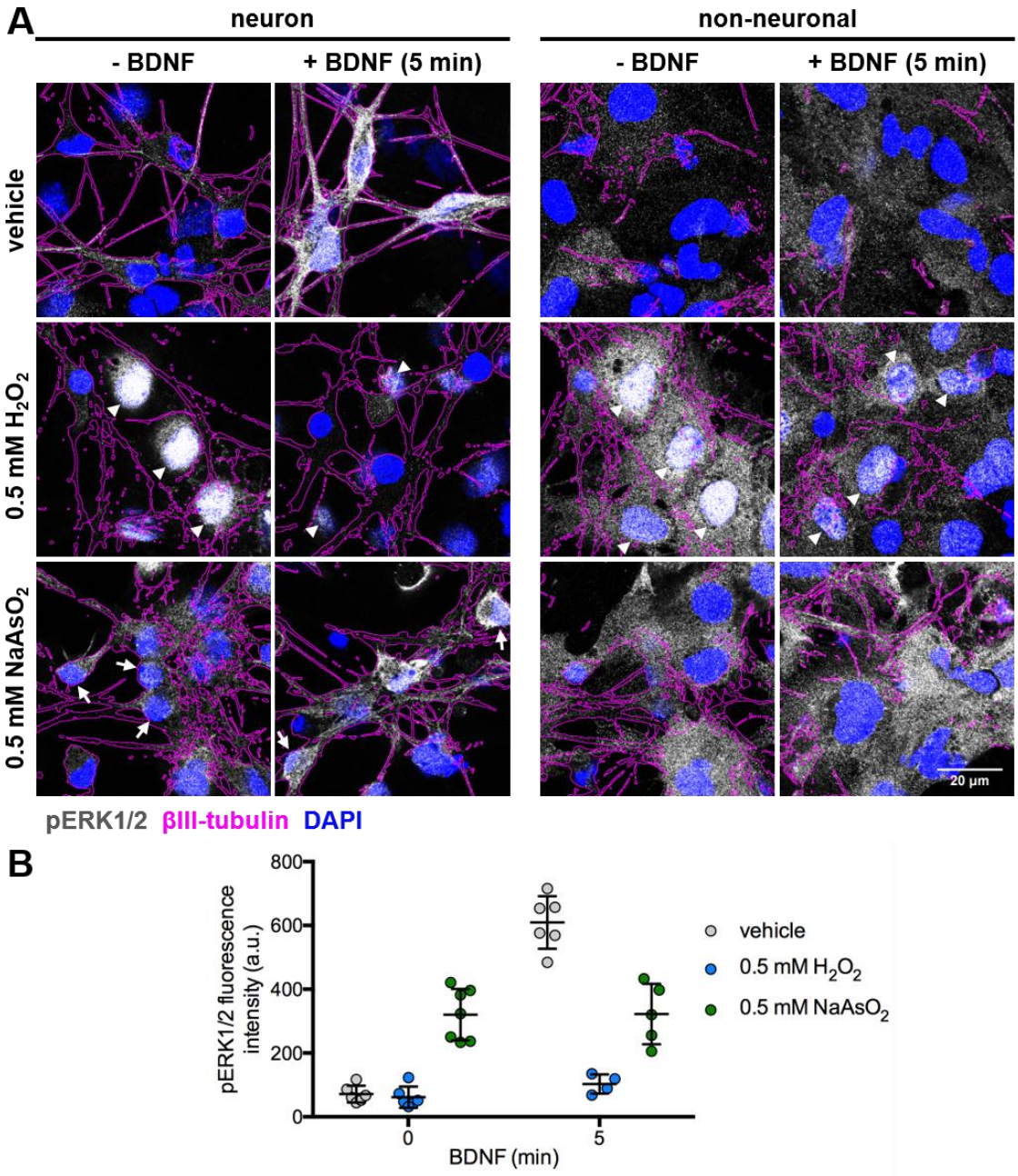

Figure 6.12 Oxidative stress affects the activation of pERK1/2.

A) pMNs were treated with vehicle, 0.5 mM hydrogen peroxide or 0.5 mM sodium arsenite, and stimulated for 5 min with or without BDNF. Next, cells were fixed, methanol-permeabilized and immunostained for pERK1/2 and βIII-tubulin (magenta outline). For each image of neuronal layer, a matching field along the Z-axis was imaged to capture the underlying non-neuronal cells, as shown in the examples. pERK nuclear staining could be observed in sodium arsenite-treated neurons (white arrows) and hydrogen peroxide-treated non-neuronal cells (white arrowheads). B) Quantification of pERK1/2 fluorescence intensity using βIII-tubulin as a mask for neurons. Between 4-7 fields were imaged per condition (n=1). All datapoints were plotted. Error bars show ±SD.

6.3 Discussion and future directions

Neurons have a very complex morphology and function, and their health relies on effective vesicular trafficking, tightly-regulated signalling and redox homeostasis. It is therefore not a surprise that these processes are implicated in age-dependent neurological disorders (Kruttgen et al., 2003; Bilsland et al., 2010; Fang et al., 2012; Wilson and González-Billault, 2015; De Vos and Hafezparast, 2017), although more research is required to understand how they precisely contribute to these diseases. The primary focus of this work was to assess the effect of oxidative stress on NTR accumulation and signalling in neuronal cells. Overall, in this chapter I demonstrated that acute oxidative stress reduced the sensitivity of neuronal cells and pMNs to BDNF stimulation, and selectively perturbed the trafficking of $p75^{NTR}$.

6.3.1 Oxidative stress selectively impairs NTR traffic

To study the effect of stress on retrograde trafficking, I utilized an anti-NTR antibody accumulation assay. In addition, CTB accumulation was employed as a measure of retrograde trafficking from the plasma membrane to the Golgi apparatus (Von Bartheld, 2004). I tested the effect of two commonly used oxidative stress inducers, sodium arsenite and hydrogen peroxide (Mahboubi and Stochaj, 2017), with the initial assumption that both stressors should have, if any, a similar effect on NTR trafficking. In addition, I assessed the cell type-specific differences, by performing the accumulation assays in the neuronal cell line N2A-FLAG-TrkB and in pMNs in culture. Using this approach, I demonstrated that oxidative stress led to a deficit in α-$p75^{NTR}$ accumulation, and partially perturbed CTB trafficking. The magnitude of this phenotype was dose dependent and differed for each stressor, and some aspects of the response was cell-type specific, since it was different between N2A-FLAG-TrkB cells and pMNs.

The perinuclear accumulation of α-$p75^{NTR}$ and CTB inversely correlated with the stressor concentration. This phenotype was comparable between N2A-FLAG-TrkB cells and pMNs when stress was elicited by sodium arsenite, but not by hydrogen peroxide (Figure 6.4; Figure 6.6; Figure 6.7). While sodium arsenite altered the morphology of N2A-FLAG-TrkB cells, I did not detect any significant changes in $p75^{NTR}$ levels at the plasma membrane (Figure 6.3A), suggesting that the loss of receptor accumulation was not due to its downregulation or lack of

trafficking to the plasma membrane. The most striking observation was the retention of internalized antibody-receptor complexes near the cell surface in N2A-FLAG-TrkB cells (Figure 6.5). At present, it is not known whether sodium arsenite induces retention of activated NTRs in pMNs, resulting in reduced somatic accumulation (Figure 6.6). Due to the massive branching of neuronal networks at DIV7, this phenotype could not be validated in cultured pMNs. As an alternative approach in future work, pMNs could be cultured in microfluidic devices (MFCs) (Park et al., 2006). Using hydrostatic pressure, MFCs allow the separation of somato-dendritic and axonal compartments. For our purpose, this would allow us to investigate the effect of somatically- or axonally-applied stress on receptor accumulation, and trafficking kinetics. Axon terminals are also easier to locate in MFCs than on coverslip. One would therefore be able to investigate the process of receptor retention, and the organization of the actin microfilaments at the active sites of endocytosis in stressed pMNs.

I demonstrated that sodium arsenite perturbed actin network organization in N2A-FLAG-TrkB cells (Figure 6.1B; Figure 6.3B) and non-neuronal cells (Figure 6.11C), which could plausibly underlie the observed deficits in NTR trafficking and signalling. Actin plays a role in early endocytic events, and is a target of redox imbalance (Wilson and González-Billault, 2015; Wilson et al., 2016), an important property of this cytoskeletal element, which drives cytokinesis (Frémont et al., 2017). Actin branching and networking is necessary for AKT localization to the plasma membrane in response to extracellular cues (Zhao et al., 2015). Furthermore, TrkA-endosomes directly associate with actin, and recruit Rac1 and cofilin to break down the actin network, allowing axon entry and retrograde transport of the signalling endosomes (Harrington et al., 2011). In addition, TrkA and TrkB associate with APPL1-early endosomes, which serve to facilitate the assembly of MAPK/AKT signalling platforms (Fu et al., 2011). Proper spatiotemporal association of APPL1-endosomes with the actin cortex, mediated by myosin VI, is also necessary for receptor-mediated propagation of downstream signalling, PI3K/AKT in particular (Masters et al., 2017). Similarly, PI3K activity is necessary for TrkA retrograde transport, but not its endocytosis (Yamashita and Kuruvilla, 2016). For these reasons, the role of actin in NTR accumulation and signalling in oxidative stress should be further investigated.

Hydrogen peroxide is a co-factor and natural by-product of many cellular processes (Lee et al., 2011; Costa et al., 2016), and plays an important role as an intracellular signalling molecule in neuronal regeneration (Duregotti et al., 2015; Negro et al., 2018). It is therefore more physiologically relevant than sodium arsenite, as it may elicit a redox imbalance in cells with high metabolic activity and compromised antioxidative capacity (Lennicke et al., 2015). However, because hydrogen peroxide treatment severely affected the structural integrity of pMNs (Figure 6.6), I was not able to investigate its effect on α-p75^{NTR} and CTB accumulation in these cells. While the observed neuronal membrane blebbing is often associated with caspase-mediated apoptosis (Wickman et al., 2013), it was not detected in this study (Figure 6.2B; Figure 6.3B; Figure 6.9C), although non-caspase cell death activation, and induction of JNK pathway by ROS, were not assessed. A hydrogen peroxide dose-response in pMNs should be re-evaluated, and its role in NTR biology further explored. Hydrogen peroxide was previously demonstrated to inhibit CNTF- and interferon-ɣ-mediated Jak/STAT1 signalling in neuronal cells (Kaur et al., 2005), and to inhibit endocytosis in yeast (Pereira et al., 2012). In addition, hydrogen peroxide facilitates ERK1/2-mediated imbalance in Ca^{2+} homeostasis, leading to cell death in cortical neurons (Numakawa et al., 2011).

Here, oxidative stress selectively perturbed NTR retrograde trafficking, demonstrated by the detection of perinuclear CTB in cells with membrane-retained α-p75^{NTR} (Figure 6.4; Figure 6.7). I speculated that the lack of α-p75^{NTR} perinuclear accumulation was not likely to be a consequence of defective retrograde traffic, because under the same stressed conditions I detected SGs (Figure 6.2A) – assembly of which relies on this transport machinery (Chernov et al., 2009; Perez-Pepe et al., 2018). A likely hypothesis for α-p75^{NTR} trafficking deficit was that SGs sequester molecular motors, making them unavailable for other types of transport. Although it was previously shown that mature SGs recruit the dynein motor complex (Loschi et al., 2009), our results contradict this hypothesis, for two main reasons: 1) I detected only mild reduction in CTB accumulation relative to α-p75^{NTR}, in spite of the fact that both transport mechanisms involved cytoplasmic dynein (Figure 6.4); 2) α-p75^{NTR} accumulation was only mildly reduced in cells treated with thapsigargin, in which SGs were comparable in size to oxidative stress-induced SGs (Figure 6.2A). In Chapter 5, I demonstrated that SGs also contain BICD1. In line with other work from our

laboratory (Terenzio et al., 2014a; Terenzio et al., 2014b), hypothetical depletion of BICD1 by SGs would more likely result in increased NTR accumulation, rather than perturbed trafficking, since degradation of α-$p75^{NTR}$ would have been prevented. Further work is necessary to understand the mechanism behind the selective downregulation of NTR trafficking, and its significance for neuronal health under oxidative stress conditions.

6.3.2 Oxidative stress hinders sensitivity to neurotrophins

Tight spatiotemporal regulation of AKT and ERK1/2 signalling amplitude and duration determines whether they will activate the survival or cell death cascade (Kaplan and Miller, 2000; Mebratu and Tesfaigzi, 2009). NTs, such as BDNF, which promote the pro-survival activation of AKT and ERK1/2 signalling (Kaplan and Miller, 2000; Yamashita and Kuruvilla, 2016), may regulate their own expression via a positive feedback-loop, and protect against ROS damage (Gardiner et al., 2009). Withdrawal of NT inputs has been shown to affect synaptic plasticity, induce ROS production and promote neuronal death (Gardiner et al., 2009). The modulation of AKT, ERK1/2 and other MAPK signalling pathways by oxidative stressors is well-documented (Carpenter et al., 2011; Hamann and Klotz, 2013; Lennicke et al., 2015; Rajesh et al., 2015). For this reason, the main purpose of this study was to assess the BDNF-mediated activation of these signalling cascades in pMNs and neuronal cells undergoing oxidative stress.

In N2A-FLAG-TrkB cells, hydrogen peroxide alone inhibited AKT and ERK1/2 phosphorylation (Figure 6.2B,C). On the other hand, sodium arsenite inhibited AKT, whilst it activated ERK1/2 in a dose-dependent manner (Figure 6.2B,C), suggesting that cells respond differently to these stressors. In addition, sodium arsenite abolished BDNF-mediated activation of AKT (Figure 6.1D-G). Unexpectedly, silencing of AKT and ERK1/2 activation in control N2A-FLAG-TrkB cells by serum-starvation proved problematic (Figure 6.2B,C), and I was not able to increase the number of repeats and quantitatively assess the effect of stress on BDNF stimulation. For this reason, pMNs seemed like a much more attractive, and physiologically-relevant, model.

Because the impact of hydrogen peroxide on pMNs was discussed above, I will focus here on the effect of sodium arsenite on BDNF signalling in pMNs, which is summarized in Figure 6.13. Unlike in N2A-FLAG-TrkB cells, sodium arsenite

alone induced mild phosphorylation of AKT and a significant activation of ERK1/2 in neurons and non-neuronal cells (Figure 6.8; Figure 6.11; Figure 6.12). Interestingly, while BDNF stimulation elicited normal phosphorylation of TrkB, downstream signal propagation was blocked by sodium arsenite (Figure 6.8), and signalling by BDNF was restored upon stress recovery (Figure 6.9C,D). Further work is necessary to better understand how sodium arsenite specifically blocks the signalling of activated TrkB. This could be pursued by analysing the activation of TrkB targets upstream of AKT and ERK1/2, and by assessing TrkB phosphorylation on other critical sites, such as the juxta-membrane Shc binding site (Stoilov et al., 2002).

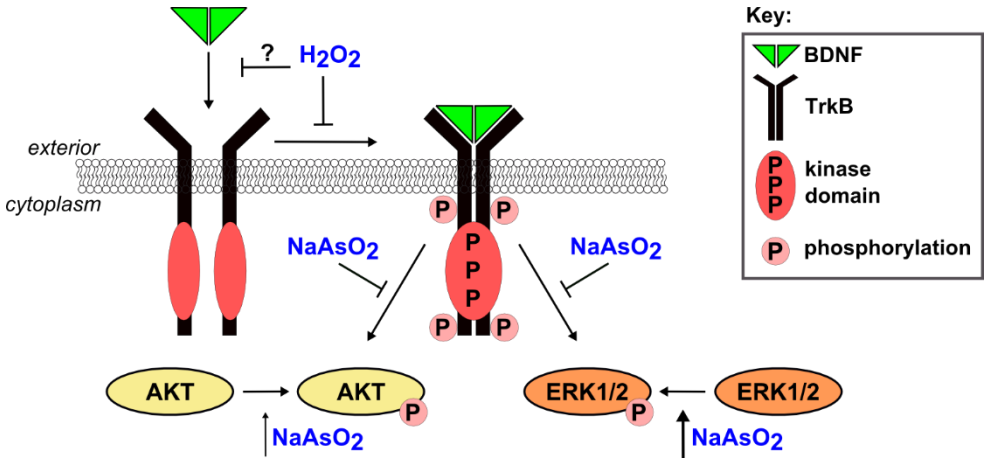

Figure 6.13 Oxidative stress perturbs TrkB signalling in pMNs.

Schematic representation of the interference of oxidative stressors with BDNF/TrkB signalling in neuronal cells. Binding of BDNF promotes TrkB dimerization, autophosphorylation and activation of downstream signalling kinase cascades, such as AKT and ERK1/2. While treatment with hydrogen peroxide (H_2O_2) inhibits TrkB phosphorylation, sodium arsenite acts downstream of TrkB, and inhibits activation of AKT and ERK1/2 in response to BDNF. At the same time however, increased AKT and ERK1/2 activation is detected in cells treated with sodium arsenite.

The localization of activated TrkB receptors in pMNs should also be assessed. Our findings from signalling (Figure 6.8) and trafficking (Figure 6.6) experiments in pMNs suggest that a phenotype similar to α-$p75^{NTR}$ membrane retention in N2A-FLAG-TrkB cells (Figure 6.5) might be observed in pMNs. Because of time constraints, I was not able to conduct a rescue experiment, such as with the use of antioxidants (Hou et al., 2014), or by pre-conditioning neurons with BDNF (Jiang et al., 2015).

6.3.3 Final conclusions

In summary, in this work I demonstrated that acute oxidative stress reduced the ability of neuronal cells to respond to NTs, by downregulating NT-mediated downstream signalling and retrograde trafficking. Given the timescale of this project, I was able to only partially explore this pathway. In addition to the experiments suggested above, it is necessary to increase the number of repeats to confirm observed trends, such as the decreased α-$p75^{NTR}$ accumulation in pMNs exposed to sodium arsenite.

7 Concluding remarks and future work

The work in this thesis brought together two seemingly unrelated topics – the neuronal neurotrophin (NT) signalling pathway and the integrated stress response (ISR). NTs play an instrumental role in the development of the nervous system (Oppenheim, 1996; Ascano et al., 2012). Therefore, appropriate spatiotemporal regulation of their signalling and trafficking is essential. These growth factors are also crucial to maintain neuronal health in the adulthood (Bronfman et al., 2007), as their withdrawal leads to the slow neuronal loss resembling that observed in neurodegeneration (Ruit et al., 1990; Xu et al., 2000). While NTs boost the antioxidative capacity of the nervous system, chronic exposure to oxidative stress may decrease the expression of NTs, further potentiating the reactive oxygen species (ROS)-induced damage (Gardiner et al., 2009). Due to high metabolic demands of the nervous system, neurons are particularly susceptible to oxidative and endoplasmic reticulum (ER) stresses during aging, which is associated with lower energy production and decreased antioxidant defence (Lin and Beal, 2006; Niedzielska et al., 2016). Perturbed trafficking, signalling, trophic support or aberrant stress granule (SG) dynamics, are strongly associated with devastating neurodegenerative diseases and cancer (Nakagawara, 2001; Bronfman et al., 2007; Anderson et al., 2015; Khotskaya et al., 2017; Khalil et al., 2018). To increase the chances of finding new promising therapeutic targets, it is essential that researchers continue to investigate how these processes are regulated in healthy and pathological conditions.

In this work, I attempted to further the understanding of the molecular machinery mediating the turnover of NTRs, as well as the regulation of this pathway in neurons undergoing stress. In addition, I explored the role of BICD1 and PTPN23 in the stress response. The key findings presented in this thesis, and future directions are summarized below.

7.1 The unusual relationship of PTPN23 with BICD1

Following the previous findings of our laboratory (Terenzio et al., 2014a; Terenzio et al., 2014b), the main aim of the work described in the first experimental chapter was to characterize the relationship between BICD1 and PTPN23. Using co-immunoprecipitations (Figure 3.1), and *in vitro* pull down assays, I demonstrated

that these proteins bind directly (Figure 3.8). Confocal microscopy indicated that this interaction is most likely to occur in the perinuclear region of neuronal cells (Figure 3.2; 3.3; 3.6), which is a sorting hub for transported cargo, abundant in organelles such as multivesicular bodies (MVBs), lysosomes and the Golgi apparatus (Huotari and Helenius, 2011).

In vitro binding assays revealed an unexpected relationship between BICD1 and PTPN23 (Figure 3.5). Previous reports strongly suggest that the N-terminal coiled coil 1 (CC1) of BICD1 mediates the interaction with the dynein complex, whilst its C-terminal CC3 binds cargoes (Hoogenraad and Akhmanova, 2016). Here, the binding of PTPN23 to CC1 (amino acids 95-265), rather than CC3, was uncovered (Figure 3.5). This finding suggests that: 1) PTPN23 does not have the ability to release the autoinhibition state of BICD1, which is achieved through the binding of a cargo to CC3 (Terawaki et al., 2015); 2) the interaction between BICD1 and PTPN23, similarly to dynein, may be possible only upon prior release of the BICD1 autoinhibition state by the CC3-cargo interaction (Liu et al., 2013); 3) PTPN23 and dynein may compete for the interaction with BICD1, potentially explaining the low level of co-localization between BICD1 and PTPN23; 4) BICD1-PTPN23 binding may promote the association between the ESCRT and trafficking machineries, necessary for cargo transport to MVBs and lysosomes (Reck-Peterson et al., 2018). In the future, it will be necessary to determine which cargos enable the BICD1-PTPN23 interaction, and the relationship of the BICD1-PTPN23 complex with cytoplasmic dynein. This would help to understand not only how this machinery operates in cargo sorting, but could also shed new light on the potential regulatory role of PTPN23 on the BICD1-dynein complex.

In the first experimental chapter, the established PTPN23-binding region on BICD1 is a fragment of CC1 (amino acids 95-265), spanning 170 amino acids (Figure 3.5). To further narrow down the interaction region between these two proteins, a synthetic peptide microarray would be a good place to start (Volkmer et al., 2012). It could be followed up with site-directed mutagenesis, to establish the critical residues required for the interaction with PTPN23. Similarly, mutagenesis of known cargo binding sites on CC3 of BICD1 (Terawaki et al., 2015) might potentially reveal whether cargo binding is necessary for the BICD1-PTPN23 interaction to occur. Similarly, the association of BICD1 with the V/CC

domain of PTPN23 has to be validated (Figure 3.8; 3.9) and could be explored further using the approaches mentioned above.

A neglected area of BICD1 biology is its potential association with kinesin motors. Interestingly, the kinesin-associated proteins, Unc33 and kinectin, were identified in the BICD1 interactome (Appendix 1). To better understand the function of this dynein adaptor in diverse trafficking events, it would be important to establish whether it associates with anterograde motors, as previously demonstrated for BICD2, BICDR1 and dBicD (Larsen et al., 2008; Splinter et al., 2010; Schlager et al., 2010). The hypothesis that BICD1 might bind kinesins is partially supported by the observation that mutant GFP-BICD1$^{\Delta 95\text{-}265}$ accumulated in the cell periphery with Rab6-positive vesicles and displayed a dominant-negative-like behaviour (Figure 3.7), similar to the previous report of BICD2-CC3 overexpression (Matanis et al., 2002). Past studies highlighted the fact that the interaction of BICD proteins with a kinesin may not be easily detectable, and may depend on cellular context, such as during a particular developmental stage or cell cycle (Larsen et al., 2008; Splinter et al., 2010; Schlager et al., 2010). In addition, a high-affinity interaction between dynein and CC1 of BICD1 may mask its potential association with kinesin motors. Upon validation of its association with the dynein complex (Matanis et al., 2002), the mutant construct, GFP-BICD1$^{\Delta 95\text{-}265}$, could be utilized to explore the hypothetical interaction of BICD1 with anterograde motors, which BICD2 binds via its middle CC2. Taken together, the findings summarised in the first experimental chapter suggest that the current model of BICD1 function is simplistic, and it should be reviewed in future studies to further our understanding of BICD1 biology.

7.2 PTPN23 is necessary for the endocytic sorting of NTRs

To date, very little is known about the function of PTPN23 in the mammalian nervous system (Toyooka et al., 2000). In non-neuronal cells, PTPN23 is essential for sorting of transmembrane proteins, such as EGFR (Doyotte et al., 2008), PDGFR (Ma et al., 2015), α5β1 integrin (Kharitidi et al., 2015) and MHC class-I (Parkinson et al., 2015). By knocking down PTPN23, these studies unanimously reported increased accumulation of ubiquitinated transmembrane proteins in early endosomes and increased receptor recycling, demonstrating

that PTPN23 is necessary for MVB-sorting and lysosomal degradation of ligand-activated signalling receptors and other membrane proteins.

In the second experimental chapter, I aimed to investigate the role of PTPN23 in NTR turnover in neurons, using anti-NTR receptor antibody accumulation assays. Indeed, I observed that PTPN23 co-labels with internalized α-TrkB (Figure 4.2), suggesting that PTPN23 associates with retrograde signalling endosomes carrying NTRs. In line with studies above, silencing PTPN23 expression by shRNA resulted in increased accumulation of α-FLAG-TrkB and α-$p75^{NTR}$ in aberrant vacuoles (Figure 4.4; 4.11). Electron microscopy revealed that the α-$p75^{NTR}$-gold-containing vacuoles have features of swollen endosomes (Figure 4.13), whilst immunostaining and confocal microscopy showed co-labelling of these compartments with the markers of the early endosome (EEA1), late endosome (Rab7) and ubiquitin (Figure 4.14; 4.15). Therefore, PTPN23 appears essential for the maturation and endocytic flow of NTR-containing endosomes in neuronal cells. Findings of this chapter correlated well with the increased accumulation of ubiquitinated NTRs, which was reported upon BICD1 knockdown (Terenzio et al., 2014a).

Further work is necessary to fully explore the identity of NTR-containing vacuoles, as well as the effect of PTPN23 depletion on receptor recycling and signalling, which was not addressed in this study. This would allow one to establish how the PTPN23 knockdown phenotype correlates with the downregulation of BICD1, and with other studies reporting PTPN23 function. Silencing of PTPN23 expression led to the accumulation of ubiquitin on vacuoles (Figure 4.15), suggesting that PTPN23 knockdown models could be a useful tool to investigate the role of this post-translational modification in the regulation of NTR function (Sanchez-Sanchez and Arevalo, 2017).

I was not able to conduct initially planned receptor recycling and signalling experiments because of shRNA2 toxicity (Figure 4.8). A significant proportion of time was spent optimising the accumulation assays using an anti-FLAG antibody and shRNA2, as well as generation of an shRNA-resistant plasmid. As a result, experiments using anti-$p75^{NTR}$ antibody and shRNA1 had to be re-optimized. The best outcome of this was the identification of a potential interaction node between BICD1, PTPN23 and the NTR scaffold Kidins220 (Figure 4.6), further placing BICD1 and PTPN23 in relation to the NT pathway.

Regrettably, I was also not able to study the function of PTPN23 in embryonic stem cell-derived motor neurons (ES-MN; Figure 4.3E), which was one of the aims of this work. Detachment of these cells from the surface of glass coverslips made it challenging to reliably conduct antibody accumulation and signalling assays. In the future, the role of PTPN23 could be investigated using an alternative culturing approach, such as in microfluidic chambers, which might prevent neuronal detachment and would serve as a better, compartmentalized platform to study receptor trafficking and sorting in neurons (Park et al., 2006).

Because of the relationship between BICD1 and PTPN23 (Chapter 3), as well as the similar phenotypes of receptor accumulation upon their downregulation (Chapter 4; Terenzio et al., 2014a), it would be interesting to determine whether BICD1 is also necessary for the endocytic flow of transmembrane receptors, the sorting of which is regulated by PTPN23. Initially, it should be established whether BICD1 plays a role in lysosomal degradation of EGFR (Doyotte et al., 2008).

7.3 BICD1 is a novel SG component, instrumental for ISR

Environmental stresses elicit the activation of the integrated stress response (ISR), which results in the stall of translational machinery and formation of stress granules (SG) (Protter and Parker, 2016). SGs are large protein-RNA assemblies, often described as membrane-less organelles. BICD1 is one of the factors necessary for SG assembly in response to oxidative and endoplasmic reticulum (ER) stresses (Loschi et al., 2009). Lack of SGs in response to stress sensitizes cells and activates premature apoptosis (Tsai and Wei, 2010; Zou et al., 2011), suggesting that BICD1 is an important player in cell survival. As its targeting to these organelles was not reported to date, the third aim of my thesis was to characterize the association of BICD1 with SGs.

The effect of oxidative and ER stresses on subcellular distribution of BICD1 in N2A-FLAG-TrkB cells and primary motor neurons (pMN) was remarkable (Figure 5.2-5.5). Not only did BICD1 associate with SGs throughout the time course of their formation and disassembly in cells (Figure 5.6, 5.7), BICD1 also significantly co-clustered with the Golgi apparatus proteins Rab6 and GM130 (Figure 5.8). In this work, I demonstrated a Rab6-independent role of BICD1, as this small GTPase was not recruited to SGs. The perturbed Golgi apparatus morphology upon cellular stress, and the increased accumulation of BICD1 and Rab6,

strongly suggests that membrane trafficking events might be compromised during cellular stress. Therefore, it would be important to assess the effect of stress on the transport pathways regulated by BICD1, in particular the Golgi-to-ER route of Rab6-positive vesicles (Matanis et al., 2002; Wanschers et al., 2007).

The mechanism of BICD1 recruitment, and its exact role during stress responses, is not fully understood. As a starting point, its relationship with SG nucleating factors should be investigated (Anderson and Kedersha, 2008). Scrutinizing FMRP would be a good starting point, since *Drosophila* BicD regulates the expression and transport of this RNA-binding protein (Bianco et al., 2010). At present, it is also not known whether BICD1 actively participates in SG disassembly, or whether it is simply retained in SGs until their clearance (Figure 5.7). Deciphering this mechanism, as well as BICD1 dynamics within SGs, would be crucial to understand its role in ISR.

The second aim of this experimental chapter was to establish whether PTPN23 plays a role in SG dynamics. The data presented in this thesis strongly implies that PTPN23 is not a component of these membrane-less organelles (Figure 5.13), and it does not influence their formation (Figure 5.14). However, its potential association with SGs during stress recovery, or the effect of PTPN23 silencing on SG disassembly, was not investigated. PTPN23 is known to interact with SG proteins involved in SG clearance, such as focal adhesion kinase (FAK) (Castiglioni et al., 2007; Tsai et al., 2008); it would therefore be important to assess whether it plays a role in this process.

Understanding SG biology is of great importance for neurodegeneration and cancer research (Wolozin, 2012; Anderson et al., 2015). Cytoplasmic inclusions containing several SG-related proteins are a histopathological hallmark of diseases such as amyotrophic lateral sclerosis (ALS) (Li et al., 2013). In addition, mutations in several ALS-related genes encode RNA-binding proteins associated with SGs, most notably C9orf72, TDP-43 and FUS, which strongly suggests that de-regulation of SGs dynamics contributes to disease pathogenesis (Li et al., 2013). The pathophysiology of ALS is highly complex, which together with its rapid progression (death usually within 3-5 years from diagnosis), makes this disease extremely difficult to target (Kiernan et al., 2011). Because SGs have been so tightly correlated with ALS, it is essential to continue to study the biology

of SGs as well as the impact of ISR activation on diverse cellular processes in neurons.

Hyper-regulation of SG dynamics is also strongly associated with tumors. Cancer cells utilize ISR as a protective mechanism against a number of chemotherapeutic agents, which led to a hypothesis that downregulating ISR and targeting SG-related proteins might have a beneficial effect on cancer treatments (Anderson et al., 2015).

7.4 NTR pathway is downregulated by oxidative stress

Components of the trafficking machinery play an essential role in protecting cells from environmental stress (Loschi et al., 2009; Tsai et al., 2009). Direct targeting of cytoplasmic dynein (Loschi et al., 2009) and BICD1 (Chapter 5) to SGs, as well as perturbed morphology of the Golgi apparatus (Figure 5.8), strongly implies that cellular transport might be affected during stress. As NT support is essential for neuronal health, and it promotes the antioxidative capacity of the nervous system, the final aim of this thesis was to explore the effect of oxidative stress on the NT pathway.

As knockdown of BICD1 leads to defective sorting of NTRs, causing them to accumulate in the neuronal soma (Terenzio et al., 2014a), I hypothesized that a similar phenotype might be observed in neurons during oxidative stress. However, antibody accumulation and signalling assays revealed a remarkable downregulation of NTR transport (Figure 6.1; 6.2; 6.4; 6.6; 6.7) and signalling in response to BDNF stimulation (Figure 6.1; 6.2; 6.8) under these conditions. Crucially, sodium arsenite appeared to differently affect AKT and ERK1/2 signalling in N2A-FLAG-TrkB cells and pMNs, therefore highlighting that motor neurons and mitotic cells respond differently to stress.

Several experiments in Chapter 6 were preliminary and require further validation, yet I provided solid evidence that activation of ISR by oxidative stress leads to downregulation of the NT pathway in neurons. The decrease in transport of α-$p75^{NTR}$, but not of cholera toxin subunit B (CTB; Figure 6.4; 6.7), which share a common retrograde trafficking route (Schmieg et al., 2014), is puzzling. This finding suggests that the effect of oxidative stress on NTR transport is selective, may affect other transmembrane receptors and differentially regulates the

ganglioside transport route to the Golgi apparatus. It also highlights that multiple probes, rather than e.g. CTB alone, should be used to monitor membrane trafficking from the plasma membrane to study the effects of stress.

While oxidative stress downregulated transport and perinuclear accumulation of α-$p75^{NTR}$, this receptor was essentially "trapped" near the cell surface in stressed N2A-FLAG-TrkB cells (Figure 6.4; 6.5). Similarly, sodium arsenite downregulated α-$p75^{NTR}$ trafficking in pMNs in a dose-dependent manner (Figure 6.6; 6.7). Although transport of α-$p75^{NTR}$ was largely reduced by sodium arsenite in pMNs (Figure 6.6; 6.7), unperturbed BDNF-dependent phosphorylation of TrkB, but not of the downstream signalling kinases, was observed (Figure 6.8). Therefore, localization of BDNF-TrkB should be examined in pMNs treated with sodium arsenite.

As only acute oxidative stress conditions were tested in this study, further assessment of the effects of chronic stress should be evaluated, as well as the long-term consequence of NT withdrawal under stress conditions. In addition, the effect of oxidative stress on signalling and transport of similar receptors should be cross-examined in MNs, because, presently, research within this area is largely focused on disease-related models. Interestingly, a TrkB trafficking deficit was previously reported in the mouse model of ALS carrying a human mutated superoxide dismutase 1 ($SOD1^{G93A}$) (Bilsland et al., 2010), which has been strongly linked to ROS damage (Ferrante et al., 1997). As oxidative stress plays an important role in the pathogenesis of neurodegenerative diseases (Barber et al., 2006), and the idea of using neurotrophins as therapy in ALS has largely failed (Federici and Boulis, 2012; Numakawa et al., 2011), it is important to continue to decipher how neurons respond and adapt to stresses and how different biological processes are regulated in these conditions.

7.5 Summary

NTs play an important role in the lifecycle of a neuron and have been of interest to scientist for many decades. The signalling elicited by these growth factors, and transport of their receptors, is relatively well-characterized. However, the molecular mechanisms regulating the turnover of NTRs, as well as the effect of pathological conditions on this pathway, are not completely understood. In addition, several processes related to cargo transport and NT signalling are

implicated in neurological disorders; it is therefore crucial to try to further determine how these processes are regulated, in order to understand the consequences of their malfunction. Using a range of biochemical approaches, the work in this thesis characterises a novel interaction between BICD1 and PTPN23, both of which mediate the sorting of NTRs. These findings may provide some new clues in uncovering the general mechanisms of cargo turnover. In addition, BICD1 was characterized as a neuronal SG component, thereby making a contribution to research focusing on decrypting the dynamics and function of these enigmatic organelles. Results presented in this thesis support the new role of BICD1 in neuronal survival. Lastly, the downregulation of the NT pathway by oxidative stress was reported herein, furthering our understanding of the role of stress on fundamental biological processes.

8 Appendix 1 – Mass spectrometry data

Mass spectrometry was performed to identify proteins co-immunoprecipitated with BICD1 (anti-BICD1 antibody, #HPA041309, Atlas Antibodies) from cell lysates of serum-starved and BDNF stimulated (15 min, 100 ng/ml) N2A cells (MNP5731) and ES-MNs (MNP5753). Scaffold and Perseus analyses were then performed to identify statistically significant proteins. Scaffold analysis allows the identification of proteins and peptides in a semi-quantitative manner. Here, it is represented as a function of BDNF stimulation. Perseus analysis verifies the significance of a selected dataset. A brief description of protein function and gene ontology (GO) is included.

The dataset attached below contains a list of significant hits only, split into following sections. The first section contains proteins previously identified as BICD1-binding partners, followed by a list of novel, previously unreported BICD1-interacting candidates. Lastly, unenriched proteins as well as proteins common in BICD1 and RAB7 pull downs are listed. Proteins identified in N2A but not in ES-MNs are coloured in green. Proteins in grey were identified in N2A cells by the Scaffold analysis, but were not verified by Perseus.

Drs. Matthew Golding and Ambrosius P. Snijders (unpublished results) performed co-IPs and mass spectrometry analyses.

MNP5731 Endogenous BICD1 immunoprecipitation from N2A cells transfected with FLAG-TrkB +/- stimulation for 15 min Scaffold analysis + Perseus Analysis

MNP5753 Endogenous BICD1 immunoprecipitation from ES-derived MN +/- stimulation for 15 min Scaffold analysis + Perseus Analysis

KNOWN PARTNERS

Gene	Ratio (-/+ BDNF) 5731	5753	Perseus	Description	GO
BICD2	12:11	5:4		Heterodimer formation? The antibody used is BICD1-specific.	
Dynein heavy chain	21:8	-		Direct interaction with p50/dynamitin and DIC.	Motor protein
Fragile X protein	2:2	-		Known binding partner of BICD in Drosophila.	RNA transport

NOVEL PARTNERS

Gene	Ratio (-/+ BDNF) 5731	5753	Perseus	Description	GO
Ptpn23/HD-PTP	7:2	4:10		Tyrosine-protein phosphatase non-receptor type 23. Endosomal cargo sorting/MBV Depletion of HD-PTP reduces transfer of EGFR to lysosomes, causes the accumulation of Ub proteins on endosomes and disrupts MVB morphogenesis PNAS 2008 105:6308-13. Interacts with CHMP4A-C, Vps26A, LRKK2 and GRB2, which is an adapter for phosphorylated receptors, including EGFR and Trks (TrkA). Phenocopies BICD1 knockdown.	Phosphatase
Ubash3b	0.5:1	0:1		Tyrosine-protein phosphatase STS1/TULA2. Complex with CBL and activated EGFR.	Phosphatase
Ptpn13	-	0:3		Tyrosine-protein phosphatase non-receptor type 13 (RIP, PTP-BL). It negatively regulates NGFR (p75) -mediated pro-apoptotic signalling, Ephrin signalling and FAS-induced apoptosis.	Phosphatase
Ppp1r12A/Mytp1	1:2	0:1		Phosphatase regulator of PPP1C. It mediates the binding to myosin. Phosphorylated by Cit.	Phosphatase
Ppp1r12C	-	0:1		Phosphatase regulator of PPP1C.	Phosphatase
CRMP2/Dpysl2/ULIP2	-	0:4		Also known as Unc33-like protein. Axonal growth.	Differentiation
CRMP4/Dpysl3/ULIP1	3:5	0:1		Also known as Unc33. Axonal growth. Mutations cause neurodegeneration. Binds to kinesins	Traffic
PlexinA	0:1	2:5		Signaling by semaphorins and remodeling of the cytoskeleton. Axon guidance and cell migration. Binds to CRMP2/Dpysl2/ULIP2 and CRMP4/Dpysl3/ULIP1	Differentiation
Ankrd17/GTAR	3:9	5:7		It is involved in vascular maturation. NFkB pathway	Tissue biogen.
Ccdc88c/Daple	-	8:13		Negative regulator of Wnt signalling	Signalling
TARA	-	1:2		TRIO and F-actin-binding protein	Cytoskeleton
Nup153	10:13	16:22		Nuclear pore	Nuclear pore

PRRC2C	9:17	6:7		?	?
MON1B	0:2	-		Part of the GEF complex for Rab7 with CCZ1; membrane recruitment of Rab7	Rab effectors
APP binding protein	2:4	-		APP trafficking and intracellular targeting	Traffic
Secretogranin	0:2	-		Secreted cargo	Traffic
Wdr62	2:4	-		WD repeat protein 62. Cortical development. Its mutations cause primary microcephaly	Centrosome
				JNK scaffold protein; stress granule	
Dmx-like protein 2	0:2	-		Rab connectin 3 interacts with RAb3A GAP on synaptic vesicles and with the Rab3GEF MADD. MADD activates ERK. Dmx-like protein 2 knockdown abolishes Notch signalling.	Rab effectors
Liprin 1beta1	1:4	-		Tyrosine-protein phosphatase receptor. It interacts with kinesin motors.	
Phosphatase/Traffic					
GORS1/GRS2	1:2	-		Involved in stacking Golgi cisternae	Traffic
Ccdc46/Macoco	0:2	-		It interacts with GABA-A receptor and Maf1 (Kittler, UCL)	Traffic
AHNAK/desmoyokin	0:3	-		Enlargeosome marker. This organelle contributes to NGF-dependent neurite outgrowth	Traffic

Unregulated/enriched in unstimulated sample (-BDNF)

Gene	Ratio (-/+ BDNF) 5731	5753	Perseus	Description	GO
JRAB/MICALL2	14:16	3:1		Rab13 and Rab8 binding protein. Actin remodelling. Role in neurite outgrowth	Rab effectors
Sec31A	22:26	34:28		COP II component ER to Golgi transport. Interacts with Sec13; Sec31B as well	Traffic
Sec13	1:2	2:2		COP II component ER to Golgi transport. Interacts with Sec13	Traffic
Kinectin	-	3:0		Kinesin binding protein	Traffic
Granulin	4:3	4:5		Secreted cargo	Traffic
Nidogen1	-	1:1		Secreted cargo	Traffic
Etl4	-	21:22		Sickle tail protein. Expressed in the notochord and other tissues.	Development
BCAR1/Cas	5:6	15:14		Docking protein in RTK signalling in cell adhesion. It interacts with Crk	Signalling
NipSnap homolog 1	5:6	3:4		L channel activation. Required for CREB activation	Signalling
NipSnap homolog 2	3:2	1:1		L channel activation. Required for CREB activation	Signalling
Pawr	2:1	2:2		PRKC apoptosis WT1 regulator protein; cell death promoting actions in motor neurons	Apoptosis
NAV1	12:15	2:2		Neural navigator 1; associated at MT plus ends; see ckap5	Cytoskeleton
Anillin	13:17	3:2		Actin binding protein	Cytoskeleton
Nckipsd	10:8	12:15		NCK-interacting protein with SH3 domain, WASBP; actin dynamics	Cytoskeleton
ARHG1	2:1	8:10		RhoGEF	Cytoskeleton
ARHG2	11:18	5:2		RhoGEF	Cytoskeleton
Arhgef26	-	18:12		RhoGEF	Cytoskeleton
Arhgap21	2:1	10:8		RhoGAP	Cytoskeleton

Srgap3	**-**	22:21		SLIT-ROBO Rho GTPase-activating protein 3	Cytoskeleton
Drebrin	**-**	8:7		actin regulation; neurite outgrowth	Cytoskeleton
Sacsin	0:1	19:17		DnaJ homolog subfamily C member 29 (DNAJC29). Mutations causes spastic ataxia of Charlevoix-Saguenay (ARSACS), a neurodegenerative disorder with spasticity and peripheral neuropathy	Chaperone
Synaptopodin2	6:3	3:6		It has an actin-binding and actin-bundling activity	Cytoskeleton
Znf512b	2:1	6:4		Prognostic factor in patients with ALS; TGF beta	?
HDAC	3:3	0:1		Histone deacetylase 4; muscle differentiation	
PRRC2B	13:11	3:2		?	?
PRRC2A	2:3	-		?	?
GAPVD1/GAPex-5	6:9	-		Rab5 activating protein 6; contains both GAP and GEF activities for Rab5 and 31. Involved in EGFR trafficking and degradation.	Rab effectors
Liprin 1beta2	12:12	-		LAR-interacting protein family	Phosphatase/Traffic
Dynamin-1	20:26	-		Pinching off of vesicles on plasma and internal membranes	Traffic
Synaptojanin-1	2:1	-		Clathrin-dependent endocytosis; clathrin release	Traffic
Mia1/Tango1	4:5	-		Cargo loading at ER exit sites by binding to COPII coat subunits (only in - BDNF Perseus)	Traffic
Tmem138	1:1	**-**		Ciliogenesis; vacuolar membrane	Cilia/Traffic
Tmem237/Als2cr4	3:2	**-**		Ciliogenesis; mutated in Joubert syndrome related disorder	Cilia/Traffic
Ccdc21/Cep85	6:8	-		Centrosome	Centrosome
Arhgef18/ARGI	9:6	-		RhoAGEF	Cytoskeleton
Cit	8:4			Citron Rho-interacting kinase	Cytoskeleton
Ckap5	2:1			Binds to the plus end of MT and regulates MT dynamics and organization	Cytoskeleton
Rab8	3:2	-		Membrane traffic	Rab / Rab effectors

Proteins in common Rab7 pY183/Y183 pull down and BICD1 pull down

Dynamin 1
Synaptojanin
Dynein HC
PTPN23 (Vps26 in Rab7)

9 Appendix 2 – Materials list

9.1 Primers used for FastCloning and sequencing

Target	Primer name	Sequence (5' -> 3')
pET28a+	FWstop	TGAGATCCGGCTGCTAAC
	REVcleav	CATATGGCTGCCGCG
pGEX-4T-1	FWstop	TGACTGACTGACGATCTGCC
	REVcleav	GGATCCACGCGGAACC
dsRed2N1	FW	CGAATTCTGCAGTCGACG
	REV	AAGCTTGAGCTCGAGATCTGAG
pEGFPC1	FWstop	TAACTGATCATAATCAGCCATACCAC
	REV	AGCTTGAGCTCGAGATCTGAGTC
PTPN23 for pET28a+ FastCloning	BroFW1	**CGCGGCAGCCATATG**ATGGAGGCCGTGCC
	BroFW8	**CGCGGCAGCCATATG**CCCATGATCTGGCTGGAC
	Tpr1/2FW250	**CGCGGCAGCCATATG**GCCGTGGCTCATCTGC
	BroREV394	**TTAGCAGCCGGATCTCA**CAGGACCTCATTCTTGTCC
	BroREV407	**TTAGCAGCCGGATCTCA**CGTCTCGGGATCCAACTG
	V/CCFW401	**CGCGGCAGCCATATG**ATGCAGTTGGATCCCGAG
	V/CCREV653	**TTAGCAGCCGGATCTCA**GGAGTTCCACTTTTGGTCC
	V/CCREV700	**TTAGCAGCCGGATCTCA**GCGGGCCTGGCAGG
	PR/HDFW703	**CCGCGCAGCCATATG**GCCCGCCAGCAGCTC
	PR/HDFW705	**CGCGGCAGCCATATG**CAGCAGCTCCTGGACAG
	PR/HDREV1134	**TTAGCAGCCGGATCTCA**AGGAGACTGAGTGCCGC
	PTPFW1188	**CCGCGCAGCCATATG**GTGGGAGCTCTGGACACTG
	PTPREV1452	**TTAGCAGCCGGATCTCA**GTGTCTCACCACTGCCTCATAG
	PTPREV1475	**TTAGCAGCCGGATCTCA**GCTGATGCTTGCACTGG
	PESTREV1636	**TTAGCAGCCGGATCTCA**TCAGGTCTTGTTGAGTGTCC
BICD1 for pGEX-4T-1 FastCloning	CC1FWHA1	**GTTCCGCGTGGATCC**TACCCATACGATGTTCCAGATTAC
	CC1FW1	**GTTCCGCGTGGATCC**ATGGCCGCAGAAGAGGTATTG
	CC1REV94	**GCAGATCGTCAGTCAG*TCA***AAGCGTTTCCTCCCGAGT
	CC1FW95	**GTTCCGCGTGGATCC**CTGCAGGAGTCAGCATCG
	CC1REV265	**GCAGATCGTCAGTCAG*TCA***GATGCTGATATGGTTATCATTGAG

	CC1REV276	**GCAGATCGTCAGTCAG*TCA***CCCATCCTCGGCAAATT TG
	CC1REV300	**GCAGATCGTCAGTCAG*TCA***ATAGTCTCCATTCAGTTT CACAAGAGG
	CC2FW314	**GTTCCGCGTGGATCC**GTCTCTGACTTATTCAGTGAGC TG
	CC2REV500	**GCAGATCGTCAGTCAG*TCA***GGTACTGTGATTTTCGTT GGC
	CC3FW662	**GTTCCGCGTGGATCC**ATGATTGATAAAGACAAGGAAG CC
	CC3REV808	**GCAGATCGTCAGTCAG*TCA***TTTGCTGCGTCGGGAC
	Sequencing	CCATGACTATGAGGTGGAC
PTPN23 for dsRed2-N1 FastCloning	FW8	**GATCTCGAGCTCAAGCTT**CCCATGATCTGGCTGGAC
	REV407	**GTCGACTGCAGAATTCG**CGTCTCGGGATCCAACTG
	REV653	**GTCGACTGCAGAATTCG**GGAGTTCCACTTTTGGTCC
	FW401	**GATCTCGAGCTCAAGCTTATG**CAGTTGGATCCCGAG
	REV712	**GTCGACTGCAGAATTCG**CAGCTCCCTGTCCAGGAG
	FW705	**GATCTCGAGCTCAAGCTTATG**CAGCAGCTCCTGGAC AG
	FW1188	**GATCTCGAGCTCAAGCTTATG**GTGGGAGCTCTGGAC ACTG
	REV1475	**GTCGACTGCAGAATTCG**GCTGATGCTTGCACTGG
	FW1452	**GATCTCGAGCTCAAGCTTATG**CACGTGGAGCAGGTC CTG
	REV1636	**GTCGACTGCAGAATTCG**GGTCTTGTTGAGTGTCCAG AGTG
BICD1 for pEGFPC1 FastCloning	FWd265	GGAAGTGATATCGGAAGT**TCAGTAGATGGACTCAAA TTTGC**
	REVd95	ACTTCCGATATCACTTCC**AAGCGTTTCCTCCCGAGTC**
	REVd1	ACTTCCGATATCACTTCC**AGCTTGAGCTCGAGATCTG AGTC**
	FW95	TCTCGAGCTCAAGCT**CTGCAGGAGTCAGCATCG**
	REV265	GATTATGATCAGTTA**GATGCTGATATGGTTATCATTG AG**
PTPN23 TCTC<CTT G mutagenesis (QuickChang e)	forward	ACGAGCAGGCCTGTATCCTGTACAACCTTGGAGCG
	reverse	CGCTCCAAGGTTGTACAGGATACAGGCCTGCTCGT
BRO$^{8-407}$ TCTC<CCT G-dsRed2N1	FW	**ACACTCAACAAGACC**CGAATTCTGCAGTCGACG
	REV	**ATCAAGGTTGTCCAC**CGTCTCGGGATCCAACTG
PTPN23 FL for mutant	FW408	GTGGACAACCTTGATGCCTACA
	REV1636	GGTCTTGTTGAGTGTCCAGAG

dsRed2N1 FastCloning		
PTPN23 sequencing primers	19-36FW	ATGCCCATGATCTGGCTG
	421-403REV	TCATGCCCTCCTCAGACAC
	482-465REV	AAGTGCTCCCGTAGGTAG
	533-514REV	ACGTTGAGCGTAAGGATCTG
	506-524FW	TGAGCCGCCAGATCCTTAC
	1016-1035FW	TGAAGCCCTTGCCAGTGAAC
	1523-1543FW	CCTCCTTCACCAACAGTGAGC
	2001-2022FW	CCTGATGAAGAAGTCGCAGGAG
	2527-2547FW	GTGGTGAGCAGTCCCTATGTG
	3038-3057FW	CCCTACACACCCAGCTCTAC
	3567-3584FW	AGCTCTGGACACTGTCTG
	4007-4025FW	TGCAGTTCCGAGACCAGAG
	4500-4517FW	CACCATTGCCAAGCTCAG
	4892-4910FW	GGACACTCAACAAGACCTG

Bold – overhang sequence complementary to a vector used in FastCloning.

9.2 Constructs and recombinant fusion proteins generated by FastCloning

Backbone	**Construct**	**Protein region (aa)**	**Predicted molecular weight (kDa)**	**Expression system**
pGEX-4T-1	GST-BICD1-CC1a	1-276	58.7	Bacteria
	GST-BICD1-CC1b	1-300	61.4	Bacteria
	GST-BICD1-CC1a.2	95-265	46.7	Bacteria
	GST-BICD1-HACC1a.1	[HA]1-94	38.4	Bacteria
	GST-BICD1-HACC1a	[HA]1-265	58.7	Bacteria
	GST-BICD1-HACC1b	[HA]1-276	59.8	Bacteria
	GST-BICD1-HACC1c	[HA]1-300	62.5	Bacteria
	GST-BICD1-HACC1/2	[HA]1-500	85.4	Bacteria
	GST-BICD1-CC2/3	314-808	82.7	Bacteria
	GST-BICD1-CC2	314-500	47.8	Bacteria
	GST-BICD1-CC3	662-808	43.3	Bacteria
pET28a	His_6-PTPN23-Bro	8-407	47.5	Bacteria
	His_6-PTPN23-Bro/VCC	8-653	75.4	Bacteria

	His_6-PTPN23-VCC1	401-653	31.1	Bacteria
	His_6-PTPN23-VCC2	401-700	36.4	Bacteria
	His_6-PTPN23-PRHD1	703-1134	46.7	Bacteria
	His_6-PTPN23-PRHD2	705-1134	46.5	Bacteria
	His_6-PTPN23-PRHD/PTP1	703-1452	82.8	Bacteria
	His_6-PTPN23-PRHD/PTP2	705-1475	85	Bacteria
	His_6-PTPN23-PRHD/PEST	705-1636	101.7	Bacteria
	His_6-PTPN23-PTP1	1188-1452	32.4	Bacteria
	His_6-PTPN23-PTP2	1188-1475	34.8	Bacteria
	His_6-PTPN23-PTP/PEST	1188-1636	51.5	Bacteria
pEGFPC1	GFP-BICD1^{WT}	1-818	123	Mammalian cells
	GFP-BICD1-ΔCC1	266-818	92.4	Mammalian cells
	GFP-BICD1-CC1.2	95-265	48.2	Mammalian cells
	GFP-BICD1-ΔCC1.2	1-808Δ95-265	103.5	Mammalian cells
DsRed2-N1	PTPN23-Bro-dsRed2	8-407	72.6	Mammalian cells
	PTPN23-Bro/VCC1-dsRed2	8-653	100.5	Mammalian cells
	PTPN23-Bro/VCC2-dsRed2	8-712	107.3	Mammalian cells
	PTPN23-VCC1-dsRed2	401-653	56.4	Mammalian cells
	PTPN23-VCC2-dsRed2	401-712	63.1	Mammalian cells
	PTPN23-HD-PEST-dsRed2	705-1636	127.1	Mammalian cells
	PTPN23-PTP-dsRed2	1188-1475	60.2	Mammalian cells
	PTPN23-sh2Bro$^{TCTC-CCTG}$-dsRed2	8-407	72.6	Mammalian cells
	PTPN23-sh2FL$^{TCTC-CCTG}$-dsRed2	408-1636	205.7	Mammalian cells
	PTPN23-FL-dsRed2	8-1636	205.7	Mammalian cells

9.3 Primary antibodies

Antigen	Name	Supplier	Species	WB
AKT	9272	Cell Signaling	Rabbit	1:1000 WB
α-tubulin	T6074	Sigma	Mouse	1:2000 WB
βIII-tubulin	ab41489	Abcam	Chicken	1:500 ICC
βIII-tubulin	mms-435p	Covance	Mouse	1:1000 ICC
BICD1	HPA041309	Atlas Antibodies	Rabbit	1:1000 WB 1:500 ICC
BICD2	HPA023013	Sigma	Rabbit	1:400 ICC
Cleaved caspase-3	9661	Cell Signaling	Rabbit	1:1000 WB 1:300 ICC
Dcp1a (56-Y)	sc-100706	Santa Cruz	Mouse	1:1000 ICC
EEA1	E41120	Transduction labs	Mouse	1:50 ICC
ERK1/2	9102	Cell Signaling	Rabbit	1:1000 WB
FLAG (M1)	F3040	Sigma	Mouse	1:500 ICC
FMRP	17722	Abcam	Rabbit	1:200 ICC
FMRP	sc-101048 (148.1)	Santa Cruz	Mouse	1:1000 WB 1:100 ICC
GAPDH	mab374	EMD Millipore	Mouse	1:5000 WB
GFP	4E12/8	CRUK	Mouse	1:2000 WB
GFP	GFP-1010	Aves Labs	Chicken	1:1000 ICC
G3BP	611127	BD Biosciences	Mouse	1:500 WB 1:200 ICC
GM130	610822	BD Biosciences	Mouse	1:100 ICC
GST	ab19256	Abcam	Mouse	1:3000 WB
HA (F310)	11867423001	Roche	Rat	1:1000 WB 1:500 ICC
His_6	70796-3MM	Novagen	Mouse	1:1000 WB
Kidins220	GSC16	CRUK	Rabbit	1:400 ICC
Kidins220	KNA	CRUK	Rabbit	1:1000 WB 1:400 ICC
LC3	ab48394	Abcam	Rabbit	1:1000 WB
$p75^{NTR}$	5410, CRD; Rat 33-194, (yellow, 0.9 mg/ml)	CRUK	Rabbit	1:1000 ICC
$p75^{NTR}$ (poly18397)	839701	Covance	Rabbit	1:1000 WB
pAKT	4060 (D9E)	Cell Signaling	Rabbit	1:1000 WB 1:400 ICC
pERK1/2	9101	Cell Signaling	Rabbit	1:1000 WB

PTPN23	sc-398711 (F-4)	Santa Cruz	Mouse	1:500 WB 1:400 ICC
pTrkA/B	4621 (C50F3)	Cell Signaling	Rabbit	1:1000 WB
Rab6	9625	Cell Signaling	Rabbit	1:400 ICC
Rab7	sc-376362	Santa Cruz	Mouse	1:1000 IF
TDP-43	12892-1-AP	ProteinTech	Rabbit	1:1000 WB
TGN46	ab16059	Abcam	Rabbit	1:100 ICC
TrkB	9872	Merck Millipore	Rabbit	1:500 ICC
TrkB (FL+T1)	07-225	Merck Millipore	Rabbit	1:1000 WB
Ubiquitin (FK2)	BML-PW8810	Enzo Life Sciences	Mouse	1:100 ICC

ICC – immunocytochemistry; WB – western blotting

9.4 Buffers and broths

Buffer	**Composition**
Acid wash (for antibody uptake)	0.2 M acetic acid, 0.5 M NaCl, pH 2.4
Coomassie Blue staining solution	0.3% Coomassie Brilliant Blue R-250, 10% v/v glacial acetic acid, 50% v/v methanol
Coomassie Blue destaining solution	10% v/v glacial acetic acid, 50% v/v methanol
DNAK wash buffer (GST purification)	50 mM Tris-HCl, pH 7.4, 10 mM $MgSO_4$, 2 mM ATP
Fractionation Buffer A	10 mM HEPES-NaOH, pH 7.8, 10 mM KCl, 0.1 mM EDTA, 0.1 mM EGTA, 1 mM DTT, 0.6% NP-40, 1 mM PMSF, protease inhibitor cocktail
Fractionation Buffer B	20 mM HEPES-NaOH, pH 7.9, 0.4 M NaCl, 1 mM EDTA, 1 mM EGTA, protease inhibitor cocktail
GFP/RFP-trap wash buffer	10 mM Tris-HCl, pH 7.5, 150 mM NaCl, 0.5 mM EDTA
GST elution buffer	50 mM Tris-HCl, pH 8.0, 10 mM reduced glutathione
GST lysis buffer	PBS, 0.05% Tween20, 2 mM EDTA, 0.1% β-mercaptoethanol, 1 mM benzamidine, 0.5 mM PMSF
His_6 lysis buffer	50 mM NaH_2PO_4, pH 8, 300 mM NaCl, 10 mM imidazole, 0.1% β-mercaptoethanol, 1 mM benzamidine, 0.5 mM PMSF
4x Laemmli sample buffer	250 mM Tris-HCl pH 6.8, 8% SDS, 40% glycerol, 0.02% Bromophenol Blue, 10% β-mercaptoethanol

LB	1% w/v tryptone, 0.5% w/v yeast extract, 1% w/v NaCl (add NaOH to pH 7.0)
LB agar	LB + 1.5% w/v agar
M9 minimal media	0.6% w/v Na_2HPO_4, 0.3% w/v KH_2PO_4, 0.05% w/v NaCl, 0.1% w/v NH_4Cl, autoclave then add: 100 mM $CaCl_2$, 1 M $MgSO_4$, 0.3% glycerol
Ni-NTA wash buffer	50 mM NaH_2PO_4, pH 8, 300 mM NaCl, 20-40 mM imidazole
NP-40 lysis/co-IP buffer	50 mM Tris-HCl, pH 7.5, 150 mM NaCl, 1 mM EDTA, 0.2-0.4% NP-40, 5% glycerol, 1:100 HALT protease and phosphatase inhibitor cocktail
PBS	137 mM NaCl, 2.7 mM KCl, 10 mM Na_2HPO_4, 1.8 mM KH_2PO_4
10x PBS	8% w/v NaCl, 0.2% w/v KCl, 1.14% w/v Na_2HPO_4, 0.24% w/v KH_2PO_4, pH 7.4
PBST	0.1% v/v Tween-20, in PBS
PBSTx	0.1% v/v Triton X-100, in PBS
RIPA buffer	50 mM Tris-HCl pH 7.5, 150 mM NaCl, 1% NP-40, 0.5% sodium deoxycholate, 0.1% SDS, 1 mM EDTA, 1 mM EGTA
SOC medium	2% w/v tryptone, 0.5% w/v yeast extract, 8.56 mM NaCl, 2.5 mM KCl, 10 mM $MgCl_2$, 10 mM $MgSO_4$, 20 mM glucose
TBE	90 mM Tris-HCl, 90 mM boric acid, pH 8.0, 2 mM EDTA
TBST	20 mM Tris, pH 7.4-7.6, 150 mM NaCl, 0.1% v/v Tween-20

9.5 Drugs

Drug	**Abbrev.**	**Target/mode of action**	**Stock conc.**	**Working conc.**	**Vehicle**
Bafilomycin A1	BafA1	inhibits V-ATPase, inhibitor of autophagy	200 µM	200 nM	DMSO
Brefeldin A	BrefA	inhibits Golgi-ER transport leading to Golgi collapse	5 mg/ml	20 µg/ml	DMSO
Cycloheximide	CHX	inhibits mRNA translation	50 mg/ml	50 µg/ml	DMSO
Hydrogen peroxide	H_20_2	oxidative stress	200 mM	0.1-1 mM	H_2O
Latrunculin B	LatB	actin depolymerisation, sequesters G-actin and prevents F-actin assembly	1 mM	0.5 µM	DMSO
MG132	MG132	Inhibits proteasome	2 mM	25 µM	DMSO
Nocodazole	Noc	disrupts microtubules by binding to β−tubulin and preventing formation of disulfide linkages, inhibiting microtubule dynamics	5 mg/ml	20 µg/ml	DMSO

Sodium arsenite	$NaAsO_2$	oxidative stress	250 mM	0.25-0.5 mM	H_2O
Thapsigargin	Thap	inhibits ER Ca^{2+} ATPase and induces ER stress	5 mM	15 µM	DMSO
Vincristine	Vinc	microtubule depolymerisation	2 mM	5 µM	MeOH

9.6 Bacterial strains

Strain	**Use**	**Supplier/Source**
BL(21)DE3	Protein expression	Invitrogen
DH5α	Plasmid amplification	Invitrogen
GCI-L3	shRNA plasmid amplification	GeneCopoeia
SoluBL21™	Protein expression	Amsbio / KCL
XL1-Blue	Plasmid amplification	CRUK
XL10-Gold	FastCloning	Stratagene

References

Akhmanova A, Hammer JA (2010) Linking molecular motors to membrane cargo. Curr Opin Cell Biol 22:479–487.

Alam U, Kennedy D (2019) Rasputin a decade on and more promiscuous than ever? A review of G3BPs. Biochim Biophys Acta - Mol Cell Res 1866:360–370.

Alazami AM et al. (2015) Accelerating novel candidate gene discovery in neurogenetic disorders via whole-exome sequencing of prescreened multiplex consanguineous families. Cell Rep 10:148–161.

Alexander EJ, Ghanbari Niaki A, Zhang T, Sarkar J, Liu Y, Nirujogi RS, Pandey A, Myong S, Wang J (2018) Ubiquilin 2 modulates ALS/FTD-linked FUS-RNA complex dynamics and stress granule formation. PNAS 115:E11485–E11494.

Ali N, Zhang L, Taylor S, Mironov A, Urbé S, Woodman P (2013) Recruitment of UBPY and ESCRT exchange drive HD-PTP-dependent sorting of EGFR to the MVB. Curr Biol 23:453–461.

Anastasia XA, Barker XPA, Chao M V, Hempstead BL (2015) Detection of p75 NTR Trimers : Implications for Receptor Stoichiometry and Activation. J Neurosci 35:11911–11920.

Anderson P, Kedersha N (2006) RNA granules. J Cell Biol 172:803–808.

Anderson P, Kedersha N (2008) Stress granules: the Tao of RNA triage. Trends Biochem Sci 33:141–150.

Anderson P, Kedersha N, Ivanov P (2015) Stress granules, P-bodies and cancer. Biochem Biophys Acta 1849:861–870.

Arévalo JC, Pereira DB, Yano H, Teng KK, Chao M V. (2006a) Identification of a switch in neurotrophin signaling by selective tyrosine phosphorylation. J Biol Chem 281:1001–1007.

Arévalo JC, Waite J, Rajagopal R, Beyna M, Chen Z-Y, Lee FS, Chao M V. (2006b) Cell survival through Trk neurotrophin receptors is differentially regulated by ubiquitination. Neuron 50:549–559.

Arimoto K, Fukuda H, Imajoh-Ohmi S, Saito H, Takekawa M (2008) Formation of stress granules inhibits apoptosis by suppressing stress-responsive MAPK pathways. Nat Cell Biol 10:1324–1332.

Ascano M, Bodmer D, Kuruvilla R (2012) Endocytic trafficking of neurotrophins in neural development. Trends Cell Biol 22:266–273.

Ascano M, Richmond A, Borden P, Kuruvilla R (2009) Axonal Targeting of Trk Receptors via Transcytosis Regulates Sensitivity to Neurotrophin Responses. J Neurosci 29:11674–11685.

Aulas A, Fay MM, Lyons SM, Achorn CA, Kedersha N, Anderson P, Ivanov P (2017) Stress-specific differences in assembly and composition of stress granules and related foci. J Cell Sci 130:927–937.

Aulas A, Stabile S, Vande Velde C (2012) Endogenous TDP-43, but not FUS,

contributes to stress granule assembly via G3BP. Mol Neurodegener 7:1–14.

Baens M, Marynen P (1997) A Human Homologue (BICD1) of the Drosophila Bicaudal-D Gene. Genomics 606:601–606.

Bali P, Pranpat M, Bradner J, Balasis M, Fiskus W, Guo F, Rocha K, Kumaraswamy S, Boyapalle S, Atadja P, Seto E, Bhalla K (2005) Inhibition of Histone Deacetylase 6 Acetylates and Disrupts the Chaperone Function of Heat Shock Protein 90. J Biol Chem 280:26729–26734.

Bamji SX, Majdan M, Pozniak CD, Belliveau DJ, Aloyz R, Kohn J, Causing CG, Miller FD (1998) The p75 neurotrophin receptor mediates neuronal apoptosis and is essential for naturally occurring sympathetic neuron death. J Cell Biol 140:911–923.

Bao W, Gu Y, Ta L, Wang K, Xu Z (2016) Induction of autophagy by the MG-132 proteasome inhibitor is associated with endoplasmic reticulum stress in MCF-7 cells. Mol Med Rep 13:796–804.

Baquet ZC, Bickford PC, Jones KR (2005) Brain-derived neurotrophic factor is required for the establishment of the proper number of dopaminergic neurons in the substantia nigra pars compacta. J Neurosci 25:6251–6259.

Barber SC, Mead RJ, Shaw PJ (2006) Oxidative stress in ALS: A mechanism of neurodegeneration and a therapeutic target. Biochim Biophys Acta - Mol Basis Dis 1762:1051–1067.

Barber SC, Shaw PJ (2010) Oxidative stress in ALS : Key role in motor neuron injury and therapeutic target. Free Radic Biol Med 48:629–641.

Barford K, Deppmann C, Winckler B (2017) The neurotrophin receptor signaling endosome: Where trafficking meets signaling. Dev Neurobiol 77:405–418.

Barrett GL, Bartlett PF (2006) The p75 nerve growth factor receptor mediates survival or death depending on the stage of sensory neuron development. Proc Natl Acad Sci 91:6501–6505.

Belyy V, Schlager MA, Foster H, Reimer AE, Carter AP, Yildiz A (2016) The mammalian dynein-dynactin complex is a strong opponent to kinesin in a tug-of-war competition. Nat Cell Biol 18:1018–1024.

Bercsenyi K, Schmieg N, Bryson JB, Wallace M, Caccin P, Golding M, Zanotti G, Greensmith L, Nischt R, Schiavo G (2014) Nidogens are therapeutic targets for the prevention of tetanus. Science 346:1118–1123.

Bertolotti A, Zhang Y, Hendershot LM, Harding HP, Ron D (2000) Dynamic interaction of BiP and ER stress transducers in the unfolded- protein response. Nat Cell Biol 2:326–332.

Bianco A, Dienstbier M, Salter HK, Gatto G, Bullock SL (2010) Bicaudal-D regulates fragile X mental retardation protein levels, motility, and function during neuronal morphogenesis. Curr Biol 20:1487–1492.

Bilsland LG, Sahai E, Kelly G, Golding M, Greensmith L, Schiavo G (2010) Deficits in axonal transport precede ALS symptoms in vivo. PNAS 107:20523–20528.

Bissig C, Gruenberg J (2014) ALIX and the multivesicular endosome: ALIX in Wonderland. Trends Cell Biol 24:19–25.

Bivik C, Bahrampour S, Ulvklo C, Nilsson P, Angel A, Fransson F, Lundin E, Renhorn J, Thor S (2015) Novel genes involved in controlling specification of Drosophila FMRfamide neuropeptide cells. Genetics 200:1229–1244.

Blomen VA, Májek P, Jae LT, Johannes W, Nieuwenhuis J, Staring J, Diemen FR Van, Olk N, Stukalov A, Marceau C, Janssen H, Carette JE, Keiryn L, Colinge J, Superti-furga G, Thijn R (2015) Gene essentiality and synthetic lethality in haploid human cells. Science 1:1092–1096.

Bodmer D, Ascaño M, Kuruvilla R (2011) Isoform-Specific Dephosphorylation of Dynamin1 by Calcineurin Couples Neurotrophin Receptor Endocytosis to Axonal Growth. Neuron 70:1085–1099.

Boeynaems S et al. (2017) Phase Separation of C9orf72 Dipeptide Repeats Perturbs Stress Granule Dynamics. Mol Cell 65:1044-1055.e5.

Boeynaems S, Bogaert E, Van Damme P, Van Den Bosch L (2016) Inside out: the role of nucleocytoplasmic transport in ALS and FTLD. Acta Neuropathol 132:159–173.

Bornhorst JA, Falke JJ (2000) Purification of proteins using polyhistidine affinity tags. Methods Enzymol 326:245–254.

Boutahar N, Reynaud E, Lassabliere F, Borg J (2010) Brain-derived neurotrophic factor inhibits cell cycle reentry but not endoplasmic reticulum stress in cultured neurons following oxidative or excitotoxic stress. J Neurosci Res 88:2263–2271.

Boyault C, Gilquin B, Zhang Y, Rybin V, Garman E, Meyer-Klaucke W, Matthias P, Müller CW, Khochbin S (2006) HDAC6-p97/VCP controlled polyubiquitin chain turnover. EMBO J 25:3357–3366.

Brangwynne CP, Eckmann CR, Courson DS, Rybarska A, Hoege C, Gharakhani J, Jülicher F, Hyman AA (2009) Germline P granules are liquid droplets that localize by controlled dissolution/condensation. Science 324:1729–1732.

Breusegem SY, Seaman MNJ (2014) Genome-wide RNAi Screen Reveals a Role for Multipass Membrane Proteins in Endosome-to-Golgi Retrieval. Cell Rep 9:1931–1945.

Brewer GJ, Cotman CW (1989) Survival and growth of hippocampal neurons in defined medium at low density: advantages of a sandwich culture technique or low oxygen. Brain Res 494:65–74.

Brewer GJ, Torricelli JR, Evege EK, Price PJ (1993) Optimized survival of hippocampal neurons in B27-supplemented neurobasal(TM), a new serum-free medium combination. J Neurosci Res 35:567–576.

Bright NA, Reaves BJ, Mullock BM, Luzio JP (1997) Dense core lysosomes can fuse with late endosomes and are re-formed from the resultant hybrid organelles. J Cell Sci 110:2027–2040.

Bronfman FC, Escudero CA, Weis J, Kruttgen A (2007) Endosomal transport of neurotrophins: Roles in signaling and neurodegenerative diseases. Dev

Neurobiol 67:1183–1203.

Bryja V, Bonilla S, Arenas E (2006) Derivation of mouse embryonic stem cells. Nat Protoc 1:2082–2087.

Bucci C, Thomsen P, Nicoziani P, McCarthy J, van Deurs B (2000) Rab7: a key to lysosome biogenesis. Mol Biol Cell 11:467–480.

Buchan JR, Kolaitis RM, Taylor JP, Parker R (2013) Eukaryotic stress granules are cleared by autophagy and Cdc48/VCP function. Cell 153:1461–1474.

Buchan JR, Parker R (2009) Eukaryotic Stress Granules: The Ins and Outs of Translation. Mol Cell 36:932–941.

Buchan JR, Yoon J-H, Parker R (2011) Stress-specific composition, assembly and kinetics of stress granules in Saccharomyces cerevisiae. J Cell Sci 124:228–239.

Budzinska M, Wicher KB, Terenzio M (2017) Neuronal Roles of the Bicaudal D Family of Motor Adaptors. In: Neurotrophins, 1st ed., pp 133–152. Elsevier Inc.

Bulgari D, Jha A, Deitcher DL, Levitan ES (2018) Myopic (HD-PTP, PTPN23) selectively regulates synaptic neuropeptide release. PNAS 115:1617–1622.

Bullock SL, Ish-Horowicz D (2001) Conserved signals and machinery for RNA transport in Drosophila oogenesis and embryogenesis. Nature 414:611–616.

Burk K, Murdoch JD, Freytag S, Koenig M, Bharat V, Markworth R, Burkhardt S, Fischer A, Dean C (2017) EndophilinAs regulate endosomal sorting of BDNF-TrkB to mediate survival signaling in hippocampal neurons. Sci Rep 7:2149.

Butowt R, Von Bartheld CS (2003) Connecting the dots: Trafficking of neurotrophins, lectins and diverse pathogens by binding to the neurotrophin receptor p75NTR. Eur J Neurosci 17:673–680.

Calderó J, Prevette D, Mei X, Oakley R a, Li L, Milligan C, Houenou L, Burek M, Oppenheim RW (1998) Peripheral target regulation of the development and survival of spinal sensory and motor neurons in the chick embryo. J Neurosci 18:356–370.

Campenot RB (1977) Local control of neurite development by nerve growth factor. Proc Natl Acad Sci U S A 74:4516–4519.

Carpenter RL, Jiang Y, Jing Y, He J, Rojanasakul Y, Liu LZ, Jiang BH (2011) Arsenite induces cell transformation by reactive oxygen species, AKT, ERK1/2, and p70S6K1. Biochem Biophys Res Commun 414:533–538.

Carter AP, Diamant AG, Urnavicius L (2016) How dynein and dynactin transport cargos: a structural perspective. Curr Opin Struct Biol 37:62–70.

Castiglioni S, Maier J a M (2012) The tyrosine phosphatase HD-PTP (PTPN23) is degraded by calpains in a calcium-dependent manner. Biochem Biophys Res Commun 421:380–383.

Castiglioni S, Maier JAM, Mariotti M (2007) The tyrosine phosphatase HD-PTP: A novel player in endothelial migration. Biochem Biophys Res Commun 364:534–539.

Catara G, Grimaldi G, Schembri L, Spano D, Turacchio G, Lo Monte M, Beccari AR, Valente C, Corda D (2017) PARP1-produced poly-ADP-ribose causes the PARP12 translocation to stress granules and impairment of Golgi complex functions. Sci Rep 7:1–17.

Caviston JP, Holzbaur ELF (2009) Huntingtin as an essential integrator of intracellular vesicular trafficking. Trends Cell Biol 19:147–155.

Ceriani M, Amigoni L, D'Aloia A, Berruti G, Martegani E (2015) The deubiquitinating enzyme UBPy/USP8 interacts with TrkA and inhibits neuronal differentiation in PC12 cells. Exp Cell Res 333:49–59.

Chantarachot T, Bailey-Serres J (2017) Polysomes, stress granules and processing bodies: a dynamic triumvirate controlling cytoplasmic mRNA fate and function. Plant Physiol 176:254–269.

Chao M V. (2003) Neurotrophins and their receptors: A convergence point for many signalling pathways. Nat Rev Neurosci 4:299–309.

Chen L, Liu B (2017) Relationships between Stress Granules, Oxidative Stress, and Neurodegenerative Diseases. Oxid Med Cell Longev 2017:1–10.

Chen Z-Y, Ieraci A, Tanowitz M, Lee FS (2005) A novel endocytic recycling signal distinguishes biological responses of Trk neurotrophin receptors. Mol Biol Cell 16:5761–5772.

Chernov KG, Barbet A, Hamon L, Ovchinnikov LP, Curmi PA, Pastré D (2009) Role of microtubules in stress granule assembly: Microtubule dynamical instability favors the formation of micrometric stress granules in cells. J Biol Chem 284:36569–36580.

Choe JY, Jung HY, Park KY, Kim SK (2014) Enhanced p62 expression through impaired proteasomal degradation is involved in caspase-1 activation in monosodium urate crystal-induced interleukin-1β expression. Rheumatology 53:1043–1053.

Claude P, Hawrot E, Dunis D, Campenot R (1982) Binding, internalization, and retrograde transport of 125I-nerve growth factor in cultured rat sympathetic neurons. J Neurosci 2:431–442.

Colin E, Zala D, Liot G, Rangone H, Borrell-Pagès M, Li XJ, Saudou F, Humbert S (2008) Huntingtin phosphorylation acts as a molecular switch for anterograde/retrograde transport in neurons. EMBO J 27:2124–2134.

Connor B, Young D, Lawlor P, Gai W, Waldvogel H, Faull RLM, Dragunow M (1996) Trk receptor alterations in Alzheimer's disease. Mol Brain Res 42:1–17.

Copani A, Uberti D, Sortino MA, Bruno V, Nicoletti F, Memo M (2001) Activation of cell-cycle-associated proteins in neuronal death: A mandatory or dispensable path? Trends Neurosci 24:25–31.

Copeland SJ, Thurston SF, Copeland JW (2016) Actin- and microtubule-dependent regulation of Golgi morphology by FHDC1. Mol Biol Cell 27:260–276.

Costa RM, Filgueira FP, Tostes RC, Carvalho MHC, Akamine EH, Lobato NS (2016) H2O2 generated from mitochondrial electron transport chain in thoracic

perivascular adipose tissue is crucial for modulation of vascular smooth muscle contraction. Vascul Pharmacol 84:28–37.

Cunha C, Brambilla R, Thomas KL (2010) A simple role for BDNF in learning and memory? Front Mol Neurosci 3:1–14.

Dao TP, Kolaitis RM, Kim HJ, O'Donovan K, Martyniak B, Colicino E, Hehnly H, Taylor JP, Castañeda CA (2018) Ubiquitin Modulates Liquid-Liquid Phase Separation of UBQLN2 via Disruption of Multivalent Interactions. Mol Cell 6:965–978.

Dastoor Z, Dreyer JL (2001) Potential role of nuclear translocation of glyceraldehyde-3-phosphate dehydrogenase in apoptosis and oxidative stress. J Cell Sci 114:1643–1653.

De Bernardez Clark E (1998) Refolding of recombinant proteins. Curr Opin Biotechnol 9:157–163.

De Vos KJ, Hafezparast M (2017) Neurobiology of axonal transport defects in motor neuron diseases: Opportunities for translational research? Neurobiol Dis 105:283–299.

Debaisieux S, Encheva V, Chakravarty P, Snijders AP, Schiavo G (2016) Analysis of Signaling Endosome Composition and Dynamics Using SILAC in Embryonic Stem Cell-Derived Neurons. Mol Cell proteomics 15:542–557.

Deinhardt K, Salinas S, Verastegui C, Watson R, Worth D, Hanrahan S, Bucci C, Schiavo G (2006) Rab5 and Rab7 Control Endocytic Sorting along the Axonal Retrograde Transport Pathway. Neuron 52:293–305.

DeJesus-Hernandez M et al. (2011) Expanded GGGGCC hexanucleotide repeat in noncoding region of C9ORF72 causes chromosome 9p-linked FTD and ALS. Neuron 72:245–256.

Delcroix J, Valletta JS, Wu C, Hunt SJ, Kowal AS, Mobley WC (2003) NGF retrograde transport in Sciatic nerve-basal root ganglia. 39:69–84.

Dewey CM, Cenik B, Sephton CF, Dries DR, Mayer P, Good SK, Johnson BA, Herz J, Yu G (2011) TDP-43 is directed to stress granules by sorbitol, a novel physiological osmotic and oxidative stressor. Mol Cell Biol 31:1098–1108.

Dienstbier M, Boehl F, Li X, Bullock SL (2009) Egalitarian is a selective RNA-binding protein linking mRNA localization signals to the dynein motor. Genes Dev 23:1546–1558.

Diggins NL, Webb DJ (2017) APPL1 is a multifunctional endosomal signaling adaptor protein. Biochem Soc Trans 45:771–779.

Dompierre JP, Godin JD, Charrin BC, Cordelières FP, King SJ, Humbert S, Saudou F (2007) Histone deacetylase 6 inhibition compensates for the transport deficit in Huntington's disease by increasing tubulin acetylation. J Neurosci 27:3571–3583.

Doyotte A, Mironov A, Mckenzie E, Woodman P (2008) The Bro1-related protein HD-PTP / PTPN23 is required for endosomal cargo sorting and multivesicular body morphogenesis. PNAS 105:6308–6313.

Driskell OJ, Mironov A, Allan VJ, Woodman PG (2007) Dynein is required for receptor sorting and the morphogenesis of early endosomes. Nat Cell Biol 9:113–120.

Duregotti E, Negro S, Scorzeto M, Zornetta I, Dickinson BC, Chang CJ, Montecucco C, Rigoni M (2015) Mitochondrial alarmins released by degenerating motor axon terminals activate perisynaptic Schwann cells. Proc Natl Acad Sci 112:E497–E505.

Eisinger-Mathason TSK, Andrade J, Groehler AL, Clark DE, Muratore-schroeder TL, Pasic L, Smith JA, Shabanowitz J, Hunt DF, Macara IG, Lannigan DA (2008) Codependent Functions of RSK2 and the Apoptosis-Promoting Factor TIA-1 in Stress Granule Assembly and Cell Survival. Mol Cell 31:722–736.

Emara MM, Fujimura K, Sciaranghella D, Ivanova V, Ivanov P, Anderson P (2012) Hydrogen peroxide induces stress granule formation independent of eIF2α phosphorylation. Biochem Biophys Res Commun 423:763–769.

Emdal KB, Pedersen AK, Bekker-Jensen DB, Tsafou KP, Horn H, Lindner S, Schulte JH, Eggert A, Jensen LJ, Francavilla C, Olsen J V (2015) Temporal proteomics of NGF-TrkA signaling identifies an inhibitory role for the E3 ligase Cbl-b in neuroblastoma cell differentiation. Sci Signal 8:1–17.

Ernfors P (2001) Local and target-derived actions of neurotrophins during peripheral nervous system development. Cell Mol Life Sci 58:1036–1044.

Esposito D, Patel P, Stephens RM, Perez P, Chao M V., Kaplan DR, Hempstead BL (2001) The Cytoplasmic and Transmembrane Domains of the p75 and Trk A Receptors Regulate High Affinity Binding to Nerve Growth Factor. J Biol Chem 276:32687–32695.

Fang C, Bourdette D, Banker G (2012) Oxidative stress inhibits axonal transport: Implications for neurodegenerative diseases. Mol Neurodegener 7:1–13.

Fay MM, Anderson P (2018) The Role of RNA in Biological Phase Separations. J Mol Biol 430:4685–4701.

Fay MM, Anderson P, Ivanov P (2017) ALS/FTD-Associated C9ORF72 Repeat RNA Promotes Phase Transitions In Vitro and in Cells. Cell Rep 21:3573–3584.

Federici T, Boulis NM (2006) Gene-based treatment of motor neuron diseases. Muscle and Nerve 33:302–323.

Federici T, Boulis NM (2012) Gene therapy for amyotrophic lateral sclerosis. Neurobiol Dis 48:236–242.

Ferrante RJ, Browne SE, Shinobu LA, Bowling AC, Baik MJ, MacGarvey U, Kowall NW, Brown RH, Beal MF (1997) Evidence of increased oxidative damage in both sporadic and familial amyotrophic lateral sclerosis. J Neurochem 69:2064–2074.

Fiesel FC, Voigt A, Weber SS, Van den Haute C, Waldenmaier A, Görner K, Walter M, Anderson ML, Kern J V, Rasse TM, Schmidt T, Springer W, Kirchner R, Bonin M, Neumann M, Baekelandt V, Alunni-Fabbroni M, Schulz JB, Kahle PJ (2010) Knockdown of transactive response DNA-binding protein (TDP-43) downregulates histone deacetylase 6. EMBO J 29:209–221.

Fisher RD, Chung HY, Zhai Q, Robinson H, Sundquist WI, Hill CP (2007) Structural and Biochemical Studies of ALIX/AIP1 and Its Role in Retrovirus Budding. Cell 128:841–852.

Flores-Rodriguez N, Kenwright DA, Chung P-H, Harrison AW, Stefani F, Waigh TA, Allan VJ, Woodman PG (2015) ESCRT-0 marks an APPL1-independent transit route for EGFR between the cell surface and the EEA1-positive early endosome. J Cell Sci 128:755–767.

Frade JM, Rodríguez-Tébar A, Barde YA (1996) Induction of cell death by endogenous nerve growth factor through its p75 receptor. Nature 383:166–168.

Frankel EB, Audhya A (2018) ESCRT-dependent cargo sorting at multivesicular endosomes. Semin Cell Dev Biol 74:4–10.

Fratta P, Mizielinska S, Nicoll AJ, Zloh M, Fisher EMC, Parkinson G, Isaacs AM (2012) C9orf72 hexanucleotide repeat associated with amyotrophic lateral sclerosis and frontotemporal dementia forms RNA G-quadruplexes. Sci Rep 2:1–6.

Frémont S, Hammich H, Bai J, Wioland H, Klinkert K, Rocancourt M, Kikuti C, Stroebel D, Romet-Lemonne G, Pylypenko O, Houdusse A, Echard A (2017) Oxidation of F-actin controls the terminal steps of cytokinesis. Nat Commun 8:1–16.

Fridolfsson HN, Ly N, Meyerzon M, Starr DA (2010) UNC-83 coordinates kinesin-1 and dynein activities at the nuclear envelope during nuclear migration. Dev Biol 338:237–250.

Frimat J-P, Xie S, Bastiaens A, Schurink B, Wolbers F, den Toonder J, Luttge R (2015) Advances in 3D neuronal cell culture. J Vac Sci Technol B 33:1–6.

Fu X, Yang Y, Xu C, Niu Y, Chen T, Zhou Q, Liu J-J (2011) Retrolinkin cooperates with endophilin A1 to mediate BDNF-TrkB early endocytic trafficking and signaling from early endosomes. Mol Biol Cell 22:3684–3698.

Fujimura K, Katahira J, Kano F, Yoneda Y, Murata M (2009) Microscopic dissection of the process of stress granule assembly. Biochim Biophys Acta - Mol Cell Res 1793:1728–1737.

Fujiwara T, Yokotas S, Takatsukig A, Ikeharan Y (1988) Brefeldin A Causes Disassembly of the Golgi Complex and Accumulation of Secretory Proteins in the Endoplasmic Reticulum. J Biol Chem 263:18545–18552.

Fumoto K, Hoogenraad CC, Kikuchi A (2006) GSK-3beta-regulated interaction of BICD with dynein is involved in microtubule anchorage at centrosome. EMBO J 25:5670–5682.

Furukawa Y, Kaneko K, Matsumoto G, Kurosawa M, Nukina N (2009) Cross-seeding fibrillation of Q/N-rich proteins offers new pathomechanism of polyglutamine diseases. J Neurosci 29:5153–5162.

Gahloth D, Heaven G, Jowitt TA, Mould AP, Bella J, Baldock C, Woodman P, Tabernero L (2017a) The open architecture of HD-PTP phosphatase provides new insights into the mechanism of regulation of ESCRT function. Sci Rep 7:9151.

Gahloth D, Levy C, Heaven G, Stefani F, Wunderley L, Mould P, Cliff MJ, Bella J, Fielding AJ, Woodman P, Tabernero L (2016) Structural Basis for Selective Interaction between the ESCRT Regulator HD-PTP and UBAP1. Structure 24:1–12.

Gahloth D, Levy C, Walker L, Wunderley L, Mould AP, Taylor S, Woodman P, Tabernero L (2017b) Structural Basis for Specific Interaction of TGFβ Signaling Regulators SARA/Endofin with HD-PTP. Structure 25:1–14.

Gal J, Kuang L, Barnett KR, Zhu BZ, Shissler SC, Korotkov K V., Hayward LJ, Kasarskis EJ, Zhu H (2016) ALS mutant SOD1 interacts with G3BP1 and affects stress granule dynamics. Acta Neuropathol 132:563–576.

Gao Y, Hubbert CC, Yao T-P (2010) The microtubule-associated histone deacetylase 6 (HDAC6) regulates epidermal growth factor receptor (EGFR) endocytic trafficking and degradation. J Biol Chem 285:11219–11226.

Garcia N, Santafe MM, TomÃ s M, Lanuza MA, Besalduch N, TomÃ s J (2009) Involvement of brain-derived neurotrophic factor (BDNF) in the functional elimination of synaptic contacts at polyinnervated neuromuscular synapses during development. J Neurosci Res 88:1406–1419.

Gardiner J, Barton D, Overall R, Marc J (2009) Neurotrophic support and oxidative stress: Converging effects in the normal and diseased nervous system. Neuroscientist 15:47–61.

Gareau C, Houssin E, Martel D, Coudert L, Mellaoui S, Huot ME, Laprise P, Mazroui R (2013) Characterization of Fragile X Mental Retardation Protein Recruitment and Dynamics in Drosophila Stress Granules. PLoS One 8:1–13.

Gauthier LR, Né B, Charrin DC, Borrell-Pagè M, Dompierre JP, Lè Ne Rangone H, Cordeliè Res FP, De Mey J, Macdonald ME, Leßmann V, Humbert S (2004) Huntingtin Controls Neurotrophic Support and Survival of Neurons by Enhancing BDNF Vesicular Transport along Microtubules. Cell 118:127–138.

Geetha T, Zheng C, Unroe B, Sycheva M, Kluess H, Babu JR (2012) Polyubiquitination of the neurotrophin receptor p75 directs neuronal cell survival. Biochem Biophys Res Commun 421:286–290.

Gibbs KL, Greensmith L, Schiavo G (2015) Regulation of Axonal Transport by Protein Kinases. Trends Biochem Sci 40:597–610.

Gilks N, Kedersha N, Ayodele M, Shen L, Stoecklin G, Dember LM, Anderson P (2004) Stress granule assembly is mediated by prion-like aggregation of TIA-1. Mol Biol Cell 15:5383–5398.

Gingras M-C, Kazan JM, Pause A (2017) Role of ESCRT component HD-PTP/ *PTPN23* in cancer. Biochem Soc Trans 45:845–854.

Gingras M-C, Kharitidi D, Chénard V, Uetani N, Bouchard M, Tremblay ML, Pause A (2009a) Expression analysis and essential role of the putative tyrosine phosphatase His-domain-containing protein tyrosine phosphatase (HD-PTP). Int J Dev Biol 53:1069–1074.

Gingras M-C, Zhang YL, Kharitidi D, Barr AJ, Knapp S, Tremblay ML, Pause A (2009b) HD-PTP is a catalytically inactive tyrosine phosphatase due to a

conserved divergence in its phosphatase domain. PLoS One 4:e5105.

Goto-Silva L, McShane MP, Salinas S, Kalaidzidis Y, Schiavo G, Zerial M (2019) Retrograde transport of Akt by a neuronal Rab5-APPL1 endosome. Sci Rep 9:1–14.

Gougeon PY, Prosser DC, Da-Silva LF, Ngsee JK (2002) Disruption of Golgi morphology and trafficking in cells expressing mutant prenylated Rab acceptor-1. J Biol Chem 277:36408–36414.

Gould TW, Oppenheim RW (2011) Motor neuron trophic factors: Therapeutic use in ALS? Brain Res Rev 67:1–39.

Granger E, McNee G, Allan V, Woodman P (2014) The role of the cytoskeleton and molecular motors in endosomal dynamics. Semin Cell Dev Biol 31:20–29.

Gray K, Ellis V (2008) Activation of pro-BDNF by the pericellular serine protease plasmin. FEBS Lett 582:907–910.

Green EG, Ramm E, Riley NM, Spiro DJ, Goldenring JR, Wessling-Resnick M (1997) Rab11 is associated with transferrin-containing recycling compartments in K562 cells. Biochem Biophys Res Commun 239:612–616.

Grigoriev I, Splinter D, Keijzer N, Wulf PS, Demmers J, Ohtsuka T, Modesti M, Maly I V., Grosveld F, Hoogenraad CC, Akhmanova A (2007) Rab6 Regulates Transport and Targeting of Exocytotic Carriers. Dev Cell 13:305–314.

Gromnitza S, Lepa C, Weide T, Schwab A, Pavenstädt H, George B (2018) Tropomyosin-related kinase C (TrkC) enhances podocyte migration by ERK-mediated WAVE2 activation. FASEB J 32:1665–1676.

Gupta VK, You Y, Gupta VB, Klistorner A, Graham SL (2013) TrkB receptor signalling: Implications in neurodegenerative, psychiatric and proliferative disorders. Int J Mol Sci 14:10122–10142.

Haapasalo A, Sipola I, Larsson K, Åkerman KEO, Stoilov P, Stamm S, Wong G, Castrén E (2002) Regulation of TRKB surface expression by brain-derived neurotrophic factor and truncated TRKB isoforms. J Biol Chem 277:43160–43167.

Hafezparast M et al. (2003) Mutations in Dynein Link Motor Neuron Degeneration to Defects. Science 300:808–813.

Halliwell B (2014) Cell culture, oxidative stress, and antioxidants: Avoiding pitfalls. Biomed J 37:99–105.

Hamann I, Klotz LO (2013) Arsenite-induced stress signaling: Modulation of the phosphoinositide 3’-kinase/Akt/FoxO signaling cascade. Redox Biol 1:104–109.

Hanahan D, Weinberg RA (2011) Hallmarks of cancer: the next generation. Cell 144:646–674.

Harada T, Hideshima T, Anderson KC (2016) Histone deacetylase inhibitors in multiple myeloma: from bench to bedside. Int J Hematol 104:300–309.

Harding HP, Zhang Y, Bertolotti A, Zeng H, Ron D (2000) Perk Is Essential for Translational Regulation and Cell Survival during the Unfolded Protein

Response. Mol Cell 5:897–904.

Harding HP, Zhang Y, Ron D (1999) Protein translation and folding are coupled by an endoplasmic-reticulum-resident kinase. Nature 397:271–274.

Harrington AW, Kim JY, Yoon SO (2002) Activation of Rac GTPase by p75 is necessary for c-jun N-terminal kinase-mediated apoptosis. J Neurosci 22:156–166.

Harrington AW, St. Hillaire C, Zweifel LS, Glebova NO, Philippidou P, Halegoua S, Ginty DD (2011) Recruitment of actin modifiers to TrkA endosomes governs retrograde NGF signaling and survival. Cell 146:421–434.

Heerssen HM, Pazyra MF, Segal RA (2004) Dynein motors transport activated Trks to promote survival of target-dependent neurons. Nat Neurosci 7:596–604.

Hein MY, Hubner NC, Poser I, Cox J, Nagaraj N, Toyoda Y, Gak IA, Weisswange I, Mansfeld J, Buchholz F, Hyman AA, Mann M (2015) A human interactome in three quantitative dimensions organized by stoichiometries and abundances. Cell 163:712–723.

Hetz C, Saxena S (2017) ER stress and the unfolded protein response in neurodegeneration. Nat Publ Gr 13:477–491.

Hideshima T, Bradner JE, Wong J, Chauhan D, Richardson P, Schreiber SL, Anderson KC (2005) Small-molecule inhibition of proteasome and aggresome function induces synergistic antitumor activity in multiple myeloma. PNAS 102:8567–8572.

Higuero AM, Sánchez-Ruiloba L, Doglio LE, Portillo F, Abad-Rodríguez J, Dotti CG, Iglesias T (2010) Kidins220/ARMS modulates the activity of microtubule-regulating proteins and controls neuronal polarity and development. J Biol Chem 285:1343–1357.

Hjerpe R, Bett JS, Keuss MJ, Solovyova A, McWilliams TG, Johnson C, Sahu I, Varghese J, Wood N, Wightman M, Osborne G, Bates GP, Glickman MH, Trost M, Knebel A, Marchesi F, Kurz T (2016) UBQLN2 Mediates Autophagy-Independent Protein Aggregate Clearance by the Proteasome. Cell 166:935–949.

Hoepfner S, Severin F, Cabezas A, Habermann B, Runge A, Gillooly D, Stenmark H, Zerial M (2005) Modulation of receptor recycling and degradation by the endosomal kinesin KIF16B. Cell 121:437–450.

Hoogenraad CC, Akhmanova A (2016) Bicaudal D Family of Motor Adaptors: Linking Dynein Motility to Cargo Binding. Trends Cell Biol 26:327–340.

Hoogenraad CC, Akhmanova A, Howell SA, Dortland BR, De Zeeuw CI, Willemsen R, Visser P, Grosveld F, Galjart N (2001) Mammalian Golgi-associated Bicaudal-D2 functions in the dynein-dynactin pathway by interacting with these complexes. EMBO J 20:4041–4054.

Hoogenraad CC, Wulf P, Schiefermeier N, Stepanova T, Galjart N, Small JV, Grosveld F, De Zeeuw CI, Akhmanova A (2003) Bicaudal D induces selective dynein-mediated microtubule minus end-directed transport. EMBO J 22:6004–6015.

Hook SS, Orian A, Cowley SM, Eisenman RN (2002) Histone deacetylase 6 binds polyubiquitin through its zinc finger (PAZ domain) and copurifies with deubiquitinating enzymes. Proc Natl Acad Sci 99:13425–13430.

Hou Y, Wang Y, Wang H, Xu Y (2014) Induction of glutathione synthesis in human hepatocytes by acute and chronic arsenic exposure: Differential roles of mitogen-activated protein kinases. Toxicology 325:96–106.

Howe CL, Valletta JS, Rusnak AS, Mobley WC (2001) NGF Signaling from Clathrin-Coated Vesicles. Neuron 32:801–814.

Hua Y, Zhou J (2004) Survival motor neuron protein facilitates assembly of stress granules. FEBS Lett 572:69–74.

Huang EJ, Reichardt LF (2001) Neurotrophins: Roles in Neuronal Development and Function. Annu Rev Neurosci 24:677–736.

Hubbert C, Guardiola A, Shao R, Kawaguchi Y, Ito A, Nixon A, Yoshida M, Wang X-F, Yao T-P (2002) HDAC6 is a microtubule-associated deacetylase. Nature 417:455–458.

Huotari J, Helenius A (2011) Endosome maturation. EMBO J 30:3481–3500.

Hurley JH (2010) The ESCRT complexes. Crit Rev Biochem Mol Biol 45:463–487.

Husedzinovic A, Neumann B, Reymann J, Draeger-Meurer S, Chari A, Erfle H, Fischer U, Gruss OJ (2014) The catalytically inactive tyrosine phosphatase HD-PTP/PTPN23 is a novel regulator of SMN complex localization. Mol Biol Cell 26:161–171.

Ichioka F, Takaya E, Suzuki H, Kajigaya S, Buchman VL, Shibata H, Maki M (2007) HD-PTP and Alix share some membrane-traffic related proteins that interact with their Bro1 domains or proline-rich regions. Arch Biochem Biophys 457:142–149.

Ivanov PA, Chudinova EM, Nadezhdina ES (2003) Disruption of microtubules inhibits cytoplasmic ribonucleoprotein stress granule formation. Exp Cell Res 290:227–233.

Jain S, Wheeler JR, Walters RW, Agrawal A, Barsic A, Parker R (2016) ATPase-Modulated Stress Granules Contain a Diverse Proteome and Substructure. Cell 164:487–498.

Ji L, Minna JD, Roth J a (2005) 3P21.3 Tumor Suppressor Cluster: Prospects for Translational Applications. Future Oncol 1:79–92.

Jiang JM, Zhou CF, Gao SL, Tian Y, Wang CY, Wang L, Gu HF, Tang XQ (2015) BDNF-TrkB pathway mediates neuroprotection of hydrogen sulfide against formaldehyde-induced toxicity to PC12 cells. PLoS One 10:1–16.

Johnson JO et al. (2010) Exome sequencing reveals VCP mutations as a cause of familial ALS. Neuron 68:857–864.

Joshi M, Kulkarni A, Pal JK (2013) Small molecule modulators of eukaryotic initiation factor 2α kinases, the key regulators of protein synthesis. Biochimie

95:1980–1990.

Kalaidzidis I, Miaczynska M, Brewinska-Olchowik M, Hupalowska A, Ferguson C, Parton RG, Kalaidzidis Y, Zerial M (2015) APPL endosomes are not obligatory endocytic intermediates but act as stable cargo-sorting compartments. J Cell Biol 211:123–144.

Kalinski AL et al. (2019) Deacetylation of Miro1 by HDAC6 blocks mitochondrial transport and mediates axon growth inhibition. J Cell Biol 5:1–20.

Kampers T, Friedhoff P, Biernat J, Mandelkow EM, Mandelkow E (1996) RNA stimulates aggregation of microtubule-associated protein tau into Alzheimer-like paired helical filaments. FEBS Lett 399:344–349.

Kaplan DR, Miller FD (2000) Neurotrophin signal transduction in the nervous system. Curr Opin Neurobiol 10:381–391.

Kapust RB, Waugh DS (1999) Escherichia coli maltose-binding protein is uncommonly effective at promoting the solubility of polypeptides to which it is fused. Protein Sci 8:1668–1674.

Karussis D, Abramsky O, Argov Z, Petrou P, Kassis I, Melamed E, Vaknin-Dembinsky A, Gotkine M, Ben-Hur T, Offen D, Gothelf Y, Levy YS (2016) Safety and Clinical Effects of Mesenchymal Stem Cells Secreting Neurotrophic Factor Transplantation in Patients With Amyotrophic Lateral Sclerosis. JAMA Neurol 73:337–344.

Kato M, Han TW, Xie S, Shi K, Du X, Wu LC, Mirzaei H, Goldsmith EJ, Longgood J, Pei J, Grishin N V., Frantz DE, Schneider JW, Chen S, Li L, Sawaya MR, Eisenberg D, Tycko R, McKnight SL (2012) Cell-free formation of RNA granules: Low complexity sequence domains form dynamic fibers within hydrogels. Cell 149:753–767.

Kaur N, Lu B, Monroe RK, Ward SM, Halvorsen SW (2005) Inducers of oxidative stress block ciliary neurotrophic factor activation of Jak/STAT signaling in neurons. J Neurochem 92:1521–1530.

Kawaguchi Y, Kovacs JJ, McLaurin A, Vance JM, Ito A, Yao TP (2003) The deacetylase HDAC6 regulates aggresome formation and cell viability in response to misfolded protein stress. Cell 115:727–738.

Kayali F, Montie HL, Rafols JA, DeGracia DJ (2005) Prolonged translation arrest in reperfused hippocampal cornu Ammonis 1 is mediated by stress granules. Neuroscience 134:1223–1245.

Kedersha N, Anderson P (2002) Stress granules: sites of mRNA triage that regulate mRNA stability and translatability. Biochem Soc Trans 30:963–969.

Kedersha N, Anderson P (2007) Mammalian Stress Granules and Processing Bodies. Methods Enzymol 431:61–81.

Kedersha N, Chen S, Gilks N, Li W, Miller IJ, Stahl J, Anderson P (2002) Evidence That Ternary Complex (eIF2-GTP-tRNAiMet)–Deficient Preinitiation Complexes Are Core Constituents of Mammalian Stress Granules. Mol Biol Cell 13:195–210.

Kedersha N, Cho MR, Li W, Yacono PW, Chen S, Gilks N, Golan DE, Anderson

P (2000) Dynamic shuttling of TIA-1 accompanies the recruitment of mRNA to mammalian stress granules. J Cell Biol 151:1257–1268.

Kedersha N, Gupta M, Li W, Miller I, Anderson P (1999) RNA-binding Proteins TIA-1 and TIAR Link the Phosphorylation of eIF-2 alpha to the Assembly of Mammalian Stress Granules. J Cell Biol 147:1431–1441.

Kedersha N, Ivanov P, Anderson P (2013) Stress granules and cell signaling: More than just a passing phase? Trends Biochem Sci 38:494–506.

Kedersha N, Panas MD, Achorn CA, Lyons S, Tisdale S, Hickman T, Thomas M, Lieberman J, McInerney GM, Ivanov P, Anderson P (2016) G3BP-Caprin1-USP10 complexes mediate stress granule condensation and associate with 40S subunits. J Cell Biol 212:845–860.

Kedersha N, Stoecklin G, Ayodele M, Yacono P, Lykke-Andersen J, Fitzler MJ, Scheuner D, Kaufman RJ, Golan DE, Anderson P (2005) Stress granules and processing bodies are dynamically linked sites of mRNP remodeling. J Cell Biol 169:871–884.

Khalil B, Morderer D, Price PL, Liu F, Rossoll W (2018) mRNP assembly, axonal transport, and local translation in neurodegenerative diseases. Brain Res 1693:75–91.

Kharitidi D, Apaja PM, Manteghi S, Suzuki K, Malitskaya E, Roldan A, Gingras M-C, Takagi J, Lukacs GL, Pause A (2015) Interplay of Endosomal pH and Ligand Occupancy in Integrin α5β1 Ubiquitination, Endocytic Sorting, and Cell Migration. Cell Rep 13:599–609.

Khong A, Jain S, Matheny T, Wheeler JR, Parker R (2018) Isolation of mammalian stress granule cores for RNA-Seq analysis. Methods 137:49–54.

Khong A, Matheny T, Jain S, Mitchell SF, Wheeler JR, Parker R (2017) The Stress Granule Transcriptome Reveals Principles of mRNA Accumulation in Stress Granules. Mol Cell 68:808–820.

Khotskaya YB, Holla VR, Farago AF, Mills Shaw KR, Meric-Bernstam F, Hong DS (2017) Targeting TRK family proteins in cancer. Pharmacol Ther 173:58–66.

Kiernan MC, Vucic S, Cheah BC, Turner MR, Eisen A, Hardiman O, Burrell JR, Zoing MC (2011) Amyotrophic lateral sclerosis. Lancet 377:942–955.

Kim J, Sitaraman S, Hierro A, Beach BM, Odorizzi G, Hurley JH (2005a) Structural basis for endosomal targeting by the Bro1 domain. Dev Cell 8:937–947.

Kim WJ, Back SH, Kim V, Ryu I, Jang SK (2005b) Sequestration of TRAF2 into Stress Granules Interrupts Tumor Necrosis Factor Signaling under Stress Conditions. Mol Cell Biol 25:2450–2462.

Kimball SR, Horetsky RL, Ron D, Jefferson LS, Harding HP (2003) Mammalian stress granules represent sites of accumulation of stalled translation initiation complexes. Am J Physiol Cell Physiol 284:273–284.

Kolobova E, Efimov A, Kaverina I, Rishi AK, Schrader JW, Ham J, Larocca MC, Goldenring JR (2009) Microtubule-dependent association of AKAP350A and

CCAR1 with RNA stress granules. Exp Cell Res 315:542–555.

Kowal J, Tkach M, Théry C (2014) Biogenesis and secretion of exosomes. Curr Opin Cell Biol 29:116–125.

Kruttgen A, Saxena S, Evangelopoulos ME, Weis J (2003) Neurotrophins and Neurodegenerative Diseases: Receptors Stuck in Traffic? J Neuropathol Exp Neurol 62:340–350.

Kuruvilla R, Ye H, Ginty DD (2000) Spatially and functionally distinct roles of the PI3-K effector pathway during NGF signaling in sympathetic neurons. Neuron 27:499–512.

Kwon SH, Zhang Y, Matthias P (2007) The deacetylase HDAC6 is an essential component of stress granules and plays a critical role in the cellular response to stress. Genes Dev 21:3381–3394.

Kwong LK, Neumann M, Sampathu DM, Lee VM-Y, Trojanowski JQ (2007) TDP-43 proteinopathy: the neuropathology underlying major forms of sporadic and familial frontotemporal lobar degeneration and motor neuron disease. Acta Neuropathol 114:63–70.

Lalli G, Schiavo G (2002) Analysis of retrograde transport in motor neurons reveals common endocytic carriers for tetanus toxin and neurotrophin receptor p75NTR. J Cell Biol 156:233–239.

LaMonte BH, Wallace KE, Holloway BA, Shelly SS, Ascaño J, Tokito M, Van Winkle T, Howland DS, Holzbaur ELF (2002) Disruption of dynein/dynactin inhibits axonal transport in motor neurons causing late-onset progressive degeneration. Neuron 34:715–727.

Lanser M, Carrington J, Fallon J (1986) Survival of motoneurons in the brachial lateral motor column of limbless mutant chick embryos depends on the periphery. J Neurosci 6:2551–2557.

Lanser M, Fallon J (1984) Development of the lateral motor column in the limbless mutant chick embryo. J Neurosci 4:2043–2050.

Lanser ME, Fallon JF (1987) Development of the brachial lateral motor column in the wingless mutant chick embryo: Motoneuron survival under varying degrees of peripheral load. J Comp Neurol 261:423–434.

Larsen KS, Xu J, Cermelli S, Shu Z, Gross SP (2008) BicaudalD actively regulates microtubule motor activity in lipid droplet transport. Schweisguth F, ed. PLoS One 3:1–12.

Lazo OM, Gonzalez A, Ascano M, Kuruvilla R, Couve A, Bronfman FC (2013) BDNF Regulates Rab11-Mediated Recycling Endosome Dynamics to Induce Dendritic Branching. J Neurosci 33:6112–6122.

Le-Niculescu H, Bonfoco E, Kasuya Y, Claret F-X, Green DR, Karin M (1999) Withdrawal of Survival Factors Results in Activation of the JNK Pathway in Neuronal Cells Leading to Fas Ligand Induction and Cell Death. Mol Cell Biol 19:751–763.

Le Roy C, Wrana JL (2005) Clathrin- and non-clathrin-mediated endocytic

regulation of cell signalling. Nat Rev Mol Cell Biol 6:112–126.

Lee J, Koga H, Kawaguchi Y, Tang W, Wong E, Gao Y, Pandey UB, Kaushik S, Tresse E, Lu J, Taylor JP, Cuervo AM, Yao T (2010) HDAC6 controls autophagosome maturation essential for ubiquitin-selective quality-control autophagy. EMBO J 29:969–980.

Lee J, Oh K-J, Lee D, Kim BY, Choi JS, Ku B, Kim SJ (2016a) Structural Study of the HD-PTP Bro1 Domain in a Complex with the Core Region of STAM2, a Subunit of ESCRT-0. PLoS One 11:1–14.

Lee KH et al. (2016b) C9orf72 Dipeptide Repeats Impair the Assembly, Dynamics, and Function of Membrane-Less Organelles. Cell 167:774–788.

Lee S, Tak E, Lee J, Rashid M, Murphy MP, Ha J, Kim SS (2011) Mitochondrial H2O2 generated from electron transport chain complex i stimulates muscle differentiation. Cell Res 21:817–834.

Lennicke C, Rahn J, Lichtenfels R, Wessjohann LA, Seliger B (2015) Hydrogen peroxide – production , fate and role in redox signaling of tumor cells. Cell Commun Signal 13:1–19.

Li C, Wen A, Shen B, Lu J, Huang Y, Chang Y (2011) FastCloning: a highly simplified, purification-free, sequence- and ligation-independent PCR cloning method. BMC Biotechnol 11:1–10.

Li X-Z, Sun Z-P, Chen Z-Y, Zhao L, Chao M V., Geng Z, Zhang K-D, Huang S-H (2009) Essential Role of Hrs in Endocytic Recycling of Full-length TrkB Receptor but Not Its Isoform TrkB.T1. J Biol Chem 284:15126–15136.

Li YR, King OD, Shorter J, Gitler AD (2013) Stress granules as crucibles of ALS pathogenesis. J Cell Biol 201:361–372.

Lin DC, Quevedo C, Brewer NE, Bell A, Testa JR, Grimes ML, Miller FD, Kaplan DR (2006) APPL1 Associates with TrkA and GIPC1 and Is Required for Nerve Growth Factor-Mediated Signal Transduction. Mol Cell Biol 26:8928–8941.

Lin G, Aranda V, Muthuswamy SK, Tonks NK (2011) Identification of PTPN23 as a novel regulator of cell invasion in mammary epithelial cells from a loss-of-function screen of the “PTP-ome.” Genes Dev 2:1412–1425.

Lin MT, Beal MF (2006) Mitochondrial dysfunction and oxidative stress in neurodegenerative diseases. Nature 443:787–795.

Liu-Yesucevitz L, Bilgutay A, Zhang YJ, Vanderwyde T, Citro A, Mehta T, Zaarur N, McKee A, Bowser R, Sherman M, Petrucelli L, Wolozin B (2010) Tar DNA binding protein-43 (TDP-43) associates with stress granules: Analysis of cultured cells and pathological brain tissue. PLoS One 5:1–15.

Liu Y, Salter HK, Holding AN, Johnson CM, Stephens E, Lukavsky PJ, Walshaw J, Bullock SL (2013) Bicaudal-D uses a parallel, homodimeric coiled coil with heterotypic registry to coordinate recruitment of cargos to dynein. Genes Dev 27:1233–1246.

Loncle N, Agromayor M, Martin-Serrano J, Williams DW (2015) An ESCRT module is required for neuron pruning. Sci Rep 5:1–11.

Loschi M, Leishman CC, Berardone N, Boccaccio GL (2009) Dynein and kinesin regulate stress-granule and P-body dynamics. J Cell Sci 122:3973–3982.

Lytton J, Westlin M, Hanley MR (1991) Thapsigargin inhibits the sarcoplasmic or endoplasmic reticulum Ca-ATPase family of calcium pumps. J Biol Chem 266:17067–17071.

Ma H, Wardega P, Mazaud D, Klosowska-Wardega A, Jurek A, Engström U, Lennartsson J, Heldin C-H (2015) Histidine-domain-containing protein tyrosine phosphatase regulates platelet-derived growth factor receptor intracellular sorting and degradation. Cell Signal 27:2209–2219.

Mackenzie IRA et al. (2007) Pathological TDP-43 distinguishes sporadic amyotrophic lateral sclerosis from amyotrophic lateral sclerosis with SOD1 mutations. Ann Neurol 61:427–434.

Maday S, Twelvetrees AE, Moughamian AJ, Holzbaur ELF (2014) Axonal Transport: Cargo-Specific Mechanisms of Motility and Regulation. Neuron 84:292–309.

Madigan NN, Staff NP, Windebank AJ, Benarroch EE (2017) Genome editing technologies and their potential to treat neurologic disease. Neurology 89:1739–1748.

Maharjan N, Künzli C, Buthey K, Saxena S (2017) C9ORF72 Regulates Stress Granule Formation and Its Deficiency Impairs Stress Granule Assembly, Hypersensitizing Cells to Stress. Mol Neurobiol 54:3062–3077.

Mahboubi H, Stochaj U (2017) Cytoplasmic stress granules: Dynamic modulators of cell signaling and disease. Biochim Biophys Acta 1863:884–895.

Manteghi S, Gingras M-C, Kharitidi D, Galarneau L, Marques M, Yan M, Cencic R, Robert F, Paquet M, Witcher M, Pelletier J, Pause A (2016) Haploinsufficiency of the ESCRT Component HD-PTP Predisposes to Cancer. Cell Rep 15:1893–1900.

Mariotti M, Castiglioni S, Beguinot L, Maier JAM (2006) The tyrosine phosphatase HD-PTP is regulated by FGF-2 through proteasome degradation. Front Biosci 11:2138–2143.

Markham A, Cameron I, Franklin P, Spedding M (2004) BDNF increases rat brain mitochondrial respiratory coupling at complex I, but not complex II. Eur J Neurosci 20:1189–1196.

Markmiller S, Soltanieh S, Server KL, Mak R, Jin W, Fang MY, Luo E-C, Krach F, Yang D, Sen A, Fulzele A, Wozniak JM, Gonzalez DJ, Kankel MW, Gao F-B, Bennett EJ, Lécuyer E, Yeo GW (2018) Context-Dependent and Disease-Specific Diversity in Protein Interactions within Stress Granules. Cell 172:590–604.

Masters TA, Tumbarello DA, Chibalina M V., Buss F (2017) MYO6 Regulates Spatial Organization of Signaling Endosomes Driving AKT Activation and Actin Dynamics. Cell Rep 19:2088–2101.

Matanis T, Akhmanova A, Wulf P, Del Nery E, Weide T, Stepanova T, Galjart N, Grosveld F, Goud B, De Zeeuw CI, Barnekow A, Hoogenraad CC (2002)

Bicaudal-D regulates COPI-independent Golgi-ER transport by recruiting the dynein-dynactin motor complex. Nat Cell Biol 4:986–992.

Mateju D, Franzmann TM, Patel A, Kopach A, Boczek EE, Maharana S, Lee HO, Carra S, Hyman AA, Alberti S (2017) An aberrant phase transition of stress granules triggered by misfolded protein and prevented by chaperone function. EMBO J 4:1–19.

Matsumoto K, Minami M, Shinozaki F, Suzuki Y, Abe K, Zenno S, Matsumoto S, Minami Y (2011) Hsp90 is involved in the formation of P-bodies and stress granules. Biochem Biophys Res Commun 407:720–724.

Matsuto M, Kano F, Murata M (2015) Reconstitution of the targeting of Rab6A to the Golgi apparatus in semi-intact HeLa cells: A role of BICD2 in stabilizing Rab6A on Golgi membranes and a concerted role of Rab6A/BICD2 interactions in Golgi-to-ER retrograde transport. Biochim Biophys Acta 1853:2592–2609.

Matteoni R, Kreis TE (1987) Translocation and clustering of endosomes and lysosomes depends on microtubules. J Cell Biol 105:1253–1265.

Mattson MP, Lovell MA, Furukawa K, Markesbery WR (1995) Neurotrophic Factors Attenuate Glutamate-Induced Accumulation of Peroxides, Elevation of Intracellular Ca2+ Concentration, and Neurotoxicity and Increase Antioxidant Enzyme Activities in Hippocampal Neurons. J Neurochem 65:1740–1751.

Mazroui R, Di Marco S, Kaufman RJ, Gallouzi I-E (2007) Inhibition of the Ubiquitin-Proteasome System Induces Stress Granule Formation. Mol Biol Cell 18:2603–2618.

Mazroui R, Huot M, Tremblay S, Filion C, Labelle Y, Khandjian EW (2002) Trapping of messenger RNA by Fragile X Mental Retardation protein into cytoplasmic granules induces translation repression. Hum Mol Genet 11:3007–3017.

McClintock MA, Dix CI, Johnson CM, McLaughlin SH, Maizels RJ, Hoang HT, Bullock SL (2018) RNA-directed activation of cytoplasmic dynein-1 in reconstituted transport RNPs. Elife 7:1–29.

McDonald KK, Aulas A, Destroismaisons L, Pickles S, Beleac E, Camu W, Rouleau GA, Vande Velde C (2011a) TAR DNA-binding protein 43 (TDP-43) regulates stress granule dynamics via differential regulation of G3BP and TIA-1. Hum Mol Genet 20:1400–1410.

McDonald KK, Aulas A, Destroismaisons L, Pickles S, Beleac E, Camu W, Rouleau GA, Velde C Vande (2011b) TAR DNA-binding protein 43 (TDP-43) regulates stress granule dynamics via differential regulation of G3BP and TIA-1. Hum Mol Genet 20:1400–1410.

McEwen E, Kedersha N, Song B, Scheuner D, Gilks N, Han A, Chen JJ, Anderson P, Kaufman RJ (2005) Heme-regulated inhibitor kinase-mediated phosphorylation of eukaryotic translation initiation factor 2 inhibits translation, induces stress granule formation, and mediates survival upon arsenite exposure. J Biol Chem 280:16925–16933.

Mebratu Y, Tesfaigzi Y (2009) How ERK1/2 activation controls cell proliferation and cell death: Is subcellular localization the answer? Cell Cycle 8:1168–1175.

Meyerowitz J, Parker SJ, Vella LJ, Ng DC, Price KA, Liddell JR, Caragounis A, Li QX, Masters CL, Nonaka T, Hasegawa M, Bogoyevitch MA, Kanninen KM, Crouch PJ, White AR (2011) C-Jun N-terminal kinase controls TDP-43 accumulation in stress granules induced by oxidative stress. Mol Neurodegener 6:1–22.

Miaczynska M, Christoforidis S, Giner A, Shevchenko A, Uttenweiler-Joseph S, Habermann B, Wilm M, Parton RG, Zerial M (2004a) APPL Proteins Link Rab5 to Nuclear Signal Transduction via an Endosomal Compartment view, signal transduction is initiated at the plasma mem- brane and, via a series of protein-protein interactions and kinase cascades, transmitted through the cytoplasm. Cell 116:445–456.

Miaczynska M, Pelkmans L, Zerial M (2004b) Not just a sink: Endosomes in control of signal transduction. Curr Opin Cell Biol 16:400–406.

Mitre M, Mariga A, Chao M V (2016) Neurotrophin signalling: novel insights into mechanisms and pathophysiology. Clin Sci 131:13–23.

Mohler J, Wieschaus EF (1986) Dominant maternal-effect mutations of Drosophila melanogaster causing the production of double-abdomen embryos. Genetics 112:803–822.

Mokos S, Mills JR, Garreau C, Fournier M-J, Robert F, Arya P, Kaufman RJ, Pelletier J, Mazroui R (2009) Uncoupling Stress Granule Assembly and Translation Initiation Inhibition. Mol Biol Cell 20:2673–2683.

Mollet S, Cougot N, Wilczynska A, Dautry F, Kress M, Bertrand E, Weil D (2008) Translationally Repressed mRNA Transiently Cycles through Stress Granules during Stress. Mol Biol Cell 19:4469–4479.

Moorhead a R, Rzomp K a, Scidmore M a (2007) The Rab6 effector Bicaudal D1 associates with Chlamydia trachomatis inclusions in a biovar-specific manner. Infect Immun 75:781–791.

Morfini GA, Burns M, Binder LI, Kanaan NM, LaPointe N, Bosco DA, Brown RH, Brown H, Tiwari A, Hayward L, Edgar J, Nave K-A, Garberrn J, Atagi Y, Song Y, Pigino G, Brady ST (2009) Axonal Transport Defects in Neurodegenerative Diseases. J Neurosci 29:12776–12786.

N'Diaye E-N, Kajihara KK, Hsieh I, Morisaki H, Debnath J, Brown EJ (2009) PLIC proteins or ubiquilins regulate autophagy-dependent cell survival during nutrient starvation. EMBO Rep 10:173–179.

Nadezhdina ES, Lomakin AJ, Shpilman AA, Chudinova EM, Ivanov PA (2010) Microtubules govern stress granule mobility and dynamics. Biochim Biophys Acta 1803:361–371.

Nakagawara A (2001) Trk receptor tyrosine kinases: A bridge between cancer and neural development. Cancer Lett 169:107–114.

Narayanan U, Achsel T, Lü Hrmann R, Gregory Matera A (2004) Coupled In Vitro Import of U snRNPs and SMN, the Spinal Muscular Atrophy Protein mechanistic studies have yet to emerge. The second theory holds that SMN performs a general cellular func- tion, and that perturbation of this activity has particularly. Mol Cell 16:223–234.

Nas GC, Timasheff SN (1982) In Vitro Vinblastine-induced Tubulin Paracrystals. J Biol Chem 257:10387–10391.

Negro S, Stazi M, Marchioretto M, Tebaldi T, Rodella U, Duregotti E, Gerke V, Quattrone A, Montecucco C, Rigoni M, Viero G (2018) Hydrogen peroxide is a neuronal alarmin that triggers specific RNAs, local translation of Annexin A2, and cytoskeletal remodeling in Schwann cells. RNA 24:915–925.

Neubrand VE, Cesca F, Benfenati F, Schiavo G (2012) Kidins220/ARMS as a functional mediator of multiple receptor signalling pathways. J Cell Sci 125:1845–1854.

Neubrand VE, Thomas C, Schmidt S, Debant A, Schiavo G (2010) Kidins220/ARMS regulates Rac1-dependent neurite outgrowth by direct interaction with the RhoGEF Trio. J Cell Sci 123:2111–2123.

Neumann M, Sampathu DM, Kwong LK, Truax AC, Micsenyi MC, Chou TT, Bruce J, Schuck T, Grossman M, Clark CM, McCluskey LF, Miller BL, Masliah E, Mackenzie IR, Feldman H, Feiden W, Kretzschmar H a, Trojanowski JQ, Lee VM-Y (2006) Ubiquitinated TDP-43 in frontotemporal lobar degeneration and amyotrophic lateral sclerosis. Science 314:130–133.

Niedzielska E, Smaga I, Gawlik M, Moniczewski A, Stankowicz P, Pera J, Filip M (2016) Oxidative Stress in Neurodegenerative Diseases. Mol Neurobiol 53:4094–4125.

Nostramo R, Varia SN, Zhang B, Emerson MM, Herman PK (2016) The Catalytic Activity of the Ubp3 Deubiquitinating Protease Is Required for Efficient Stress Granule Assembly in Saccharomyces cerevisiae. Mol Cell Biol 36:173–183.

Numakawa T, Matsumoto T, Numakawa Y, Richards M, Yamawaki S, Kunugi H (2011) Protective action of neurotrophic factors and estrogen against oxidative stress-mediated neurodegeneration. J Toxicol 2011.

Nykjaer A, Lee R, Teng KK, Jansen P, Madsen P, Nielsen MS, Jacobsen C, Kliemannel M, Schwarz E, Willnow TE, Hempstead BL, Petersen CM (2004) Sortilin is essential for proNGF-induced neuronal cell death. Nature 427:843–848.

Nykjaer A, Willnow TE, Petersen CM (2005) p75NTR - Live or let die. Curr Opin Neurobiol 15:49–57.

Obrig TG, Culp WJ, McKeehan WL, Hadesty B (1971) The Mechanism by which Cycloheximide Glutarimide Antibiotics Inhibit Peptide Synthesis on Reticulocyte Ribosomes. J Biol Chem 246:174–181.

Ohshima D, Arimoto-Matsuzaki K, Tomida T, Takekawa M, Ichikawa K (2015) Spatio-temporal Dynamics and Mechanisms of Stress Granule Assembly. PLoS Comput Biol 11:1–22.

Omer A, Patel D, Lian XJ, Sadek J, Marco S Di, Pause A, Gorospe M, Gallouzi IE (2018) Stress granules counteract senescence by sequestration of PAI- 1. EMBO Rep 19:1–16.

Oppenheim RW (1989) The neurotrophic theory and naturally occurring motoneuron death. Trends Neurosci 12:252–255.

Oppenheim RW (1996) The concept of uptake and retrograde transport of neurotrophic molecules during development: History and present status. Neurochem Res 21:769–777.

Oppenheim RW, Prevette D, Tytell M, Homma S (1990) Naturally occurring and induced neuronal death in the chick embryo in vivo requires protein and RNA synthesis: Evidence for the role of cell death genes. Dev Biol 138:104–113.

Orrù S, Coni P, Floris A, Littera R, Carcassi C, Sogos V, Brancia C (2016) Reduced stress granule formation and cell death in fibroblasts with the A382T mutation of TARDBP gene: evidence for loss of TDP-43 nuclear function. Hum Mol Genet 25:4473–4483.

Panas MD, Ivanov P, Anderson P (2016) Mechanistic insights into mammalian stress granule dynamics. J Cell Biol 215:313–323.

Park JW, Vahidi B, Taylor AM, Rhee SW, Jeon NL (2006) Microfluidic culture platform for neuroscience research. Nat Protoc 1:2128–2136.

Parkinson MDJ, Piper SC, Bright NA, Evans JL, Boname JM, Bowers K, Lehner PJ, Luzio JP (2015) A non-canonical ESCRT pathway, including histidine domain phosphotyrosine phosphatase (HD-PTP), is used for down-regulation of virally ubiquitinated MHC class I. Biochem J 471:79–88.

Pereira C, Bessa C, Saraiva L (2012) Endocytosis inhibition during H 2O 2-induced apoptosis in yeast. FEMS Yeast Res 12:755–760.

Perez-Pepe M, Fernández-Alvarez AJ, Boccaccio GL (2018) Life and Work of Stress Granules and Processing Bodies: New Insights into Their Formation and Function. Biochemistry 57:2488–2498.

Picher-Martel V, Renaud L, Bareil C, Julien JP (2018) Neuronal Expression of UBQLN2P497H Exacerbates TDP-43 Pathology in TDP-43G348C Mice through Interaction with Ubiquitin. Mol Neurobiol 10:1–17.

Podzuweit T, Nennstiel P, Müller A (1995) Isozyme selective inhibition of cGMP-stimulated cyclic nucleotide phosphodiesterases by erythro-9-(2-hydroxy-3-nonyl) adenine. Cell Signal 7:733–738.

Pradhan-Sundd T, Verheyen EM (2014) The role of Bro1- domain-containing protein Myopic in endosomal trafficking of Wnt/Wingless. Dev Biol 392:93–107.

Proenca CC, Song M, Lee FS (2016) Differential effects of BDNF and neurotrophin 4 (NT4) on endocytic sorting of TrkB receptors. J Neurochem 138:397–406.

Progida C, Malerod L, Stuffers S, Brech A, Bucci C, Stenmark H (2007) RILP is required for the proper morphology and function of late endosomes. J Cell Sci 120:3729–3737.

Progida C, Spinosa MR, De Luca A, Bucci C (2006) RILP interacts with the VPS22 component of the ESCRT-II complex. Biochem Biophys Res Commun 347:1074–1079.

Protter DSW, Parker R (2016) Principles and Properties of Stress Granules. Trends Cell Biol 26:668–679.

Qamar S et al. (2018) FUS Phase Separation Is Modulated by a Molecular Chaperone and Methylation of Arginine Cation-π Interactions. Cell:720–734.

Rajesh K, Krishnamoorthy J, Kazimierczak U, Tenkerian C, Papadakis AI, Wang S, Huang S, Koromilas AE (2015) Phosphorylation of the translation initiation factor eIf2α at serine 51 determines the cell fate decisions of Akt in response to oxidative stress. Cell Death Dis 6:1–11.

Rajesh K, Papadakis AI, Kazimierczak U, Peidis P, Ferbeyre G, Kaufman RJ, Koromilas AE (2013) eIF2 α phosphorylation bypasses premature senescence caused by oxidative stress and pro - oxidant antitumor therapies. Aging 5:884–901.

Reck-Peterson SL, Redwine WB, Vale RD, Carter AP (2018) The cytoplasmic dynein transport machinery and its many cargoes. Nat Rev Mol Cell Biol 19:382–398.

Reed NA, Cai D, Blasius TL, Jih GT, Meyhofer E, Gaertig J, Verhey KJ (2006) Microtubule Acetylation Promotes Kinesin-1 Binding and Transport. Curr Biol 16:2166–2172.

Renton AE et al. (2011) A hexanucleotide repeat expansion in C9ORF72 is the cause of chromosome 9p21-linked ALS-FTD. Neuron 72:257–268.

Repici M, Hassanjani M, Maddison DC, Garção P, Cimini S, Patel B, Szegö ÉM, Straatman KR, Lilley KS, Borsello T, Outeiro TF, Panman L, Giorgini F (2019) The Parkinson's Disease-Linked Protein DJ-1 Associates with Cytoplasmic mRNP Granules During Stress and Neurodegeneration. Mol Neurobiol 56:61–77.

Rink J, Ghigo E, Kalaidzidis Y, Zerial M (2005) Rab conversion as a mechanism of progression from early to late endosomes. Cell 122:735–749.

Rogers S, Wells R, Rechsteiner M (1986) Amino Acid Sequences Common to Rapidly Degraded Proteins: The PEST Hypothesis. Science 234:364–268.

Roossien DH, Miller KE, Gallo G (2015) Ciliobrevins as tools for studying dynein motor function. Front Cell Neurosci 9:1–10.

Roskoski R (2012) ERK1/2 MAP kinases: Structure, function, and regulation. Pharmacol Res 66:105–143.

Roux PP, Barker P a. (2002) Neurotrophin signaling through the p75 neurotrophin receptor. Prog Neurobiol 67:203–233.

Ruit K, Osborne P, Schmidt R, Johnson E, Snider W (1990) Nerve growth factor regulates sympathetic ganglion cell morphology and survival in the adult mouse. J Neurosci 10:2412–2419.

Sahoo PK, Lee SJ, Jaiswal PB, Alber S, Kar AN, Miller-randolph S, Taylor EE, Smith T, Singh B, Ho TS, Urisman A, Chand S, Pena EA, Burlingame AL, Woolf CJ, Fainzilber M, English AW, Twiss JL (2018) mRNA translation and nerve regeneration. Nat Commun 9:1–14.

Salahuddin P, Siddiqi MK, Khan S, Abdelhameed AS, Khan RH (2016) Mechanisms of protein misfolding: Novel therapeutic approaches to protein-misfolding diseases. J Mol Struct 1123:311–326.

Sanchez-Sanchez J, Arevalo JC (2017) A review on ubiquitination of neurotrophin receptors: Facts and perspectives. Int J Mol Sci 18:1–11.

Sandow SL, Heydon K, Weible MW, Reynolds AJ, Bartlett SE, Hendry IA (2000) Signalling organelle for retrograde axonal transport of internalized neurotrophins from the nerve terminal. Immunol Cell Biol 78:430–435.

Sasi M, Vignoli B, Canossa M, Blum R (2017) Neurobiology of local and intercellular BDNF signaling. Pflugers Arch 469:593–610.

Schein CH (1989) Production of Soluble Recombinant Proteins in Bacteria. Nat Biotechnol 7:1141–1149.

Schlager M a, Kapitein LC, Grigoriev I, Burzynski GM, Wulf PS, Keijzer N, de Graaff E, Fukuda M, Shepherd IT, Akhmanova A, Hoogenraad CC (2010) Pericentrosomal targeting of Rab6 secretory vesicles by Bicaudal-D-related protein 1 (BICDR-1) regulates neuritogenesis. EMBO J 29:1637–1651.

Schlager M a, Serra-Marques A, Grigoriev I, Gumy LF, Esteves da Silva M, Wulf PS, Akhmanova A, Hoogenraad CC (2014) Bicaudal d family adaptor proteins control the velocity of Dynein-based movements. Cell Rep 8:1248–1256.

Schmieg N, Menendez G, Schiavo G, Terenzio M (2014) Signalling endosomes in axonal transport: Travel updates on the molecular highway. Semin Cell Dev Biol 27:32–43.

Scholz-Starke J, Cesca F (2016) Stepping Out of the Shade: Control of Neuronal Activity by the Scaffold Protein Kidins220/ARMS. Front Cell Neurosci 10:1–12.

Schreij AMA, Fon EA, McPherson PS (2016) Endocytic membrane trafficking and neurodegenerative disease. Cell Mol Life Sci 73:1529–1545.

Scott CC, Vacca F, Gruenberg J (2014) Endosome maturation, transport and functions. Semin Cell Dev Biol 31:2–10.

Seaman MNJ (2012) The retromer complex - endosomal protein recycling and beyond. J Cell Sci 125:4693–4702.

Senger DL, Campenot RB (1997) Rapid retrograde tyrosine phosphorylation of trkA and other proteins in rat sympathetic neurons in compartmented cultures. J Cell Biol 138:411–421.

Sette P, Mu R, Dussupt V, Jiang J, Snyder G, Smith P, Xiao TS, Bouamr F (2011) The Phe105 loop of Alix Bro1 domain plays a key role in HIV-1 release. Structure 19:1485–1495.

Seyb KI, Ansar S, Bean J, Michaelis ML (2006) β-Amyloid and Endoplasmic Reticulum Stress Reponses in Primary Neurons: Effects of Drugs That Interact With the Cytoskeleton. J Mol Neurosci 28:111–124.

Shao Y, Akmentin W, Toledo-Aral JJ, Rosenbaum J, Valdez G, Cabot JB, Hilbush BS, Halegoua S (2002) Pincher, a pinocytic chaperone for nerve growth factor/TrkA signaling endosomes. J Cell Biol 157:679–691.

Shaw DJ, Eggleton P, Young PJ (2008) Joining the dots: Production, processing and targeting of U snRNP to nuclear bodies. Biochim Biophys Acta - Mol Cell Res

1783:2137–2144.

Shaw PJ, Ince PG, Falkous G, Mantle D (1995) Oxidative damage to protein in sporadic motor neuron disease spinal cord. Ann Neurol 38:691–695.

Shendelman S, Jonason A, Martinat C, Leete T, Abeliovich A (2004) DJ-1 Is a redox-dependent molecular chaperone that inhibits α-synuclein aggregate formation. PLoS Biol 2:1764–1773.

Shenton D, Smirnova JB, Selley JN, Carroll K, Hubbard SJ, Pavitt GD, Ashe MP, Grant CM (2006) Global translational responses to oxidative stress impact upon multiple levels of protein synthesis. J Biol Chem 281:29011–29021.

Shields SB, Piper RC (2011) How ubiquitin functions with ESCRTs. Traffic 12:1306–1317.

Sigismund S, Argenzio E, Tosoni D, Cavallaro E, Polo S, Di Fiore PP (2008) Clathrin-Mediated Internalization Is Essential for Sustained EGFR Signaling but Dispensable for Degradation. Dev Cell 15:209–219.

Smigiel R, Landsberg G, Schilling M, Rydzanicz M, Pollak A, Walczak A, Stodolak A, Stawinski P, Mierzewska H, Sasiadek MM, Gruss OJ, Ploski R (2018) Developmental epileptic encephalopathy with hypomyelination and brain atrophy associated with PTPN23 variants affecting the assembly of UsnRNPs. Eur J Hum Genet 26:1502–1511.

Somasekharan SP, El-Naggar A, Leprivier G, Cheng H, Hajee S, Grunewald TGP, Zhang F, Ng T, Delattre O, Evdokimova V, Wang Y, Gleave M, Sorensen PH (2015) YB-1 regulates stress granule formation and tumor progression by translationally activating G3BP1. J Cell Biol 208:913–929.

Soncini C, Berdo I, Draetta G (2001) Ras-GAP SH3 domain binding protein (G3BP) is a modulator of USP10, a novel human ubiquitin specific protease. Oncogene 20.

Sönnichsen B, De Renzis S, Nielsen E, Rietdorf J, Zerial M (2000) Distinct membrane domains on endosomes in the recycling pathway visualized by multicolor imaging of Rab4, Rab5, and Rab11. J Cell Biol 149:901–914.

Soppina V, Rai AK, Ramaiya AJ, Barak P, Mallik R (2009) Tug-of-war between dissimilar teams of microtubule motors regulates transport and fission of endosomes. Proc Natl Acad Sci 106:19381–19386.

Sorenson EJ et al. (2008) Subcutaneous IGF-1 is not beneficial in 2-year ALS trial. Neurology 71:1770–1775.

Souquere S, Mollet S, Kress M, Dautry F, Pierron G, Weil D (2009) Unravelling the ultrastructure of stress granules and associated P-bodies in human cells. J Cell Sci 122:3619–3626.

Sowada N, Hashem MO, Yilmaz R, Hamad M, Kakar N, Thiele H, Arold ST, Bode H, Alkuraya FS, Borck G (2017) Mutations of PTPN23 in developmental and epileptic encephalopathy. Hum Genet 136:1455–1461.

Splinter D, Tanenbaum ME, Lindqvist A, Jaarsma D, Flotho A, Yu K Lou, Grigoriev I, Engelsma D, Haasdijk ED, Keijzer N, Demmers J, Fornerod M,

Melchior F, Hoogenraad CC, Medema RH, Akhmanova A (2010) Bicaudal D2, Dynein, and Kinesin-1 Associate with Nuclear Pore Complexes and Regulate Centrosome and Nuclear Positioning during Mitotic Entry. PLoS Biol 8:1–20.

Srivastava SP, Kumar KU, Kaufman RJ (1998) Phosphorylation of eukaryotic translation initiation factor 2 mediates apoptosis in response to activation of the double-stranded RNA-dependent protein kinase. J Biol Chem 273:2416–2423.

Stefan CJ et al. (2017) Membrane dynamics and organelle biogenesis-lipid pipelines and vesicular carriers. BMC Biol 15:1–24.

Stefani F, Zhang L, Taylor S, Donovan J, Rollinson S, Doyotte A, Brownhill K, Bennion J, Pickering-Brown S, Woodman P (2011) UBAP1 is a component of an endosome-specific ESCRT-I complex that is essential for MVB sorting. Curr Biol 21:1245–1250.

Steward R, Nüsslein-Volhard C (1986) The genetics of the dorsal-Bicaudal-D region of Drosophila melanogaster. Genetics 113:665–678.

Stoilov P, Stamm S, Castren E (2002) Analysis of the human TrkB gene genomic organization reveals novel TrkB isoforms, unusual gene length, and splicing mechanism. Biochem Biophys Res Commun 290:1054–1065.

Suter B, Romberg LM, Steward R (1989) Bicaudal-D , a Drosophila gene involved in developmental asymmetry : localized transcript accumulation in ovaries and sequence similarity to myosin heavy chain tail domains. Genes Dev 3:1957–1968.

Swan a, Nguyen T, Suter B (1999) Drosophila Lissencephaly-1 functions with Bic-D and dynein in oocyte determination and nuclear positioning. Nat Cell Biol 1:444–449.

Tabernero L, Woodman P (2018) Dissecting the role of His domain protein tyrosine phosphatase / PTPN23 and ESCRTs in sorting activated epidermal growth factor receptor to the multivesicular body. Biochem Soc Trans 46:1037–1046.

Takahashi M, Higuchi M, Matsuki H, Yoshita M, Ohsawa T, Oie M, Fujii M (2013) Stress granules inhibit apoptosis by reducing reactive oxygen species production. Mol Cell Biol 33:815–829.

Tanase C-A (2010) Histidine domain-protein tyrosine phosphatase interacts with Grb2 and GrpL. PLoS One 5:1–10.

Taylor JP, Brown RH, Cleveland DW (2016) Decoding ALS: From genes to mechanism. Nature 539:197–206.

Tejeda GS, Díaz-Guerra M (2017) Integral characterization of defective BDNF/TrkB signalling in neurological and psychiatric disorders leads the way to new therapies. Int J Mol Sci 18:1–24.

Terawaki S-I, Yoshikane A, Higuchi Y, Wakamatsu K (2015) Structural basis for cargo binding and autoinhibition of Bicaudal-D1 by a parallel coiled-coil with homotypic registry. Biochem Biophys Res Commun 460:451–456.

Terenzio M, Golding M, Russell MRG, Wicher KB, Rosewell I, Spencer-Dene B,

Ish-Horowicz D, Schiavo G (2014a) Bicaudal-D 1 regulates the intracellular sorting and signalling of neurotrophin receptors. EMBO J 33:1–17.

Terenzio M, Golding M, Schiavo G (2014b) siRNA screen of ES cell-derived motor neurons identifies novel regulators of tetanus toxin and neurotrophin receptor trafficking. Front Cell Neurosci 8:1–12.

Terenzio M, Schiavo G (2010) The more, the better: the BICD family gets bigger. EMBO J 29:1625–1626.

Terenzio M, Schiavo G, Fainzilber M (2017) Compartmentalized Signaling in Neurons: From Cell Biology to Neuroscience. Neuron 96:667–679.

Teyssou E et al. (2017) Novel UBQLN2 mutations linked to amyotrophic lateral sclerosis and atypical hereditary spastic paraplegia phenotype through defective HSP70-mediated proteolysis. Neurobiol Aging 58:1–10.

Tourrière H, Chebli K, Zekri L, Courselaud B, Blanchard JM, Bertrand E, Tazi J (2003) The RasGAP-associated endoribonuclease G3BP assembles stress granules. J Cell Biol 160:823–831.

Toyooka S, Ouchida M, Jitsumori Y, Tsukuda K, Sakai a, Nakamura a, Shimizu N, Shimizu K (2000) HD-PTP: A novel protein tyrosine phosphatase gene on human chromosome 3p21.3. Biochem Biophys Res Commun 278:671–678.

Tsai N-P, Wei L (2010) RhoA / ROCK1 signaling regulates stress granule formation and apoptosis. Cell Signal 22:668–675.

Tsai NP, Ho PC, Wei LN (2008) Regulation of stress granule dynamics by Grb7 and FAK signalling pathway. EMBO J 27:715–726.

Tsai NP, Tsui YC, Wei LN (2009) Dynein motor contributes to stress granule dynamics in primary neurons. Neuroscience 159:647–656.

Turner MR, Kiernan MC, Leigh PN, Talbot K (2009) Biomarkers in amyotrophic lateral sclerosis. Lancet Neurol 8:94–109.

Uings IJ, Farrow SN (2000) Cell receptors and cell signalling. J Clin Pathol - Mol Pathol 53:295–299.

Ullrich O, Reinsch S, Urbé S, Zerial M, Parton RG (1996) Rab11 regulates recycling through the pericentriolar recycling endosome. J Cell Biol 135:913–924.

Ure DR, Campenot RB (1997) Retrograde transport and steady-state distribution of 125I-nerve growth factor in rat sympathetic neurons in compartmented cultures. J Neurosci 17:1282–1290.

Uttara B, Singh A V, Zamboni P, Mahajan RT (2009) Oxidative Stress and Neurodegenerative Diseases: A Review of Upstream and Downstream Antioxidant Therapeutic Options. Curr Neuropharmacol 7:65–74.

Uversky VN (2017) Protein intrinsic disorder-based liquid–liquid phase transitions in biological systems: Complex coacervates and membrane-less organelles. Adv Colloid Interface Sci 239:97–114.

Valdez G, Akmentin W, Philippidou P, Kuruvilla R, Ginty DD, Halegoua S (2005) Pincher-mediated macroendocytosis underlies retrograde signaling by

neurotrophin receptors. J Neurosci 25:5236–5247.

Van Treeck B, Parker R (2019) Principles of Stress Granules Revealed by Imaging Approaches. Cold Spring Harb Perspect Biol 11:a033068.

Van Treeck B, Protter DSW, Matheny T, Khong A, Link CD, Parker R (2018) RNA self-assembly contributes to stress granule formation and defining the stress granule transcriptome. Proc Natl Acad Sci 115:2734–2739.

Vanderweyde T, Youmans K, Liu-Yesucevitz L, Wolozin B (2013) Role of stress granules and RNA-binding proteins in neurodegeneration: A mini-review. Gerontology 59:524–533.

Vanderweyde T, Yu H, Varnum M, Liu-Yesucevitz L, Citro A, Ikezu T, Duff K, Wolozin B (2012) Contrasting Pathology of the Stress Granule Proteins TIA-1 and G3BP in Tauopathies. J Neurosci 32:8270–8283.

Vega L, Ostrosky-Wegman P, Fortoul TI, Díaz C, Madrid V, Saavedra R (1999a) Sodium arsenite reduces proliferation of human activated T-cells by inhibition of the secretion of interleukin-2. Immunopharmacol Immunotoxicol 21:203–220.

Vidaurre ÓG, Gascón S, Deogracias R, Sobrado M, Cuadrado E, Montaner J, Rodríguez-Peña Á, Díaz-Guerra M (2012) Imbalance of neurotrophin receptor isoforms TrkB-FL/TrkB-T1 induces neuronal death in excitotoxicity. Cell Death Dis 3:1–12.

Villarroel-Campos D, Schiavo G, Lazo OM (2018) The many disguises of the signalling endosome. FEBS Lett 592:3615–3632.

Volkmer R, Tapia V, Landgraf C (2012) Synthetic peptide arrays for investigating protein interaction domains. FEBS Lett 586:2780–2786.

Von Bartheld CS (2004) Axonal Transport and Neuronal Transcytosis of Trophic Factors, Tracers, and Pathogens. J Neurobiol 58:295–314.

Von Bartheld CS, Altick AL (2011) Multivesicular bodies in neurons: Distribution, protein content, and trafficking functions. Prog Neurobiol 93:313–340.

Waelter S, Boeddrich A, Lurz R, Scherzinger E, Lueder G, Lehrach H, Wanker EE (2001) Accumulation of mutant huntingtin fragments in aggresome-like inclusion bodies as a result of insufficient protein degradation. Mol Biol Cell 12:1393–1407.

Walters RW, Muhlrad D, Garcia J, Parker R (2015) Differential effects of Ydj1 and Sis1 on Hsp70-mediated clearance of stress granules in Saccharomyces cerevisiae. Cold Spring Harb Lab Press 21:1660–1671.

Wang T, Hong W (2006) RILP interacts with VPS22 and VPS36 of ESCRT-II and regulates their membrane recruitment. Biochem Biophys Res Commun 350:413–423.

Wanschers BFJ, van de Vorstenbosch R, Schlager M a, Splinter D, Akhmanova A, Hoogenraad CC, Wieringa B, Fransen J a M (2007) A role for the Rab6B Bicaudal-D1 interaction in retrograde transport in neuronal cells. Exp Cell Res 313:3408–3420.

Wheeler JR, Jain S, Kong A, Parker R (2017) Isolation of yeast and mammalian stress granule cores. Methods 126:12–17.

Wheeler JR, Matheny T, Jain S, Abrisch R, Parker R (2016) Distinct stages in stress granule assembly and disassembly. Elife 5:1–25.

Whone A et al. (2019a) Randomized trial of intermittent intraputamenal glial cell line-derived neurotrophic factor in Parkinson's disease. Brain 142:512–525.

Whone AL et al. (2019b) Extended Treatment with Glial Cell Line-Derived Neurotrophic Factor in Parkinson's Disease. J Parkinsons Dis 45:1–13.

Wichterle H, Lieberam I, Porter J a, Jessell TM (2002) Directed differentiation of embryonic stem cells into motor neurons. Cell 110:385–397.

Wickman GR, Julian L, Mardilovich K, Schumacher S, Munro J, Rath N, Zander SAL, Mleczak A, Sumpton D, Morrice N (2013) Blebs produced by actin – myosin contraction during apoptosis release damage-associated molecular pattern proteins before secondary necrosis occurs. Cell Death Differ 20:1293–1305.

Wilczynska A, Aigueperse C, Kress M, Dautry F, Weil D (2005) The translational regulator CPEB1 provides a link between dcp1 bodies and stress granules. J Cell Sci 118:981–992.

Wilson C, González-Billault C (2015) Regulation of cytoskeletal dynamics by redox signaling and oxidative stress : implications for neuronal development and trafficking. Front Cell Neurosci 9:1–10.

Wilson C, Terman JR, González-Billault C, Ahmed G (2016) Actin filaments—A target for redox regulation. Cytoskeleton 73:577–595.

Wolozin B (2012) Regulated protein aggregation: Stress granules and neurodegeneration. Mol Neurodegener 7:1–12.

Woodman P (2016) ESCRT-III on endosomes: new functions, new activation pathway. Biochem J 473:e5–e8.

Wu A, Ying Z, Gomez-Pinilla F (2004) The interplay between oxidative stress and brain-derived neurotrophic factor modulates the outcome of a saturated fat diet on synaptic plasticity and cognition. Eur J Neurosci 19:1699–1707.

Xie X, Matsumoto S, Endo A, Fukushima T, Kawahara H, Saeki Y, Komada M (2018) Deubiquitylases USP5 and USP13 are recruited to and regulate heat-induced stress granules through their deubiquitylating activities. J Cell Sci 131:1–11.

Xu B, Zang K, Ruff NL, Zhang YA, McConnell SK, Stryker MP, Reichardt LF (2000) Cortical Degeneration in the Absence of Neurotrophin Signaling: Dendritic Retraction and Neuronal Loss after Removal of the Receptor TrkB. Neuron 26:233–245.

Yamashita N, Joshi R, Zhang S, Zhang Z-Y, Kuruvilla R (2017) Phospho-Regulation of Soma-to-Axon Transcytosis of Neurotrophin Receptors. Dev Cell 42:626-639.e5.

Yamashita N, Kuruvilla R (2016) Neurotrophin signaling endosomes: biogenesis,

regulation, and functions. Curr Opin Neurobiol 39:139–145.

Yang WH, Bloch DB (2007) Probing the mRNA processing body using protein macroarrays and “autoantigenomics”. RNA 13:704–712.

Yano H, Lee FS, Kong H, Chuang J-Z, Arevalo J, Perez P, Sung C-H, Chao M V. (2001a) Association of Trk neurotrophin receptors with components of the cytoplasmic dynein motor. J Neurosci 21:1–7.

Yano H, Lee FS, Kong H, Chuang J, Arevalo J, Perez P, Sung C-H, Chao M V. (2001b) Association of Trk neurotrophin receptors with components of the cytoplasmic dynein motor. J Neurosci 21:RC125.

Yoshii SR, Mizushima N (2017) Monitoring and measuring autophagy. Int J Mol Sci 18:1–13.

Youn JY, Dunham WH, Hong SJ, Knight JDR, Bashkurov M, Chen GI, Bagci H, Rathod B, MacLeod G, Eng SWM, Angers S, Morris Q, Fabian M, Côté JF, Gingras AC (2018) High-Density Proximity Mapping Reveals the Subcellular Organization of mRNA-Associated Granules and Bodies. Mol Cell 69:517–532.

Yu T, Calvo L, Anta B, López-Benito S, Southon E, Chao M V., Tessarollo L, Arévalo JC (2011) Regulation of Trafficking of Activated TrkA Is Critical for NGF-Mediated Functions. Traffic 12:521–534.

Zala D, Hinckelmann M-V, Yu H, Lyra da Cunha MM, Liot G, Cordelières FP, Marco S, Saudou F (2013) Vesicular glycolysis provides on-board energy for fast axonal transport. Cell 152:479–491.

Zerial M, Marsico G, Conte-Zerial P Del, Kalaidzidis Y, Hengstler JG, Koteliansky V, Kuchimanchi S, Nonaka H, Peng CG, Zeigerer A, Epstein-Barash H, Bogorad RL, Ruda VM, Seifert S, Gilleron J (2012) Rab5 is necessary for the biogenesis of the endolysosomal system in vivo. Nature 485:465–470.

Zhang F, Ström AL, Fukada K, Lee S, Hayward LJ, Zhu H (2007) Interaction between familial Amyotrophic Lateral Sclerosis (ALS)-linked SOD1 mutants and the dynein complex. J Biol Chem 282:16691–16699.

Zhang K, Daigle JG, Cunningham KM, Coyne AN, Ruan K, Grima JC, Bowen KE, Wadhwa H, Yang P, Rigo F, Taylor JP, Gitler AD, Rothstein JD, Lloyd TE (2018) Stress Granule Assembly Disrupts Nucleocytoplasmic Transport. Cell 173:958–971.

Zhang S, Fan G, Hao Y, Hammell M, Wilkinson JE, Tonks NK (2017) Suppression of protein tyrosine phosphatase N23 predisposes to breast tumorigenesis via activation of FYN kinase. Genes Dev 31:1939–1957.

Zhang Y, Moheban DB, Conway BR, Bhattacharyya a, Segal R a (2000) Cell surface Trk receptors mediate NGF-induced survival while internalized receptors regulate NGF-induced differentiation. J Neurosci 20:5671–5678.

Zhao Y, Lin Y, Zhang H, Mañas A, Tang W, Zhang Y, Wu D, Lin A, Xiang J (2015) Ubl4A is required for insulin-induced Akt plasma membrane translocation through promotion of Arp2/3-dependent actin branching. Proc Natl Acad Sci 112:9644–9649.

Zheng J, Shen WH, Lu TJ, Zhou Y, Chen Q, Wang Z, Xiang T, Zhu YC, Zhang C, Duan S, Xiong ZQ (2008) Clathrin-dependent endocytosis is required for TrkB-dependent Akt-mediated neuronal protection and dendritic growth. J Biol Chem 283:13280–13288.

Zhu X, Raina AK, Perry G, Smith MA (2004) Alzheimer's disease: The two-hit hypothesis. Lancet Neurol 3:219–226.

Zou T, Yang X, Pan D, Huang J, Sahin M, Zhou J (2011) SMN deficiency reduces cellular ability to form stress granules, sensitizing cells to stress. Cell Mol Neurobiol 31:541–550.